



NORTHWEST GEOLOGY

The Journal of The Tobacco Root Geological Society

Volume 41, July 2012

37th Annual Field Conference

Yellowstone National Park

July 26—July 29, 2012



Published by The Tobacco Root Geological Society, Inc.

P.O. Box 2734

Missoula, Montana 59806

<http://trgs.org>

Edited by: Marie M. Garsjo and Richard I. Gibson

*Cover: Touring Yellowstone in the Sylvan Lake area, 1916
Above: Souvenir folder mailed to Anaconda, Montana, in 1916
National Park Service photos.*

The Tobacco Root Geological Society, Inc.

P.O. Box 2734
Missoula, Montana 59806



Officers, 2012:

President: Mike Stickney, Montana Bureau of Mines and Geology, Butte, MT
Vice-President: Katie McDonald, Montana Bureau of Mines and Geology, Butte, MT
Treasurer: Ted Antonioli, Montana Mining Association, Missoula, MT
Secretary: Ann Marie Crites, Libby, MT
Webmaster: Dick Gibson, Consultant, Butte, MT

Board of Directors, 2012:

Ann Marie Crites, Libby, MT
Bruce E. Cox, (ret.) Hecla Mining Co., Idaho
Marie Marshall Garsjo, Natural Resources Conservation Service (ret.), Ft. Worth, TX
Richard I. Gibson, Gibson Consulting, Butte, MT
Larry Johnson, Consultant, Missoula, MT
Larry N. Smith, Dept. of Geological Engineering, Montana Tech, Butte, MT
Robert C. Thomas, Dept. of Environmental Sciences, U. of Montana-Western, Dillon, MT
Emily Geraghty Ward, Geology Dept., Rocky Mountain College, Billings, MT

Conference Organizer, Yellowstone Field Conference:

Michael C. Stickney
Editors: Marie M. Garsjo and Richard I. Gibson

ISSN: 0096-7769
© 2012 The Tobacco Root Geological Society, Inc.
<http://trgs.org>



NORTHWEST GEOLOGY

The Journal of The Tobacco Root Geological Society

Volume 41, July 2012

Yellowstone National Park

and other papers

Table of Contents

Author	Page	Title
E. A. (Skip) Yates and Michael A. Ellis	1	Locating the next Yellowstone Caldera
Elizabeth Lincoln Mathieson	11	Earthquake detective work on the Madison Range Fault, Montana – A retrospective
Chris Shaw	21	Radiocarbon age date of a mountain bison and rock fall in the Anaconda Range, Montana
D. H. Vice, Arnold Doden, and Bridget Lynne	25	Geothermal activity along a segment of the Lewis and Clark Line
Joseph H. Baird	34	The Wasatch Line (Neogene)/East Pacific Rise Plate Tectonic Model: Viable for multiple working hypothesis evaluation against “Slab Gap”?
J. Alcock and Peter Muller	47	A Paleoproterozoic sedimentary basin within the Wyoming craton exposed in the Ruby Range, SW Montana: Identified by field relations and geochronology
Paul Mueller, David Mogk, and Joseph Wooden	63	Age and composition of crystalline basement in the Armstead Anticline, southwestern Montana
FIELD GUIDES		
Michael Stickney	71	Road log for the Hebgen Lake earthquake area
Dan Moore, Chris Sant, Rebecca Wood, Barry Miller, Steve Hansen, Ryan Shurtliffe, and Samuel Grover	83	Field guide to the Eocene igneous rocks of the Centennial and Henry’s Mountains, Idaho and Montana
Marc S. Hendrix	95	The Yellowstone Volcano caldera margin, Quaternary volcanics, and selected thermal features between Norris Geyser Basin and the Upper Geyser Basin, Yellowstone National Park
B.E. Cox and Jo-Ann Sherwin	109	Centennial Valley — East to west: A field trip crossing the Great Divide (twice)
Kevin Lielke and Robert C. Thomas	117	Field guide to the sedimentary deposits, tectonic setting, paleoenvironment, and basin evolution of the Paleogene Renova Formation in the Upper Ruby River Basin of southwestern Montana
Kevin Lielke and Robert C. Thomas	139	Field guide to Paleogene volcanics, sedimentary deposits, tectonic setting, paleoenvironment, and basin evolution of the Beaverhead Canyon,





**TRGS HAMMER AWARD
RECIPIENTS**
Awarded for distinguished achievement
in the study of the geology of the
Northern Rocky Mountains

**TRGS CHARTER
MEMBERS**

Stanley W. Anderson
Clyde Cody
William S. Cordua
Lanny H. Fisk
Richard I. Gibson†
Thomas Hanley
Stephen W. Henderson
Thomas E. Hendrix
Mac R. Hooton
Inda Immega
Steven W. Koehler
Marian Millen Lankston†
Robert W. Lankston†
J. David Lazor
Joe J. Liteheiser, Jr.
Judson Mead*
Marvin R. Miller
Vicki M. Miller
Allen H. Nelson
Alfred H. Pekarek
Patricia Price*
Donald L. Rasmussen
Raymond M. Rene

1993: Ed Ruppel
1994: Dick Berg
2003: Don Winston
2004: Dean Kleinkopf
2009: Betty Skipp
2010: Jim Sears
2011: John Childs
2012: J. Michael O'Neill

TRGS HONORARY MEMBERS

1980: Charles J. Vitaliano*

2008: Elizabeth Younggren
(also honorary Board member)

2010: Dick Berg
2010: Bruce Cox
2010: Dean Kleinkopf
2010: Dave Lageson
2011: Marie Marshall Garsjo
2011: Paul Link
2011: Rob Thomas
2012: Jeff Lonn
2012: Mitch Reynolds

TRGS LIFETIME MEMBERS

Rob Foster
Joan (Mrs. Jack) Harrison*

† = co-founder
* = deceased

2012 Scholarship Recipients

- **Zachary Adam** (Harrison Scholarship) Montana State Univ.: *Characterizing the Mesoproterozoic microfossil record of the Belt Supergroup, Montana*
- **Neal Auchter** (Michael Thompson Foster Scholarship) U. of Montana: *Interpretation of coastal incision fill deposits in the Santonian-Campanian Eagle Formation, south-central Montana*
- **Whitney Bausch** (TRGS Scholarship) U. of Montana: *Timing and extent of post-orogenic magmatic and tectonic events in the northern Cordillera: Petrogenetic and kinematic investigation of an Eocene dike swarm, southwest Montana*
- **Lane Boyer** (TRGS Scholarship) U. of Arkansas: *Highland Gneiss Dome*
- **Jessie Chadwick** (TRGS Scholarship) Montana State U.: *Metamorphism, Anatexis, and Deformation in Metasupracrustal Enclaves in the Spanish Peaks, Madison Range, SW Montana: Evidence of Cryptic 2.55, 2.45 or 1.8 Ga Thermotectonic Events*
- **Cailey Condit** (Harrison Scholarship) U. of Colorado: *Integrated geologic history of the Archean rocks of the Madison Range, Montana: implications for lower crustal deformational processes and the assembly of Laurentia*
- **Breanna Hennessy** (TRGS Scholarship) Montana State U.: *Sedimentology and Stratigraphy of the Late Cretaceous Livingston Group in Central Montana*
- **Sarah Jeffrey** (TRGS Scholarship) Montana State U.: *Structurally-controlled diagenesis of Paleozoic reservoir rocks exposed in the Little Belt Mountains and Big Snowy Uplift, Montana*
- **Lauren Kay** (TRGS Scholarship) Montana State U.: *Tectonic deformation as a taphonomic process: using fossilized bones as strain indicators*
- **Tetsuro Nagase** (TRGS Scholarship) U. of Montana: *Investigating depositional processes and sedimentary environments of Late Devonian organic-rich mudrock of the Bakken Formation, central Montana*
- **Laura Neser** (TRGS Scholarship) U. of North Carolina - Chapel Hill: *The timing of Laramide deformation in the northern Rocky Mountains*
- **Jacob Thacker** (Michael Thompson Foster Scholarship) Montana State U.: *Structural and mineralogic characterization of the South Prairie fault in the Stillwater Complex, Beartooth Mountains, MT*
- **Stephanie Wafforn** (Michael Thompson Foster Scholarship) Oregon State U.: *Structural Geology of the Mount Polley porphyry copper district: Reconstruction of post-mineral faults and tilting for the purpose of future exploration*

[Donate to scholarships at www.trgs.org/scholar.htm](http://www.trgs.org/scholar.htm)



*Grand Canyon of the Yellowstone and Lower Falls.
Photo by Richard I. Gibson.*

LOCATING THE NEXT YELLOWSTONE CALDERA

E. A. (Skip) Yates

Yates & Sherry, Inc., 237 Cap de Villa, Lolo, Montana 59847

Michael A. Ellis

British Geological Survey, Keyworth, Nottingham NG12 5GG

Abstract

We assemble here a suite of geophysical, geochemical, and geomorphological data sets that provides compelling evidence for the existence of a ring structure and early regional tumescence that signals the next, or fourth, Yellowstone caldera-forming eruptive cycle. The extent of the ring structure is defined by the here-named Mirror Plateau Feature (MPF), a region of relatively high elevation and low relief bordered discontinuously by ranges with higher relief, and by evidence for relatively higher rates of surface uplift. The existence of relatively shallow silicic magma under the MPF is supported by calculated Curie depths, the spatial and geochemical characteristics of geothermal features, anomalies in both gravity and magnetic potential fields, and anomalies in shallow seismic velocities. Patterns of fluvial incision argue for Holocene and active surface uplift of the entire MPF, but that uplift is presently dictated by the Lamar Valley fault, which forms the northeast and eastern boundary to the MPF. We suggest that this is a ring-fracture fault forming the boundary of the next Yellowstone eruptive center.

Introduction

Yellowstone is arguably part of the most explosive active volcanic system on earth. Over the past two million years and in three distinct cycles, the Yellowstone system has erupted more than 6,500 cubic kilometers of volcanic material (Christiansen, 2001). Each cycle culminated in massive, caldera-

forming eruptions, followed by relatively quiet, caldera-filling eruptions of both rhyolitic and basaltic flows. The most recent cycle formed the Yellowstone Caldera ~640,000 years ago and ejected more than 1,000 cubic kilometers of material, resulting in the deposition of the Lava Creek Tuff, most of it inside Yellowstone National Park. The eruption of the Yellowstone Caldera is estimated to have been about 1,000 times larger than the 1980 eruption of Mt. St. Helens.

Volcanoes of the Yellowstone type are a natural hazard that, more than most, have the potential to fundamentally affect global human civilization (Sparks et al., 2005). In this paper, we summarize a variety of geophysical, geological, and geomorphological evidence that strongly indicates that the current focus of the volcanic system has migrated to the northeast of the Yellowstone Caldera and lies now under the Mirror Plateau Feature as defined below (Figure 1).

The origin of the Yellowstone magmatic system is linked to motion of the North American Plate over a mantle plume (Wilson, 1973), as is much of the regional faulting and present seismicity (Anders, 1994). The existence and nature of plumes has been critically questioned in recent years (Anderson, 1994; Christiansen et al., 2002; Foulger, 2002; Courtillot et al., 2003; Geol. Soc. London, 2002), and the nature of the Yellowstone plume, in particular, is enigmatic. P-wave velocities in the upper mantle beneath Yellowstone and adjacent

regions are interpreted as melt-induced convection within the asthenosphere (Saltzer and Humphreys, 1997), rather than to classic deep-rooted plumes (Humphreys et al., 2000; Schutt and Humphreys, 2004; Yuan and Dueker, 2005). Regardless of the origin of the Yellowstone magmatic system, it has retained its focused and persistent course toward the northeast over at least the last ten million years (Anders, 1994) at a constant rate of 2.2 cm/y (Anders, 1994) or between 2 and 4 cm/y (Smith and Braile, 1994). These velocities predict that the current focus of melt release is likely to be under the Mirror Plateau Feature (Figure 1).

Observational and geophysical evidence

The Mirror Plateau Feature (MPF) as defined here is a large, circular, geomorphic feature located northeast of and partially within the 640,000-year-old Yellowstone Caldera. We suggest that the MPF represents an emerging ring-fracture zone and forms the boundary of the next eruptive cycle. The MPF is readily recognizable on almost any scale satellite image (Figure 1), radar image, or aerial photograph, and can be identified on topographic, relief, and geologic maps of Yellowstone National Park. The feature is $\sim 1,250$ km² and roughly bounded by the Yellowstone River (on the southwest), Tower Creek (northwest), Lamar River (northeast), Pelican Creek (southeast) and Yellowstone Lake (south). The circular nature of the MPF in an active volcanic terrain suggests that its origin is likely related to magmatic or volcanic processes.

Smith and Braile (1994) estimated depths to the Curie isotherm to assess the locations of excess heat of the crust in the Yellowstone volcanic system. This was done by comparing the observed gravity field to a magnetically derived pseudogravity field, to try to correct for widespread variations

in the Yellowstone heat flow (Smith and Braile, 1994). These data clearly show a prominent, shallow, upper-crustal heat source under the MPF (Figure 2A) and, by contrast, a cooler source under the bulk of the modern Yellowstone Caldera.

Extensive hydrothermal activity, pervasive alteration, and the region's highest heat flow (Figure 2A) strongly suggest to us that magma is emplaced at shallow levels under the MPF. The largest hydrothermal basin in the Park (Hot Springs Basin) is near the center of the MPF, indicating high heat flow in that area. Numerous smaller basins and features, mostly deep vapor-phase systems (Fournier, 1989) also are found in this area, including Mud Volcano, Washburn Hot Springs, Joseph's Coat Hot Springs, Grand Canyon of the Yellowstone, Seven Mile Hole, Bog Creek Hot Springs, Rainbow Springs, and Calcite Springs. Additionally, Soda Butte Hot Spring, Crater Hills Hot Spring Basin, and hydrothermal features recently discovered in the northern end of Yellowstone Lake appear to be located along the edge of the MPF circular feature.

Alteration is evident throughout the MPF, particularly in the Grand Canyon of the Yellowstone, which dissects the feature. According to Fournier (1989), old geyser mounds and sinter deposits are found throughout the Mirror Plateau. The highest ³He/⁴He anomaly in hydrothermal waters, indicative of a magmatic source, is found along the edge of MPF at Mud Volcano (16 times air ratio) and Crater Hills (10.4 times) (Fournier, 1989). Hot springs at Crater Hills yield the highest chloride concentrations and highest geothermometer temperatures (270-300 degrees C) of any thermal water in Yellowstone National Park, and appear to represent the direct upward migration of fluid from deep in the system (Fournier, 1989). Mud Volcano and the

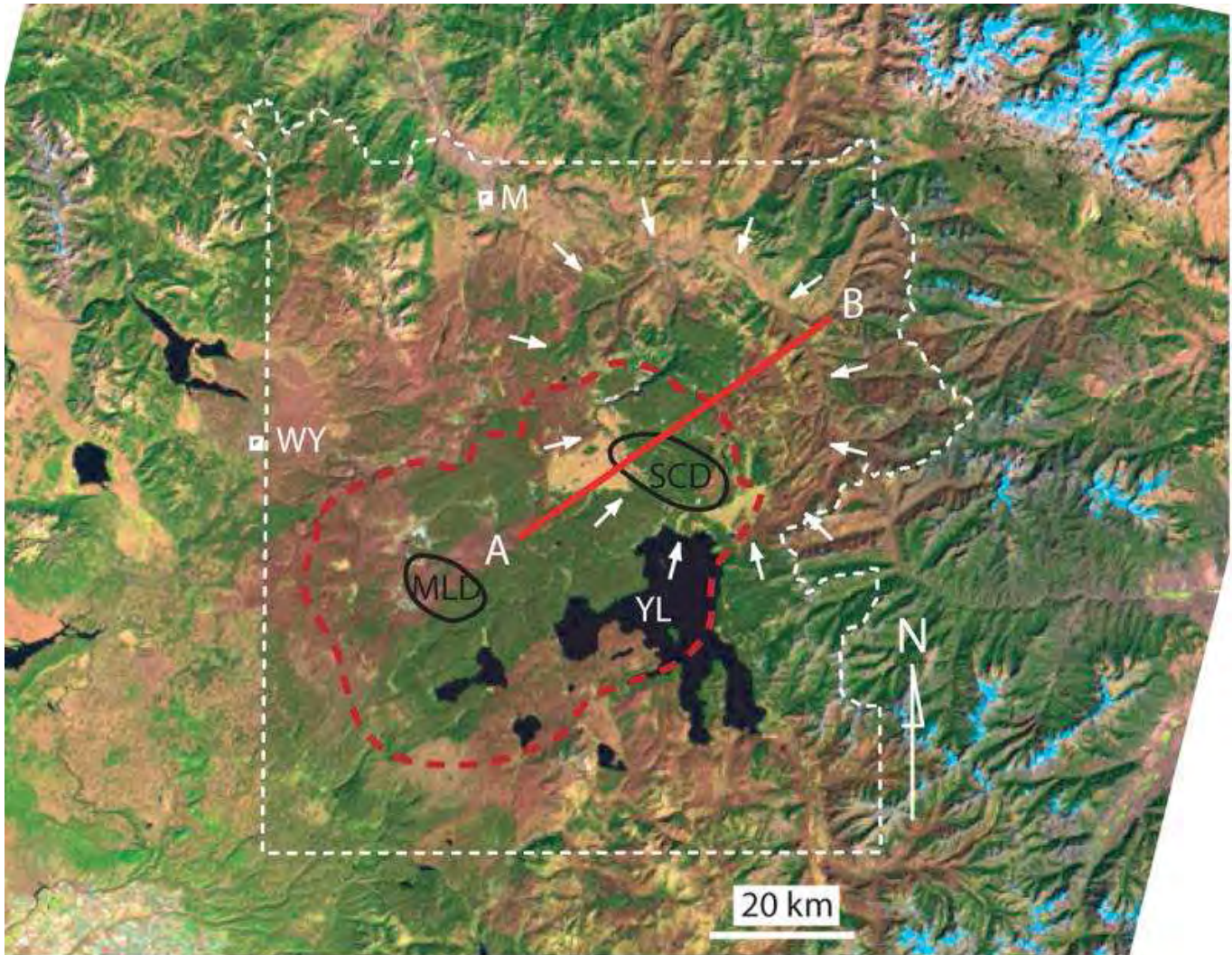


Figure 1. Landsat 5 (1993) image of Yellowstone National Park showing the circular shaped Mirror Plateau Feature (MPF) outlined by white arrows and the Yellowstone Caldera (dashed red). The calculated range of hotspot movement (2 to 4 cm/yr), including the uncertainties, is shown by the solid red line labeled A-B; the most likely position of the present volcanic center (hot-spot) is within the MPF. WY, West Yellowstone; M, Mammoth; YL, Yellowstone Lake; SCD, Sour Creek Dome; MLD, Mallard Lake Dome.

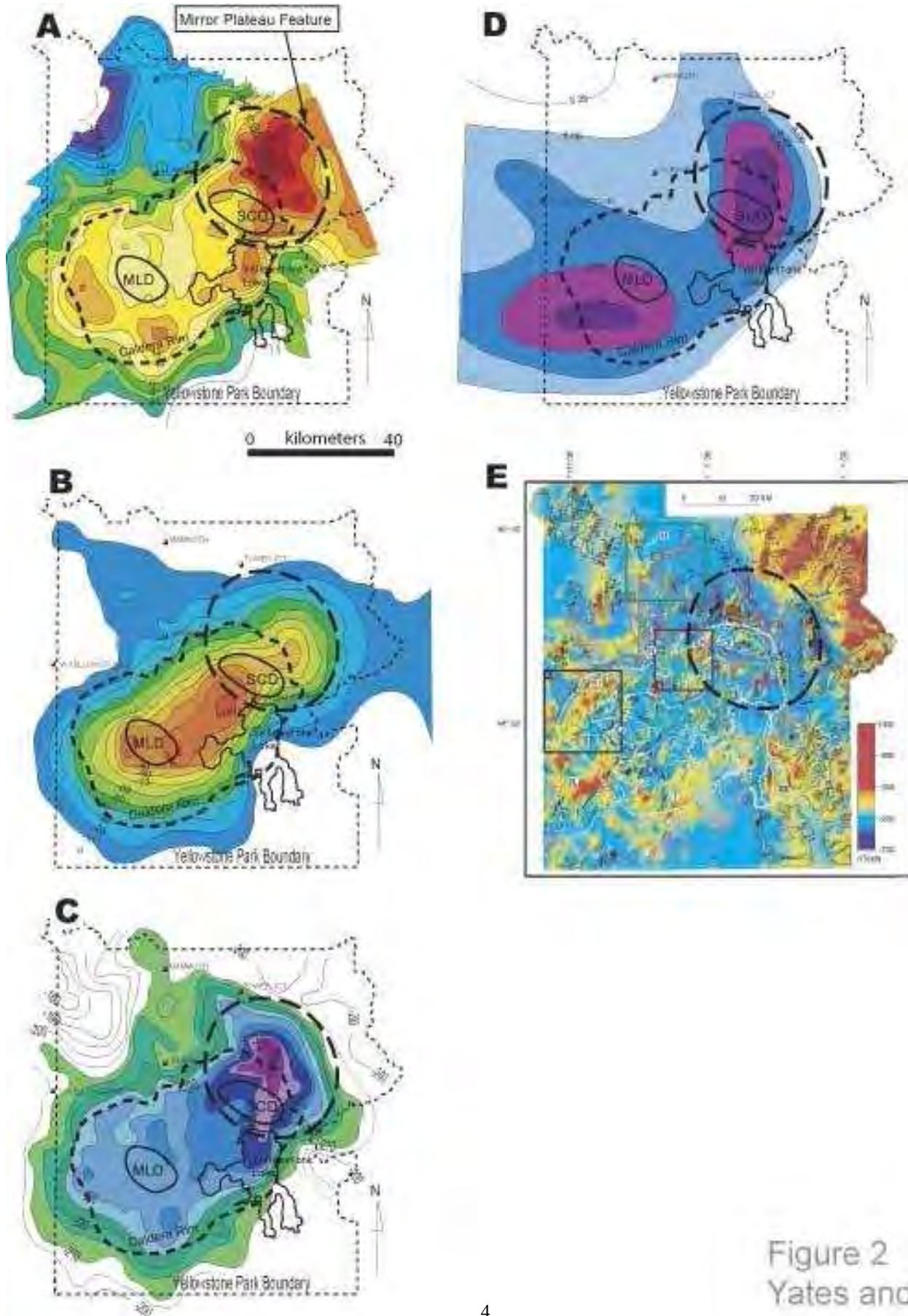


Figure 2
Yates and Ellis

Crater Hills are located along the western edge of the MPF, and are possible ring structures that may provide conduits for magmatic waters. Fournier (1989) suggested that magmatic temperatures are likely to exist at depths below about four to five kilometers in the northeast part of the caldera, accounting for the large convective heat flux and the lack of earthquakes below this depth.

Surface deformation has been measured inside the Yellowstone Caldera since 1923 (Wicks et al., 1998). A long period of uplift was followed by a period of subsidence between 1987 and 1994 (Figure 2B) (Meertens et al., 1992) followed by renewed uplift (Wicks et al., 1998). Surface deformation, measured by leveling surveys and space-based geodesy, is documented within the Yellowstone Caldera, and notably extends outside the caldera into the MPF (Figure 2B). Analyses of radar interferometry also reveal surface deformation occurring both within the MPF and in the Yellowstone Caldera (Wicks et al., 1998).

A Bouguer gravity map of the Yellowstone Plateau (Lehman et al., 1982) shows the lowest gravity readings form a “bull’s-eye”

on the MPF (Figure 2C), consistent with the existence of low-density material, possibly silicic magma, at shallow levels beneath the MPF. The existence of a large gradient in the Bouguer gravity anomaly toward the Lamar Valley is consistent with our proposal that magmatic material does not extend outside the northeast boundary of the MPF.

P-wave velocities in the Yellowstone area (Figure 2D) show a marked low-velocity zone centered on the MPF, consistent with molten rock in the subsurface (Lehman et al., 1982). These authors interpret the P-wave anomalies as a low-density ($\sim 2,400 \text{ kg/m}^3$) body at 1-10 km depth, consistent with hydrothermally altered material underlain by silicic partial melt. Miller and Smith (1999) used three-dimensional P- and S-wave velocity distributions to model the structure of the Yellowstone volcanic field. They observed a caldera-wide 15% velocity decrease at a depth of six to twelve kilometers, which they interpret as a silicic partial melt. These authors also note a more pronounced 10 by 20 km area of reduced velocity (37% reduction in V_p , 33% reduction in V_s) underlying the center of the MPF, which they named the Hot Spring Basin

Figure 2 (opposite): Mirror Plateau Feature (dashed oval) geophysical anomalies. A: Heat flow, estimated depths to the Curie isotherm calculated using residual gravity field (mGal). Positive residual anomalies correspond to temperatures in excess of the Curie isotherm (modified from Smith and Braile, 1994). The highest calculated heat flow is centered on the MPF, suggesting a large-scale, shallow heat source. B: Subsidence (mm) in the Yellowstone Plateau from 1987 to 1989, (modified from Meertens et al., 1992). Note that surface deformation extends outside the Yellowstone Caldera only within the MPF. C: Bouguer gravity map of the Yellowstone Plateau, modified from Lehman et al. (1982). Contour interval is five mGal. The lowest gravity readings bull’s-eye the MPF, indicating that low-density, possibly magmatic material underlies this feature. D: P-wave velocity contours modified from Benz and Smith (1984). The lowest velocity P-waves, which indicate the lowest density material, are centered on the MPF. E: Color shaded-relief image of high-resolution, reduced-to-the-pole aeromagnetic data, modified from Finn and Morgan (2002). Note the broad, prominent negative magnetic anomaly covering the MPF, and the marked lows (dark blue) along the proposed ring fracture zone of the MPF.

velocity anomaly; they note it is strongly coincident with a -20 mGal gravity anomaly. They interpret this anomaly as a saturated, possibly hydrothermally altered mass underlying the Hot Spring Basin. We suggest that the coupled seismic and gravity anomalies indicate the shallow accumulation of silicic magma below the MPF.

High-resolution aeromagnetic data acquired over Yellowstone National Park show a broad, negative reduced-to-pole magnetic anomaly over much of the Yellowstone Caldera that is most prominent in the MPF (Finn and Morgan, 2002). Magnetic lows in volcanic terrains are commonly due to the destruction of magnetic minerals, either from high temperatures or from hydrothermal alteration. Anomalously low magnetic readings occur along much of the proposed ring fracture zone of the MPF, also suggesting intense alteration or high heat flows in this zone.

The MPF also offers a suite of geomorphic characteristics that are consistent with recent surface uplift. Most notable is the nature of Specimen Ridge, which forms the northeastern boundary of the MPF and which is bounded by the Lamar River on its northeastern flank (Figures 1 and 3). Specimen Ridge is strongly asymmetric: the northeastern-facing range front is sharply defined within the Lamar River valley and the highest elevations occur at the peaks of triangular facets that rise above the floor of the valley. The range divide occurs farther east of the highest elevations, beyond which elevations fall gradually toward the Yellowstone River. This first-order profile shape of the range is distinctive of normal-fault-bounded ranges in the Basin and Range; the high peaks reflect the remnant tectonic envelope (King and Ellis, 1990; Ellis et al., 1999; Densmore et al., 2004) and the drainage divide is the subsequent and still transient adjustment of the land-

scape to local base levels (Ellis and Densmore, 2003, 2004). The distribution of hypsometries within the range-front basins (Figure 3) is consistent with a relatively recent lowering of base level along the Lamar valley, and the variation of hypsometries along the range suggests that that lowering is related to faulting along the range front, rather than to a regional base-level drop.

The Lamar Valley fault is not well known. Howard's (1937) description is the most detailed and earliest description that we can find, but beyond Love's (1961) revisit, there appears to be no recent investigation of this fault. These authors estimate a total offset of ~ 300 m, most of which was accumulated during the Quaternary (Love, 1961), though this is poorly constrained. Specimen Ridge therefore is likely to be an active footwall block to the Lamar Valley fault. This is also consistent with the pattern of incision to the southeast of the current range divide (Figure 3). Tributaries of Deep Creek and Shallow Creek (Figure 3) that drain toward the northeast toward the range divide are markedly less incised than those that drain toward the southwest, away from the divide. Toward the southern end of Specimen Ridge, the range divide steps abruptly to the southwest, to a position that we regard as closer to the original (or pre-Lamar fault) fluvial pattern. Evidence for active divide migration is seen along this part of the range divide where the head of a stream that used to drain to the northeast has been captured and now drains toward the southeast (Figure 3).

The pattern of footwall stream incision is consistent with active uplift and tilting of the Specimen Ridge footwall block and although we currently have no constraints on the timing nor rates of uplift, it is likely that much of the topography we now see in the back-tilted footwall is largely Holocene,

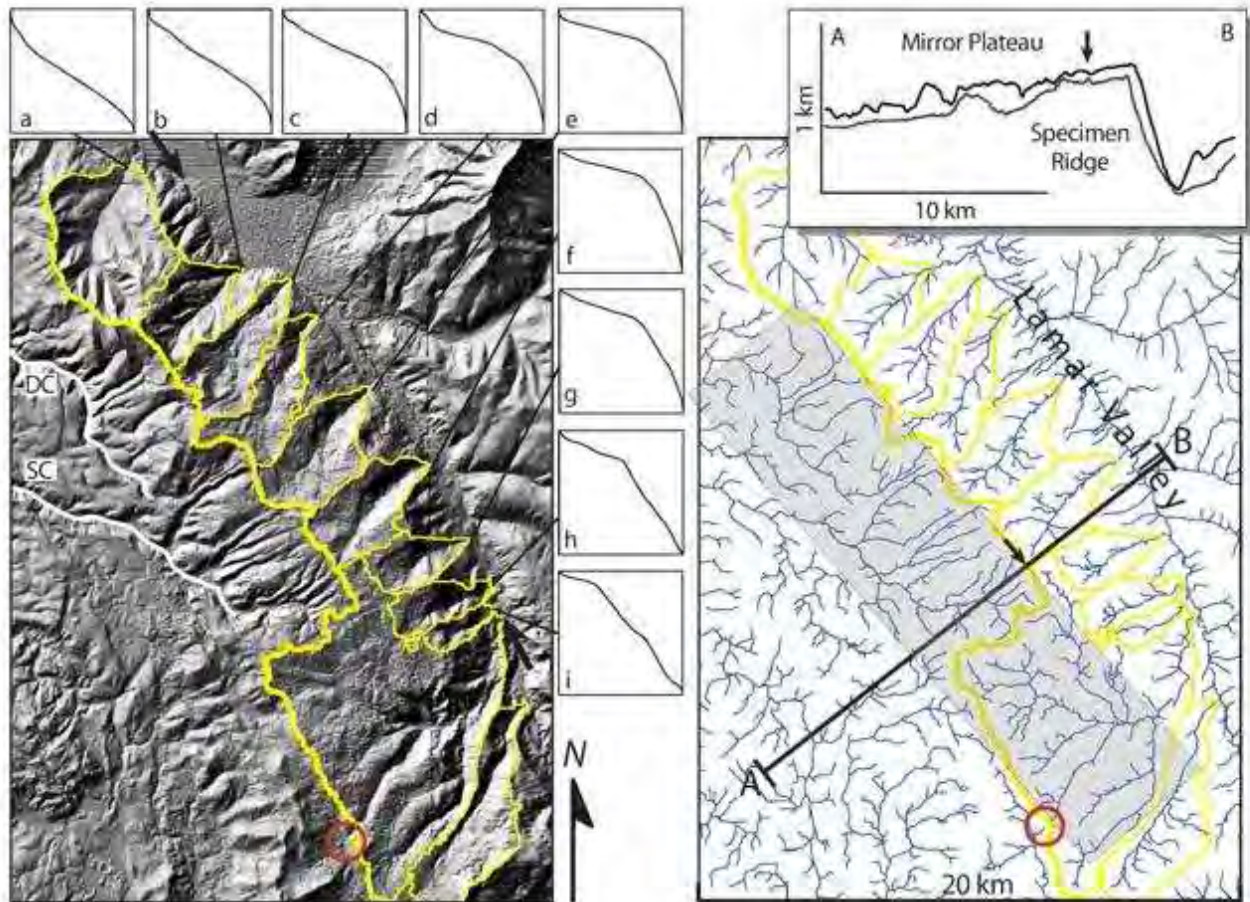


Figure 3. Geomorphic characteristics of the eastern part of the MPF are shown with a shaded relief image of USGS NED 30 m DEM (left) and the derived fluvial network (right). The Lamar Valley fault, visible discontinuously as prominent east-facing scarps, lies between the black arrows in the shaded-relief image and defines the eastern flank of Specimen Ridge. Watersheds that drain the eastern flank of Specimen Ridge (yellow) define the prominent triangular facets typical of active normal faults. Normalized hypsometries of these watersheds (plots a-i) show a signature systematic variation along the length of the fault consistent with an active tip-to-tip displacement field. Topographic profile (top inset, elevations are maxima and minima) along A-B reveals the tilted footwall block to the Lamar Valley fault. The small black arrow marks the range divide, which is not coincident with the peaks of Specimen Ridge, again typical of active normal faults. The light gray region on the footwall is underlain by evidence of active tilting to the southwest; note the difference in incision of tributaries to Deep Creek (DC) and Shallow Creek (SC). Those that drain toward the southwest are significantly more incised than those that drain toward the northeast, as expected if the surface was being tilted to the southwest. Active stream capture is occurring along the southern part of the drainage network (under the red circle), consistent with southwest tilt and a northeastward migration of the main drainage divide. Note also the multiple fault scarps within the footwall and Mirror Plateau; many of these show northeast-facing scarps and are consistent with their role as subsidiary ring-fracture faults.

since this region was covered by a mobile ice-sheet that likely reset the topography of the MPF. The downward displacement of the northeast side of the steeply dipping Lamar Valley fault is consistent with its role as part of the proposed ring structure of the next, fourth, eruptive cycle caldera.

Other geomorphic indicators of relatively high rates of surface uplift of the MPF include the incision of Yellowstone River, which starts at the Upper Yellowstone Falls, near the southwestern edge of the MPF, and remains significant until immediately downstream of the confluence with the Lamar River (Figure 3). The Yellowstone River is confined to a relatively narrow, but not particularly deep, gorge as it cuts through the Washburn Range (Figure 1), the northwestern boundary of the MPF. The pattern of incision across the range is consistent with relatively high rates of uplift.

Discussion and Conclusion

The various individual features described in the preceding section, with the exception of aspects of the geomorphology, are well known, but their discussion has been framed largely in the context of the current Yellowstone Caldera. We have attempted to show here that the integration of these features may be telling us more about the next, or fourth, caldera cycle of the Yellowstone volcanic system.

If the MPF is the locus of the next eruptive cycle, then the circular boundary is a ring-fracture zone forming above an ascending silicic melt. Curvilinear fault zones mapped on the eastern and southern sides of the MPF (Christiansen, 2001) may reflect these ring structures. The steeply dipping Lamar Valley fault is the clearest candidate for a ring-structure fault. Minor faults within its footwall (Figure 3) have typically been in-

terpreted as caldera-collapse structures, but field evidence of eastward-facing scarps suggests that some of these faults may instead be related to the development of a ring structure.

Silicic volcanic centers undergo seven stages, called the caldera cycle, during their development (Smith and Bailey, 1968), including regional tumescence and generation of ring fractures; eruption of pyroclastic material along ring fractures; caldera collapse; pre-resurgent volcanism and intracaldera sedimentation; resurgent doming; major ring-fracture volcanism (lava flows); and terminal fumarolic and hot spring activity. Yellowstone Caldera is probably in the terminal seventh stage, the sixth stage having ended ~70,000 years ago with the last associated ring-fracture rhyolite eruptions. The MPF, as defined here, represents the first stage of the next caldera cycle. The volume of material calculated to erupt from the MPF, derived from its area relative to that of earlier Yellowstone calderas, is estimated here to be in the range of 550 to 700 cubic kilometers. Volcanic hazards include phreatic explosions along the postulated ring structure, especially under the northern end of Yellowstone Lake, small (less than five cubic kilometers) ash eruptions, lava flows, intense seismic activity, landslides, lahars, and a catastrophic caldera-forming eruption with worldwide impacts.

Acknowledgements

We are grateful to Sander Geophysics Inc. for generating the reduced aeromagnetic data used here, and to Richard Sherry, Nancy Hinman and Barb Korzendorfer for insightful comments on an earlier draft of this manuscript. CERI contribution number 486.

References

- Anderson, D.L., 1994, The sublithospheric mantle as the source of continental flood basalts: The case against the continental lithosphere and plume head reservoirs: *Earth and Planetary Science Letters*, v. 123, p. 269–280.
- Christiansen, R.L., 2001, The Quaternary and Pliocene Yellowstone plateau volcanic field of Wyoming, Idaho and Montana: U.S. Geological Survey Professional Paper, 729-G, 145 p.
- Christiansen, R.L., Foulger, G.R., and Evans, J.R., 2002, Upper-mantle origin of the Yellowstone hotspot: *Geologic Society of America Bulletin*, v. 114, p. 1245-1256.
- Courtillot, V., Davaille, A., Besse, J., and Stock, J., 2003, Three distinct types of hot-spots in the Earth's mantle: *Earth and Planetary Science Letters*, v. 205, p. 295-308.
- Densmore, A. L., Dawers, N.H., Gupta, S., Guidon, R., and Goldin, T., 2004, Foot-wall topographic development during continental extension: *Journal of Geophysical Research*, 109, F03001, doi:10.1029/2003JF000115.
- Ellis, M.A., Densmore, A.L., and Anderson, R.S., 1999, Development of mountainous topography in the Basin Ranges, USA: *Basin Research*, 11, p. 21-41.
- Ellis, M.A. and Densmore, A.L., 2003, Position of the topographic divide as a measure of tectonics, steady-state, and bulk rock strength: *EOS, Trans. AGU*, 83, Fall Meeting Supplement.
- Ellis, M., and Densmore, A., 2004, Shaping mountains over blind thrust faults: European Geophysical Union, Annual meeting proceedings.
- Finn, C.A., and Morgan, L.A., 2002, High-resolution aeromagnetic mapping of volcanic terrain, Yellowstone National Park: *Journal of Volcanology and Geothermal Research*, v. 115, p. 207-231.
- Foulger, G.R., 2002, Plumes, or plate tectonic processes?: *Astronomy & Geophysics*, v. 43, p. 6.19-6.23.
- Geological Society of London, 2005: www.geolsoc.org.uk/plumesdebate.
- Fournier, R.O., 1989, Geochemistry and dynamics of the Yellowstone National Park hydrothermal system: *Annual Review of Earth and Planetary Sciences*: v. 17, p. 13-53.
- Lehman, J.A., Smith R.B., Schilly, M.M., and Braile, L.W., 1982, Upper crustal structure of the Yellowstone caldera from delay time analyses and gravity correlations: *Journal of Geophysical Research*, v. 87, p. 2713-2730.
- Meertens, C.M., Smith, R.B., and Vasco, D.M., 1992, Crustal deformation of the Yellowstone caldera from first GPS measurements: 1987-1989: *Geophysical Research Letters*, v. 18, p. 1763-1766.
- Miller, D.S., and Smith, R.B., 1999, P- and S-velocity structure of the Yellowstone volcanic field from local earthquake and controlled source tomography: *Journal of Geophysical Research*, v. 104, no. B7, p. 15.
- Saltzer, R.L., and Humphreys, E.D., 1997, Upper mantle P-wave velocity structure of the eastern Snake River Plain and its relationship to geodynamic models of the region: *Journal of Geophysical Research*, v. 102, p. 11,829–11,841.
- Schutt, D. L., and Humphreys, E.D., 2004, P- and S-wave velocity and Vp/Vs in the wake of the Yellowstone Hot Spot: *Journal*

of Geophysical Research, B, Solid Earth and Planets, v. 109, B08302,
doi:10.1029/2003JB002442.

Smith, R.B., Shuey, R.T., Friedline, R.O., Otis, R.M., and Alley, L.B., 1974, Yellowstone hot spot: New magnetic and seismic evidence: *Geology*, v. 2, p. 451-455.

Smith, R.B., and Braile, L.W., 1994, The Yellowstone Hotspot: *Journal of Volcanology and Geothermal Research*, v. 61, p. 121-187.

Smith, R.L., and Bailey, R.A., 1968, Resurgent cauldrons: *in* Coats, R.R., Hay, R.L., and Anderson, C.A., eds., *Studies in volcanology—a memoir in honor of Howell Williams*: Geological Society of America Memoir 116, p. 613-662.

Sparks, S., et al., 2005, Super-eruptions: global effects and future threats: Report of a Geological Society of London Working Group, www.geolsoc.org.uk/supereruptions.

Wicks, C., Jr., Thatcher, W., and Dzurinsin, D., 1998, Migration of fluids beneath Yellowstone caldera inferred from satellite radar interferometry: *Science*, v. 282, p. 458-462.

Wilson, J.T., 1973, Mantle plumes and plate motions: *Tectonophysics*, v. 19, p. 149-164.

Yuan, H., and Dueker, K., 2005, Teleseismic P-wave tomogram of the Yellowstone plume: *Geophysical Research Letters*, v. 32, L07304, doi: 10.1029/2004GL022056.

*Tower Fall, by Thomas Moran, date unknown.
Courtesy National Park Service.*



EARTHQUAKE DETECTIVE WORK ON THE MADISON RANGE FAULT, MONTANA – A RETROSPECTIVE

Elizabeth Lincoln Mathieson

Exponent Failure Analysis Associates, Oakland, CA, emathieson@exponent.com

Finding Faults

In August 1981 I was an M.S. degree candidate in the Engineering Geology program at Stanford University. “Only” my thesis remained. I had been working as a geologist at Kaiser Cement Corporation at the Permanente limestone quarry southeast of San Francisco since January, enjoying the income and full benefits but knowing I should stop procrastinating and finish school. I wanted to study an active fault but had been turned down by California landowners who didn’t want me finding faults and devaluing their real estate. Then Kaiser sent me to Montana for two weeks to map the new Clark Gulch limestone property near the cement plant at East Helena. Kaiser’s local plant manager, Bob O’Hara, was a geologist himself. He and his wife Sally warmly welcomed me to Montana, and Bob

enlightened me about his state’s active seismicity and suggested some possible thesis areas.

Over the next several months I contacted past and current investigators in the region—by snail mail and phone—to narrow my choices for a thesis area and to be sure I wouldn’t be treading on anyone else’s turf. Ed Bingler of the Montana Bureau of Mines and Geology suggested I study the Madison Range Fault (Figure 1), a major normal fault trending north-northwest with a prominent Holocene scarp that trends for a distance of about 65 km. A 3.2-km segment of the fault had been reactivated by the 1959 M 7.1 Hebgen Lake Earthquake. As much as one meter of vertical offset was expressed by newly-formed scarps that were steep and discontinuous, but these had drawn much less attention than the larger,



Figure 1. Northward view along western base of the Madison Range in the study area. Holocene scarp appears as a dark, sinuous slope (right center). Mouth of Upper Madison Canyon is just right of center.

more accessible 1959 scarps on the Hebgen and Red Canyon Faults. Ed suggested that I contact Robert Wallace at the U.S. Geological Survey.

Bob Wallace had studied the degradation of the 1959 Hebgen Lake Earthquake scarps. He had flown along and photographed the southern portion of the Madison Range Fault and had measured one topographic scarp profile. He explained to me that that Madison Range Fault would be complicated for an M.S. thesis due to the “broken” glacial stratigraphy. He suggested that I begin with an air-photo study and choose one or two canyons where the glacial stratigraphy was well displayed. He hoped that I would be able to determine the recurrence interval of ground-rupturing earthquakes on the Madison Range Fault to add to his work (Wallace, 1981). He was comparing aver-

age earthquake recurrence intervals on the San Andreas Fault (short) with those of more eastern faults, increasing progressively eastward until interrupted by Utah’s Wasatch Fault and its relatively short recurrence interval. Bob referred me to his colleague Irving Witkind at the U.S. Geological Survey.

Irv Witkind had been camped at the epicenter during the Hebgen Lake Earthquake and quickly became an expert on its surface effects. He declared to me that the Madison Range Fault was “extraordinarily important.” He mentioned a growing “environmental geology” influence in Congress which had generated an interest in the impacts of geologic events on the public. Irv suggested the mouth of Little Mile Creek as good study area. I contacted a few more investigators then began arranging for

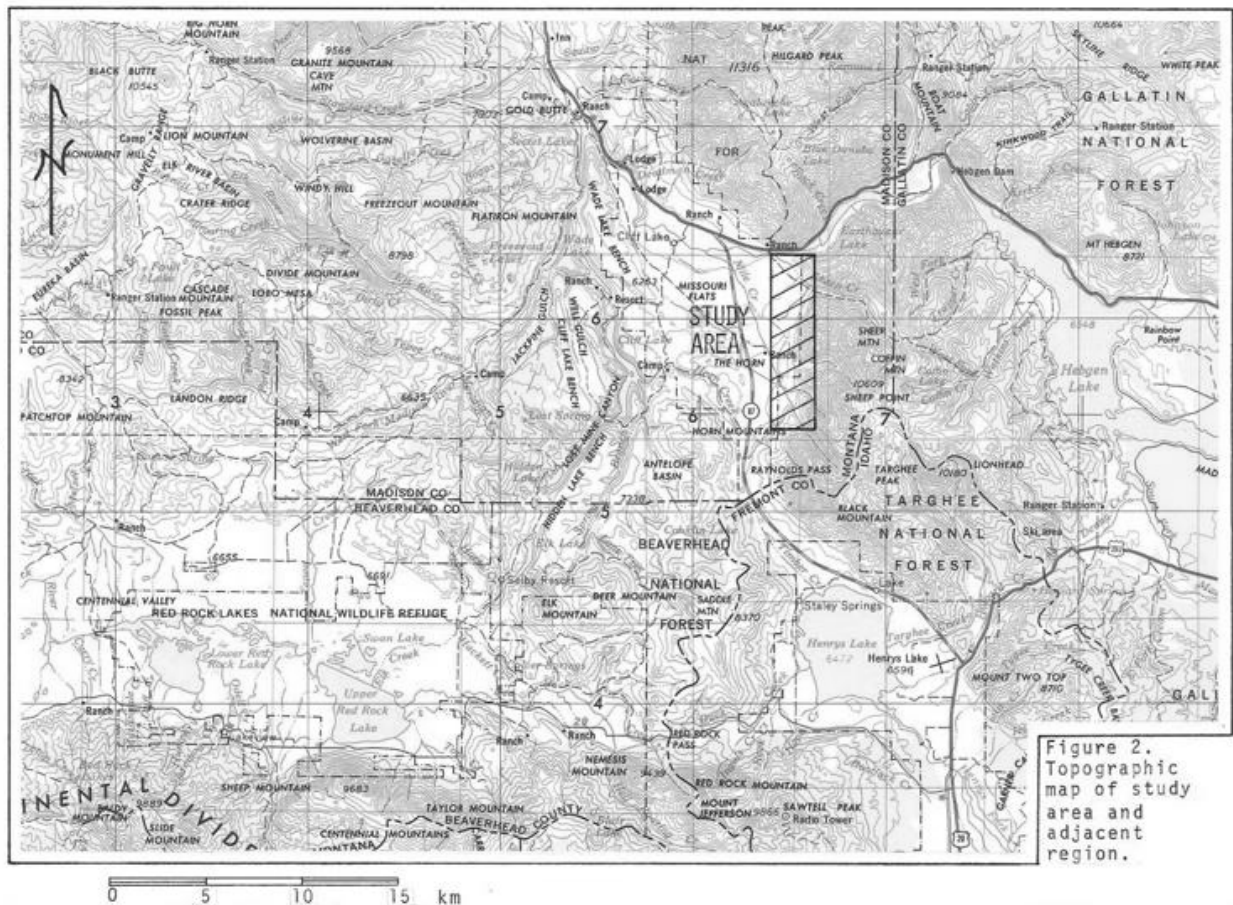


Figure 2. Topographic map of study area and adjacent region.

private-property access along the range front south of the Madison River (Figure 2).

A Disaster Freak's Dream

My interest in Montana extended beyond its active faults. During the brief limestone-mapping trip to Helena I had also fallen in love with the region's Victorian houses and mining history. I was eager for my geologist-and-fellow-old-house-lover husband to visit Montana with the thought of perhaps moving to Big Sky Country. I wanted to see Montana at its worst, so we visited my future thesis area in January 1982 (just as copper prices plummeted and job prospects for out-of-state geologists evaporated). Our trip through the Madison Valley gave us a clear view of the Holocene scarp of the Madison Range Fault and the opportunity to record names and addresses on mailboxes and on billboards advertising 20-acre lots that few people knew were bisected by the fault. Our efforts to visit the Madison River Canyon Earthquake Area were thwarted by a thick coating of tire-chain-proof ice on old Highway 287 where the rebuilt road climbed the steep rockpile deposited by the Madison Canyon Slide.

Despite the icy roads and the 20-below-zero temperature, I was sold on studying the 1959 rupture of the Madison Range Fault. It was a perfect topic for me, an admitted disaster freak. My senior year of high school I had finally realized that many of the disasters that I had loved reading about during my childhood were actually geologic processes. Don West, a fellow student at my geology field camp in 1976, was an engineering geologist at Woodward-Clyde and actually got paid to investigate and reduce the impacts of geologic hazards on people. By the time my thesis research began in 1982 I was on my way to becoming an engineering geologist myself.

The Hebgen Lake Earthquake was a true geologic disaster. Twenty-eight people were killed, most of them in the Rock Creek Campground where they were entombed beneath the Madison Canyon Slide. In other campgrounds, fault scarps sliced through fire pits and beneath picnic tables and bisected at least one ranch building. The basin of Hebgen Lake permanently tilted northward, stranding boat docks at vacation cabins on the south shore and partially submerging cabins on the north shore. The concrete core of Hebgen Dam cracked, and a seiche overtopped the dam repeatedly. Several stretches of Highway 287 slumped into Hebgen Lake, and the roadway below the dam—the parts of which were not buried by the catastrophic rockslide—was inundated by the rising waters of the newly formed Earthquake Lake. Downstream towns were evacuated in preparation for a flood like the one that had followed the failure of the Gros Ventre landslide dam in Wyoming in 1925. The area of the Madison Range Fault was a disaster freak's dream.

The Work Begins

Richard Jahns, my Stanford advisor, approved of my choice of a field area. He was particularly impressed with the Madison Range Fault's superb surface expression and historic activity. He encouraged me to emphasize paleoseismology as a recent breakthrough in deciphering fault behavior and earthquake recurrence intervals. I enlisted Ernie Rich, who had taught my air photo interpretation course, as my second thesis advisor. I also intended to rely on skills of interpreting soil stratigraphy that I had learned from Roy Shlemon in another Stanford course.

I obtained a Research Grant from the Geological Society of America and a grant from the Shell Fund at Stanford University.

My plan was to decipher the Holocene history of the Madison Range Fault by studying scarp morphology the way paleoseismologists were doing on other faults. In June 1982 I resigned my temporary position at Kaiser Cement and prepared for a summer of field work in Montana.



Figure 3. View of 1959 rupture trace with the author (six ft) for scale, north of unnamed canyon north of Little Mile Creek. Fiberglass tape used for scarp profiling at left.

I collected and pored over maps, literature, and air photos while making logistical arrangements and, coincidentally, working with my husband Scott to secure our small Victorian house in San Jose to its brand-new foundation before heading to Montana. I borrowed my parents' Dodge van—a living room on wheels—for a field vehicle and recruited my fine-arts-major mother as my field assistant for the first three weeks.

(Now, a generation later, I know that fifty-something is not old, even for field work!) Scott would be my field assistant for the second half.

My field headquarters was The Slide Inn, at the northern end of my study area and just downstream from the Madison Canyon Slide. This sunny campground offered showers, mail service, and ice cream bars (I mentioned the ice cream bars in the Acknowledgements section of my thesis, but my "Expenses" notebook also documents frequent purchases of beer).

Recalculating...

As I mentioned, my study was planned to emphasize scarp morphology as a tool for deciphering the Holocene history of faulting. Such a study ordinarily involves interpretations of composite fault scarps that display multiple facets, each of which records a distinct displacement event. At the time, this method had been used successfully in areas with arid climates (e.g., Wallace, 1977). The wetter climate of southwestern Montana, however, causes more rapid degradation of fault scarps and hence the erasure of older facets. I eventually discovered that only the 1959 scarp facets near the mouth of one canyon were clearly recognizable on the composite scarp of the Madison Range Fault (Figure 3).

The direction of my research therefore evolved to emphasize detailed topographic and geologic mapping of Quaternary deposits traversed by the Holocene scarp at the mouths of three canyons (Figure 4). I measured the surface offset of each deposit displaced by the fault and assigned an approximate age to each deposit. From this, displacement directions and amounts, average displacement rates, and average earthquake recurrence intervals could be estimated.

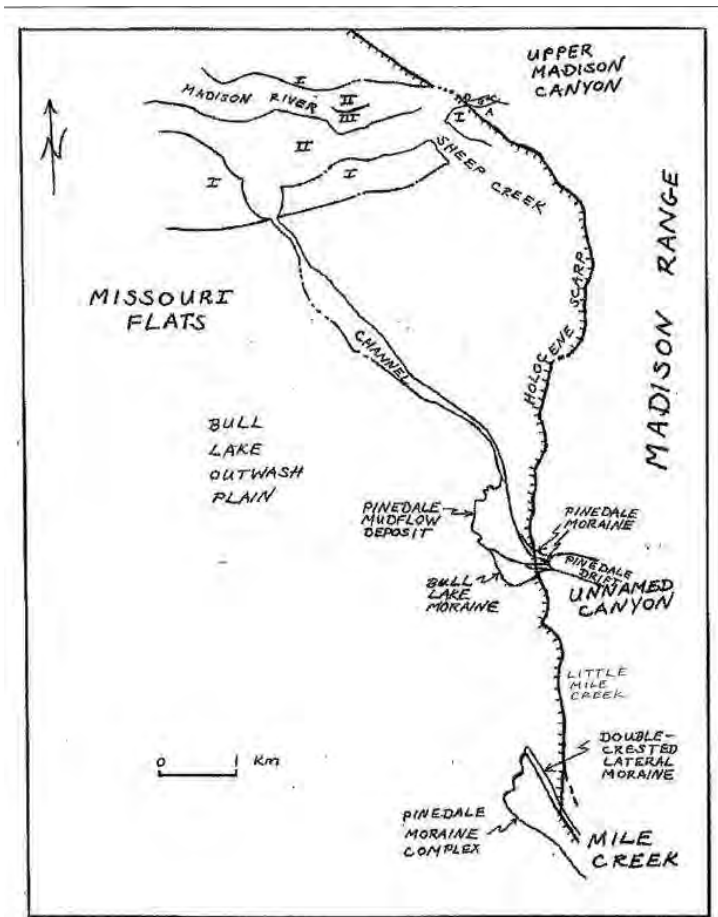


Figure 4. Sketch map showing selected late Quaternary features in study area. River terrace correlations (Montagne, 1965): I – higher Bull Lake, II – lower Bull Lake, III – Pinedale.

With my mother's assistance I made detailed 1:500-scale topographic maps using now-obsolete equipment: a Teledyne Gurley telescopic alidade, a plane table (Figure 5), and a four-meter folding stadia rod. We documented vertical displacements ranging from 4.7 to 15.4 m of river and stream terraces, lateral moraines and moraine complexes, and a boulder mudflow deposit (Figure 6). My mother's jobs were to hold the stadia rod steady and to collect "baked potato"-sized and -shaped rocks, tie flagging around them, and label the flagging with a felt-tipped pen for use in marking future survey points. Much to our surprise,

some of the rocks were moved overnight by a mystery animal or animals who must have picked the rocks up by the flagging and carried them from place to place, messing with my mapping efforts.

I interpreted discontinuous breaks in thin colluvium on bedrock spurs between Slide Creek and the unnamed canyon north of Little Mile Creek as 1959 surface ruptures that had been described by Myers and Hamilton (1964). These features were free faces as high as 0.8 m, extending along upper parts of the prehistoric scarp or across the ground above the scarp. The faces sloped at angles of 50 to 70 degrees. To learn what I could from topographic profiling, I constructed ten scarp profiles with a fiberglass tape, stadia rod, and Abney hand level. Scott and I measured scarp heights, measured slope angles to within 0.5 degrees, and documented the locations of breaks in slope.

We dug nine shallow soil pits, one in each deposit of interest, to provide quick insights into subsurface composition and soil profile development. The southern Madison Range consists predominantly of Precambrian dolomite-quartz marble, with metagray-



Figure 5. Alidade and plane table in south-eastward view along fault scarp with graben. Canyon of Sheep Creek is in background.



Figure 6. Vertical aerial photograph showing range front and mudflow complex of Pinedale age (center left) at mouth of unnamed canyon north of Little Mile Creek. Arrows indicate channel of Bull Lake age (left) and treeless scarp of Madison Range Fault (right).

wacke, biotite schist, amphibolite, and quartzite. The marble component in the source areas provides a source of caliche on the bottoms of cobbles and boulders in the glacial deposits. Unfortunately, however, the thickness of caliche varied markedly within individual deposits and turned out to have little or no correlation with the age of the deposit. My field observations revealed no datable materials, such as volcanic ash or carbonaceous matter, in the deposits. And because the Madison Valley contained no large glacial lake during Pleistocene time, no datable shorelines are present.

No detailed investigations of glacial chronology in the Madison Range had been made. Reconnaissance investigators had assigned deposits to specific glacial stages primarily by using criteria of morphology and topographic position, and I did the same.

All new age assignments were based on relative-dating criteria that permitted correlation of the Pleistocene deposits with deposits dated by Pierce (1979) in the nearby northern part of Yellowstone National Park. The age assignments were based on obsidian-hydration dates from the unusual volcanic source area. Approximate age assignments for glacial and fluvio-glacial deposits in my study are based primarily on morphologic features, the presence or absence of a loess mantle, and various cross-cutting relationships.

The Fun of Field Work

The difficulties of deciphering the subtleties of scarp morphology and soil stratigraphy were balanced by the pleasures of working outdoors in Montana. My mother learned that a nearby bush is better than a distant bathroom. Together we learned to read the weather. From our position high on the Holocene scarp we evaluated the daily afternoon thunder showers as they approached. If it was a “thin storm,” we’d wait it out in the van and resume our field work after the rain passed. If it was a “thick storm” we’d pack up our equipment and head for the campground. Our recipe for bratwurst was governed by the evening showers: cook it until it starts to rain then slap it between two pieces of bread, jump in the van, and eat it.

After a couple of weeks at The Slide Inn, on the banks of the Madison River which we knew was a blue-ribbon trout stream, we wondered why we never smelled fish

cooking in the campground. Upon asking around we learned that only catch-and-release fishing was allowed. Then we knew that we were surrounded by truly dedicated anglers. One night we inadvertently caught and released some wildlife of our own; a bat found a temporary home inside the mechanism of the sliding door on the side of our van. Fortunately, we succeeded in convincing him or her to depart without injury (to any of us). We also discovered that antelopes are not silent creatures but can make noise with their mouths. Curious pronghorns would pause in their graceful sprints, stare at us from a distance, and make a noise that sounded like a sneeze. I suspect they were signaling to each other rather than trying to scare us; the noise was cute, not frightening.

Occasionally, for a special treat, we traveled down the road for burgers and shakes at the Grizzly Bar, a rustic establishment frequented by fishermen and locals. (During a return trip a decade ago we discovered the Grizzly Bar, along with the rest of the upper Madison Valley, had gone upscale. The burgers and shakes had been replaced by lobster ravioli and martinis. And the grocery store at The Slide Inn had become a luxurious fly fishing shop. The only groceries they sold were cans of beer.) One evening at the Grizzly Bar we quickly identified a scruffy-looking group of young beer drinkers as geology field-camp students. They and their professor, Paul Pushkar, were from

Wright State University in Ohio. They invited me to take a break from my field work, travel with them to spend the night at their camp, and hike with them to Black Butte the next day. After the hike we dined together at the Longbranch, and they delivered me back to the Madison Valley and the reality of having to wrestle with the complexities of my favorite active fault.

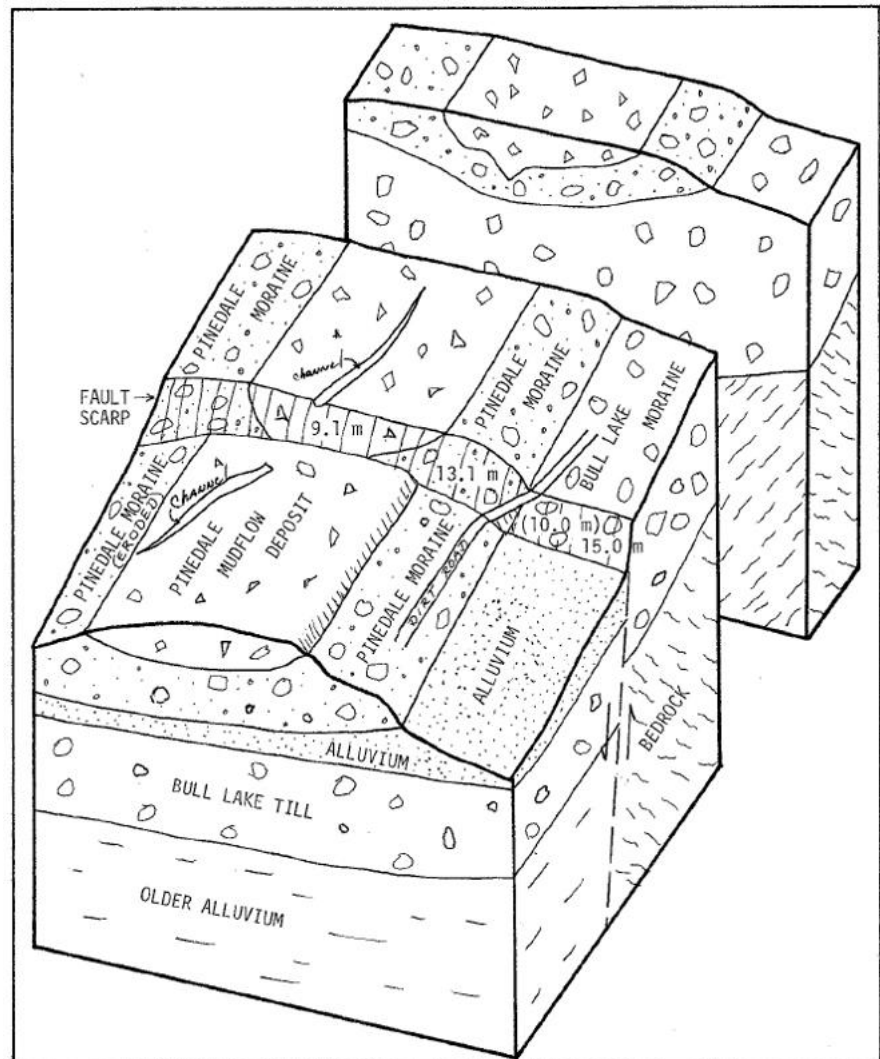


Figure 7. Generalized block diagram of fault-scarp area at mouth of unnamed canyon north of Little Mile Creek, looking east-northeastward (not to scale). Numbers on scarp indicate measured vertical surface offsets.

Just-in-Time Geology

I finished my field work in early September as summer waned, 80-degree days alternated with 30-degree nights, and the aspen leaves turned yellow. We left the Madison Valley just before the first snow of the season. Back at Stanford I began my data analysis and a series of brainstorming sessions with Dick Jahns. We discussed issues such as the tectonic vs. climatic significance of glacial outwash terraces on the upthrown and downthrown fault blocks, and the relative ages of the glacial moraines, outwash channels, and the large mudflow deposit displaced by the fault (Figures 6 and 7). My collection of diverse observations began to make sense, so I put pen to paper (not really; I used a Wang word processor) and began to share drafts of my initial chapters with Dick and with Ernie Rich. A few months later Dick, convalescing after heart surgery, read the final draft of my thesis and approved it in time for June graduation. My thesis, "Late Quaternary Activity of the Madison Range Fault Along its 1959 Rupture Trace, Madison County, Montana," was bound in red cloth and added to the shelf of the Branner Earth Sciences Library at Stanford.

The Meaning of It All

Here's what I figured out. The detailed topographic mapping of the mouths of three canyons, together with scarp profiling and regional age correlations for glacial and fluvioglacial deposits, yielded estimates of average vertical displacement rates, maximum displacement amounts, and average earthquake recurrence intervals since late Pleistocene time. Differential offsets of Bull Lake (135,000-160,000 years BP) moraines and Pinedale (15,000-30,000 years BP) moraines and outwash terraces and a Pinedale mudflow complex (glacial chronologies by Pierce, 1979, from northern

Yellowstone National Park) indicated that the prominent range-front scarp represents multiple prehistoric faulting events.

The estimated average vertical displacement rate is 0.01-0.04 m/yr for post-Bull Lake/pre-Pinedale time, and the estimated average rate is 0.3-0.4 mm/yr for post-Pinedale time. These values suggest an order-of-magnitude increase in average vertical displacement rate during late Pleistocene time and suggest that the southern segment of the Madison Range Fault may have been relatively quiescent during much of the Sangamon Interglaciation, 75,000-125,000 yrs BP.

The composite scarp in my thesis area lacks prominent facets that could be attributed to individual prehistoric Holocene earthquakes; only the scarplets formed in 1959, with maximum heights of about one meter, were specifically identified. It has been suggested that the relatively rapid degradation of fault scarps here is due to the greater humidity of the region as compared with areas of the Great Basin where prominent facets have been recognized. Nevertheless, geomorphic features suggest that three meters may be the average vertical displacement rate for individual faulting events on the southern part of the Madison Range Fault and that such events may have recurred every 7,500-10,000 years, on the average, during the past 15,000-30,000 years. An earthquake with a maximum Richter magnitude of 7.3 might be expected. It is possible, however, that the total scarp height is the result of a series of one-meter displacements similar to the 1959 rupture. The estimated average recurrence interval for such displacements is 2,200-3,800 years, but it could be as short as 1900 years. Earthquakes of M 6.8 might be expected to have accompanied such more frequent displacements.

Epilogue

I have been working as a full-time consulting engineering geologist (Figure 8) since completing my degree and couldn't have chosen a more suitable profession. I'm still a disaster freak. At the 2001 annual meeting of the Association of Engineering Geologists (AEG,) Montana State University M.S. student Cal Ruleman (now at the U.S. Geological Survey in Denver) introduced himself and said he was working on the Madison Range Fault. I gave him a copy of my thesis, and he later sent me a copy of his, "Quaternary Tectonic Activity within the Northern Arm of the Yellowstone Tectonic Parabola and Associated Seismic Hazards, Southwest Montana." I was excited to learn that great advances had been made in investigators' understanding of the regional tectonic setting and equally pleased to see that the slip rates I had estimated for the southern part of the Madison Range Fault still appeared to be reasonable. I'm looking forward to this summer's field conference to hear and see what else has been learned in the three decades since I crawled the scarps along the Madison Range Fault.

REFERENCES

Montagne, John, 1965, Terraces and Quaternary faulting along the Madison Valley: *in* Northern and middle Rocky Mountains, 7th Congress, Colorado, 1965, Guidebook for Field Conference E: International Association for Quaternary Research, p. 50-51.

Myers, W.B., and Hamilton, Warren, 1964, Deformation accompanying the Hebgen Lake earthquake of August 17, 1959: *in*



Figure 8. Disaster freak (the author) at work on an undisclosed site in the Rocky Mountains in 2011.

The Hebgen Lake, Montana earthquake of August 17, 1959: U.S. Geological Survey Professional Paper 435, p. 55-98.

Pierce, K.L., 1979, History and dynamics of glaciation in the northern Yellowstone National Park area: U.S. Geological Survey Professional Paper 729-F, 90 p.

Wallace, R.E., 1977, Profiles and ages of young fault scarps, north-central Nevada: *Geological Society of America Bulletin*, v. 88, p. 1267-1281.

Wallace, R.E., 1981, Active faults, paleoseismology, and earthquake hazards in the western United States: *in* Earthquake prediction – an international review: *American Geophysical Union Maurice Ewing Series* 4, p. 209-216.



*Rope descent, Uncle Tom's Trail, Grand Canyon of the Yellowstone, pre-1905.
Courtesy National Park Service.*

RADIOCARBON AGE DATE OF A MOUNTAIN BISON AND ROCK FALL IN THE ANACONDA RANGE, MONTANA

Chris Shaw

Mine Geologist, Turquoise Ridge Joint Venture, Golconda, NV 89414

Abstract

This paper is a follow-up to Shaw (2010) providing carbon-14 age dates that had not been determined at the time of his original work. A bison skull and parts of its skeleton, the subject of the original paper, were found in the Anaconda Range, 40 km southwest of Anaconda. They were found pinned under a rock fall at the north side of Warren Peak in 1977. A conventional radiocarbon C-14 age date has been obtained for some of the bones, providing an age of 70 ± 30 years BP (before present, where “present” is defined as AD 1950) for the Maloney Basin Bison. This date sets the age of the death of the bison with a 95 percent probability from AD 1810 to 1920. A horn core width of one meter suggests it is a mountain or wood bison, which are extinct in the lower 48 states. The left horn core shows evidence of deformity caused by bacterial infection. A two-meter rock pinned the skull to the ground, indicating the rock fall may have killed the animal. The radiocarbon age date of 70 ± 30 years BP is the maximum age of the rock fall.

Introduction

A bison skull and pieces from its skeleton were found by the author in 1977 at an elevation of 2,515 m in the Anaconda Range, 40 km southwest of Anaconda (Shaw,

2010). Measurements of the horn core show it to be larger than the largest plains bison, indicating it is a mountain bison (*Bison bison athabasca*). Although there may be hybrids of mountain bison and plains bison in Yellowstone National Park, Wyoming (Jackson, 2008), pure mountain bison (Wilson and Strobeck, 1999) are extinct in the western U.S. (Meagher, 1973). A radiocarbon date was needed to determine when bison inhabited this area. The resulting age date shows it died between AD 1810 and 1920 (Beta Analytic Inc., 2012). The Maloney Basin Bison may be the last mountain bison to be found and age dated in western Montana.



Figure 1. The Maloney Basin Bison skull as found in 1977, with a 9-cm knife for scale.

More Bison Bones Found during 2011

A field trip to Maloney Basin in 2011 by Russel Shaw and the author found nine more bison bones under the rock fall. Bison jawbone with teeth, two vertebrae, four rib bones, a broken pelvis, and an intact tail-bone were found and left at the site (Figure 1). One of the vertebrae found has a very high hump projection consistent with that of a mountain bison.



Figure 2. Photograph of additional bison bones found under rock. Note the high hump projection consistent with a mountain bison on one of the vertebrae. Jawbone is 40 cm long.

Radiocarbon Age Dates both the Bison and Rock Fall

Bone fragments from the base of the skull and jawbone (Figure 3) were submitted for conventional carbon-14 age dating. Laboratory number beta-320212 (Beta Analytic Inc., 2012, Figure 4) returned a measured age of 100.1 ± 0.4 pMC (percent modern carbon), with a $^{13}\text{C}/^{12}\text{C}$ ratio of -19.9‰ , providing a conventional age of 70 ± 30 years BP. The 2-sigma calibration has a 95% probability of age of death at AD 1810 to 1920.

The bison skull was found buried beneath a rock that is two meters across. The rock fall may have killed the bison. Alternatively, if the bison died before it occurred, the rock fall would be younger than the bison. Therefore the radiometric age date of the bison is the maximum possible age of the rock fall.

Horn Core Infection

The Maloney Basin Bison shows evidence of infection in its left horn core (Shaw, 2010). Bovine brucellosis and tuberculosis are common infections found in other Holocene-aged bison (Jolly and Messier, 2004), and these diseases still exist in the wild populations today. Currently, the Fort Peck and Fort Belknap Indian Tribes are moving Yellowstone bison to the Fort Peck Indian Reservation with transportation provided by U.S. Fish and Wildlife Service and cooperation from Yellowstone National Park. This program is causing controversy as Montana stock growers are concerned about the potential for tuberculosis or brucellosis bacteria spreading to their herds (Hansen, 2012).



Figure 3. Photograph of bison bone used for radiocarbon dating. Tool for scale is 14 cm long.

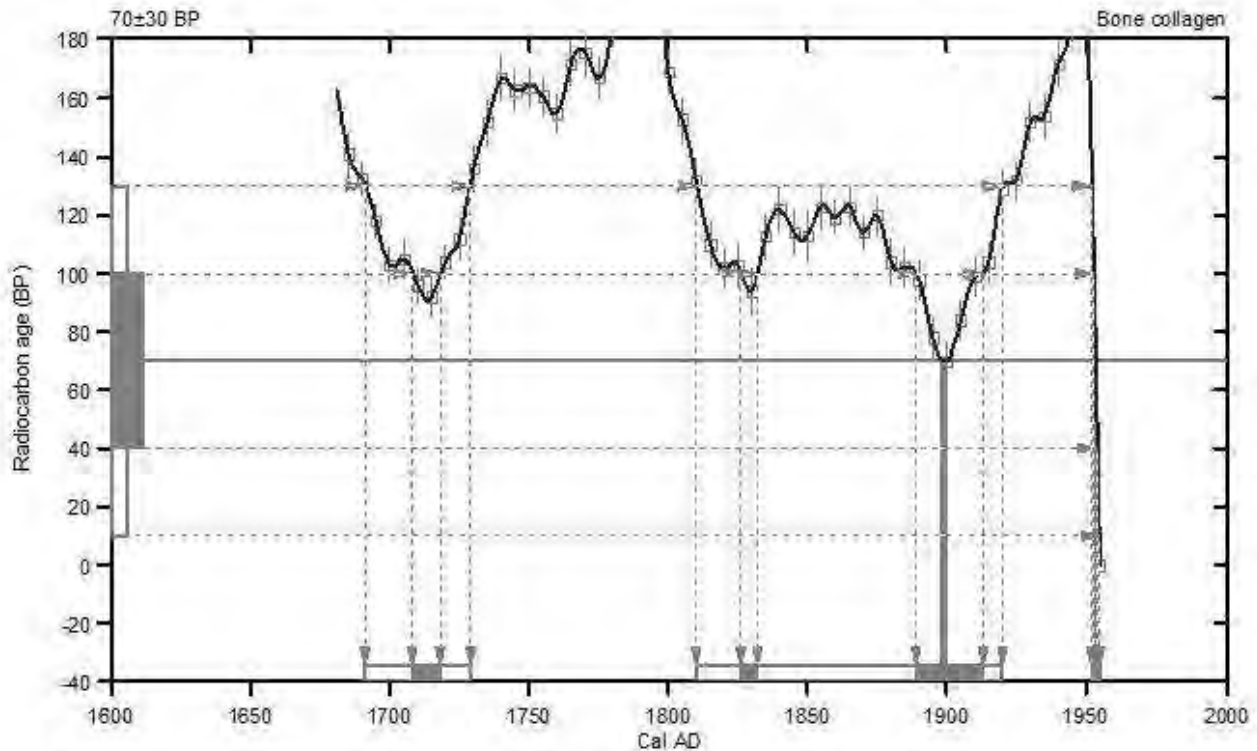


Figure 4. Maloney basin bison graph of radiocarbon age vs. calendar years. Cal AD is Calendar Years AD. This graph represents the calibration of radiocarbon age to calendar years. The radiocarbon age based on C13/C12 ratios is on the y-axis; the x axis is calendar years at the 2-sigma statistical range of C14 content.

Conclusion

The radiocarbon age date of 70 ± 30 years BP of the Maloney Basin Bison shows that this mountain bison may be the most recently dated mountain bison in Montana, and it also dates the maximum age of the rock fall. This animal also had a bacterial infection likely to have been bovine brucellosis or tuberculosis which are thought to be common in wild bison.

The author would like to acknowledge Barrick Gold of North America for funding the radiocarbon age date.

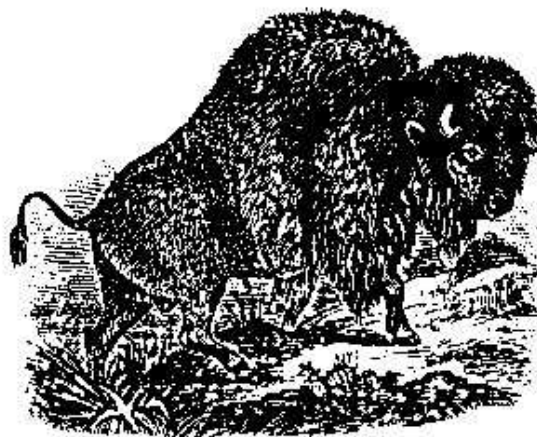
REFERENCES

- Beta Analytic Inc., 2012: unpublished report of radiocarbon dating analyses, beta-320212, sample MB-1, report date 5-1-12, p. 1-3.
- Hansen, P., 2012, Saga of Spotted Dog, a culture clash in Montana between stockmen and bison lovers: Range Magazine, v. 20, no. 2, Summer 2012, p. 88-90.
- Jackson, B., 2008, The mountain bison of Yellowstone, a breed apart: peer.org/docs/nps/08_23_4_yellowstone_mountain_bison.pdf
- Jolly, D.O., and Messier, F., 2004, Factors affecting apparent prevalence of tuberculosis and brucellosis: Jour. of Animal Eco., v. 7, n. 4, p. 623-631.

Meagher, M., 1973, The bison of Yellowstone National Park: Scientific Monograph Series Number One, National Park Service, Washington, D.C., 161 p.

Shaw, C.W., 2010, Late Holocene rock fall on a mountain bison in the Anaconda Range, Montana: Northwest Geology, v. 39, p. 25-29.

Wilson, G.A., Strobeck, C., 1999, Genetic variation within and relatedness among wood and plains bison populations: Genome, v. 42, no. 3, p. 483-496.



GEOHERMAL ACTIVITY ALONG A SEGMENT OF THE LEWIS AND CLARK LINE

D. H. Vice

Penn State Hazleton, 76 University Drive, Hazleton, PA 18202

Arnold Doden

State College, PA

Bridget Lynne

Auckland, New Zealand

Abstract

Burlington Northern (BN) conducted Thermal Infrared (TIR) surveys and performed reconnaissance geologic mapping and geochemical sampling to determine the geothermal potential of the Garnet Range in Western Montana. The study was conducted between 1974 and 1981. The TIR imagery was used because it detects variations in the thermal flux of the ground and thus can indicate leakage from a subsurface geothermal reservoir. The recent development of binary technology allows lower temperature geothermal systems to be used to produce electricity. The authors reviewed geothermal data from the Garnet Range to determine if any of the geothermal systems were suitable for producing electricity.

The Garnet Range area is part of a major crustal zone or break known as the Lewis and Clark Line. Several mineral springs and tufa deposits occur along the southeastern margin of the Garnet Range. Most of these indicators are suggestive of low temperature geothermal systems except for an anomalous tufa deposit on Warm Springs Creek near Garrison that has stringers of chalcedony/silica in it. The system does not appear to be active at the present time but the presence of silica suggests that when the system was active approximately

25,000 years ago, its temperature was close to 200 degrees C. The authors are updating this information and making it available to the public.

Introduction

The purpose of this article is to review the geothermal data for the Garnet Range to determine if the commercial development of binary systems has made any of the moderate geothermal systems along the Garnet Range suitable for producing electricity. Most the geologic and geochemical data and remote sensing imagery included in this paper is from the Burlington Northern (BN) geothermal exploration program. The exploration program was started in 1974 when the resources group was a department of the Burlington Northern railroad, and was continued when they were spun off to form Burlington Resources. The BN geothermal program was closed down in 1982 and most of the geologic and geochemical data and the remote sensing imagery have been sitting in files since then. Very little of the information has been made public. The authors are updating this information and making the remote sensing imagery available to the public.

BN became interested in the southeastern part of the Garnet Range in 1974 because there were warm springs on Warm Springs

Creek near Garrison and on the Warm Springs Creek tributary to Carpenter Creek near Avon, as well as warm springs near Nimrod and Bearmouth. BN was also interested in the area because the company has significant blocks of both fee and mineral land within the area. The purpose of the BN exploration program was to find and develop a geothermal prospect that could be used to interest a company in leasing and developing the prospect (Vice, 2011b).

The senior author and some assistants conducted field reconnaissance, geochemical water sampling, and remote sensing surveys in the Garnet Range area as part of the exploration project. BN chose to use Thermal Infrared (TIR) imagery as part of its exploration tools because this remote sensing method can cover a lot of ground rapidly and is effective in areas of rugged topography or heavy timber or both. In addition, TIR can directly identify areas of elevated temperature which could represent leakage from a subsurface geothermal system (Vice, 2007). Two TIR surveys were conducted in the Garnet Range, one in the Warm Springs Creek area near Garrison in 1976 (Figure 3), and the second in the eastern half of the range in 1981 (Figure 4).

Geothermal energy is present everywhere beneath the Earth's surface due to the increase in temperatures with depth in the Earth's interior (Duffield and Sass, 2003). There are two distinct types of geothermal systems, which are differentiated by their source of heat. A magmatic system obtains its heat from nearby intrusive or extrusive igneous activity. As the magma rises, it brings heat from the interior of the earth to the near surface and then transfers heat to the groundwater. A tectonic system obtains its heat from water that circulates deeply within the earth's crust and is heated by the normal geothermal gradient. The existing technology can only produce power from the magmatic geothermal system.

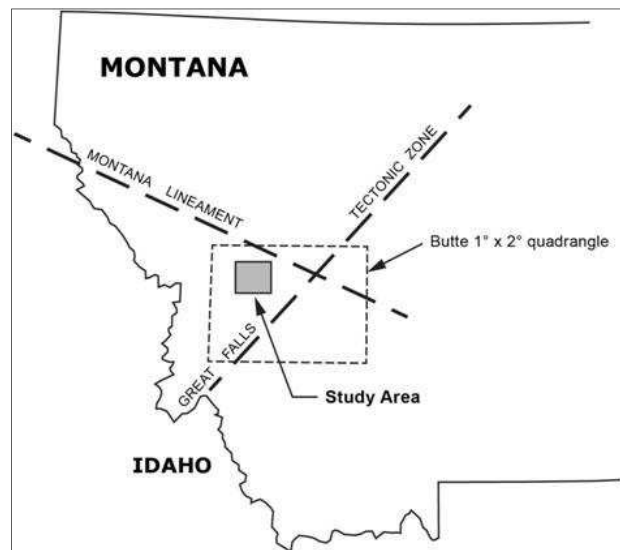


Figure 1. Location map of survey area (modified from Figure 1 of Sonderegger et al., 1982).

The new binary technology uses a secondary fluid (e.g., isobutane) to run turbines and thus generate electricity (Duffield and Sass, 2003), and it has allowed geothermal systems with temperatures as low as 76 degrees C to be used (Benoit et al., 2007). Binary technology has widened the available resource that can be used to generate electricity but again, it is limited to the magmatic type of geothermal system.

Regional Structure

The Garnet Range is a rugged, east-west trending mountain range in Missoula, Granite, and Powell Counties in western Montana (Figure 1). Relief can be as great as 2,000 to 3,000 feet. Precambrian to Quaternary rocks are present in a structurally complex, intermingled pattern within the range (Figure 2, Vice, 1989).

The Garnet Range is unusual in that it cuts across the general NNW-SSE trend of the Rocky Mountains in northwestern Montana. The reason for this cross-grain structure is that the Garnet Range is within the

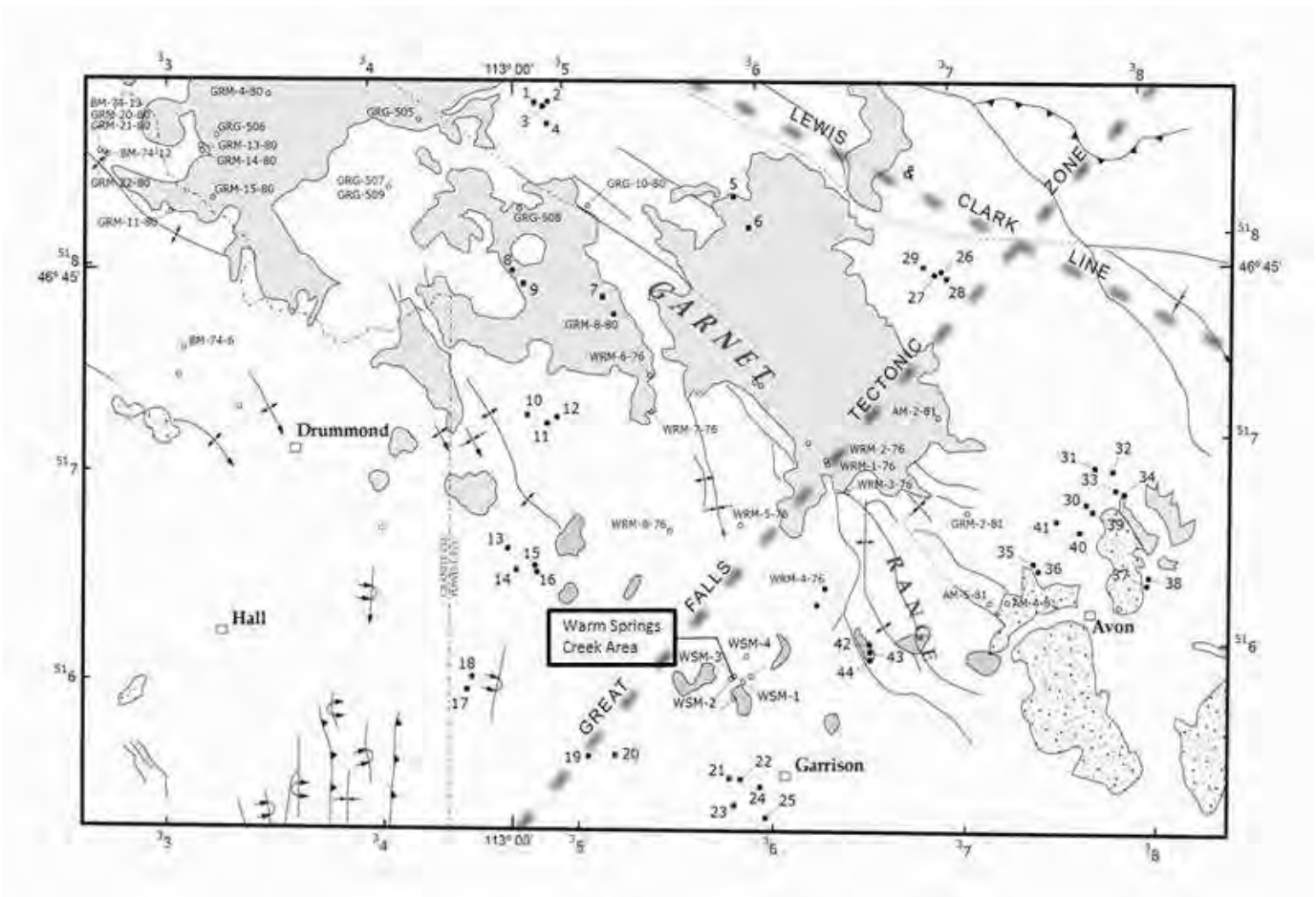


Figure 2. Geologic map of the Warm Springs Creek-Garrison-Avon area of the Garnet Range in western Montana.

Lewis and Clark Line (Vice, 1989), a complex system of strike-slip, dip-slip, and oblique-slip faults representing a deep-seated crustal structure. It extends about 300 miles from Coeur d'Alene, Idaho, eastward to the Lake Basin fault zone north of Billings, Montana (Wallace et al., 1990; Harrison et al., 1974; Douglas and Crosby, 1973). Lorenz (1984) suggested that this structure serves as a boundary between two major crustal blocks and that different amounts of crustal compression have occurred on either side of this line. There is an estimated 60 miles or more of compression in the fold and thrust belt on the north side, and approximately 31 miles of shortening on the south side (Vice, 2011a).

Geology and Geothermal Indicators

The core of the Garnet Range contains several igneous intrusions, while a sequence of Paleozoic and Mesozoic sediments is present in folds on the southeastern side of the range in the Garrison and Avon areas (Vice, 1989). Northwest-trending faults cut through most of the range (Vice, 1989). Some of these faults are shown in Figure 2. The Paleozoic and Mesozoic sediments appear as a WNW-ESE trending zone, shown to have low magnetic values in a 1984 USGS aeromagnetic map, suggesting that the sequence is quite thick and extends deep into the subsurface. Eocene Lowland Creek Volcanics overlie the sediments (Schmidt et al., 1994).

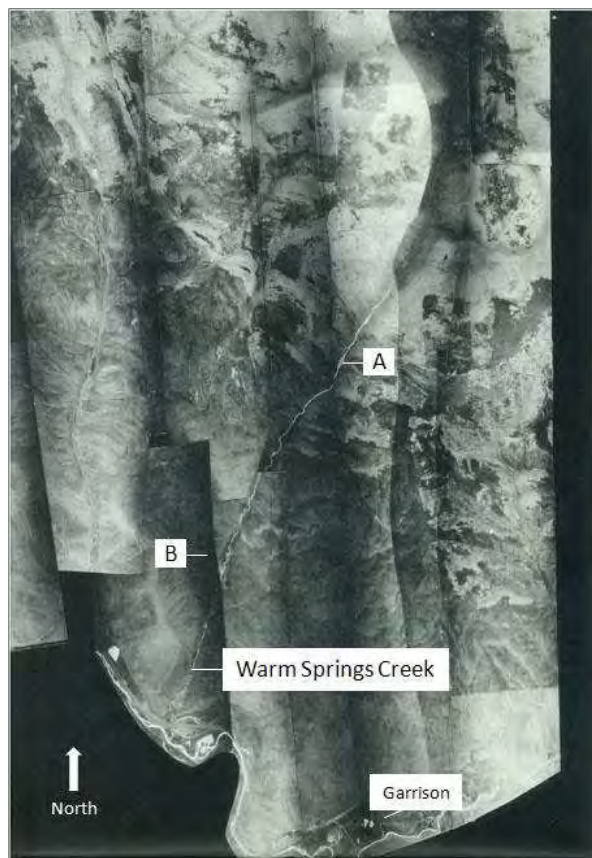


Figure 3. Thermal infrared imagery of Warm Springs Creek area in the southeastern part of the Garnet Range. This imagery is considered to have an approximate scale of 1:62,500, but there is no lens so an actual scale cannot be determined.

Most of the igneous intrusions and volcanic flows within the Garnet Range area are Cretaceous or early Tertiary in age. Luedke and Smith's 1983 map of Montana, Idaho, Wyoming, and South Dakota shows that the youngest igneous occurrences in the Garnet Range are a couple of small rhyolitic bodies in the Nevada Creek valley northwest of Avon. They are ten to sixteen million years old. The small size and older age of these volcanics argue against any residual heat being retained in the subsurface (Duffield and Sass, 2003).

Geothermal indicators in the Garnet Range include warm springs and a tufa deposit at

Nimrod, and warm springs and tufa deposits along Warm Springs Creek near Garrison (T9-10N, R9-10W). There are also warm springs along the Warm Springs Creek near Avon (sections 14 and 23, T10N, R8W).

Geochemical Data

Geochemical data obtained from some of the mineral springs along the southeastern margin of the Garnet Range are shown in Table 1. These data include samples from the largest spring on Warm Springs Creek near Avon (Sample GRM-1) and three samples (WSM-1, WSM-2, and WSM-3) collected along the Warm Springs Creek near



Figure 4. Thermal infrared imagery of the Warm Springs Creek that is tributary to Carpenter Creek near Avon, Site C is the largest spring on Warm Springs Creek; Site D shows bifurcation of Threemile Creek.

Table 1. BN Geochemical data from the Southeastern Portion of the Garnet Range

Sample	GRM-1-80-ROM ¹	WSM-1-80-ROM ¹	WSM-2-80-ROM ¹	WSM-3-80-ROM ¹	AFE 393-59 ³	AFE 601-39 ⁴
Location	NENE Sec. 23, 10N, 8W	SESWNE Sec. 3, 9N, 10W	NWSENW Sec. 3, 9N, 10W	marshy stream, NWSWNE Sec. 3, 9N, 10W	Well, Avon section house	Well, depot at Garrison
Na ²	68.00	16.00	27.00	27.00	6.85	20.54
Ca ²	51.00	37.00	34.00	34.00	70.18	23.97
Mg ²	14.00	9.00	4.00	5.00	35.95	6.85
Sulfate ²	140.00	23.00	21.00	20.00	15.41	77.03
Chloride ²	13.00	7.00	8.00	9.00	11.98	13.69
Bicarbonate ²	210.00	143.00	143.00	144.00	112.97	159.20
Total Solids (Calculated)	403	166	168	170	140	146
F ²	5.10	0.41	0.35	0.32		
Li ²	0.52	0.02	0.04	0.03		
SiO ₂ ²	40.60	29.90	25.60	25.60		6.85
pH	7.3	7.6	7.6	7.5	7.5	8.5

¹Analyses by Energy Labs, Billings, Montana

²Analyses in milligrams/liter

³ Analysis by unknown lab for Northern Pacific RR, 1959, converted from grains/gal.

⁴ Analysis by unknown lab for Northern Pacific RR, 1940, converted from grains/gal.

Garrison (section 34, T10N, R10W and section 3, T9N, R10W). In addition, geochemical data obtained from two Northern Pacific water wells (Well AFE 393-59 at Avon, with a depth of 59 feet, and Well AFE 601-39 at Garrison, with a depth of 172 feet) are included as background.

Only the chemistry of the GRM-1 sample near Avon is discussed because it shows the least amount of mixing with near-surface waters. The concentrations of fluorine (F) and lithium (Li) are slightly above the levels in the background sample (AFE 393) which suggests that some type of geothermal system may be present. However, the silica concentrations (40 m/l) are only slightly elevated and suggest that subsurface geothermal temperatures are rather low, probably no more than 90 degrees C.

The low silica concentrations, fluorine, and lithium indicators suggest that the current geothermal activity is of the tectonic type.

There is one anomalous area of tufa deposits (Figure 4) on lower Warm Springs Creek near Garrison (Site B in Figure 3) that contains stringers of chalcedony, suggesting that a magmatic geothermal system occurred there. Two carbon-14 radiometric dates provide an age of approximately 25,000 years (Vice, 1984). This is the strongest indicator of higher temperature geothermal systems in the Garnet Range area and occurs in sections 33 and 34, T10N, R10W, and section 3, T9N, R10W (Vice, 1984). The presence of the silica suggests that the reservoir temperature may have been 200 degrees C or higher.



Figure 5. Tufa mound shown on TIR imagery, Figure 3, Site A on Warm Springs Creek.

The Thermal Infrared Survey Theory and General Background

TIR is a passive remote sensing method that detects variations in the amount of heat emitted from the surface of the earth (Sabins, 1997). Blackbodies are theoretical materials that absorb all the radiant energy that strikes them and radiate or emit all of this energy back in a wavelength-dependent pattern (Sabins, 1997). The Earth's surface can be considered an imperfect blackbody which emits heat both from solar heating and the internal heat of the Earth (i.e., geothermal heat). This emitted heat is referred to as radiant flux. The brightness of the TIR imagery is related to the radiant flux and so can be used as a close approximation of the surface temperature (Vice, 2007). However, the radiant flux emitted from the Earth's surface is not uniform because of the interplay of varying factors including the albedo of a surface, which is the fraction of solar energy (shortwave radiation) reflected from the Earth back into space; surface roughness; topographic slope; soil moisture; water temperature relative to the soil; and type of vegetative cover (Vice, 2007). To separate surface factors from geothermal anomalies, a combination of

field-checking and visual interpretation of the imagery by a skilled interpreter is needed (Vice, 2007).

TIR Survey

As part of its exploration program in Montana, BN conducted one TIR survey of the area of Warm Springs Creek in the southeastern part of the Garnet Range near Garrison in 1976 (Vice, 1984) and another over most of the eastern half of the range in 1981 (Crowley Environmental and Planning Associates, Inc., 1982; Vice and Crowley Associates, 1983). In addition, BN performed considerable reconnaissance geologic mapping and geochemical water sampling of thermal springs in the Garnet Range from 1974 through 1981.

The purpose of using TIR imagery was to identify structural controls (i.e., faults) that would allow geothermal fluids to leak to the surface from a subsurface reservoir, and to identify subtle surface anomalies relating to this leakage. Threemile Creek north of Avon showed evidence of recent faulting by the bifurcation of a segment of the creek (Vice and Crowley Associates, 1983).

There is an instructive example for the application of TIR imagery in King County, Washington. There is a natural meadow close to Lester Hot Springs, and it serves as an example of one of the subtle features that can be detected using TIR imagery. It had not been considered a surface geothermal feature until a TIR survey was conducted over the Lester area (Vice, 2008). Thermal waters come to the top of the water table underneath the meadow and then spread laterally toward the Green River. The heat from the thermal waters creates a short-grass prairie and prevents the growth of normal forest vegetation (Vice, 2008). The meadow represents a large extension of the area of geothermal activity.



Figure 6. Anomalous tufa at Figure 3, Site B on lower Warm Springs Creek that contains silica stringers.

This study has included TIR imagery from the southeastern portion of the Garnet Range, including all or parts of T10 -11N, and R8-11W in Powell County. Several of the springs along Warm Springs Creek and elsewhere in this area show warmth in the TIR imagery (e.g., site A in Figure 3). The anomalous tufa shown in Figure 6, at Site B on Figure 3, does not appear in the TIR imagery. The relatively straight, south-southwest trend of Warm Springs Creek in the TIR imagery is suggestive of fault control.

Conclusions

A number of warm springs were identified along the southern margin of the Garnet Range, both from published sources and TIR imagery. The lack of volcanics younger than five million years old in the Garnet Range or nearby areas along this segment of the Lewis and Clark Line suggests that these springs represent a tectonic type of geothermal system rather than the magmatic type. In addition, geochemical data suggest that these warm springs do not have sufficiently high temperatures to be of interest for generating electricity.

One reason BN conducted geothermal exploration in the Garnet Range even though no recent volcanics were present and there were only limited indications of geothermal activity (e.g., warm springs) was that movement along the bifurcating fault north of Avon appears to have occurred in fairly recent times. This movement could have kept the fault structures open and possibly allowed a higher temperature geothermal system to operate in the recent past.

An anomalous tufa deposit along Warm Springs Creek near Garrison contains silica deposits, which suggests a geothermal system with significantly higher temperatures. This tufa deposit has a radiometric age date of approximately 25,000 years which supports periodic movement along segments of the Lewis and Clark Line.

Acknowledgements

The author wishes to thank several people who have helped at different stages in this project and with the research paper, including Richard Mahood who served as a field assistant during some of the time that work was conducted in the Garnet Range. The thermal infrared imagery and geochemical data have been provided courtesy of Burlington Resources, Inc.

Burlington Resources Inc. has not participated in this study and does not endorse any views, statements, or conclusions reached by the author in this study.

References

Benoit, D., Holdmann, G., and Blackwell, D., 2007, Low cost exploration, testing, and development of the Chena geothermal resource: Geothermal Resources Council Transactions, v. 31, p. 147-152.

- Crowley Environmental and Planning Associates, Inc., 1982, Review of the BN-Meridian geothermal remote sensing program: Unpublished report prepared for Meridian Land and Mineral Co., October, 26 p.
- Douglas, J.K., and Crosby, G.W., 1973, Geophysical study of the Montana lineament: Preprint, Department of Geology, University of Montana, 21 p.
- Duffield, W.A., and Sass, J.H., 2003, Geothermal energy-clean power from the Earth's heat: U. S. Geological Survey Circular C1249, 36 p.
- Harrison, J.E., Griggs, A.B., and Wells, J.D., 1974, Tectonic features of the Belt Basin and their influence on post-Belt structures: U. S. Geological Survey, Professional Paper 866.
- Lorenz, J.C., 1984, The function of the Lewis and Clark fault system during the Laramide orogeny: Montana Geological Society, 1984 field conference guidebook and symposium, Northwest Montana and Adjacent Canada, p. 221-230.
- Luedke, R.G., and Smith, R.L., 1983, Map showing distribution, composition, and age of late Cenozoic volcanic centers in Idaho, western Montana, west-central South Dakota, and northwestern Wyoming: U.S. Geological Survey, Miscellaneous Investigations Series, Map I-1091-E.
- Sabins, F.F., 1997, Remote sensing: Principles and interpretation: W.H. Freeman and Company, New York, Third Edition, 494 p.
- Schmidt, R.G., Loen, J.S., Wallace, C.A., and Mehnert, M.L., 1994, Geology of the Elliston region, Powell and Lewis and Clark Counties, Montana: U. S. Geological Survey Bulletin 2045.
- Sears, J.W., 2000, Rotational kinematics of the Rocky Mountain thrust belt of northern Montana: *in* Shalla, R.A., and Johnson, E.H., eds., Montana/Alberta thrust belt and adjacent foreland: Montana Geological Society, 50th Anniversary Symposium, p. 143-149.
- U.S. Geological Survey, 1984, Aeromagnetic map of the Butte 1° X 2° quadrangle, Montana: U.S. Geological Survey Open-file report 84-278.
- Vice, D.H., 2011a, A study of the structure in the northwestern Montana overthrust belt using side-looking airborne radar imagery: Northwest Geology, v. 40.
- Vice, D.H., 2011b, The Burlington Northern mineral exploration program: Geothermal Resources Council *Transactions*, v. 35, p. 77-80.
- Vice, D.H., 2008, Lester Meadow, Washington, a geothermal anomaly: Geothermal Transactions, v. 32, p. 175-179.
- Vice, D.H., 2007, Application of airborne thermal infrared imagery to geothermal exploration: Geothermal Resources Council Transactions, v. 31, p. 369-372.
- Vice, D.H., 1989, The mineral potential of the Garnet Range, west-central Montana: Montana Geological Society, 1989 Field Conference guidebook: Montana centennial edition, v. 1, p. 411-414.
- Vice, D.H., 1984, Geothermal activity at the intersection of the Montana and Great Falls lineaments: *in* McBane, J.D., and Garrison, P.B., eds., Northwest Montana and adjacent Canada: Montana Geological Society, Field Conference and Symposium guidebook, p. 315-320.
- Vice, D.H., and Crowley Associates, 1983, Garnet Range East and West Geothermal

IR Report: Unpublished report prepared for Meridian Land and Mineral Company, 26 p.

Wallace, C.A., Lidke, D.J., and Schmidt, R.G., 1990, Faults of the central part of the Lewis and Clark Line and fragmentation of the Late Cretaceous foreland basin in west-central Montana: *Geol. Soc. America Bull.*, v. 102, p. 1021-1037.



Norris Geyser Basin, 1912. Courtesy National Park Service.

THE WASATCH LINE (NEOGENE)/EAST PACIFIC RISE PLATE TECTONIC MODEL: VIABLE FOR MULTIPLE WORKING HYPOTHESIS EVALUATION AGAINST “SLAB GAP”?

Joseph H. Baird

Baird Hanson Williams LLP, Boise, Idaho

ABSTRACT

The author proposes a plate tectonic model for the U.S. and Mexican Cordillera in which the Neogene aspects of the tectonic feature described by Dr. William Lee Stokes as the “Wasatch Line” is interpreted to be a northern subsialic portion of the East Pacific Rise spreading center. Within it, the Wasatch Line/East Pacific Rise spreading center has been *an active, not incipient* spreading center generating two divergent basaltic plates directly beneath the sialic North American Plate (NAP) for approximately 14 million years (Stokes, 1976). The Neogene Wasatch Line/East Pacific Rise plate tectonic model (Wasatch/EPR Model or just “Model”) interprets current U.S. Cordilleran topography and late Cenozoic geology to result substantially from the operation of the full plate tectonic cycle of the East Pacific Rise under the NAP, from initial basalt generation, to plate subduction (defined as a basalt plate sinking into the mantle), through partial melting, and finally magma eruption. The author presents some preliminary evidence supporting the Model and suggests that it merits (1) additional evaluation, comment, criticism and refinement; and (2) a “multiple working hypothesis” evaluation against “slab gap” theory. This paper is presented in the spirit of Professor Chamberlin’s multiple working hypothesis paradigm for study and evaluation of new concepts (Chamberlin, 1965).

WASATCH LINE (NEOGENE)/EAST PACIFIC RISE PLATE TECTONIC MODEL: SUMMARY DESCRIPTION

Wasatch Spreading Center

The Model interprets current Cordilleran topography and late Cenozoic geology to be primarily the result of the East Pacific Rise operating under the North American Plate (NAP). The full plate tectonic cycle is evidenced under the NAP, from initial basalt plate generation to plate subduction (defined as a basalt plate sinking into the mantle), partial melting, and eruption. The topography of the Wasatch Front/Mogollon Rim is an effect of the Wasatch Line/East Pacific Rise spreading center (Wasatch Spreading Center), but the actual position of the Wasatch Line/East Pacific Rise is the Intermountain Seismic Belt (IMSB), typically located to the east of the topographic Wasatch Front/Mogollon Rim. The Yellowstone Hot Spot is an Icelandic analogue that is integral to the Wasatch Spreading Center. Geographically, the Model’s Wasatch Line runs from approximately Glacier National Park through Yellowstone National Park, the Wasatch Front, and the Mogollon Rim (Figure 1), and then conceptually, the Wasatch Line continues along the eastern edge of the Mexican basin and range before reconnecting with the East Pacific Rise in the Pacific basin. In part, the Model’s “Wasatch Line” concept is extrapolated, but substantially modified, from Dr. Stokes’ Wasatch Line (Stokes, 1976, 1986).

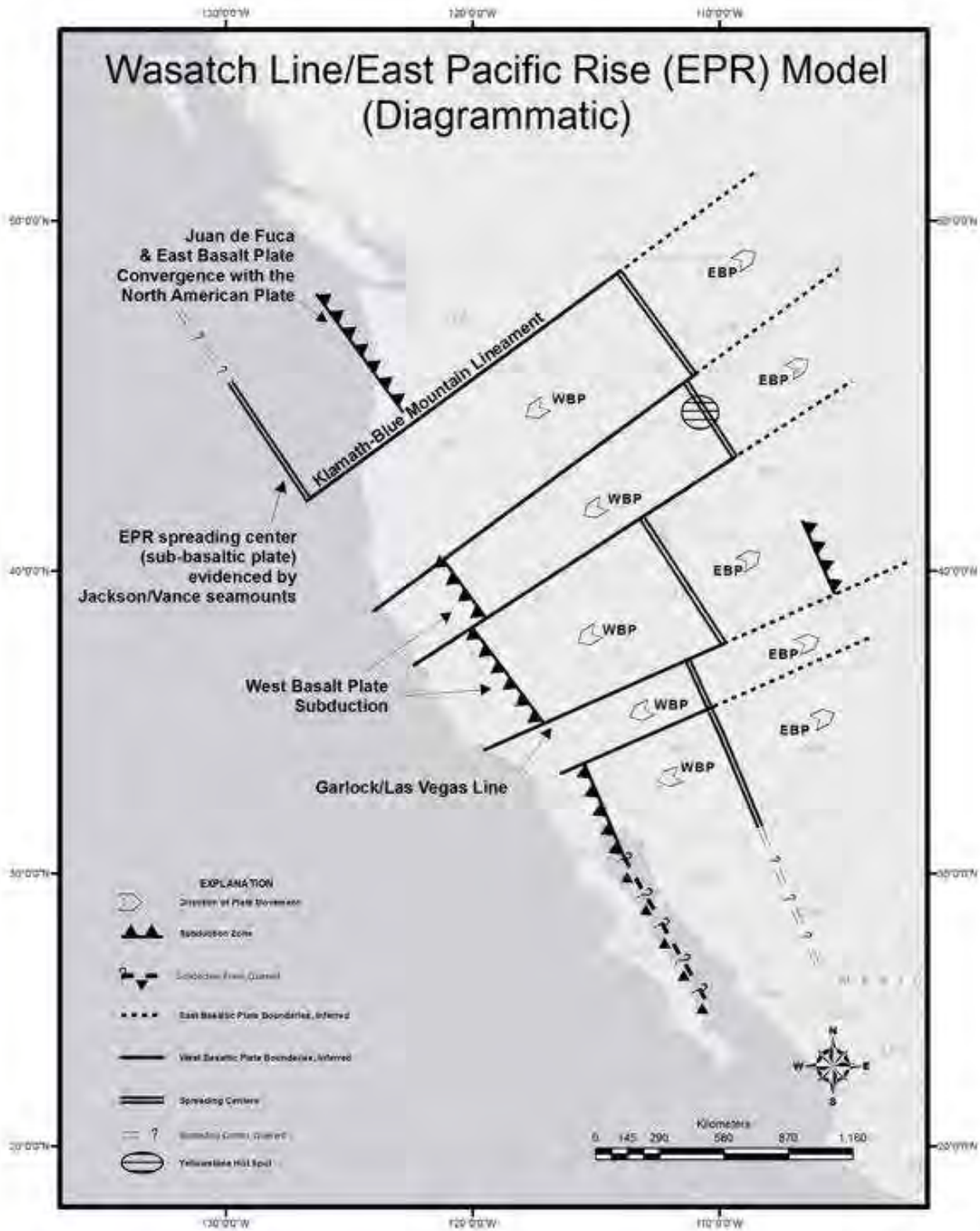


Figure 1 – Wasatch Line/East Pacific Rise Model

The Wasatch Spreading Center (WSC) has been generating two hot, fast-moving, divergent basaltic plates that have been sliding horizontally away from the Wasatch Spreading Center directly beneath the NAP for approximately 14 million years. The West Basalt Plate (WBP) moves southwest-erly. The East Basalt Plate (EBP) moves northeasterly. Utah's "rift pil-lows" (Wanamaker et al., 2001, Figure 21) provide evidence for magma generation at the Wasatch Spreading Center. The WBP and EBP are buoyed by intrinsic heat that forces the WBP/EBP system up against the bottom of the NAP across most of the Cor-dillera. This intrinsic heat is not easily dis-sipated through the insulating NAP. Thus, the WBP and EBP maintain petrologic con-ditions favorable for generating pressure-relief magmatism wherever extension in the NAP creates a system of fractures provid-ing plumbing to the surface.

Once the NAP moves across the Wasatch Spreading Center, the NAP is physically transferred onto the WBP, which is moving more rapidly than the overlying NAP. In-deed, "[e]vidence exists that the Colorado Plateau at its western margin is being con-verted to lithosphere with rifted Great Ba-sin properties" (Wanamaker et al., 2001). The velocity differentials create extension in the NAP, initially creating horst and gra-ben faulting, and later stretching into listric configuration. Great Basin extension is concentrated along its eastern margins (Wanamaker et al., 2001) consistent with the mechanisms of this Model. West of the Wasatch Spreading Center, the NAP is a relatively passive block dominated by the kinetics of the underlying WBP. Great Ba-sin regional mafic "under-plating" (Wanamaker et al., 2001) as well as "possible double-Moho reflections, ani-sotropy, flatness of the Moho, low-angle faults, and opportunities to trace deep struc-tures back to the surface," (GreatBreak,

2004, p. 3) are consistent with the existence of the WBP under the Great Basin.

WBP sinking begins at the Walker Lane Belt/Gulf of California trough: the WBP contacted and tilted the Sierra Nevada and Baja California (Baja) batholiths, maintain-ing the angle of WBP sinking; this tilting is also reflected by the distinct regional to-pography of the Sierra Nevada and Baja regions. WBP sinking is further evidenced by apparent southwesterly "delamination of the Sierra Nevada," Great Valley "mantle drips", and young coastal-range volcanism, as discussed below.

In the Model, the Mojave block plateau lies over a segment of the WBP that initially locked against the Pacific Plate and has re-mained essentially horizontal because it was insufficiently cool to subduct. The ap-proximate location of the northern edge of this non-subducting WBP segment is marked by the southwesterly trace of Stokes' Las Vegas Seismic Line, which arises from Stokes' Marysvale Bifurcation and extends to the Garlock fault (Stokes, 1976). The topographic clarity of the ele-vated Mojave/Marysvale Block underlain by this WBP segment is obscured by Ceno-zoic erosion created by the Colorado River and extension in the basin and range prov-ince. Nevertheless, immediately to the north of the Mojave/Marysvale Block (i.e., north of the Garlock fault) and to the south (i.e., the Salton trough) there are dramatic topographic and structural lows: respec-tively, Death Valley and the Gulf of Cali-fornia.

The Mojave/Marysvale Block is a regional topographic and structural high that creates an apparent north-south topographic break between the Sierra Nevada and Baja batholiths, the Walker Lane Belt and the Gulf of California trough, the basin and range prov-ince, and Wasatch Front/Mogollon Rim.

Each of these paired features would otherwise be deemed singular topographic features requiring singular geologic and tectonic explanations, such as provided by the Model. To the north of the Sierra Nevada, the NAP topography suggests that the WBP is not subducting, but instead is engaged in laminar movement immediately under the sialic crust, which when combined with WBP rotation discussed below gives rise to the Plio-Pleistocene Klamath Block uplift.

East Basaltic Plate Movement and Incipient Subduction

The EBP moves from the Wasatch Spreading Center in a northeasterly direction, demonstrating incipient subduction at the Colorado/Wyoming Rocky Mountain Front Range. As the EBP starts sinking into the mantle, countervailing mantle forces cause the EBP to buckle slightly up and “backwards” to the southwest causing a regional bowing that also creates the 14,000-foot peaks of the Colorado Front Range. South of Colorado’s Canyon City embayment, this incipient subduction seems to give way to the EBP’s northeasterly laminar movement directly under the NAP, which characterizes most of the eastern Cordillera. Neither the Rio Grande “Rift” nor the Jemez Lineament, which runs from Springerville in eastern Arizona through (and beyond) Raton, New Mexico, are integral parts of the Wasatch/East Pacific Rise system; thus the Model assumes a conventional interpretation of these features as being pre-existing zones of weakness in the NAP. They provide scattered local opportunities for pressure-relief melting of the EBP, but are older than their associated volcanism (Sanford and Lin, 1989). Collectively, this gives rise to the mafic volcanism of scattered ages and varied locations of the Jemez Lineament that confounds any easy magma-tectonic interpretation. The Socorro Fault Zone (Sanford

and Lin, 1989) may indicate the location of another transverse fault line in the Wasatch/East Pacific Rise system.

Klamath-Blue Mountain Transverse Vector and the Juan de Fuca System

The Model interprets the Klamath-Blue Mountain Lineament (KBML) (Riddhough et al., 1986) to be a transform fault connecting the Wasatch Spreading Center/East Pacific Rise under the NAP with the northernmost remnant of the old Farallon basaltic plate of the East Pacific Rise, located off the coast of the Pacific Northwest. Traditionally, this remnant of the East Pacific Rise is deemed to be the Juan de Fuca (JdF) spreading center. The JdF basaltic plate is generated perpendicularly, and deemed to migrate to the southeast. However, the actual direction of JdF convergence with the NAP is northeasterly (Swanson et al., 1989, p. 2; Jordan et al., 2004, Figure 1), suggesting that the JdF plate growth vector is inconsistent with the direction of the mantle flow driving its convergence with the NAP. In contrast, the KBML transform fault’s strike is consistent with the northeasterly direction of JdF/NAP convergence and with the apparent direction of mantle flow. North of the KBML transform, Cascadia subduction more closely resembles traditional concepts (with the notable exception of the Yakima fold belt, discussed below). However, since the Model deems the KBML to be the northwestern edge of the WBP, then per the Model, south of the KBML there is a complex interaction of continued WBP laminar movement to the southwest; the JdF plate passively sinking due to the weight of the cold, dense plates; and clockwise rotation of the KBML linear magma chamber described further below.

The KBML continues offshore under the Cascades and continental shelf (Riddhough et al., 1986; Blackwell et al.,

1990). Based upon the logic of the Model and its intriguing bathymetry, the KBML transform structure appears to continue southwesterly to terminate underneath and in the middle of the Gorda Plate. Here, another segment of the East Pacific Rise spreading center seems to strike to the northwest at 90 degrees from the KBML's southwestern terminus, and then continue on-strike to the President Jackson and, perhaps, Vance Seamounts, underneath the mafic plate generated by JdF spreading center. Following the Model's basic "plate under plate" paradigm, this suggests the existence of both: (1) a lower plate (i.e., an EBP analogue) generated and driven by direct mantle convection; and (2) an upper plate (i.e., the JdF/Gorda plate) driven by cold-pull subduction that actually floors the Pacific Ocean basin. Importantly, seismic reflection of the JdF "has delineated two slabs of oceanic lithosphere underlying Vancouver Island, one that is currently being subducted and one that is underplated," (Green et al., 1986, Figure 3, p. 3) which is generally consistent with the Model.

Klamath-Blue Mountain Lineament and Oregon Time-Transgressive Rhyolite Rotation

Late Cenozoic silicic volcanism in southeastern Oregon manifests a chronologically repeating and westerly shortening line of northwesterly time-transgressive rhyolite domes (TTR) ranging in age from approximately 10 Ma through the Holocene (Jordan et al., 2004). The most recent line of Oregon TTR consists of two rhyolite domes within Newberry Crater which is slightly to the southwest of and on parallel strike with the KBML. The Model interprets the Oregon time-transgressive rhyolite as evidencing the movement and rotation of the KBML under the NAP. To reiterate and emphasize, the KBML is also the northwest

edge of the WBP. The rotating track of the KBML starts about 12 Ma at the Steens/Black Rock Range escarpment (Steens Topographic Line), where the WBP edge first forced its way under the piece of the NAP bounded on the southeast by the Steens Topographic Line. The WBP pushes the NAP up and out of the way, creating a linear pressure-relief magma chamber just to the northwest of the KBML, called the KBML Chamber. The KBML Chamber is floored by mantle, walled to the southeast by the WBP and roofed by the NAP; thus, partial melting of the mantle and WBP can parent a variety of mafic melts on a wide chemical continuum. As the KBML advances and rotates to the northwest, the KBML Chamber immediately precedes it. In advance of the KBML, the overlying NAP is in compression, so the aligned KBML Chamber melts must migrate upward and assimilate silicic NAP, erupting as lines of rhyolite. In contrast, when the KBML Chamber advances under the generous plumbing of the old Western Cascades, the KBML Chamber erupts the wide variety of complex mafic rocks that is the signature of the southern High Cascades. As the KBML rotates under the slower moving NAP, the NAP is dragged, extended, and thinned, generating pressure-relief magma and plumbing sourced from the WBP. This obviates the need for "back-arc" models of more recent mafic volcanism in eastern Oregon. The Model ascribes central and southern Oregon's limited andesitic volcanism to anemic subduction of the traditional JdF plate because it is descending only by intrinsic cold-pull subduction; the JdF plate descent is oblique to, and therefore cannot be aided by, the apparent direction of mantle convection. In fact, southern Cascadia evidences little indication of subduction seismicity or a trench (Wood and Kinle, 1990, p. 148); this is also consistent with the Model. Rotation of the KBML would also create the northerly compression of the

NAP necessary to generate the Yakima fold belt, which is anomalous to conventional Cascadian subduction models.

**WASATCH LINE/EAST PACIFIC
RISE SPREADING CENTER:
DR. STOKES' DIRECTED INQUIRY –
DRIVING MECHANISM**

The Wasatch Line “is, by any standard, one of the most important geologic features in North America” (Stokes, 1986, p. 11). Although Stokes suggests the origins of the Wasatch Line to be Paleozoic or older, he also draws a distinction between this ancient correlation and the Cenozoic topographic and seismic characteristics of the Neogene Wasatch Line (Stokes, 1976; 1986). Thus, even though the Model’s Wasatch Line has been significantly extrapolated and modified from Stokes’ Wasatch Line (Neogene), his concept and terminology remain a useful foundation for the Model. Importantly, Stokes provides a line of directed inquiry.

Stokes’ fundamental question is “*What is the Wasatch Line?*” The Model proposes the Wasatch Line is the East Pacific Rise operating under the NAP. The Model deems the Wasatch Line/East Pacific Rise to be at the Intermountain Seismic Belt (IMSB) (<http://earthquake.usgs.gov/regional/imw>). The IMSB’s geographic pattern describes impressive regional-scale, right-angle intersections, similar to the map view pattern of mid-ocean ridge transform fault systems. Importantly, this generally orthogonal pattern of the IMSB at the Wasatch Line is similar in structure to late Cenozoic volcanic patterns throughout the Cordillera. (See Smith and Luedke, 1984, figures 4.2 through 4.8, pp. 50–54). This pattern, including an apparently preferential northeasterly axis of approximately N50E, is deemed to be “Smith-Luedke Fabric.”

Nevada evidences Smith-Luedke Fabric on a smaller, state-wide scale for gravity anomalies, geologic blocks, and major transverse structures (Shawe, 1991, Figures 3, 4, and 5, p. 203-5) suggesting that Smith-Luedke Fabric may profoundly influence all aspects of Cordilleran geology. The Wasatch Line/EPR Model provides a common source for the origin of Smith-Luedke Fabric throughout the Cordillera.

Stokes asks, “*What is the Marysvale Bifurcation?*” (Stokes, 1986). He describes the Marysvale Bifurcation in Utah as the point where the Las Vegas Seismic Line strikes southwesterly from the Wasatch Line to merge with the Mojave’s Garlock fault system, while the main Wasatch Line strikes southeasterly through Arizona (Stokes, 1976). The Model interprets Stokes’ Las Vegas Seismic Line to be a transverse fault within the WBP that departs from the Wasatch Spreading Center at Marysvale, Utah, and then strikes southeasterly to merge with the left-lateral Garlock fault system of the Mojave Block. Importantly, Stokes’ Las Vegas Seismic Line appears coincident with the “Southern Nevada transverse zone,” (Kreemer et al., 2010, Figure 1A, also referred to as the Pahrnagat Shear Zone), providing a left-lateral, transverse aspect to the Las Vegas Seismic Line. It is fully consistent with the Model’s interpretation of Stokes’ Marysvale Bifurcation and the Las Vegas Seismic Line, as well as its connectivity to the Garlock fault system.

Stokes queries, “*Is the Wasatch Line Migrating?*” and offers geophysical and volcanic observations suggesting the Wasatch Line is migrating eastward (Stokes, 1986, p. 23). Regionally, time transgressive mafic volcanism (TTM) moving northeastwardly has been long observed in Idaho, Montana, Wyoming, Colorado, Utah, New Mexico, Arizona, and eastern Nevada (Smith and Luedke, 1984, p. 63). Subsequent work has

significantly added to its understanding and elaborated upon the TTM. The “Oregon Nevada Rift Zone” has been portrayed as a north-south line of the volcanic fields erupting in the period between 17-14 Ma. (herein called the 17-14 Zone), including, among other things, the Yellowstone Hot Spot with its mafic heat source (Pierce et al., 2000, Figure 3). The Model proposes that the 17-14 Zone extends southerly to include the volcanics of the San Francisco mafic sequence near Prescott, Arizona that initiated the 15 Ma to Holocene TTM described by Reynolds et al. (1986).

The San Francisco mafic sequence describes a shorter geographic vector, but clearly mirrors the Yellowstone Hotspot’s TTM over the last 15 million years. Importantly, the Springerville field on the Arizona-New Mexico border exhibits “migration ... essentially identical to that seen in the San Francisco volcanic field” (Condit et al., 1989, p. 7975). Additionally, the Pahranaagat-San Rafael belt (15-3.5 Ma.) of Nevada and Utah is “similar to the Yellowstone trend” (Nelson and Tingey, 1997, p. 1249, 1252). All of these TTM trends “terminate” in the vicinity of the Wasatch Line in the Plio-Pleistocene. If a synchronous line of the Wasatch Line TTM is plotted from Pierce et al.’s (2000) Oregon-Nevada Rift Zone, which is now inclusive of synchronous Arizona fields, to the IMSB/Wasatch Line, this plot generally describes a north-south TTM line “moving” from southwest to northeast. This is a synchronous *line*, not just several isolated hot spots; and, in fact, “... [i]t is difficult to equate each of the many [volcanic] loci of such a large region with its own deep-mantle plume” (Smith and Luedke, 1984, p. 63). Stokes was correct; the Wasatch Line is migrating. The Model provides a specific mechanism to explain Wasatch Line TTM.

Arizona volcanism at 20 Ma has been attributed to final foundering of the Farallon Plate (Spencer and Reynolds, 1989, p. 542). Metamorphic mineralization of 18-17 Ma rocks in southwestern Arizona suggests “that the cause of regional extension, reheating, K-metasomatism, and low-grade mineralization along detachment faults could be an overridden, post-collision, portion of the East Pacific Rise that survived” (Brooks, 1985). Then, circa 15 to 13 Ma, Arizona evidences a fundamental change in magma chemistry (Spencer and Reynolds, p. 541). In the Model this represents the reestablishment of the stable mantle convection cells supporting the East Pacific Rise that enables the resumption of basaltic plate generation all along the north-south 17-14 Zone.

WALKER LANE/SIERRA NEVADA/ GREAT VALLEY SUBDUCTION ZONE

The asymmetric pattern of seismicity and rising magma blebs associated with Long Valley volcanism (Hill, 2006, Figure 12, p. 18) illustrates an idealized subduction zone cross-section minus a descending plate. Southwesterly directed asymmetric mafic “delamination” from under the Sierra Nevada is described as “a nearly horizontal shear zone accommodating the detachment of the [presumed] ultramafic root from its granitoid batholith” (Zandt et al., 2004); the Model deems this to be continued sinking of the WBP. This “delaminating” slab then manifests as the lower of the two plates of “Great Valley Ophiolite,” (Brocher et al., 2000, Figure 3A, p. 235), which is depicted to be the thickness of *two* oceanic plates with the lower plate (i.e., the presumed WBP) in dip-slip motion descending southwesterly relative to the upper ophiolite plate (Brocher et al., 2000, Figure 3A, p. 235). Importantly, the Isabella “mantle drip” is no longer necessarily “a single,

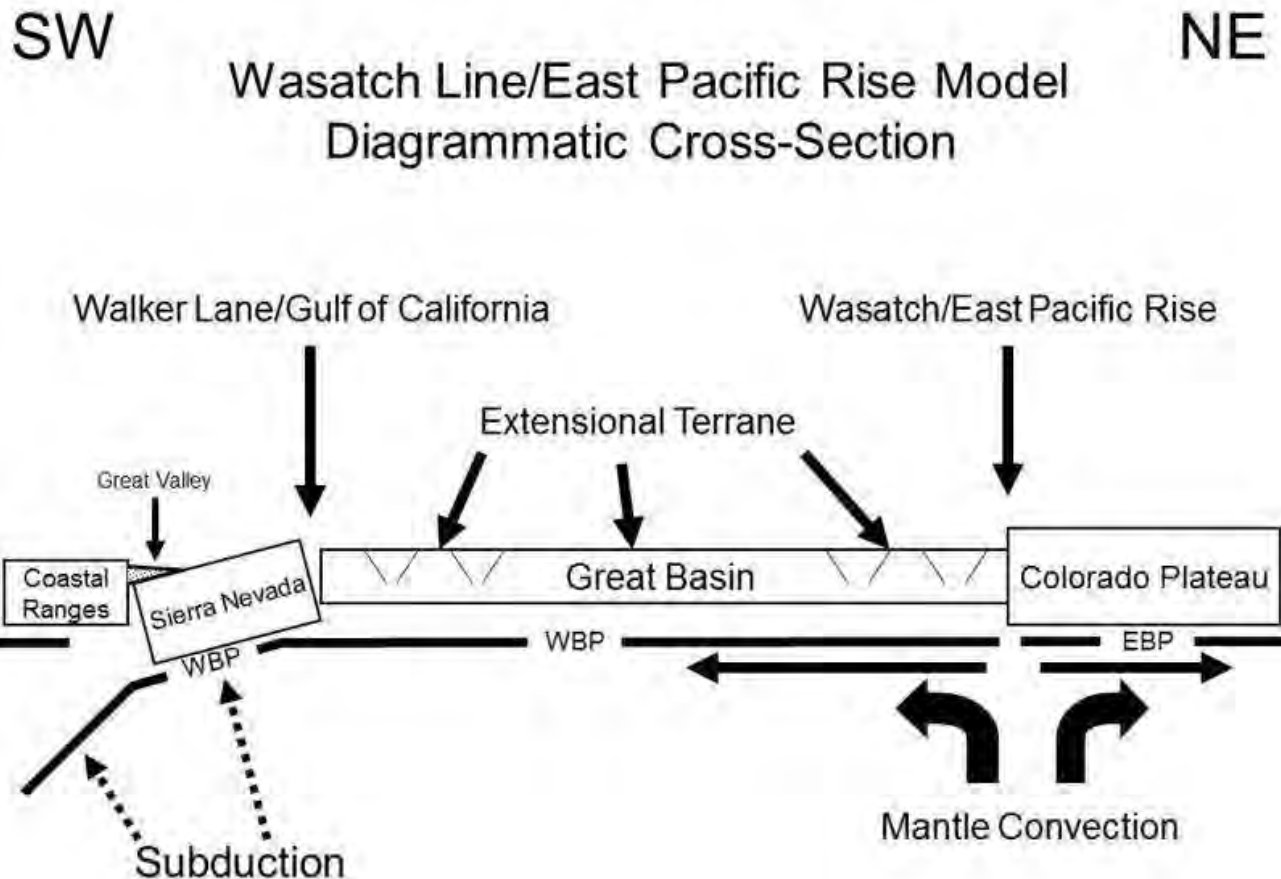


Figure 2 – Wasatch Line/East Pacific Rise Model – Cross-Section

limited, foundering event, it might be the oldest of a northward younging series of instabilities in the mantle lithosphere,” (IRIS, 2006, p. 14) therefore this line of mafic material foundering may actually evidence WBP subduction. Additionally, “... it appears the bright Moho conversion commonly found in the Basin and Range extends well into the Sierras, suggesting some Cenozoic modification of Moho” (IRIS, 2006, p. 13). The Wasatch Line/East Pacific Rise Model is predicated upon late Cenozoic continuity between the BandR and the SN at the Moho; thus, the Model deems this “continuity” to be the WBP (see Figure 2). Finally, recent California coastal range volcanism has been attributed to the effects of “young, hot oceanic slab ... [because this would] explain the observed crustal structure, heat flow,

and sparse Neogene [Coastal Range] volcanism” (Brocher et al., 2000); this would seem to be more readily explained by southwesterly subduction of the younger WBP than by easterly convergence of the much older remnant of the Farallon plate.

CORDILLERA-WIDE REGIONAL ROTATION OF THE WSC/WBP/EBP

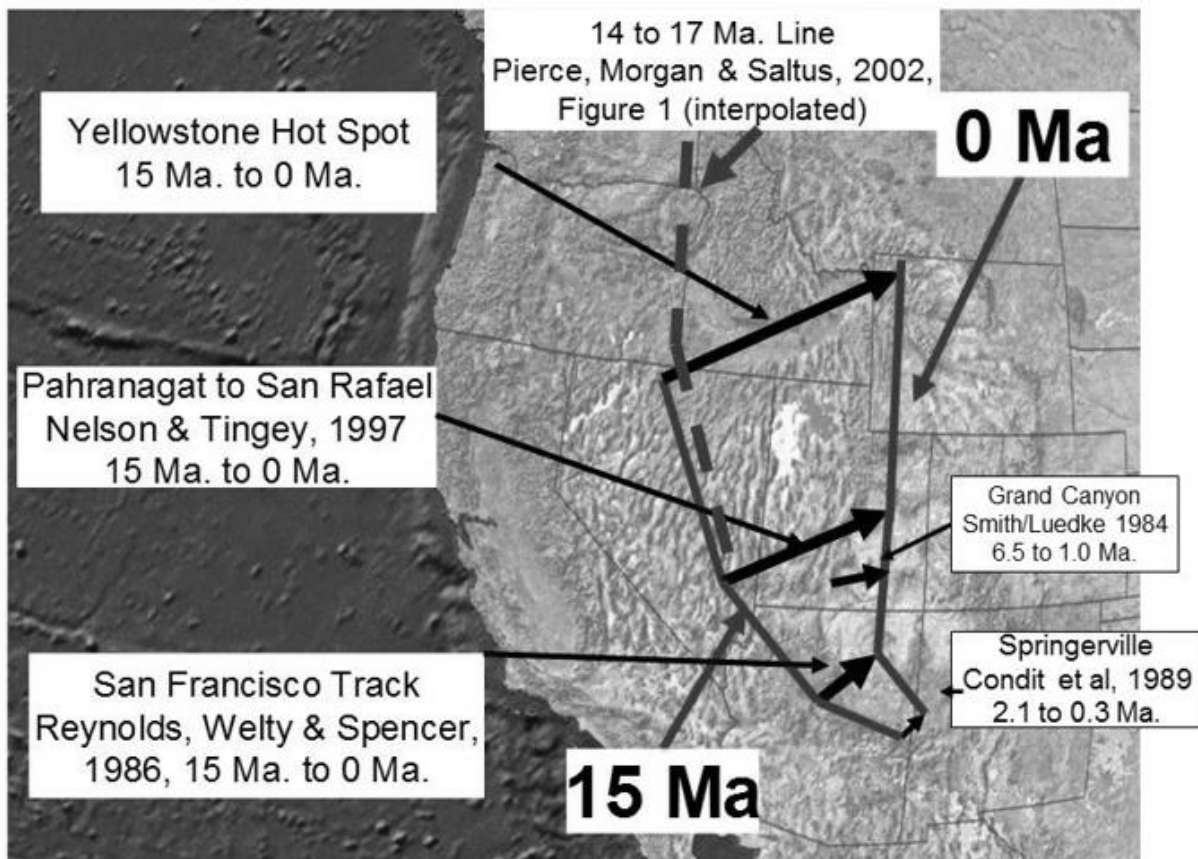
As discussed above, TTM volcanism associated with the Wasatch Spreading Center suggests that the Wasatch Line “moves,” but the Wasatch Line TTM appears to be “moving” more rapidly in the north at the Yellowstone Hot Spot than in the south (e.g., Arizona’s San Francisco volcanic sequence). Assuming the TTM volcanism represents the NAP moving across relatively stationary volcanic sources, the pat-

tern of Wasatch Line TTM suggests the NAP is also *rotating counterclockwise* over the line of volcanic sources (see Figure 3). This would be highly anomalous behavior, since GPS studies show the NAP is rotating clockwise, logically moving north along the point of contact with the Pacific plate (Wells and Simpson, 2001). The Model interprets this anomalous NAP counterclockwise “movement” to be largely apparent; the NAP and the Wasatch Line are both rotating clockwise, but the Wasatch Line is rotating clockwise more rapidly than the NAP. As noted above, once the NAP crosses to the west of the Wasatch Spreading Center, the NAP is merely “along for the ride” on the WBP and all significant NAP tectonic kinetics are imparted to the

NAP. Thus, per the Model, the kinetic linkage between the Cordillera and the Pacific plate/mantle system (Pacific System) is driven by the interaction between it and the WBP. The interaction between the NAP and the Pacific System is only a secondary effect of WBP/Pacific System dynamics.

As was also discussed above, regional rotation of the northwestern edge of the WBP (i.e., the KBML transform) underneath the NAP has profoundly affected southeastern Oregon’s terrain and petrology since about 12 Ma. Opportunistically, the Garlock fault segment of the Mojave/Marysville Block discussed above also presents a northwest facing and rotating WBP “edge” that, per the Model, might yield additional evidence

Figure 3 - Wasatch Line Time Transgressive Volcanism
Multiple Hot Spots or Linear Spreading Center?



of the WBP rotating underneath the NAP. However, any attempted rotation of this edge in California would be impeded by the downward projection of the westward tilted blocks of the Sierra Nevada and the Great Valley Ophiolite, at least initially. In fact, the northwestern edge of the WBP may have finally worked its way under the Sierra Nevada block, and might be evidenced by the compressive reverse faulting of the White Wolf fault. This fault lies north of and parallel to the more quiescent Garlock fault and is highly active. If the primary kinetic linkage to the Pacific System of the Cordilleran is the WBP and not the NAP, then the Model provides intriguing possibilities for reevaluating the relationship between the NAP and the Pacific plate, as well as California seismicity, generally, and the Eastern California Shear Zone/Walker Lane, specifically.

CONCLUSIONS

The author respectfully suggests the Model presents a comprehensive, integrated paradigm that is sufficiently tenable to be worthy of further evaluation using Chamberlin's multiple working hypothesis. If the Model survives criticism, it will be corrected and modified as necessary. Then, I believe the Model will merit a multiple working hypothesis evaluation against "slab gap." I believe that the Wasatch/EPR Model has significant predictive capability potential for both plate tectonic and mineral exploration purposes.

References

Baird, J. H., and Williams, W.K., 2011, Abstract, *in* Proceedings of the Geological Society of America, Rocky Mountain (63rd Annual) and Cordilleran (107th Annual) Sections Joint Meeting.

Blackwell, D.D., Steele, J.L., Frohme, M.K., Murphey, C.F., Priest, G.R., and Black, G.L., 1990, Heat flow in the Oregon Cascade Range and its correlation with regional gravity, Curie point depths, and geology: *Journal of Geophysical Research*, v. 95, no. B12, p. 19,475-19,493.

Brocher, T.M., ten Brink, U.S., and Abramovitz, T. 2000, Synthesis of crustal structure and implications for the concept of a slab gap beneath coastal California: *in* Ernst, W.G. and Coleman, R.G., eds., *Tectonic Studies of Asia and the Pacific Rim*, GSA.

Brooks, W.E., 1985, The East Pacific Rise, Part II: Proceedings of the Geological Society of America, Cordilleran Section, 81st Annual, #70494.

Chamberlin, T.C., 1965, *Science*, v. 148, p. 754-759; reprinted from *Journal of Geology*, 1897.

Condit, C., et al., 1989, Patterns of volcanism along the southern margin of the Colorado Plateau: The Springerville field: *Journal of Geophysical Research*, v. 94, #B6, pp 7975 – 7986.

Green, A.G., Clowes, R.M., Yorath, C.J., Spencer, C., Kanasewich, E.R., 1986, Seismic reflection imaging of the subducting Juan de Fuca plate: *Nature*, v. 319, No. 6050, pp. 210-213.

GreatBREAK Workshop: Preparing for EarthScope in the Great Basin, June 21-23, 2004, Tahoe City, California: Notes of the Proceedings. http://crack.seismo.unr.edu/greatbreak/contents/Report/Workshop_Report-v7-a.doc

Hill, D.P., 2006, Unrest in Long Valley Caldera, California, 1978 – 2004: *in* Troise, C., De Natale, G., and Kilburn, C.R.J., eds.,

Mechanisms of activity and unrest at large calderas: Geological Society, London, Special Publications, 269, 1-24.

Kreemer, C., Blewitt, G., and Hammond, W.C., 2010, Evidence for an active shear zone in southern Nevada linking the Wasatch fault to the Eastern California shear zone: *Geology*, May 2010, p. 475-478.

Jordan, B.T., Grunder, A.L., Duncan, R.A., and Deino, A.L., 2004, Geochronology of age-progressive volcanism of the Oregon High Lava Plains: Implications for the plume interpretation of Yellowstone: *Journal of Geophysical Research*, v. 109, B10202.

Nelson, S.T., and Tingey, D.G., 1997, Time transgressive and extension related basaltic volcanism in southwest Utah and vicinity: *GSA Bulletin*, v. 109, pp. 1249 – 1265.

Pierce, K.L., Morgan, L.A., and Saltus, R.W., 2000, Yellowstone Plume Head: Postulated tectonic relations to the Vancouver Slab, continental boundaries, and climate: USGS Open-File Report 00-498, <http://pubs.usgs.gov/of/2000/ofr-00-0498/ofr-00-0498.pdf>

Reynolds, S.J., Welty, J.W., and Spencer, J.E., 1986, Volcanic History of Arizona: Fieldnotes, Arizona Bureau of Geology and Mineral Technology, v. 16, No. 2, p. 5.

Riddihough, R.C., Finn, C. and Couch, R., 1986, Klamath-Blue Mountain lineament, Oregon: *Geology*, v. 14, p. 528-531.

Sanford, A.R. and Lin, Kuo-wan, 1989, Evidence for a 1400-km-long Socorro Fault Zone: Geophysics Open-File Report, Earth and Environmental Science Institute, New Mexico Institute of Mining and Technology, Socorro, New Mexico.

Shawe, D.R., 1991, Structurally controlled gold trends imply large gold resources in

Nevada: *in* *Geology and Ore Deposits of the Great Basin*, Geological Society of Nevada, p. 199-212.

Smith, R.L., and Leudke, R.G., 1984, Potentially active volcanic lineaments and loci in western coterminous United States: *in* *Studies in Geophysics - Explosive Volcanism: Inception, Evolution, and Hazards*, p. 47-66.

Spencer, J. E., and Reynolds, S.J., 1989, Middle Tertiary tectonics of Arizona and adjacent areas: Jenney, J.P., and Reynolds, S.J., eds., *Geologic Evolution of Arizona*, Arizona Geological Society Digest 17, p. 539-574.

Stokes, W.L., 1976, What is the Wasatch Line?: *in* *Geology of the Cordilleran Hingeline*, Rocky Mountain Association of Geologists, p. 11-25.

Stokes, W.L., 1986, *Geology of Utah*: Utah Geological and Mineral Survey, Salt Lake City, Utah, p. 11-36.

Swanson, D.A., Cameron, K.A., Evarts, R.C., and Pringle, P.T., 1989, Cenozoic volcanism in the Cascade Range and Columbia Plateau, southern Washington and northernmost Oregon: New Mexico Bureau of Mines and Mineral Resources, Memoir 47.

Wanamaker, P.E., Bartley, J.M., Sheehan, A.F., Jones, C.H., Lowry, A.R., Dumitru, T.A., Ehlers, T.A., Holbrook, W. S., Farmer, G. L., Unsworth, M.J., Hall, D.B., Chapman, D.S., Okaya, D.A., John, B.E., and Wolfe, J.A., 2001, Great Basin-Colorado Plateau transition in central Utah: an interface between active extension and stable interior: *Proceedings of the J. Mackin Symposium*, Utah Geological Association and AAPG.

Wells, R.E., and Simpson, R.W., 2001, Northward migration of the Cascadia forearc in the northwestern U.S. and implications for subduction deformation: *Earth Planets Space*, v. 53, p. 275-283.

Wood, C.A., and Kienle, J., 1990, *Volcanoes of North America: United States and Canada*: Cambridge University Press, N.Y.

Gilbert, H., et al., 2004, *Nature*, v. 431, p. 41-46.

An early Yellowstone visitor. Courtesy National Park Service.



A PALEOPROTEROZOIC SEDIMENTARY BASIN WITHIN THE WYOMING CRATON EXPOSED IN THE RUBY RANGE, SW MONTANA: IDENTIFIED BY FIELD RELATIONS AND GEOCHRONOLOGY

J. Alcock

Geosciences, Pennsylvania State University, Abington College, Abington, PA 19001, jea4@psu.edu

Peter Muller

Alpha Geoscience, 636 Burnham Road, Philadelphia, PA 19119, mullerpd@gmail.com

Abstract

Metasedimentary rocks of the Montana Metasedimentary terrain within the Wyoming craton are generally thought to be derived from Archean protoliths. Among these are a small belt of schists exposed in the southern Ruby Range in southwestern Montana. They have traditionally been correlated with the Archean Pre-Cherry Creek sequence of the Madison Range because these rocks do not contain either marble or banded-iron formation. However, field relations, metamorphic grade, and geochronologic constraints indicate that the schists are a distinct unit that is Paleoproterozoic in age. They are named herein the Garnet Mine Schist.

Zircon included in the schist, analyzed by laser ablation techniques, yielded ten nearly concordant ages and a single weighted-mean $^{207}\text{Pb}/^{206}\text{Pb}$ age of 1769 ± 2.6 Ma. No significantly older ages were obtained, indicating that the schist had not been metamorphosed during an earlier regional Proterozoic event that affected the Montana Metasedimentary terrain ≈ 2450 Ma. In addition, the schists contain both muscovite and sillimanite while the surrounding metamorphics experienced conditions above the second sillimanite isograd. Finally, the garnet leucogneiss that intruded the older Dillon gneiss adjacent to the schists is not found within them. Nine high-U and high-

common Pb zircons from the leucogneiss yielded weighted-mean $^{207}\text{Pb}/^{206}\text{Pb}$ ages ranging from 2413 ± 9 to 2438 ± 9 Ma, depending on the age of included common lead. The geochronologic evidence presented here is the first to confirm that the protoliths of some metasedimentary rocks within the Montana Metasedimentary terrain were deposited in a Paleoproterozoic sedimentary basin.

Keywords: Montana Metasedimentary terrain, Ruby Range, U-Pb geochronology, Archean metasedimentary rocks, Early Proterozoic sedimentary basin

Introduction

Basement complexes occur in Laramide uplifts throughout southwestern Montana, exposing Archean and Paleoproterozoic rock of the Wyoming craton (Figure 1A). Together, the ranges of the area comprise the Montana Metasedimentary terrain (Mogk et al., 1992; Mueller et al., 1993), a mix of granitoid gneiss and metasedimentary gneiss, schist, and marble. Two distinct metasedimentary sequences have been recognized and correlated throughout the region based on the presence or absence of marble and banded-iron formation. Rock sequences with these lithologies are correlated with the Cherry Creek sequence and those without are inferred to correspond to the Pre-Cherry Creek suite. The implied

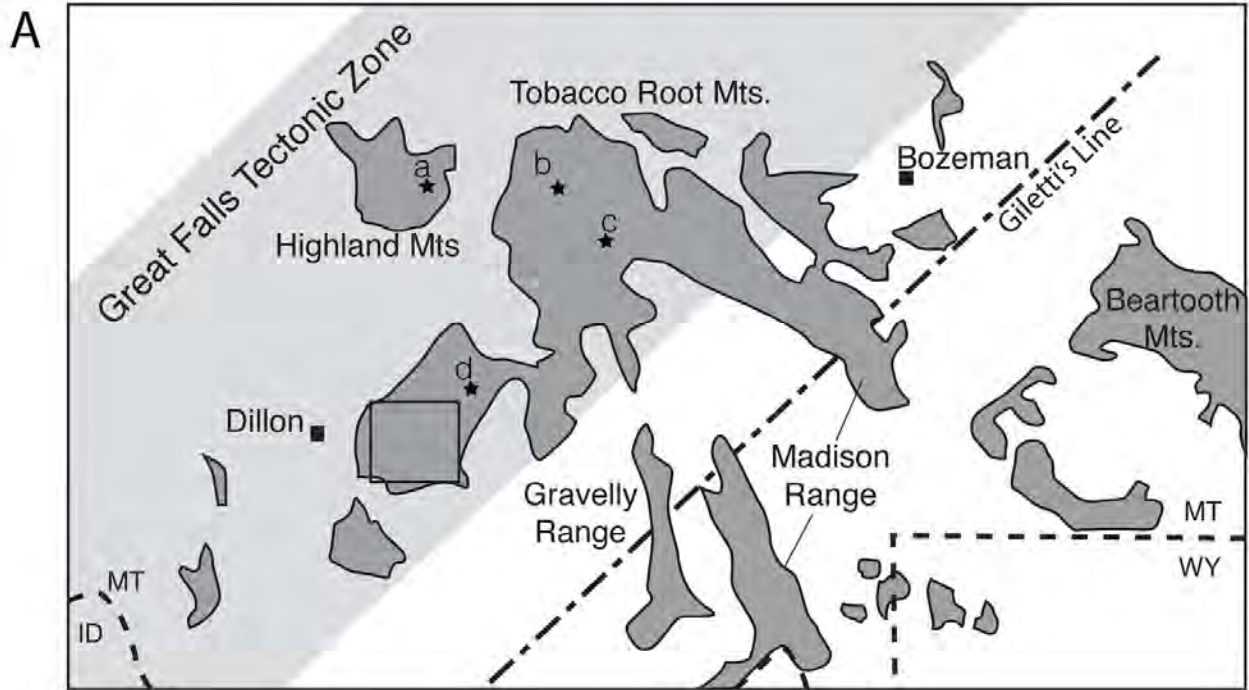


Figure 1A: Generalized geology of the northwest Wyoming craton exposed in Laramide-aged basement uplifts of southwest Montana. Gilletti's line separates rocks that experienced post-2000 Ma metamorphism to the northwest from those that did not. The Great Falls tectonic zone is an area that experienced intense deformation and metamorphism during the ≈ 1780 -Ma Big Sky Orogeny. Stars indicate approximate locations of dated samples within the Montana Metasedimentary terrain outside area discussed in detail: a – 1780^m Ma; b – 2060^z and 1760^m Ma; c – 3300^z , 2780^m and 2450^m ; and d – 2740^z , $2450^{z,m}$ and 1760^m (Cheney et al., 2004; Dahl and Hamilton, 2002; Jones, 2008; Jones et al., 2004; Mueller et al., 2004; Roberts et al., 2002). The z and m superscripts indicate zircon or monazite ages respectively. Map follows Mueller and others (2005) and references therein. Square indicates location of Figure 1B.

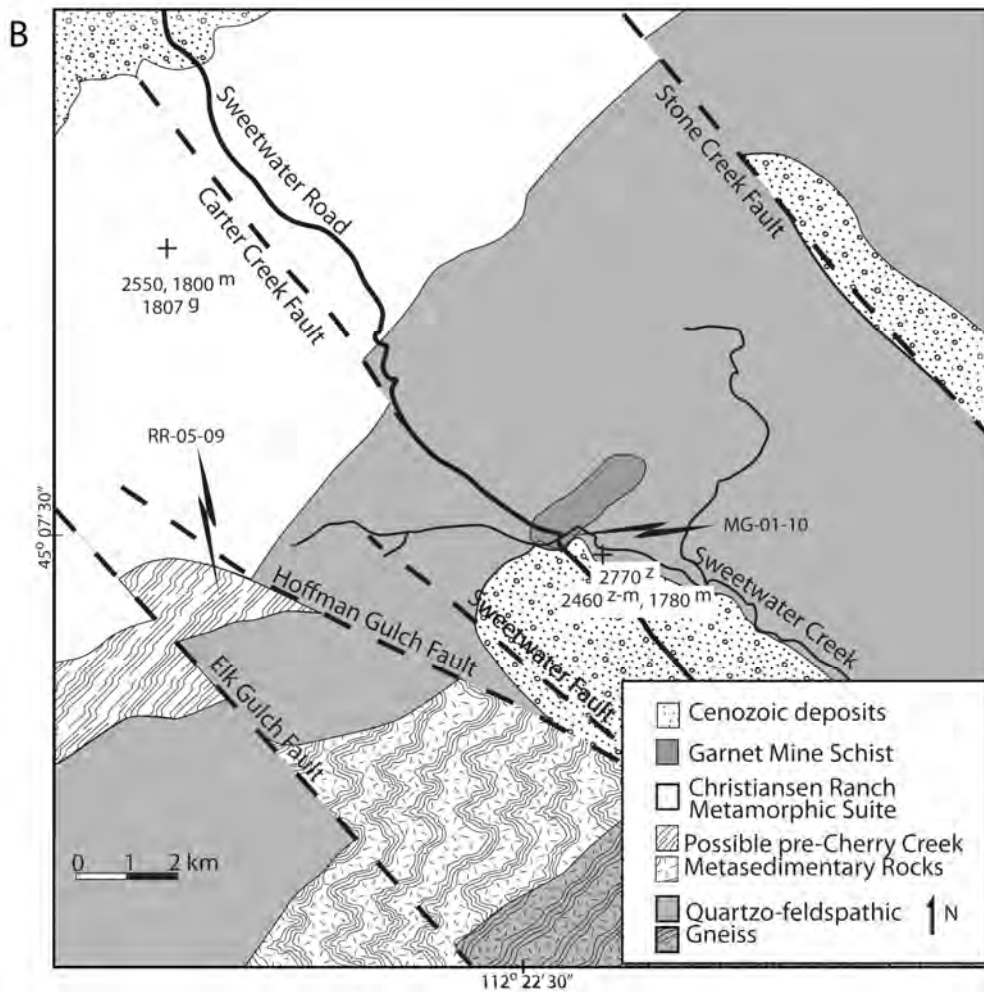


Figure 1B: Geologic map of the southern Ruby Range showing distribution of lithologies (Garihan, 1973; Karasevich, 1980; Karasevich et al., 1981; Okuma, 1971, author's unpublished data) and the approximate locations of previously dated samples (Jones, 2008; Roberts et al., 2002). Superscripts are z – zircon, m – monazite, and g – garnet. Approximate locations of the garnet leucogneiss, RR-05-09, and Garnet Mine Schist, Mg-01-10, are indicated by sample number and arrow. UTM coordinates for RR-05-09 are 12 T 385031 E, 4996749 N.

relative ages of the suites are derived from structural relationships observed in the Gravelly and Madison Ranges where the sequences were first described (Erslev, 1983; Erslev and Sutter, 1990; Hadley, 1969). An additional metasedimentary sequence has also been tentatively identified in the Gravelly Range (O'Neill and Christiansen, 2004). These rocks are of lower metamorphic grade and so might be Paleoproterozoic in age (O'Neill and Christiansen, 2004). However, field rela-

tions are inconclusive because no Cherry Creek sequence rocks are found between the Pre-Cherry Creek rocks and the lower-grade metamorphics.

Both the Cherry Creek and Pre-Cherry Creek correlatives have been identified in the Ruby Range (Figure 1B). The Christensen Ranch metamorphic suite, located to the northwest, is dominated by metasedimentary rocks with banded-iron formation and abundant marble. It has been associated with the Cherry Creek sequence (Dahl, 1979; Garihan, 1973; James, 1990; Karasevich, 1980; Karasevich et al., 1981; Okuma, 1971). In the eastern

parts of the range there are limited exposures of metasedimentary rocks that do not include marble and, therefore, have been assumed to be Pre-Cherry Creek rocks. Among these is a small area of metasedimentary rocks exposed northeast of Sweetwater Creek that is mostly hornblende-biotite-garnet and biotite-garnet schists with muscovite or sillimanite or both, named herein the Garnet Mine Schist (Figures 1 and 2).

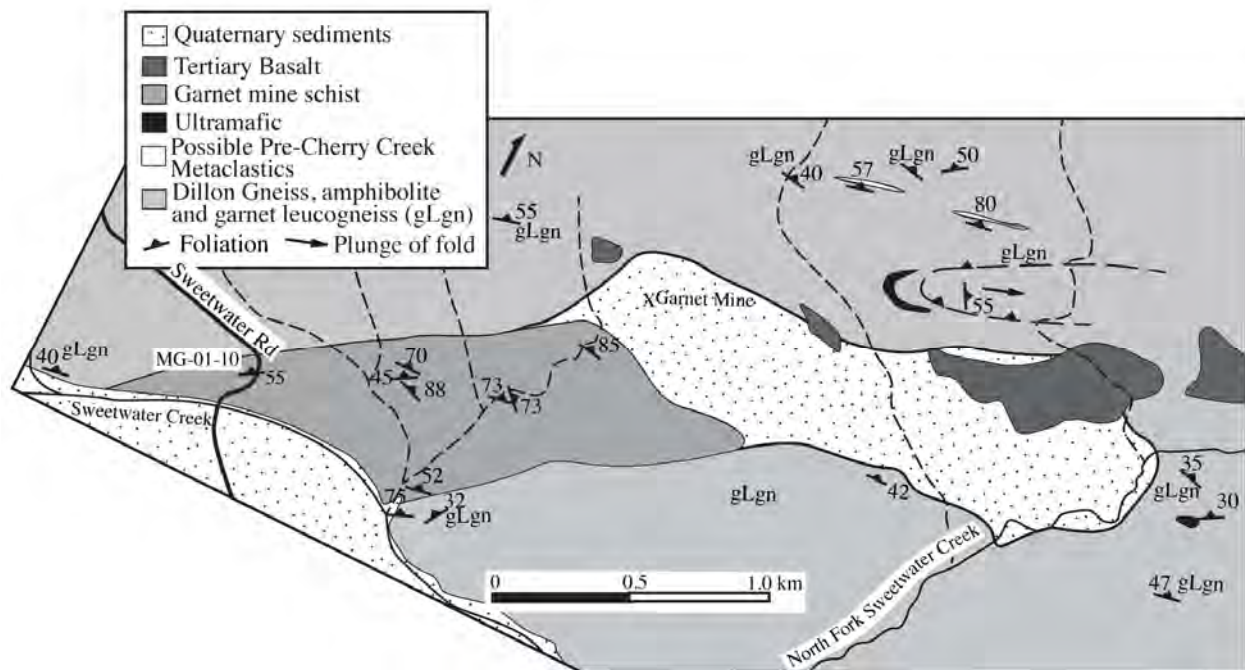


Figure 2: Geologic map of portion of the Sweetwater Basin showing outcrop pattern of Garnet Mine Schist. Area is dominated by Dillon gneiss that includes garnet leucogneiss, amphibolite, and minor metaclastics that are primarily quartzite. Outcrops with garnet leucogneiss indicated by gLgn. UTM coordinates for MG-01-10 are 12T, 392198 E and 4997780 N.

A sample of hornblende-biotite-garnet schist from this locale was collected for geochronologic analysis as part of a study attempting to establish relationships among the metasedimentary rocks of the southeastern Ruby Range that lie structurally below the Christiansen Ranch sequence (Figures 1 and 2). The expectation was that zircons extracted from the schist would yield metamorphic ages ≈ 2450 and ≈ 1780 Ma, similar to ages obtained from a granitic gneiss that lies within a kilometer of the sampled schist (Jones, 2008; Jones et al., 2004; Roberts et al., 2002). However, only ages ≈ 1770 Ma were obtained. Subsequent field work has confirmed these rocks surpassed the first but not the second sillimanite isograd and so are lower grade than the surrounding gneiss. Garnet leucogneiss, common within the older Dillon gneiss adjacent to the schists, is not found within them. Weighted mean $^{207}\text{Pb} / ^{206}\text{Pb}$ ages ranging

from 2413 to 2438 Ma, depending on the age of common lead found in the zircons, were obtained for zircons from the leucogneiss and are inferred to date emplacement of the gneiss protolith.

When combined, these data indicate that the Garnet Mine Schist does not belong to the Archean Pre-Cherry Creek sequence. Instead its protoliths were deposited after the ≈ 2450 -Ma regional metamorphism and garnet leucogranite intrusions. These data provide evidence that a Paleoproterozoic sedimentary basin formed within the Montana Metasedimentary terrain after ≈ 2450 Ma but prior to the ≈ 1780 -Ma Big Sky Orogeny. The Big Sky Orogeny is thought to be related to collision of the Wyoming craton with the Medicine Hat Block to the northwest (Dahl et al., 1999; Mueller et al., 2005; O'Neill, 1998).

Geologic Setting

The Wyoming craton is a mostly Archean terrain that has been subdivided into three provinces, including the Montana Metasedimentary terrain of southwestern Montana (Mogk et al., 1992; Mueller et al., 1993; Roberts et al., 2002). This terrain includes metasedimentary rocks and granitoid gneisses with ages of 3200-3300 Ma and 2700-2800 Ma. The terrain experienced major metamorphic events at ≈ 2700 , ≈ 2450 , and ≈ 1780 Ma in the northwestern part of the terrain (Cheney et al., 2004; Erslev and Sutter, 1990; James and Hedge, 1980; Jones, 2008; Mueller et al., 2004; Roberts et al., 2002). Rocks that experienced this later event lie to the northwest of Giletti's line (Giletti, 1966) and either southeast of or within the Great Falls tectonic zone that marks the northwestern boundary of the craton (Figure 1A). The Great Falls tectonic zone includes Paleoproterozoic and older rock metamorphosed during the ≈ 1780 Big Sky Orogeny.

Two metasedimentary sequences have been identified within the Montana Metasedimentary terrain and correlated across the region even though differences among the correlated lithologies have been recognized between ranges. The Cherry Creek sequence was originally described in the Gravelly Range, extended to the Madison Range (Erslev, 1983; Erslev and Sutter, 1990; Hadley, 1969) and then across the broader region. It includes marbles and banded-iron formation as well as other metasedimentary rocks, amphibolites, and orthogneiss. Its lower contact with granitoid gneiss and associated metasedimentary rocks as observed in the Madison Range was determined to be a metaconglomerate and interpreted to represent an unconformity (Erslev, 1983). The second suite of rocks, basement to the Cherry Creek sequence, is dominated by quartzofeldspathic

gneiss with distinctive metasedimentary rocks that do not include either marble or banded-iron formation. Because this sequence lies beneath the unconformity, it was named the Pre-Cherry Creek sequence. Archean ^{40}Ar - ^{39}Ar ages indicating Archean protoliths were obtained from hornblende, biotite, and muscovite from both sequences in the Madison Range (Erslev and Sutter, 1990).

O'Neill and Christiansen (2004) reported a possible third metamorphic suite including metasedimentary rocks and metagabbro in the northern Gravelly Range. The base of this sequence lies on Pre-Cherry Creek metamorphics and is separated from the Cherry Creek sequence by sediments in an extensive Tertiary to Quaternary basin. Because these rocks are of lower metamorphic grade than the Cherry Creek and Pre-Cherry Creek sequences, they were interpreted to be a distinct Paleoproterozoic unit that was deposited after the ≈ 2450 regional metamorphic event. However, it is also possible that they are the same age as the Cherry Creek rocks but represent a higher structural level that experienced less intense metamorphism.

In the Ruby Range, the Christiansen Ranch metamorphic suite (James, 1990) has been correlated with the Cherry Creek sequence. These rocks are predominantly metasediments that include banded-iron formation and abundant dolomitic marble. They comprise the majority of rocks exposed on the western slope of the southern half of the range (Figure 1B). The Christiansen Ranch suite structurally overlies the Dillon gneiss. Immediately to the east the gneiss includes relatively thin but laterally extensive marble bodies (Garihan, 1973; James, 1990; Karasevich, 1980; Karasevich et al., 1981; Okuma, 1971). Further east, the marble disappears and the remainder of the range is dominated by quartzofeldspathic gneiss

with amphibolite and minor metaclastic rock (Garihan, 1973; Karasevich, 1980; Karasevich et al., 1981; Okuma, 1971; authors' unpublished data). Within this expanse of gneiss there is a small area, about two km², of garnetiferous schist with both muscovite and sillimanite (Figures 1 and 2).

Contacts between the schists and the surrounding gneiss are not exposed, but foliations appear to be structurally conformable, dipping moderately to steeply to the northwest. Because these metasedimentary rocks lie structurally below the Christiansen Ranch sequence and because they contain neither marble nor banded-iron formation, they have been correlated with the Pre-Cherry Creek sequence (Garihan, 1973; James, 1990; Karasevich, 1980; Karasevich et al., 1981; Okuma, 1971).

U-Pb dating of zircon and monazite has yielded consistent ages across the Montana Metasedimentary terrain (Figure 1). Protolith ages for granitoid gneiss are ≈ 3300 and 2780 Ma (Cheney et al., 2004; Dahl et al., 2002; Jones, 2008; Jones et al., 2004; Mueller et al., 2004; Roberts et al., 2002). Both an Archean and an early Proterozoic metamorphic event have been inferred from zircon and monazite as occurring at ≈ 2700 and 2450 Ma (Cheney et al., 2004; Jones, 2008; Jones et al., 2004; Mueller et al., 2004; Roberts et al., 2002). A third event, the ca ≈ 1780 -Ma Big Sky Orogeny is limited in extent to areas west of Giletti's line that separates rocks that experienced the Big Sky Orogeny from those that did not (Cheney et al., 2004; Jones, 2008; Jones et al., 2004; Mueller et al., 2004; Roberts et al., 2002). One other age of significance, 2060 Ma, is reported as the intrusive age of a metamorphosed mafic dike in the Tobacco Root Mountains (Mueller et al., 2005). The intrusion of mafic magma may represent a period of crustal extension and possible rifting.

Age data specific to the Ruby Range (Figure 1B) include a protolith age for the Dillon gneiss at ≈ 2770 Ma (Alcock and Muller, 2010; Jones, 2008; Jones et al., 2004). Zircons from some of these gneisses also provide evidence for metamorphism at ≈ 2450 Ma (Jones, 2008; Jones et al., 2004). Younger zircon ages, limited to highly discordant ages obtained from thin rims visible in backscatter images, may indicate the later Big Sky event. Monazite from the gneiss yields both ≈ 2450 Ma and ≈ 1780 Ma ages and so indicate that the Ruby Range also experienced the periods of Paleoproterozoic metamorphism inferred from age data obtained elsewhere in the Montana Metasedimentary terrain (Jones, 2008; Jones et al., 2004).

Christiansen Ranch metasedimentary rocks yield ages recording a ≈ 1780 -Ma event (Jones, 2008; Jones et al., 2004; Roberts et al., 2002). A single age of 2550 Ma from monazite within garnet provides tentative evidence that the protolith dates from the Archean (Jones, 2008). Zircons from a Christiansen Ranch quartzite yielded only one, probably metamorphic, age younger than 2850 Ma. The absence of younger detrital zircons would be consistent with the Christiansen Ranch metasedimentary rocks having originally been deposited in the Archean (Mueller et al., 1998). However neither datum is conclusive in establishing an Archean origin for the metasedimentary rocks.

Sample descriptions

Mg-01-10, Garnet Mine Schist

This sample of schist was collected in the Sweetwater Basin from an outcrop along the Sweetwater Road near the western edge of an area with abundant metasedimentary rocks. The schist has mafic and felsic layering. The more mafic layers consist primar-

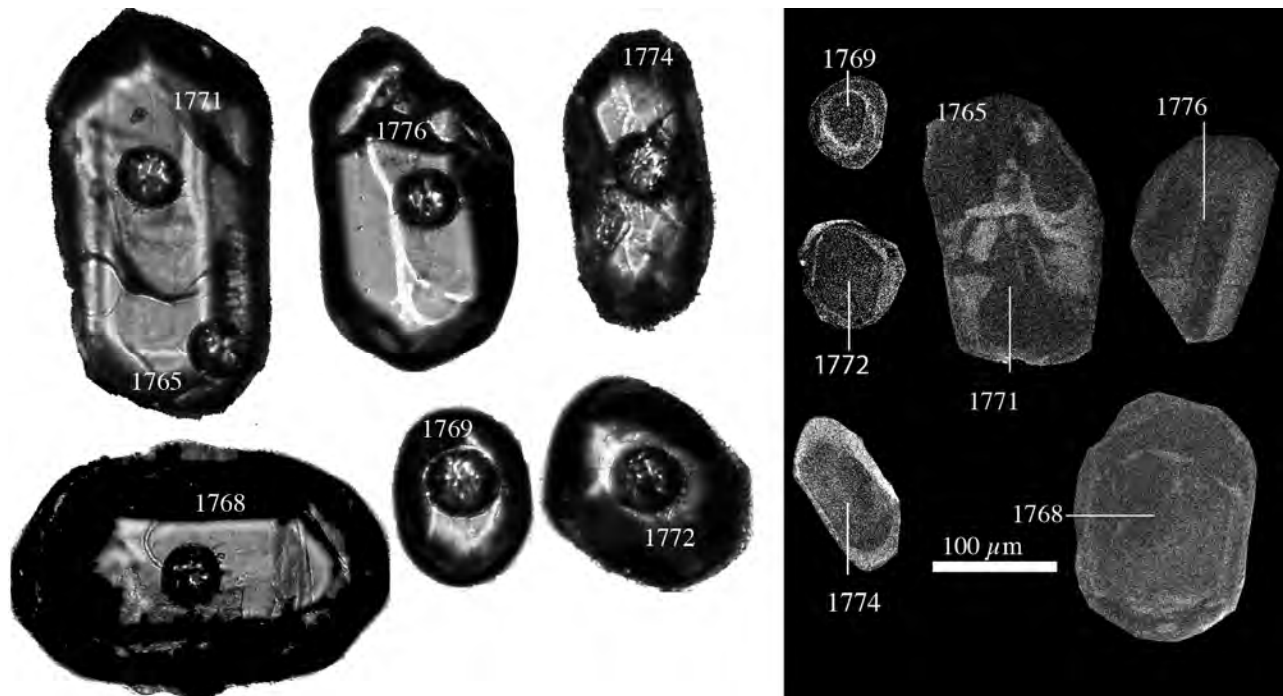


Figure 3: Images taken in plane-polarized light of representative zircons showing morphology and location of laser-ablation analyses. Ages (in Ma) are given for accepted spot analyses that can be identified by pit visible in image. Inset: Cathodoluminescent images that have been enhanced to increase zoning contrast. Ages can be used to correlate images.

ily of hornblende, biotite and garnet. Felsic layers contain mostly quartz and two feldspars. Neither primary muscovite nor sillimanite is present in the sample, but both occur in other schists of the area. Secondary sericite and chlorite are present. Zircon grains seen in thin section are small, generally $< 50 \mu\text{m}$, within biotite or hornblende, identifiable by high birefringence and pleochroic haloes.

RR-05-09, Garnet leucogneiss

The garnet leucogneiss with associated garnet pegmatite and garnet leucogranite is a common lithology found within Dillon gneiss and associated metasedimentary rocks that occur structurally below the Christiansen Ranch metamorphic suite. Gneiss, granite, and pegmatite are predominantly quartz and microcline with areas of abundant garnet and minor biotite and sillimanite. In some locations, pyroxene occurs, seemingly in place of garnet. Sample RR-

05-09 is from a leucogneiss that cuts a calcisilicate-rich marble. Zircon is a common accessory, visible in thin section as intergranular grains.

Methods

Approximately five kilograms of each sample were crushed and the zircons separated from the powder using standard heavy liquid and magnetic techniques. Analytical procedures used to determine U and Pb isotopic contents of the zircon are those of the University of Arizona LaserChron Center for Laser Ablation-Multicollector-Inductively Coupled Plasma-Mass Spectrometry (LA-ICPMS). Details of analytical methods are described in Gehrels et al. (2008). Raw data are reduced using the NUagecalc software prepared by the Center and Isoplot software (Ludwig, 2008) for determining isochron and weighted mean ages.

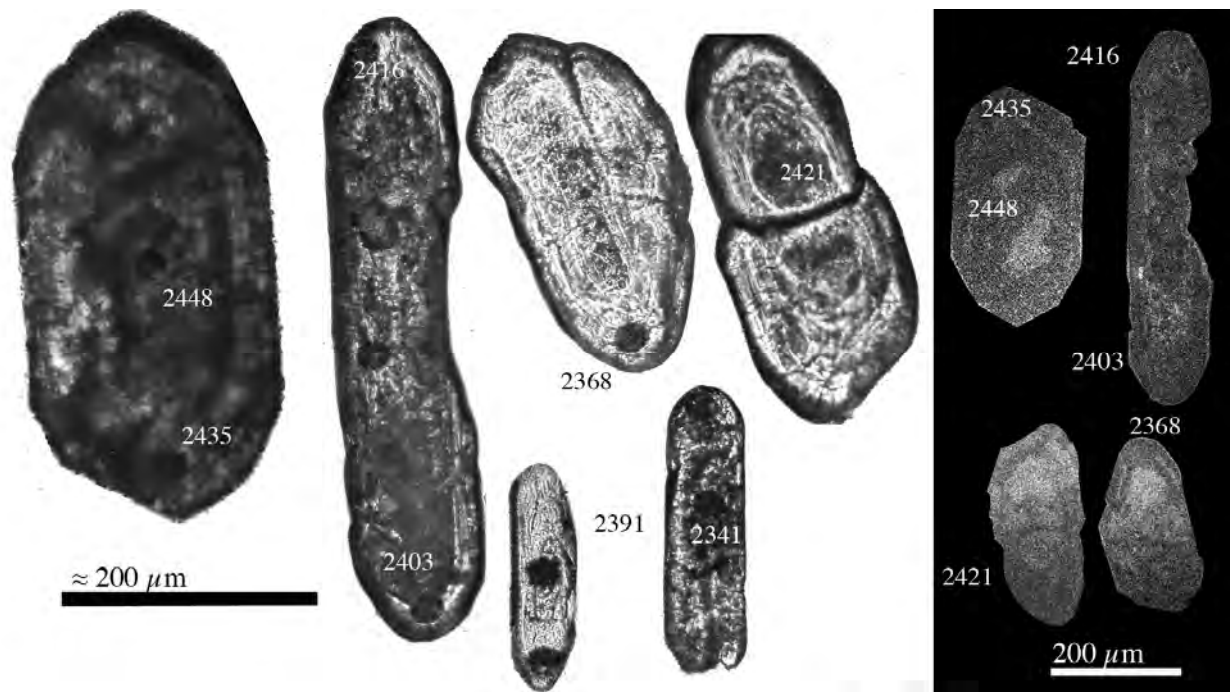


Figure 4: Images taken in plane-polarized light of representative zircons showing morphology and location of laser-ablation analyses. Ages (in Ma) are given for accepted spot analyses that can be identified by pit visible in image. Inset shows cathodoluminescent images that have been enhanced to increase zoning contrast. Limited contrast is probably a result of radiation damage resulting from high uranium content. However, the apparent concentric zoning in both plane-polarized light and cathodoluminescence is consistent with a magmatic origin.

Geochronology

Garnet Mine Schist, Mg-01-10

Zircons from Mg-01-10 are mostly equant with an approximate aspect ratio between 1:1 and 2:1 and $\leq 100 \mu\text{m}$ in diameter (Figure 3A). A few grains are larger and others more prismatic. Color ranges from clear to lavender. Cathodoluminescent images reveal irregular, faint zoning (Figure 3B).

Sixteen grains were subjected to eighteen analyses. Ten of the analyses yielded concordant or nearly concordant ages with low error (Table 1 and Figure 5). Together they give a weighted mean $^{207}\text{Pb}/^{206}\text{Pb}$ age of $1769 \pm 2.6 \text{ Ma}$ (2s). Of the eight other analyses two yielded somewhat older ages, $\approx 1850 \text{ Ma}$. Both had large error, $>100 \text{ Ma}$,

and were, therefore, not statistically distinct from the mean age. Other ages were similar to 1770 Ma or younger. Neither grain size nor analysis location within a grain affected the results.

Garnet leucogneiss, RR-05-09

Zircons from RR-05-09 are prismatic, mostly greater than $200 \mu\text{m}$ in the long dimension. In plane polarized light, the grains are dark brown to clear, contain numerous small inclusions, and appear to be metamict (Figure 4). Cathodoluminescent images reveal faint zoning, some concentric, and other irregular.

Twenty-five analyses were conducted on 15 grains. All were rich in uranium and contained high levels of common lead. Th/U ratios are low, all but one less than 0.1

Table 1: U-Pb geochronologic analyses.

Analysis	U		U/Th		Isotope ratios			Apparent ages (Ma)						Conc (%)					
	206Pb (ppm)	204Pb	206Pb*	207Pb*	235U*	206Pb* (%)	238U (%)	206Pb* (%)	238U (%)	206Pb* (Ma)	235U (Ma)	206Pb* (Ma)	207Pb* (Ma)		Best age (Ma)	± (Ma)			
RR0509-1A1	5336	518	18.8	6.2753	1.6	11.3928	30.4	0.5185	30.4	1.00	2692.9	670.8	2555.8	291.6	2448.8	26.5	2448.8	26.5	110.0
RR0509-1A2	6202	374	6.6	6.3262	1.3	8.6906	24.4	0.3987	24.4	1.00	2163.2	448.9	2306.1	226.1	2435.1	22.8	2435.1	22.8	88.8
RR0509-1B1 <i>a</i>	4585	394	19.4	6.0958	1.6	12.4626	7.6	0.5510	7.5	0.98	2829.3	171.2	2639.9	71.9	2497.8	26.7	2497.8	26.7	113.3
RR0509-1C1	5112	449	54.2	6.3789	0.4	10.4358	7.2	0.4828	7.2	1.00	2539.5	151.8	2474.2	67.2	2421.1	6.6	2421.1	6.6	104.9
RR0509-3B1 <i>a</i>	4407	230	19.2	6.6112	12.7	3.4622	17.0	0.1660	11.4	0.67	990.1	104.4	1518.6	135.0	2360.2	217.6	2360.2	217.6	41.9
RR0509-3B2 <i>a</i>	4454	631	35.9	6.5802	0.4	5.3138	3.4	0.2536	3.4	0.99	1457.0	44.5	1871.1	29.4	2368.2	6.8	2368.2	6.8	61.5
RR0509-3C	4251	137	54.7	6.6847	5.3	9.1257	39.9	0.4424	39.6	0.99	2361.5	786.6	2350.7	382.6	2341.3	91.2	2341.3	91.2	100.9
RR0509-5C1	4219	313	30.0	6.3278	4.1	8.7454	13.0	0.4014	12.3	0.95	2175.3	227.4	2311.8	118.8	2434.7	69.6	2434.7	69.6	89.3
RR0509-5C2	6759	155	10.6	6.5786	4.4	5.6228	33.0	0.2683	32.7	0.99	1532.0	446.7	1919.6	292.3	2368.6	74.3	2368.6	74.3	64.7
RR0509-5C3	5319	232	24.9	6.2104	1.8	11.1546	3.5	0.5024	3.0	0.85	2624.2	64.8	2536.1	32.8	2466.4	31.0	2466.4	31.0	106.4
RR0509-6A1 <i>a</i>	3630	231	29.4	6.4914	3.4	4.4737	5.6	0.2106	4.5	0.80	1232.1	50.2	1726.1	46.5	2391.4	57.3	2391.4	57.3	51.5
RR0509-6A2 <i>a</i>	4298	189	22.7	6.8314	9.3	2.8951	22.0	0.1434	19.9	0.91	864.1	161.1	1380.6	167.3	2304.1	159.8	2304.1	159.8	37.5
RR0509-6C1 <i>a</i>	3842	2235	91.1	6.6858	0.6	10.2132	5.8	0.4952	5.8	1.00	2593.3	123.4	2454.3	53.8	2341.0	9.6	2341.0	9.6	110.8
RR0509-8A1 <i>a</i>	4904	311	19.6	6.7010	3.8	10.6053	6.9	0.5154	5.7	0.83	2679.8	124.9	2489.2	63.9	2337.1	65.8	2337.1	65.8	114.7
RR0509-8A2	3908	275	20.0	6.4443	0.8	7.5665	5.5	0.3536	5.4	0.99	1952.0	91.2	2180.9	49.1	2403.7	13.1	2403.7	13.1	81.2
RR0509-8A3	4918	432	12.8	6.3948	1.5	9.1218	7.3	0.4231	7.2	0.98	2274.4	137.1	2350.3	67.0	2416.9	25.9	2416.9	25.9	94.1
RR0509-10A <i>a</i>	3974	1674	23.5	6.1908	0.5	12.0425	7.6	0.5407	7.6	1.00	2786.4	171.6	2607.7	71.3	2471.7	8.1	2471.7	8.1	112.7
RR0509-10A2 <i>a</i>	3341	534	25.7	6.0690	1.4	17.1359	14.8	0.7543	14.7	1.00	3623.2	408.6	2942.5	142.8	2505.2	23.3	2505.2	23.3	144.6
MG-01-10-5A	2162	1962	4.9	9.7187	0.6	2.8034	2.0	0.1976	1.9	0.95	1162.4	20.2	1356.5	14.9	1677.0	11.0	1677.0	11.0	69.3
MG-01-10-5B	1290	52237	16.0	9.6636	0.7	2.3302	2.4	0.1633	2.3	0.96	975.2	20.8	1221.5	17.1	1687.5	13.1	1687.5	13.1	57.8
MG-01-10-5C1	920	2164	14.8	8.9582	6.7	5.3799	14.4	0.3495	12.7	0.89	1932.4	212.9	1881.7	123.8	1826.1	121.4	1826.1	121.4	105.8
MG-01-10-5C2	1680	11175	58.9	10.3214	0.9	1.7506	4.7	0.1310	4.7	0.98	793.8	34.8	1027.4	30.6	1565.0	16.9	1565.0	16.9	50.7
MG-01-10-15A	567	902641	4.4	9.2467	0.2	4.8671	2.0	0.3264	2.0	0.99	1820.9	31.8	1796.6	17.0	1768.4	4.3	1768.4	4.3	103.0
MG-01-10-15B	937	7461	4.1	9.2254	0.5	4.7950	2.9	0.3208	2.9	0.98	1793.8	45.2	1784.0	24.7	1772.6	9.8	1772.6	9.8	101.2
MG-01-10-15C	408	188114	3.2	9.2615	0.3	4.7808	1.9	0.3211	1.8	0.99	1795.2	28.9	1781.5	15.7	1765.5	5.7	1765.5	5.7	101.7
MG-01-10-15D	590	368461	15.9	9.2332	0.2	4.8423	1.0	0.3243	1.0	0.98	1810.5	15.4	1792.3	8.4	1771.1	3.1	1771.1	3.1	102.2
MG-01-10-14B	274	130525	6.3	9.3083	0.6	4.7359	3.7	0.3197	3.6	0.98	1788.4	56.6	1773.6	30.8	1756.3	11.6	1756.3	11.6	101.8
MG-01-10-14D <i>a</i>	863	5845	16.3	9.3627	0.4	4.2274	3.8	0.2871	3.8	0.99	1626.8	54.5	1679.4	31.3	1745.6	7.3	1745.6	7.3	93.2
MG-01-10-12A	269	10068	2.3	9.2511	0.7	4.7693	1.7	0.3200	1.6	0.92	1789.7	24.7	1779.5	14.4	1767.5	12.4	1767.5	12.4	101.3
MG-01-10-12B	689	49623	14.5	9.2685	0.3	4.7355	3.2	0.3183	3.2	0.99	1781.6	50.2	1773.5	27.2	1764.1	6.3	1764.1	6.3	101.0
MG-01-10-12BC	538	182938	5.9	9.2208	0.4	4.7436	1.3	0.3172	1.2	0.96	1776.2	19.1	1775.0	10.8	1773.5	6.6	1773.5	6.6	100.2
MG-01-10-10C	553	256829	3.1	9.2445	0.4	4.7244	1.3	0.3168	1.2	0.95	1773.9	18.9	1771.6	10.7	1768.9	7.1	1768.9	7.1	100.3
MG-01-10-10B	424	93417	2.5	9.2304	0.6	4.6718	1.4	0.3128	1.3	0.90	1754.3	19.2	1762.2	11.6	1771.6	11.1	1771.6	11.1	99.0

a - Analyses not included in weighted mean age determinations for excess error or discordance

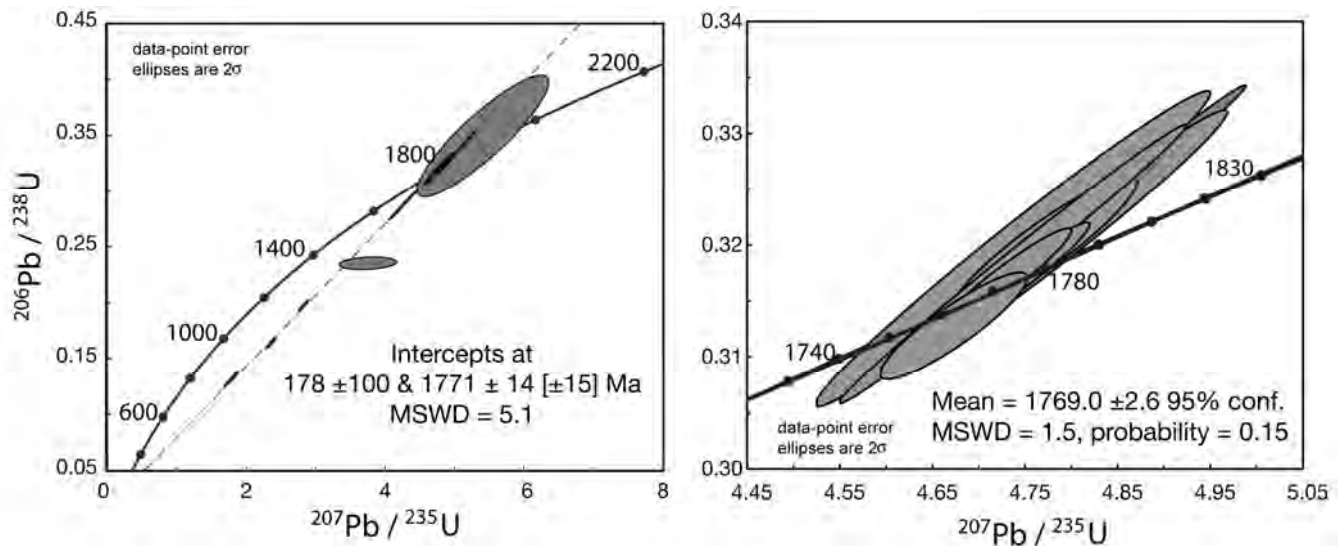


Figure 5: Concordia diagrams presenting results of U-Pb isotopic analysis of zircons from sample MG-01-10, Garnet Mine Schist. All analyses except one with very high error are included to produce an isochron indicating an age of 1771 ± 14 Ma with high MSWD (mean square of weighted deviates). B. Weighted mean of $^{207}\text{Pb}/^{206}\text{Pb}$ ages of 1769 ± 2.6 Ma and low MSWD for ten low-error, nearly concordant zircon analyses.

(Table 1). Seven analyses were rejected for ratios of $^{206}\text{Pb}/^{204}\text{Pb}$ that were less than 125. An additional eight were excluded for high error (> 100 Ma, 2σ) or severe discordance ($< 60\%$ or $> 110\%$ concordant). Nine of the remaining ten analyses from seven grains yield a weighted mean $^{207}\text{Pb}/^{206}\text{Pb}$ age of 2420 ± 8.1 Ma ($2s$). All 25 analyses yielded $^{207}\text{Pb}/^{206}\text{Pb}$ ages between 2305 and 2580 Ma. Neither grain size, location within the grain, nor grain appearance could be correlated with age.

The high common lead content of the zircons increases uncertainty regarding the robustness of the $^{207}\text{Pb}/^{206}\text{Pb}$ age given above. Because the source and age of common lead contamination is uncertain, correcting for its presence introduces an error. To better estimate the size of the error, one may establish a range of possible ages for the leucogneiss by correcting for common lead with different ages. To do this, the common lead correction procedure used by the NUagecalc data reduction program was altered to make corrections assuming various common lead ages between 0 and 3500

Ma. The effect of common lead age on the apparent age of the leucogneiss is small. Calculated age varies between 2413 ± 9 and 2438 ± 9 Ma (2σ) (Figure 6).

Discussion

The ≈ 1770 Ma $^{207}\text{Pb}/^{206}\text{Pb}$ ages of zircon from the Garnet Mine Schist are consistent with metamorphism during the regional Big Sky Orogeny, and the ages are much younger than 2450 Ma. It is therefore unlikely that the metapelite experienced high-grade regional metamorphism at either ≈ 2700 or ≈ 2450 Ma, implying that its protolith was deposited after those events.

Two alternative interpretations might be considered. First, the ≈ 1770 -Ma metamorphic event could have caused all of the older zircon to be dissolved so that the zircon U-Pb system was entirely reset. However, zircon is commonly included within biotite and hornblende. Therefore, not only zircon, but also all biotite and hornblende from the earlier events would have to have been entirely recrystallized. There is no

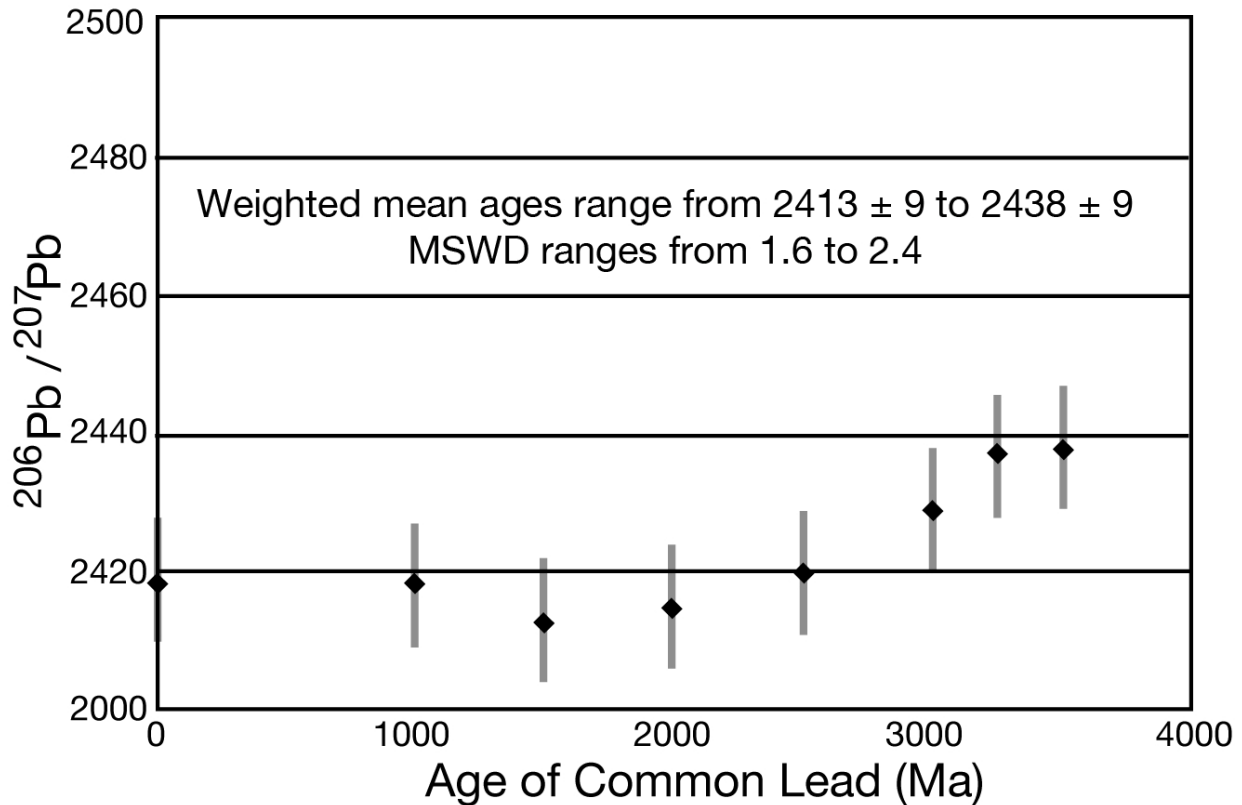


Figure 6: Weighted mean $^{207}\text{Pb}/^{206}\text{Pb}$ ages for 10 analyses from sample RR-05-09 that are between 60% and 110% concordant and with a 2σ error < 100 Ma. Different ages for common lead are used to correct for high common lead found in the zircons. Each data point represents the weighted mean age and 2σ error obtained for a particular common lead age using the NUagecalc data reduction software. Although potential error in any reported age is higher than the standard deviation because of high amounts of common lead, the data indicate that the garnet leucogneiss is unlikely to be derived from an Archean protolith.

evidence for reactions like biotite dehydration melting that would have caused it to recrystallize, nor is there evidence for major dissolution and regrowth induced by deformation. For these reasons it seems unlikely that an earlier population of zircons was eliminated from the assemblage.

A second possibility is that sampling produced a biased population of ages. Although this possibility cannot be eliminated, the same is true for every attempt to use accessory minerals to date a sample. Methods of separation might cause a small population of distinct grains to be missed. However, of the zircons separated and mounted, care was given to analyze grains

of different appearance and to analyze different locations within grains. No correlation was observed between age and appearance or location.

Other evidence supports the inference that the protolith of the Garnet Mine Schist did not originate in the Archean. For example, the ≈ 2420 Ma $^{207}\text{Pb}/^{206}\text{Pb}$ age of the garnet leucogneiss is interpreted to date the intrusion of the gneiss protolith towards the end of the ≈ 2450 -Ma regional metamorphic event. The prismatic habit and the faint concentric zoning of many grains visible in the cathodoluminescent images are typical of magmatic zircons. Although the very low Th/U ratios are more typical of meta-

morphic zircons, their habit and appearance as well as their occurrence within a metaigneous rock suggest that the zircons do not have a metamorphic origin.

Instead, the low Th/U ratio may reflect the origin of the protolith's magma. Garnet leucogranite is thought to form during decompression-driven melting of metapelites (Harris and Massey, 1994; Patiño Douce and Harris, 1998; Streule et al., 2010). If this is the origin of the leucogneiss, then the magma might form in association with a metamorphic fluid that would impact the trace element chemistry of the magma and the zircons that formed during later crystallization. Because the ≈ 2420 -Ma age is somewhat younger than the previously identified ≈ 2450 -Ma metamorphic event, and because garnet leucogranite is associated with decompression melting in other orogenic belts, we propose that age of the leucogneiss dates a period of extensional collapse following crustal thickening ≈ 2450 Ma.

For the purpose of this study, the intrusive age of leucogneiss is significant because it sets an upper limit on the age of the Garnet Mine Schist. The leucogneiss is a common lithology found within Dillon gneiss and related amphibolite and metaclastic rock that surround the Garnet Mine Schist, but it is not found within the schist (Figure 2). It follows, therefore, that the schist protolith is younger than the leucogneiss. Thus the effect of common lead on the preciseness of the apparent age of the leucogneiss is less important than the potential range of ages that might result under reasonable assumptions for the age of the common lead. So long as the maximum likely intrusive age of the leucogneiss is ≈ 2450 Ma, then added uncertainty caused by the presence of common lead in the zircon is not critical to the discussion and conclusions of this paper.

As discussed above, a range of possible ages was determined. The results indicate that the age of the gneiss is similar to the previously recognized regional metamorphism ≈ 2450 , and it is reasonable to conclude that its protolith intruded during that early Proterozoic metamorphic event. Because the leucogranite did not intrude the Garnet Mine Schist, it follows that the schist protolith was deposited in a Paleoproterozoic sedimentary basin after the ≈ 2450 -Ma regional metamorphism and intrusion of the leucogneiss protolith.

A possible origin for such a sedimentary basin might be either continued extension and crustal thinning after 2420 Ma, as inferred from the age of the garnet leucogneiss, or during a younger period of extension and possible rifting that has been inferred from the 2060-Ma intrusive age of a metamorphosed mafic dike in the Tobacco Root Mountains (Mueller et al., 2005). There are numerous small- to moderate-sized ultramafic bodies of unknown age in the Ruby Range that might be related to the Spuhler Peak mafic dikes and also indicate crustal thinning and mantle melting. If this happened at ≈ 2060 Ma, a sedimentary basin would be expected. The Garnet Mine metasedimentary rocks of the Sweetwater Basin may preserve a small part of that sedimentary history.

The geochronologic evidence presented here is the first to confirm that some metasedimentary rocks within the Montana Metasedimentary terrain have a Paleoproterozoic protolith. Because these metasedimentary rocks had previously been correlated with the Pre-Cherry Creek sequence of the Madison Range, the age of their protolith requires that prior inferences of the original ages for other metasedimentary rocks in the region that are external to the Madison and Gravelly Ranges be re-examined. For example, monazite and garnet ages from the

Christiansen Ranch Metasedimentary Sequence in the western Ruby Range do not provide conclusive evidence for early Proterozoic metamorphism and by extension for an Archean origin, although the rocks of the Christiansen Ranch sequence appear to be quite similar lithologically to the Archean Cherry Creek sequence of the Madison and Gravelly Ranges.

Detrital zircons establish a maximum age of 2.85 Ga (Mueller et al., 1998). A single monazite grain from within a garnet yielded an age ≈ 2550 Ma (Jones, 2008) perhaps indicative of garnet and monazite growth at that time. However, it is worth noting that the igneous protolith of quartzofeldspathic gneiss of the Ruby Range has an age of ≈ 2770 Ma, and so is distinctly younger than those of the other ranges. Without additional data, the age and source of the Christiansen Ranch sequence remains problematic.

Rocks of the Tobacco Root Mountains to the north of the Ruby Range also present problems of correlation. Mueller et al. (2004) studied detrital and metamorphic zircons from that region. Within the three units studied, two yielded strong evidence for metamorphism during the ≈ 2450 Ma event. The third, the Spuhler Peak Metamorphic Suite, did not. One zircon extracted from a quartzite from the Spuhler Peak suite yielded a ≈ 2450 -Ma age while the great majority of ages were older than 3000 Ma. Mueller and others (2004) recognized that interpretation of the ≈ 2450 -Ma zircon is problematic as it is unclear if it is detrital or if it grew *in situ* during a metamorphic event. However, they favored interpreting the grain as metamorphic, which would imply an Archean protolith.

In the same volume, Cheney et al. (2004) reported monazite ages from a number of metasedimentary rocks and amphibolites

from the Tobacco Roots. Again, two of three units preserve ample evidence of a ≈ 2450 -Ma metamorphic event. However, monazites from the Spuhler Peak Metamorphic Suite yield ages of only ≈ 1770 Ma. Cheney et al. (2004) considered that the distinct metamorphic history of the Spuhler Peak suite suggested it is an allochthonous terrain added to the Montana Metasedimentary terrain during the Big Sky Orogeny.

In a discussion of possible tectonic provenance of the Spuhler Peak suite, Cheney et al. (2004) interpret the chemistry of its mafic rocks to indicate that it has an oceanic origin, possibly in a back arc basin (Harms et al., 2004). If this interpretation is correct, the Spuhler Peak suite is most likely Proterozoic in age. The evidence from the Ruby Range that a sedimentary basin formed in what is now southwestern Montana after 2450 Ma raises the possibility that the Garnet Mine Schists and the Spuhler Peak suite originated in different parts of a single basin. The schist protoliths were perhaps deposited in a near-shore environment on continental crust while the Spuhler Peak suite originated as oceanic crust and deepwater sediments that formed as the basin expanded.

Conclusion

A metamorphic age of ≈ 1770 Ma for the Garnet Mine Schist from the Sweetwater basin of the Ruby Range establishes that the protolith was deposited after a regional ≈ 2450 -Ma event. This interpretation is supported by the fact that ≈ 2420 -Ma garnet leucogneiss that is common within Dillon gneiss and related rocks surrounding the Garnet Mine Schist does not occur within it. It follows that the Garnet Mine protoliths were deposited in the Paleoproterozoic. Recognition of early Proterozoic sedimentation within the Montana Metasedimentary terrain requires a more careful re-

evaluation of the age of other metasedimentary rocks in the region and the assumed correlation of units among the various ranges of southwestern Montana.

Acknowledgements

Research has been supported by several Faculty Development Grants provided by Pennsylvania State University, Abington College.

References cited

- Alcock, J., and Muller, P.D., 2010, Contact anatexis at circa 2100 Ma in metapelites adjacent to Wolf Creek ultramafics, southern Ruby Range, SW Montana: Geological Society of America, Abstracts with Programs, v. 42(5), p. 415.
- Cheney, J.T., Webb, A.A., Coath, C.D., and McKeegan, K.D., 2004, In situ ion microprobe $^{207}\text{Pb}/^{206}\text{Pb}$ dating of monazite from Precambrian metamorphic suites, Tobacco Root Mountains, Montana: *in* Brady, J.B., Burger, H.R., Cheney, J.T., and Harms, T.A., eds., Precambrian geology of the Tobacco Root Mountains, Montana: Geological Society of America Special Paper 337, p. 151-179.
- Dahl, P.S., 1979, Comparative geothermometry based on major-element and oxygen isotope distributions in Precambrian metamorphic rocks of Southwestern Montana: *American Mineralogist*, v. 64, p. 1280-1293.
- Dahl, P.S., Holm, D.K., Gardner, E.T., Hubacher, F.A., and Foland, K.A., 1999, New constraints on the timing of Early Proterozoic tectonism in the Black Hills (South Dakota) with implications for the docking of the Wyoming province with Laurentia: *Geological Society of America Bulletin*, v. 98, p. 1335-1349.
- Dahl, P.S., Hamilton, M.A., Terry, M.P., Roberts, H.J., Kelley, S.P., Frei, R., Jercinovic, M.J., and Williams, M.L., 2002, Comparative ion and electron microprobe dating of Wyoming Province monazite, with tectonic and analytical implications: *Geological Society of America, Abstracts with Programs*, v. 31(1).
- Erslev, E.A., 1983, Pre-Beltian geology of the southern Madison Range, Southwestern Montana: Montana Bureau of Mines and Geology Memoir 55, 26 p.
- Erslev, E.A., and Sutter, J.F., 1990, Evidence for Proterozoic mylonitization in the northwestern Wyoming province: *Geological Society of America Bulletin*, v. 102, p. 1681-1694.
- Garihan, J.M., 1973, Geology and talc deposits of the central Ruby Range, Madison County, Montana: Ph.D. thesis, Geosciences, Pennsylvania State University, University Park, PA.
- Gehrels, G.E., Valencia, V.A., and Ruiz, J., 2008, Enhanced precision, accuracy, efficiency, and spatial resolution of U-Pb ages by laser ablation-multicollector-inductively coupled plasma-mass spectrometry: *Geochimistry Geophysics Geosystems*, v. 9(3). doi:10.1029/2007GC001805.
- Giletti, B.J., 1966, Isotopic ages from southwestern Montana: *Journal of Geophysical Research*, v. 71 p. 4029-4036.
- Hadley, J.B., 1969, Geologic map of the Cameron quadrangle, Madison County, Montana: U.S. Geological Survey Geologic Quadrangle Map GQ-813, scale 1:62500.
- Harms, T.A., Brady, J.B., Burger, H.R. and Cheney, J.T., 2004, Advances in the geology of the Tobacco Root Mountains, Montana, and their implications for the history

of the northern Wyoming province: *in* Brady, J.B., Burger, H.R., Cheney, J.T., and Harms, T.A., eds., Precambrian geology of the Tobacco Root Mountains, Montana: Geological Society of America Special Paper 337, p. 227-243.

Harris, N., and Massey, J., 1994, Decompression and anatexis of Himalayan metapelites: *Tectonics*, v. 13, p. 1537-1546.

James, H.L., 1990, Precambrian geology and bedded iron deposits of the southwestern Ruby Range, Montana: U.S. Geological Survey Professional Paper 1495.

James, H. L., and Hedge, C.E., 1980, Age of basement rocks of southwest Montana: *Geological Society of America Bulletin*, v. 91 p. 11-15.

Jones, C.L., Dahl, P.S., Wooden, J.L., Mazdab, F.K., and Tracy, R.J., 2004, Geochronology of U-bearing accessories from Precambrian metamorphic rocks, Ruby Range, SW Montana: Deciphering geological events that shaped the NW Wyoming Province: *Geological Society of America Abstracts with Programs*, v. 36(5), p. 568.

Jones, C.L., 2008, U-Pb geochronology of monazite and zircon in Precambrian metamorphic rocks from the Ruby Range, SW Montana: Deciphering geological events that shaped the NW Wyoming province: M.Sc. thesis, Kent State University, Kent, OH.

Karasevich, L.P., 1980, Structure of the pre-Beltian metamorphic rocks of the northern Ruby Range, Southwestern Montana: M.Sc. thesis, Pennsylvania State University, University Park, PA.

Karasevich, L.P., Garihan, J.M., Dahl, P.S., and Okuma, A.F., 1981, Summary of Precambrian metamorphic and structural his-

tory, Ruby Range, southwest Montana: *Montana Geological Society Field Conference and Symposium Guidebook to Southwest Montana*, p. 225-237.

Ludwig, K., 2008, Isoplot 3.70, A geochronological toolkit for Microsoft Excel: Berkeley Geochronology Center Special Publication No. 4.

Mogk, D., Mueller, P., and Wooden, J., 1992, The significance of Archean terrane boundaries: evidence from the northern Wyoming Province: *Precambrian Research*, v. 55, p. 155-168.

Mueller, P.A., Shuster, R.D., Wooden, J.L., Erslev, E.A., and Bowes, D.R., 1993, Age and composition of Archean crystalline rocks from the southern Madison Range, Montana: Implications for crustal evolution in the Wyoming Craton: *Geological Society of America Bulletin*, v. 105, p. 437-446.

Mueller, P.A., Wooden, J.L., Nutman, A.P., and Mogk, D.W., 1998, Early Archean crust in the northern Wyoming province: Evidence from U-Pb ages of detrital zircons: *Precambrian Research*, v. 91, p. 285-307.

Mueller, P.A., Burger, H.R., Heatherington, A., Wooden, J., Mogk, D.W., and D'Arcy, K., 2004, Age and evolution of the Precambrian crust, Tobacco Root Mountains, Montana: *in* Brady, J.B., Burger, H.R., Cheney, J.T., and Harms, T.A., eds., Precambrian geology of the Tobacco Root Mountains, Montana: Geological Society of America Special Paper 337, p. 181-202.

Mueller, P.A., Burger, H.R., Wooden J.L., Brady, J.B., Cheney, J.T., Harms, T.A., Heatherington, A.L., and Mogk, D.W., 2005, Paleoproterozoic metamorphism in the Northern Wyoming Province: Implications for assembly of Laurentia: *Journal of Geology*, v. 113, p. 169-179.

Okuma, A.F., 1971, Structure of the southwestern Ruby Range near Dillon, Montana: Ph.D. thesis, Pennsylvania State University, University Park, PA.

O'Neill, J.M., 1998, The Great Falls tectonic zone, Montana-Idaho: an early Proterozoic collisional orogen beneath and south of the Belt Basin: *in* R.B. Berg, ed., Belt Symposium III, Montana Bureau of Mines and Geology, Special Publication 112, p. 222-228.

O'Neill, J.M., and Christiansen, R.L., 2004, Geologic map of Hebgen Lake quadrangle, Beaverhead, Madison, and Gallatin Counties, Montana, Park and Teton Counties, Wyoming, and Clark and Fremont Counties, Idaho: U.S. Geological Survey Scientific Investigations Map 2816, scale 1:100,000.

Patiño Douce, A.E., and Harris, N., 1998, Experimental constraints on Himalayan anatexis: *Journal of Petrology*, v. 39, p. 689-710.

Roberts, H., Dahl, P., Kelly, S., and Frei, R., 2002, New ^{207}Pb - ^{206}Pb and ^{40}Ar - ^{39}Ar ages from SW Montana, USA: constraints on the Proterozoic and Archaean tectonic and depositional history of the Wyoming Province: *Precambrian Research*, v. 117, p. 119-143.

Streule, M.J., Searle, M.P., Waters, D.J., and Horstwood, M.S.A., 2010, Metamorphism, melting and channel flow in the Greater Himalayan Sequence and Makalu leucogranite: Constraints from thermobarometry, metamorphic modeling, and U-Pb geochronology: *Tectonics*, v. 29: TC5011, doi:10.1029/2009TC002533.

*Lower Falls of the Yellowstone,
by William Henry Jackson, 1871.
Courtesy National Park Service.*



AGE AND COMPOSITION OF CRYSTALLINE BASEMENT IN THE ARMSTEAD ANTICLINE, SOUTHWESTERN MONTANA

Paul Mueller

Department of Geological Sciences, University of Florida, Gainesville, FL 32605

David Mogk

Department of Earth Science, Montana State University, Bozeman, MT 59715

Joseph Wooden

Department of Earth Sciences, Stanford University, Stanford, CA 94305

Abstract

Precambrian crystalline basement is exposed in the core of the Armstead anticline in Beaverhead County, Montana. U-Pb ages of zircon from two samples of quartzofeldspathic gneiss exposed near Clark Canyon Reservoir suggest the protolith formed in the late Archean (2729 ± 15 Ma), but was likely overprinted twice in the Paleoproterozoic (~ 2.45 and ~ 1.8 Ga). Rare earth element abundances show a typical granitic pattern with (chondrite) normalized La of ~ 300 and strong negative Eu anomalies for both samples. Sm-Nd isotopic data yield depleted mantle model ages in the Mesoarchean (~ 3.3 - 3.5 Ga). The primary age of ~ 2730 Ma is uncommon in the major basement uplifts of southwestern Montana (e.g., Ruby, Tobacco Root, Madison, and Highland Ranges), but does match ages of migmatitic gneisses and the youngest detrital zircons reported from the Gravelly Range. This age does, however, correspond closely with the emplacement of the

Stillwater Complex, which suggests a possible link to post-orogenic collapse of the ~ 2800 Ma Beartooth orogen.

Introduction

The Armstead anticline (Figure 1) is one of several Sevier thrust structures in southwestern Montana that has exposed crystalline basement (e.g., O'Neill et al., 1990; Figure 1). Previous work (e.g., Kellogg et al., 2004; Foster et al., 2006) demonstrated that many of the exposures (e.g., Tendoy Mountains, Pioneer Mountains, Biltmore

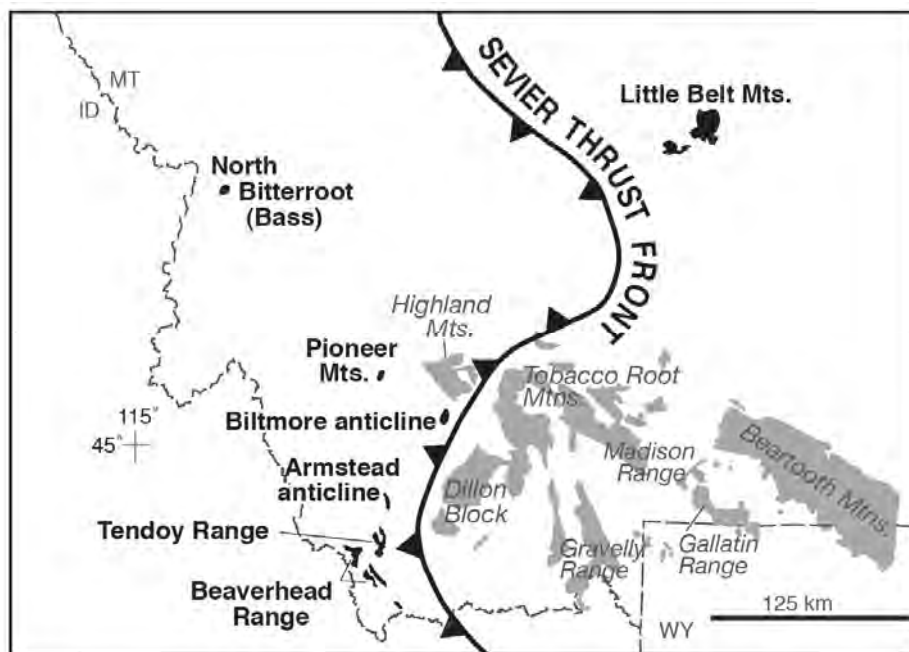


Figure 1. Schematic map of basement uplifts and structures in southwest Montana showing location of Armstead anticline (from Foster et al., 2006).

anticline, etc.) were exclusively Paleoproterozoic (1.7-2.5 Ga). In addition, Mueller et al. (2005, 2011) demonstrated that Archean crust in the Highland and Tobacco Root Mountains was remobilized during the Great Falls orogeny (also known as Big Sky Orogeny) at ~1800 Ma and by an earlier event at ~2450 Ma (herein named the Tendoy Orogeny). The Tendoy event is poorly understood, but pervasive in crystalline basement of southwestern Montana. Although a previous report by our group showed that crystalline basement west of the Blacktail Mountains is typically Proterozoic, no data were reported from the Armstead anticline (Foster et al., 2006). In this paper we present trace element and isotopic data, including U-Pb zircon geochronologic data that show that crystalline basement exposed in the Armstead anticline (Armstead gneiss) has a primary Archean age that is distinctly younger than the vast majority of Archean basement exposed in the Tobacco Root, Highland, and Ruby Ranges immediately to the east. These data may reflect recycling of this older basement based on Sm-Nd model ages and distinct, negative Eu anomalies.

Samples and Methods

Samples (~10 kg) were collected on Henneberry Ridge along Forest Service Road 1893 (N44.59.922, W112.53.943). Whole rocks were crushed and prepared for geochemical analysis of major elements (XRF), trace elements (high resolution ICP), isotopic compositions (multi-collector ICP), and U-Pb zircon geochronology (SHRIMP-RG). Details of these methods can be found in Mueller et al. (2010).

Results

U-Pb geochronology

Zircons previously imaged using cathodoluminescence were analyzed for U and Th concentrations along with Pb isotopic compositions *in situ* using ~30 micrometer diameter primary ion beams of the SHRIMP-RG ion microprobe. The resulting data for sample AA-1 (32 analyses) and AA-2 (4 analyses) are shown in Table 1. Of the 32 analyses of AA-1, ten have Th/U ratios of 0.1 or less, which is indicative of hydrothermal growth. These ages are commonly viewed as representative of a period of

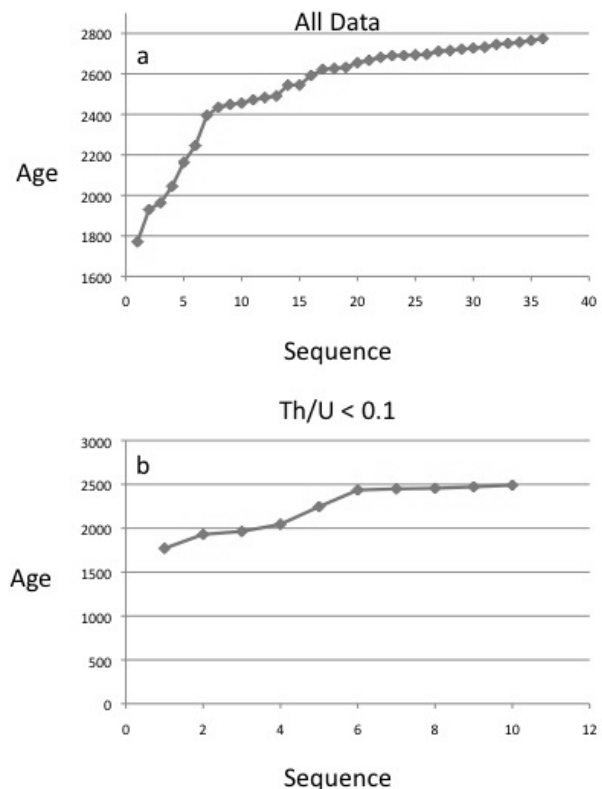


Figure 2. U-Pb ages ($^{207}\text{Pb}/^{206}\text{Pb}$) plotted sequentially for: a) all data regardless of discordance and b) all data with $\text{Th}/\text{U} < 0.1$. There is a clear tendency for the highest ages in (a) to be concentrated in the 2700-2750 Ma range and for low Th/U data to be concentrated in the 2400-2500 Ma range (b).

Table 1.

Sample/Grain	U ppm	Th ppm	Th/U	²⁰⁶ Pb/ ²⁰⁶ Pbc	²⁰⁶ Pb/ ²³⁸ U Age	1σ err	²⁰⁷ Pb/ ²⁰⁶ Pb Age	1σ err	%D	²³⁸ U/ ²⁰⁶ Pb	% err	²⁰⁷ Pb/ ²⁰⁶ Pb	% err	²⁰⁷ Pb/ ²³⁵ U	% err	²⁰⁶ Pb/ ²³⁸ U	% err
AA1-1	50	37	0.77	0.000	2780	59	2732	13	-2	1.854	2.6	0.189	0.8	14.04	2.7	0.539	2.6
AA1-2	223	90	0.42	0.000	2688	55	2691	10	0	1.933	2.5	0.184	0.6	13.14	2.6	0.517	2.5
AA1-3	45	28	0.64	0.000	2693	58	2696	14	0	1.929	2.6	0.185	0.9	13.21	2.8	0.518	2.6
AA1-4	194	178	0.95	0.025	2750	56	2722	7	-1	1.879	2.5	0.188	0.4	13.77	2.5	0.532	2.5
AA1-5	197	43	0.23	0.019	2152	46	2395	9	10	2.523	2.5	0.154	0.6	8.44	2.6	0.396	2.5
AA1-6	55	42	0.78	0.032	2735	58	2727	13	13	1.892	2.6	0.188	0.8	13.72	2.7	0.528	2.6
AA1-7	86	37	0.44	0.345	2099	16	2545	17	21	2.598	0.9	0.169	1.0	8.96	1.3	0.385	0.9
AA1-8	107	44	0.43	0.000	2291	20	2667	60	16	2.343	1.0	0.182	3.6	10.68	3.7	0.427	1.0
AA1-9	884	654	0.77	0.021	2293	8	2690	6	17	2.341	0.4	0.184	0.4	10.84	0.6	0.427	0.4
AA1-10	71	32	0.46	0.000	2401	46	2592	31	8	2.216	2.3	0.174	1.8	10.80	2.9	0.451	2.3
AA1-11	575	272	0.49	0.014	2458	9	2694	7	10	2.154	0.4	0.185	0.4	11.81	0.6	0.464	0.4
AA1-12	1080	32	0.03	0.007	2253	7	2449	26	9	2.390	0.4	0.159	1.5	9.19	1.6	0.418	0.4
AA1-13	2659	1444	0.56	0.005	2244	4	2632	4	17	2.401	0.2	0.178	0.2	10.21	0.3	0.416	0.2
AA1-14	940	781	0.86	0.000	2473	7	2655	8	7	2.139	0.4	0.180	0.5	11.62	0.6	0.467	0.4
AA1-15	648	72	0.12	0.000	1949	8	2163	10	11	2.832	0.5	0.135	0.5	6.57	0.7	0.353	0.5
AA1-16	88	59	0.69	0.039	3570	23	2712	18	6	2.042	1.1	0.187	1.1	12.60	1.5	0.490	1.1
AA1-17	57	30	0.55	0.749	2108	23	2483	72	18	2.585	1.3	0.163	4.3	8.67	4.5	0.387	1.3
AA1-18	929	816	0.91	0.009	2493	6	2682	4	8	2.118	0.3	0.183	0.3	11.92	0.4	0.472	0.3
AA1-19.1	236	193	0.85	0.000	2432	13	2715	10	12	2.182	0.6	0.187	0.6	11.81	0.9	0.458	0.6
AA1-20	180	49	0.28	0.094	2286	17	2627	23	15	2.350	0.9	0.177	1.4	10.40	1.6	0.426	0.9
AA1-21	192	59	0.32	0.000	2366	13	2622	11	11	2.255	0.7	0.177	0.6	10.80	0.9	0.443	0.7
AA1-22R	1917	48	0.03	0.018	1729	4	1771	7	2.376	3.250	0.3	0.108	0.4	4.59	0.5	0.308	0.3
AA1-23R	933	40	0.04	0.759	1944	6	1663	26	1.0087	2.841	0.4	0.120	1.6	5.85	1.6	0.352	0.4
AA1-24R	628	26	0.04	0.125	2158	13	2435	21	12.86	2.516	0.7	0.158	1.2	8.66	1.4	0.398	0.7
AA1-25R	1209	29	0.02	0.090	1648	5	2045	9	10.656	3.012	0.3	0.126	0.5	5.78	0.6	0.332	0.3
AA1-26R	1105	46	0.04	0.377	1615	6	1930	15	6.3409	3.075	0.4	0.118	0.9	5.30	0.9	0.325	0.4
AA1-27R	695	20	0.03	0.071	2018	6	2246	7	11.271	2.720	0.3	0.142	0.4	7.17	0.5	0.368	0.3
AA1-28	103	64	0.65	0.053	2677	23	2756	55	2.9658	1.943	1.0	0.192	3.3	13.60	3.5	0.515	1.0
AA1-29	416	127	0.31	0.874	1920	8	2544	10	32.491	2.882	0.5	0.169	0.6	8.07	0.8	0.347	0.5
AA1-30R	699	33	0.05	0.068	2286	8	2456	8	2.9384	2.233	0.4	0.160	0.5	9.88	0.6	0.448	0.4
AA1-31R	1239	55	0.05	0.067	2465	7	2472	5	0.2869	2.147	0.3	0.162	0.3	10.37	0.5	0.466	0.3
AA1-32R	481	45	0.10	0.045	2403	9	2491	29	3.6782	2.214	0.5	0.163	1.7	10.17	1.8	0.452	0.5
AA-2																	
AA2-1.1	396	178	0.46	0.035	2638	11	2750	7	4	1.977	0.5	0.191	0.4	13.31	0.7	0.506	0.5
AA2-2.1	455	185	0.42	0.024	2716	10	2745	7	1	1.909	0.5	0.190	0.4	13.75	0.6	0.524	0.5
AA2-3	419	261	0.64	0.000	2671	11	2774	7	4	1.948	0.5	0.194	0.4	13.71	0.7	0.513	0.5
AA2-4	400	172	0.44	0.000	2620	12	2765	12	5	1.994	0.5	0.193	0.7	13.32	0.9	0.501	0.5

Table 1-A. Summary of U-Pb and Sm-Nd isotopic data for samples AA-1 and AA-2.

AA-1			AA-2		
Element	ppm	Cn	Element	ppm	Cn
La	92.4	290	La	109.9	345
Ce	180.9	221	Ce	222.8	272
Pr	19.0	157	Pr	24.5	203
Nd	71.9	117	Nd	88.4	144
Sm	14.1	70	Sm	22.1	111
Eu	2.5	33	Eu	1.1	14
Gd	14.0	52	Gd	23.8	89
Tb	2.4	48	Tb	4.8	97
Dy	14.6	44	Dy	30.7	93
Ho	3.0	40	Ho	6.1	81
Er	9.0	42	Er	17.5	81
Tm	1.3	41	Tm	2.5	75
Yb	8.5	38	Yb	14.3	65
Lu	1.3	40	Lu	1.9	58
Sr	21.3		Sr	5.0	
Y	88		Y	164.0	
Sm/Nd	0.196		Sm/Nd	0.250	
$^{143}\text{Nd}/^{144}\text{Nd}$	0.51103		$^{143}\text{Nd}/^{144}\text{Nd}$	0.51179	
Tdm	3.46		Tdm	3.30	

Notes:

Italics are data with Th/U < 0.1

206c = common 206Pb in %

all isotopic ratios corrected for common Pb using measured 204Pb prior to age calculation

r = radiogenic (after common Pb correction)

%D = % discordant based on 206/238 age vs. 207/206 age

error columns are all 1 sigma (percent or absolute)

Cn = normalized to chondrites

Table 1-B. Trace elemental data for samples AA-1 and AA-2.

metamorphism during which oxidizing fluids enhanced the mobility of U relative to Th, typically leading to growth of new zircon with low Th/U ratios and high U contents. For example, the ten analyses with Th/U < 0.1 average ~1,000 ppm U; those with Th/U > 0.1 average ~400 ppm U. Using these criteria, a mean, somewhat ad hoc, crystallization age of 2706 ± 11 Ma for the protolith of sample AA-1 can be obtained from the ten oldest analyses with Th/U > 0.1.

Only four zircons from sample AA-2 were analyzed, and none had Th/U < 0.1. Because the ages from AA-1 and AA-2

slightly overlap, they are combined in Figure 2a, which shows a continuum of ages from ~1770 to ~2750 Ma; Figure 2b shows only the low Th/U data (ages from ~1700 to ~2500 Ma). The pattern in Figure 2a suggests that Pb-loss has occurred to a significant degree (up to 32% discordance) in sample AA-1, even in zircons which do not show Th/U < 0.1.

Figure 3 demonstrates the positive correlation between Th/U and $^{207}\text{Pb}/^{206}\text{Pb}$ age for the overall population of zircons analyzed. Using the 13 oldest ages from the combined data set of AA-1 and AA-2 yields an age of 2729 ± 15 Ma for zircons which

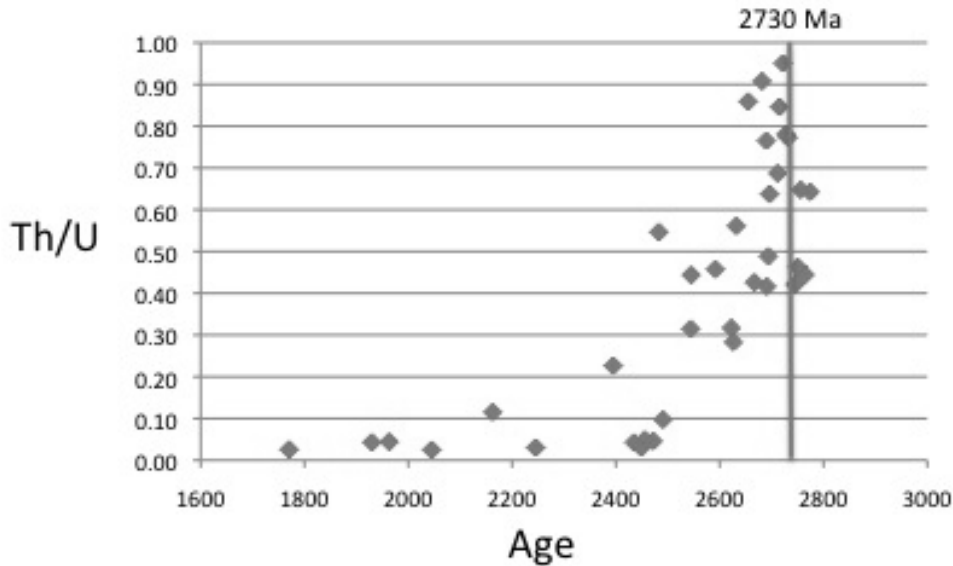


Figure 3. Plot of age ($^{207}\text{Pb}/^{206}\text{Pb}$) for all analyses vs. Th/U ratio showing a clear pattern of decreasing age with decreasing Th/U, even for samples with Th/U > 0.1. Vertical line represents our best estimate of protolith age as discussed in the text.

show discordance <12% no relationship between Th/U and age. This age is within error of the independent age estimate for AA-1 (2706 ± 11 Ma). Within the limitations of the present data, this age (2729 ± 15 Ma) is the best estimate for the time of crystallization of the protolith of the Armstead gneiss.

It is clear from the number of grains with low Th/U ratios in AA-1 and the overall relationship between Th/U and age (Figure 3) that sample AA-1 was affected by hydrothermal alteration during one or more periods in the Proterozoic. The continuum of ages makes it difficult to specify the age or ages of these events, but Figure 2b shows that there is a relatively well defined plateau of ages at ~ 2450 Ma. The youngest age is 1771 ± 7 Ma (2% discordant), within error of the time of crustal anatexis in the

Highland and Tobacco Root Ranges (1777 ± 6 Ma; Mueller et al., 2005). As seen in Table 1, these ages come exclusively from the outer portions of individual zircons (noted by an R next to the grain number in Table 1). It appears likely that the Armstead gneiss also experienced both events because both of these ages (~ 2450 and ~ 1770 Ma) have been reported from

other ranges in southwestern Montana that lie both east and west of the sample locality (Roberts et al., 2002; Cheney et al., 2004; Brady et al., 2004; Mueller et al., 2005, 2011). The limited low Th/U data for sample AA-1, however, means the identification of the 1770 Ma event at Armstead remains tenuous.

Geochemistry

Trace element, particularly rare earth element (REE), abundances in conjunction with Sm-Nd isotopic data suggest the protolith(s) of the Armstead gneiss were mid-crustal, anatectic melts of older crust. For example, Figure 4 shows that REE patterns for samples AA-1 and -2 are similar in three key features: 1) low La/Yb ratios (~ 9), which indicate that minerals that strongly partition any of the REE were not important in the petrogenesis of the protolith; 2) negative Eu anomalies, which require either extensive fractionation of plagioclase from the original magma or that the protolith was simply derived from a plagioclase-bearing source; and 3) the heaviest REEs (e.g., Yb and Lu) are >10 times chondritic abundances, which largely

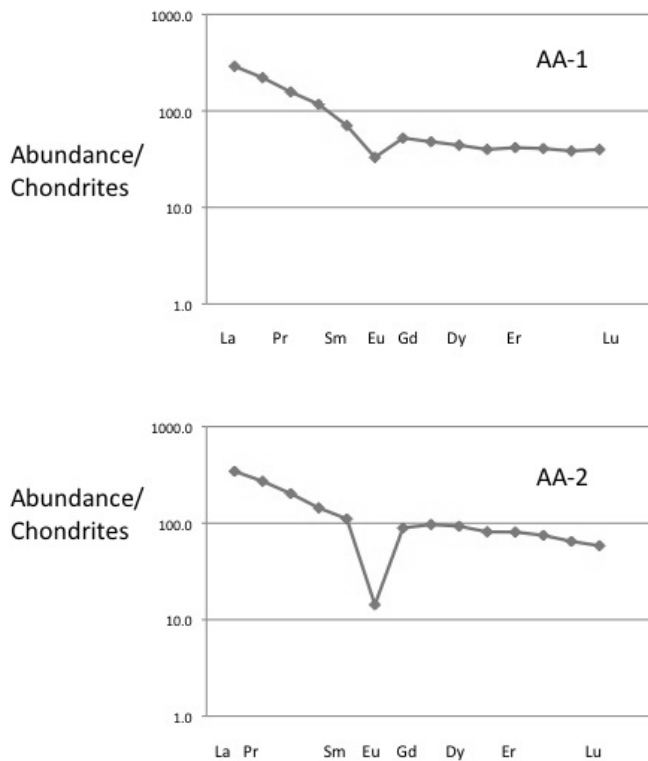


Figure 4. Chondrite normalized REE abundances for samples AA-1 and -2.

precludes equilibrium with garnet, and even makes amphibole an unlikely residual phase. In addition, the low Sr/Y ratios of these two samples also argue against residual garnet in the source and are far too low for common convergent margin magmas such as adakites or Archean tonalite-trondhjemite-granodiorite (TTG) suites (e.g., Martin et al., 2005; Castillo, 2006). In particular, the Sr contents are very low, in consort with the negative Eu anomalies.

The lack of zircon xenocrysts makes it impossible to directly determine the age of the source of the protolith. Sm-Nd depleted mantle model ages (T_{dm}), however, can provide some useful constraints. In this case, both samples AA-1 and -2 yield T_{dm} of ~3400 Ma (Table 1). This model age corresponds to a common crystallization age of metaigneous rocks throughout south-

western Montana (e.g., Mogk et al., 1988, 1992; Mueller et al., 1993, 2004). Many of these rocks represent relatively juvenile magmas, so they also exhibit T_{dm} in the range ~3400 Ma.

Discussion

Confirming an Archean age of the Armstead gneiss, specifically its ~2730 Ma age, helps clarify the distribution of Archean ages previously reported from southwestern Montana. Mueller and Cordua (1976) and later James and Hedge (1980) suggested that much of the crystalline basement of southwestern Montana recorded a tectonothermal event at about 2750 Ma ago based on whole-rock Rb-Sr analyses of quartzofeldspathic gneisses from the Tobacco Root, Ruby, and Gallatin Ranges.

Subsequent, more accurate U-Pb zircon analyses showed that many, if not most, of the basement gneisses were >3000 Ma (e.g., Mueller et al., 1993, 2004; Krogh et al., 2011) and the ~2750 Ma age proposed by James and Hedge (1980) was specifically considered erroneous by Roberts et al. (2002). What is clear at this point, however, is that rocks ~2750 Ma in age do occur in southwestern Montana and the reconnaissance study of James and Hedge (1980) and the site specific study of Mueller and Cordua (1976) did reflect a true geologic event. Later U-Pb zircon-based studies showed metasupracrustal rocks of this age occur in the southern Madison Range (Mueller et al., 1993), are present in detrital zircon suites in low metamorphic grade Archean metasedimentary rocks in the Gravelly Range (Mogk et al., 2004), and correspond to the crystallization age of migmatitic gneisses in the Gravelly Range (Mogk et al., 2004).

Although recognized in several localities, the nature of this event remains cryptic. If

2730 Ma accurately reflects the time of this event, it is only ~50 Ma younger than the major magmatic episode that generated the TTG suite in the Beartooth Mountains (e.g., Mueller et al., 2010). The isolation of this event in time and space, its limited isotopic expression, and the varied rock types yielding this age suggests that this event may be associated with some form of extension. If this is the case, then it may reflect post-orogenic collapse of the Beartooth margin subsequent to the cessation of arc-magmatism at ~2790 Ma. This episode of extension likely lasted until at least ~2700 Ma when the mafic-ultramafic magmas of the Stillwater complex were emplaced in the eastern Beartooth Mountains (Premo et al., 1990) and, perhaps, is the time when other low-grade, apparently allochthonous, supracrustal assemblages were emplaced in the Gravelly Range, southern Madison Range, and the Jardine area of the South Snowy Block (Beartooth Mountains and Yellowstone National Park).

Acknowledgements

Financial support provided by the N.S.F. (EAR-0538133) and the U.S.G.S. (05HQGR0156). D. Spake and G. Kamenov assisted with elemental and isotopic analyses.

References Cited

Brady, John B., Kovaric, Dana N., Cheney, John T., Jacob, Lisa J., and King, Jonathan T., 2004, $^{40}\text{Ar}/^{39}\text{Ar}$ Ages of Metamorphic Rocks from the Tobacco Root Mountains, Montana: *in* Brady, John B., Burger, H. Robert, Cheney, John T., and Harms, Tekla A., eds., Precambrian Geology of the Tobacco Root Mountains, Montana: Geological Society of America Special Paper 377, p. 131-150.

Castillo, P., 2006. An overview of adakite

petrogenesis: Chinese Science Bulletin, v. 51, p. 257-268.

Cheney, John T., Webb, A., Coath, C., and McKeegan, K., 2004, In situ ion microprobe $^{207}\text{Pb}/^{206}\text{Pb}$ dating of monazite from Precambrian metamorphic rocks, Tobacco Root Mountains, Montana: *in* Brady, John B., Burger, H. Robert, Cheney, John T., and Harms, Tekla A., eds., Precambrian Geology of the Tobacco Root Mountains, Montana: Geological Society of America Special Paper 377, p. 151-180.

Foster, D., Mueller, P., Vogl, J., Mogk, D., and Wooden, J., 2006, Proterozoic evolution of the western margin of the Wyoming Craton: Implications for the tectonic and magmatic evolution of the northern Rocky Mountains: Canadian Journal of Earth Science, v. 43, p. 1601-19.

James, H.L., and Hedge, C.E., 1980, Age of the basement rocks of southwest Montana: Geological Society of America Bulletin, v. 91, p. 11-15.

Kellogg, K., Snee, L., and Unruh, D., 2004, The Mesoproterozoic Beaverhead impact structure and its tectonic setting, Montana-Idaho: $^{40}\text{Ar}/^{39}\text{Ar}$ and U-Pb constraints: Journal of Geology, 111: 639-652.

Krogh, T., Kamo, S., Hanley, T., Hess, D., Dahl, P., and Johnson, R., 2011, Geochronology and geochemistry of Precambrian gneisses, metabasites, and pegmatite from the Tobacco Root Mountains, northwestern Wyoming craton, Montana: Canadian Journal of Earth Science, v. 48, p. 161-185.

Mogk, D., Mueller, P., and Wooden, J., 2004, Tectonic implications of late Archean-early Proterozoic supracrustal rocks in the Gravelly Range, SW Montana: Geological Society of America Abstracts with Programs, v. 36, no. 5, p. 507.

Mogk, D., Mueller, P., and Wooden, J., 1992, The significance of Archean terrane boundaries: Evidence from the northern Wyoming Province: *Precambrian Research*, v. 55 p. 155-168.

Mogk, D.W., Mueller, P.A., and Wooden, J.L., 1988, Tectonic aspects of Archean continental development in the North Snowy Block, Beartooth Mountains, Montana: *Journal of Geology*, v. 96 p. 125-141.

Mueller, P., Wooden, J., Mogk, D., Henry, D., and Bowes, D., 2010, Rapid growth of an Archean continent by arc magmatism: *Precambrian Research*, v. 183, p. 70-88.

Mueller, P., Burger, H., Wooden, J., Brady, J., Cheney, J., Harms, T., Heatherington, A., and Mogk, D., 2005, Age and tectonic implications of Paleoproterozoic metamorphism in the northern Wyoming Province: *Journal of Geology*, v. 111, p. 169-179.

Mueller, P., Wooden, J., Heatherington, A., Burger, H., Mogk, D. and D'Arcy, K., 2004, Age and evolution of the Precambrian crust of the Tobacco Root Mountains: *in* Brady, John B., Burger, H. Robert, Cheney, John T., and Harms, Tekla A., eds., *Precambrian Geology of the Tobacco Root Mountains, Montana*: Geological Society of America Special Paper 377, p. 181-202.

Mueller, P.A., Shuster, R., Wooden, J., Erslev, E., and Bowes, D., 1993, Age and composition of Archean crystalline rocks from the southern Madison Range: Implications for crustal evolution in the Wyoming craton: *Geological Society of America Bulletin*, v. 105, p. 437-446.

Mueller, P.A., and Cordua, W.S., 1976, Rb-Sr whole rock age of gneisses from the Horse Creek Area, Tobacco Root Mountains, Montana. *Ischron/West*, no. 16, pp. 33-36.

O'Neill, M., Schmidt, C., and Genovese, P., 1990, Dillon cutoff-Basement-involved tectonic link between the disturbed belt of west-central Montana and the overthrust belt of extreme southwestern Montana: *Geology*, v. 18, p. 1107-1110.

Premo, W., Helz, R., Zientek, M., and Langston, R., 1990, U-Pb and Sm-Nd ages for the Stillwater Complex and its associated sills and dikes, Beartooth Mountains, Montana: Identification of a parent magma: *Geology*, v. 18, p. 1065-1068.

Roberts, H., Dahl, P., Kelley, S. and Frei, R., 2002, New 207Pb-206Pb and 40Ar-39Ar ages from SW Montana, USA: constraints on the Proterozoic and Archean tectonic and depositional history of the Wyoming Province: *Precambrian Research*, v. 117, p. 119-143.



Old Faithful. Courtesy National Park Service.

ROAD LOG FOR THE HEBGEN LAKE EARTHQUAKE AREA

Michael Stickney

*Montana Bureau of Mines and Geology, 1300 W Park St., Butte, MT 59701,
mstickney@mtech.edu*

Introduction

This road log describes features related to the August 17, 1959, magnitude 7.3 Hebgen Lake earthquake, which are still visible after more than 50 years. The geologic interpretations are based on decades of geologic mapping and studies by dozens of earth scientists. Stop 5 will require walking on a half-mile trail that is normally decent, but it may be muddy if wet; sturdy hiking shoes are recommended.

The field trip begins at the Earthquake Lake Visitor's Center in Madison Canyon. To reach the Visitor's Center from West Yellowstone, drive north on Highway 191 for 8.7 miles (14.0 km) and turn left (west) on Highway 287. Drive 20.2 miles (32.5 km) west to the Madison slide and turn right (north) into the Earthquake Lake Visitor Center. Follow the paved road to the left to the uppermost parking lot. Figure 1 shows the field trip route.

STOP 1

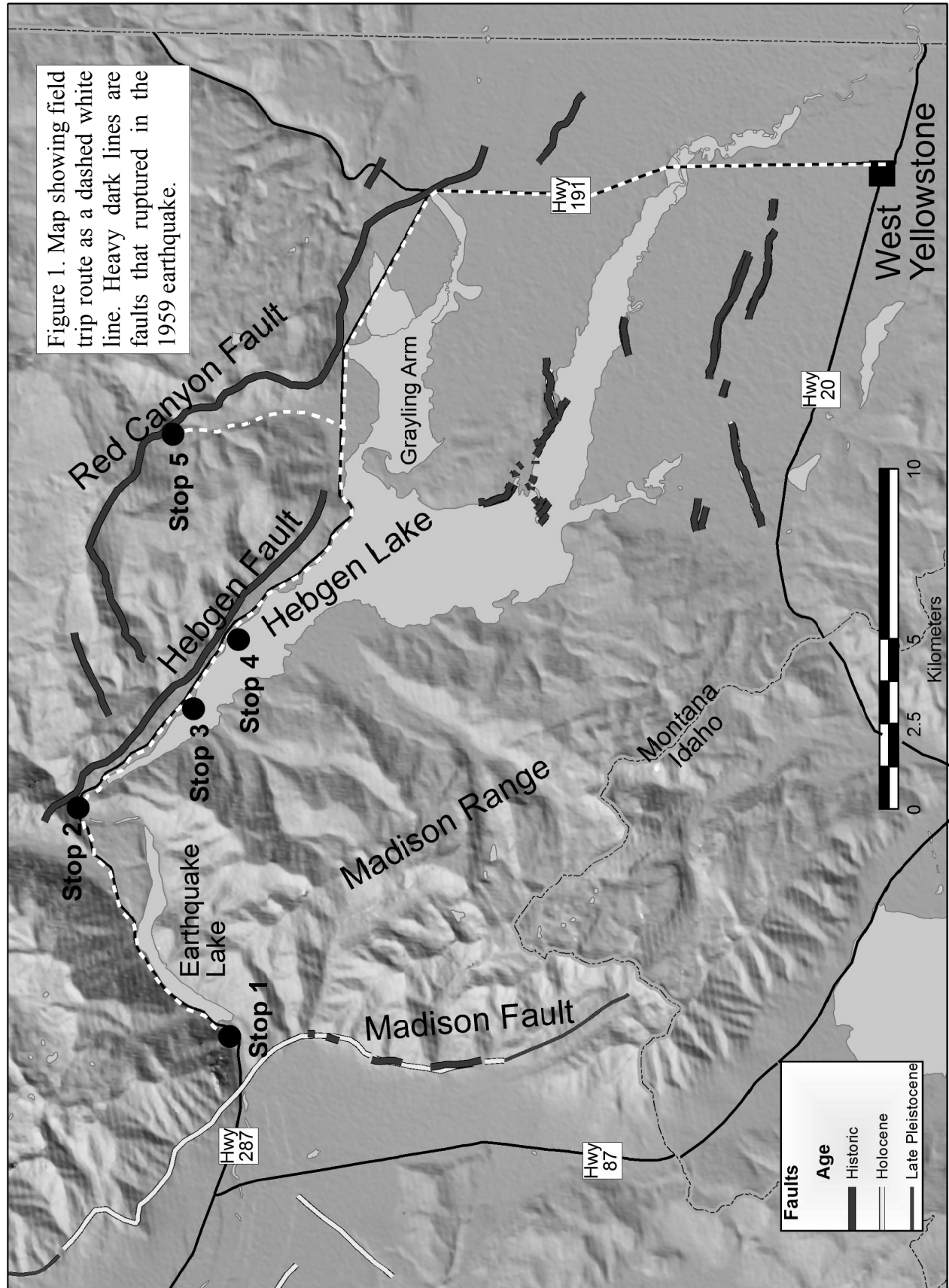
Stop 1—Upper parking lot at the Earthquake Lake Visitor Center.

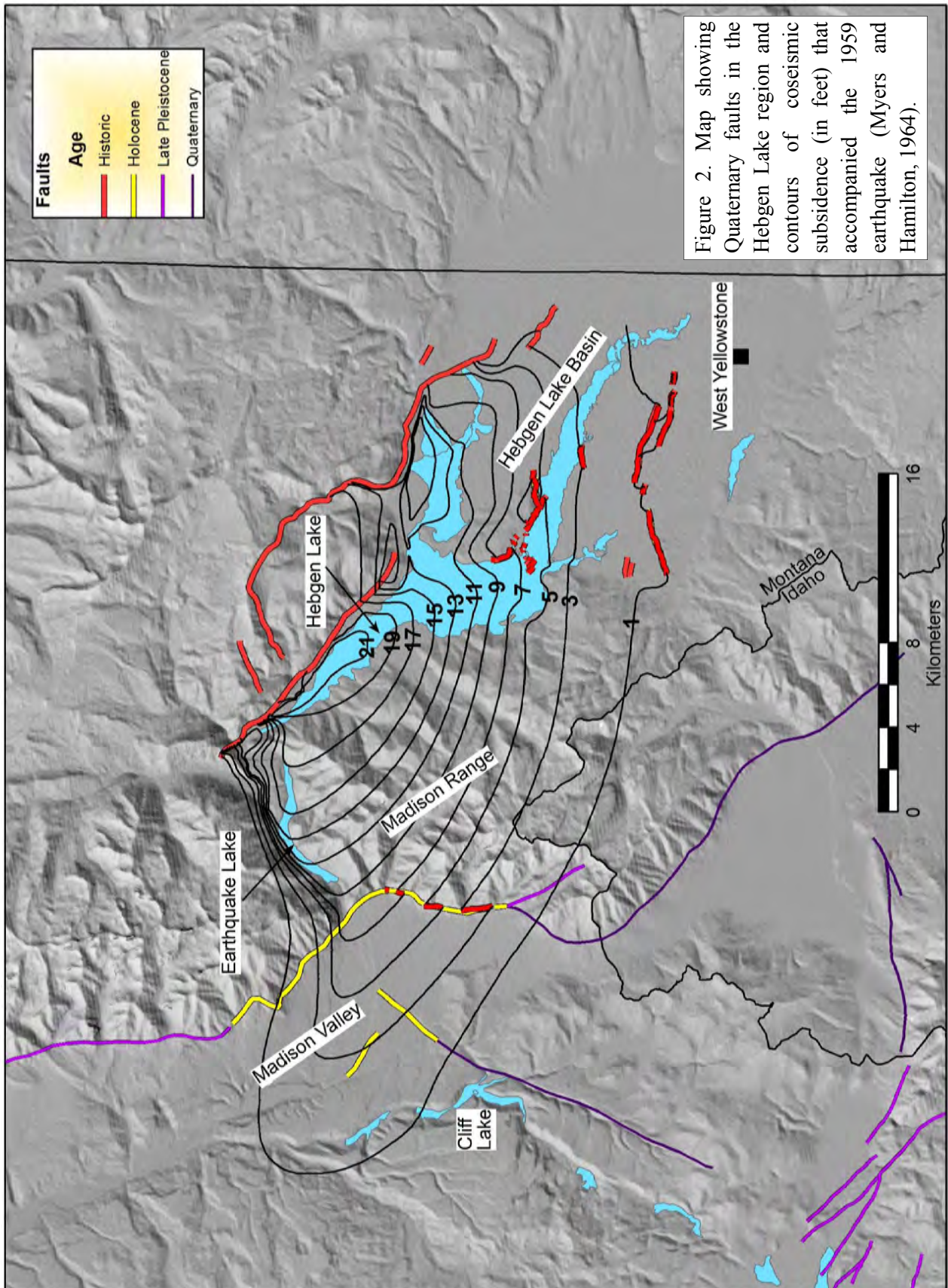
We are standing on top of the largest seismically triggered landslide in North America to occur in historic times. An estimated 28 million cubic yards of rock, weighing 60 million tons, catastrophically slid into Madison Canyon from an area on the south canyon wall about 30 seconds after the strongest seismic shaking that accompanied the 11:36 p.m., August 17, 1959, Hebgen Lake earthquake. The leading edge, or toe, of the slide crossed the river and came to

rest 400 feet (122 m) up the north canyon wall near our present location. Hadley (1964) estimated the final volume of the slide mass at 37 million cubic yards. The slide velocity was estimated at over 100 miles per hour (161 km per hour), generating hurricane-force winds around the perimeter of the slide.

The eastern edge of the slide covered part of the Rock Creek Campground, which was fully occupied, killing 26 people. The memorial boulder, just above where we are now standing, commemorates these victims. For those not directly in the slide path, the severe wind blast and a wave of thick, muddy water carrying trees, driftwood, and small rocks that was pushed ahead of the slide mass were the most destructive. The blast tumbled cars and trailers outward away from the slide mass.

If you look to the north up above our position, the uppermost edge of the slide deposit is visible above the parking lot. You will notice that most clasts are pinkish-tan dolomite and that, looking southward back towards the main headscarp, most clasts are composed of dark-colored schist and gneiss. Looking across the river near the base of the headscarp, you can see the light-colored dolomite forming a prominent band trending westward along the lower part of the canyon wall. The dolomite dips steeply into the canyon and apparently formed a buttress that held the upslope mass of gneiss and schist in place. This dolomite buttress fractured and broke apart during the strong seismic shaking, allowing the gneisses and schists upslope to slide





into the canyon. The slide mass moved as a coherent unit, evidenced by the band of dolomite from the bottom of the south canyon wall that is now distributed along the leading edge of the slide above the parking lot. Trees growing on the pre-slide canyon wall remain on the slide surface—many of their grey-weathered trunks aligned with the direction of slide movement are still visible.

The Madison slide covered the canyon bottom to a maximum depth of 220 feet (67 m) and dammed the Madison River to form Earthquake Lake. The following morning, emergency responders feared that the rising water in Earthquake Lake would overtop the dam if not controlled. Had this occurred, it may have rapidly cut a new outlet channel, resulting in catastrophic flooding affecting the downstream populations.

At the request of the Governor of Montana, the U.S. Army Corps of Engineers mobilized a fleet of earthmoving equipment and began excavating an outlet channel across the top of the slide. Water began to flow through the new outlet on September 10th, 24 days after the earthquake. The initial channel was too steep so work continued to excavate the spillway to a more stable configuration 50 feet (15 m) lower. Total cost of the project was \$1.715 million (U.S. Army Corps of Engineers, 1960). There is a bathtub ring of drowned trees that encircles Earthquake Lake above the current surface showing the maximum height of the original lake and the extent of the outlet channel modifications.

The Madison Fault lies just downstream of the slide at the mouth of Madison Canyon. This fault bounds the western side of the north-trending Madison range (through which Madison Canyon is cut) and is marked by fault scarps that offset late Pleistocene deposits. There is a two-mile (3.2-

km) section of the Madison Fault just southwest of our position that moved during the 1959 earthquake, producing a scarp up to three feet (0.9 m) high. There is no evidence of historic movement along the Madison Fault either north of Madison Canyon or near its southern terminus.

The relatively minor movements on the Madison Fault together with measured changes in the land-surface elevation are shown in Figure 2 (Myers and Hamilton, 1964). These coseismic elevation changes led to two competing theories to explain the subsurface faulting of the 1959 earthquake. In the so-called “dual basin concept”, Fraser et al. (1964) argued that measured subsidence in both the southern Madison Valley and the Hebgen Lake Basin resulted solely from slip along their respective valley-bounding normal faults, and that measured subsidence in the upper Madison Canyon near Beaver Creek resulted only from shaking-induced compaction of alluvial materials.

In contrast, Myers and Hamilton (1964) argued that a deep-seated, east-west-trending normal fault controlled the elongate zone of measured subsidence extending from the southern Madison Valley eastward to the Norris Geyser Basin in Yellowstone National Park. Movement on this deeper fault resulted in a broad zone of subsidence manifested at the surface by faults that developed along optimally-oriented bedding planes, and in regions lacking those, simple warping of the land surface. This so-called “single basin concept” suggests that surface faulting along the Madison, Hebgen, and Red Canyon Faults represents reactivation of existing structures; the southern part of the Madison Range subsided along with the Madison Valley to the west and the Hebgen Lake basin to the east. The seismologically-determined orientation

of the 1959 earthquake fault plane (Ryall, 1962; Dewey et al., 1973; Doser, 1985), the distribution of early aftershocks (Dewey et al., 1973; Doser, 1985), and later deformation in the Hebgen Lake Basin (Savage et al., 1985, 1993) all seem to favor the single basin concept.

0.0 0.0 Reset odometer to zero here. Values indicate cumulative (left) and interval (right) mileage.

0.3 0.3 Proceed to the Earthquake Lake Visitor Center entrance and turn left (east) on Highway 287.

0.6 0.3 Cross the upstream edge of the Madison Slide.

1.2 0.6 Bouldery deposit exposed in road cut mapped as Bull Lake Till (approximately 140,000 years old) by Myers and Hamilton (1964).

2.5 1.3 Beaver Creek end moraine visible ahead on north side of Earthquake Lake.

2.9 0.4 Highway 287 leaves the shoreline of Earthquake Lake.

3.4 0.5 Remnant of the pre-earthquake highway on right is now used as a boat launch.

4.4 1.0 Cross Beaver Creek. A re-leveling survey in 1964 determined 6-13 feet (1.8-4.0 m) of earthquake-related subsidence in this area (Myers and Hamilton, 1964).

4.8 0.4 Beaver Creek road on left.

5.0 0.2 Refuge point on right. This hill is formed on the Beaver Creek moraine and is underlain by the Bull Lake Till. It was used as a gathering point for campers trapped

between the Madison slide and the landslides that damaged the highway along Hebgen Lake. This point of refuge was high enough to escape the rising waters of Earthquake Lake and above the elevation of Hebgen Dam, making it a safe haven in the event that the dam might fail.

5.7 0.7 Cabin Creek Campground on left.

5.8 0.1 Cross Cabin Creek, turn left into Cabin Creek fault scarp exhibit. Park and gather at scarp exhibit sign.

Stop 2—Cabin Creek scarp on the Hebgen Fault. **STOP 2**

The scarp crossing the Cabin Creek drainage is near the northern terminus of the 8-mile (13 km) long Hebgen Fault. At this location, the lowest terrace along Cabin Creek, dated at 800-1,400 years (Van der Woerd et al., 2000), was offset 10.2 feet (3.1 m) by the 1959 earthquake. Southeastward along the fault, directly behind the sign, the scarp is 17.4 feet (5.3 m) high. A 7.2-foot (2.2 m) fault scarp existed at this location prior to the 1959 earthquake, so this scarp represents the combined offset of two large earthquakes.

In 1990, the Hebgen Lake Paleoseismology Working Group, comprised of personnel from the U.S. Geological Survey, Montana State University, and Lawrence Livermore National Laboratory, teamed up to conduct paleoseismic studies of the Hebgen Lake and Red Canyon Faults. Trenching produced evidence for one pre-1959 earthquake that radiocarbon dates show to be older than 1,000 years (Pierce et al., 2000). Although still a very fresh scarp in geomorphic terms, Wallace (1980) measured modification of the 1959 scarp at Cabin Creek (and other locations) that resulted from 19

years of weathering and erosion. He documented the upslope retreat of scarp crests and the lowering of average scarp angles from about 70° to slightly more than 40° in the center portion of the scarp face.

6.1 0.3 Exit Cabin Creek scarp parking loop and turn left (east) on Highway 287.

6.7 0.6 Hebgen Dam, on right, was damaged by the 1959 earthquake but did not fail. The dam consists of an earthfill embankment, outlet works which extend through the dam along the left abutment, and a spillway along the right abutment. The embankment is 721-feet long and up to 85-feet high above original ground surface. It consists of rock and soil fill excavated from nearby hillsides that was dumped in place from rail cars without compactive effort. The concrete core wall is founded on rock, up to 122.5 feet below the top of the dam, and extends from the left abutment to a point about 50 feet left of the spillway structure. The remainder of the core wall is founded on natural alluvium/landslide debris comprising the right abutment of the dam and about 15 feet below the spillway floor (U.S. Society on Dams, 2011).

Earthfill on the downstream side of the concrete core slumped and settled up to two feet (0.6 m), and up to five feet (1.5 m) on the upstream side. The core wall cracked in several places, and a series of four seismically generated waves, or seiches, overtopped the dam. They gullied the downstream face and damaged the old spillway beyond repair. Despite this extensive damage, the Hebgen Dam remained functional. The Hebgen Fault is less than 250 yards upslope from the northeast dam abutment.

7.6 0.9 Turn right into Building Destruction interpretive display area and park.

STOP 3

Stop 3—Subsidence and landslides.

We are standing on the pre-1959 highway. About 1,500 feet (457 m) to the northwest, a 350,000 cubic-yard landslide in alluvial fan and colluvial deposits removed a 525-foot (160 m) long section of highway 287. The Hebgen Fault is less than 600 feet (183 m) upslope from the headscarp of the landslide, which was triggered by strong seismic shaking in the saturated, unconsolidated sediments. A short trail down to the lakeshore leads to one of several cabins that were built along the shore of Hebgen Lake before 1959. This site sits on the hanging wall of the Hebgen Fault and the earthquake caused the lakeshore here to drop as much as 22 feet (6.7 m). The subsidence was greater near this location than along the lake's southern reaches, the sudden drop in the water level caused large seiche waves to rush into this area. Seiches are a large wave that oscillated back and forth across the lake basin for 12 hours (Myers and Hamilton, 1964). The period of oscillation is estimated to have been 17 minutes between successive waves. The elevation of the first four waves was high enough to overtop Hebgen Dam. The initial waves washed several cabins built near this shore off their foundations.

7.9 0.3 Exit Building Destruction interpretive site and turn right (east) on Highway 287.

9.4 1.5 This new section of highway was built after the pre-1959 section failed and was inundated by lake waters.

10.2 0.8 Park on right side of highway.

STOP 4 Stop 4—Hebgen Fault at “Section 31 Site.”

At this stop, we will examine the Hebgen Fault scarp where it crosses a small alluvial fan. The Hebgen Lake Paleoseismic Working Group named it the “Section 31 site” and trenched it in 2000 (Hecker et al., 2000) and again in 2002 (Hecker et al., 2002). Photographs of this scarp taken soon after the 1959 earthquake clearly show a compound fault scarp, with an older, rounded crest above the fresh scarp; evidence that a pre-1959 earthquake had also offset the surface of this alluvial fan. The Working Group found evidence of two pre-historic earthquakes. The penultimate earthquake occurred no more than 3,370 to 3,840 years before the 1959 earthquake (Hecker et al., 2000) and the oldest event occurred 8,000 to 16,500 years ago (Schwartz et al., 2009). Surficial evidence for the oldest event has largely been removed by retreat and modification of the 1959 scarp. Stable isotope estimates of the age of the surface of the alluvial fan range from 11,000-15,000 years (Hecker et al., 2002).

Just to the east, a landslide has obliterated the 1959 scarp. Further to the east along the north side of Highway 287, the Mission Canyon Formation preserves a bedrock scarp in the footwall surface of the Hebgen Fault. A study describing cosmogenic chlorine-36 dates of samples spanning the height of this bedrock scarp postulates that six earthquakes over the past 24,000 years incrementally exposed this bedrock scarp (Zreda and Noller, 1998). Zreda and Noller’s surprising result drastically overestimates the number of recent earthquakes recorded in the adjacent late Quaternary deposits and motivated the Hebgen Lake Paleoseismic Working Group to conduct their studies. Return to vehicles and continue east on Highway 287.

13.8 3.6 The Great Unconformity (Cambrian Flathead Formation overlying Archean metamorphic rocks) is exposed on the hillside to left. Straight ahead, the narrows connects the Grayling Arm to Hebgen Lake. The peninsula to the south is composed of Bull Lake Till and represents the end moraine of the glacier that flowed westward from Yellowstone approximately 140,000 years ago.

15.5 1.7 Turn left (north) on Red Canyon road, U.S.F.S. road 681.

18.2 2.7 Park at Red Canyon trail head.

Stop 5—Red Canyon Fault scarp. This stop includes a 0.5 mile (0.8 km) hike up the Red Canyon trail to view the Red Canyon Fault scarp. The trail is decent but may be muddy if wet; sturdy hiking shoes are recommended. This segment of the Red Canyon Fault ruptured in the 1959 earthquake, extending 13 miles (21 km) in an arcuate pattern. It trends northeastward near the west end of Kirkwood Ridge, southerly along the lower reaches of Red Canyon, turning eastward north of Grayling Arm, and finally southeastward to the boundary of Yellowstone Park. The Red Canyon Fault is unusual because the northwestern two-thirds of the fault trace cuts through mountainous terrain high on Kirkwood Ridge, and does not bound a structural basin except at its southeastern end. At our destination, where the Red Canyon Fault crosses Red Canyon Creek, the 1959 scarp is 19 feet (5.8 m) high with 14 to 15 feet (4.3-4.6 m) of displacement. In this area, the fault faithfully follows the steeply dipping contact between the Mission Canyon and Amsden Formations (Witkind et al., 1964). The Red Canyon and Hebgen Faults are normal faults that are likely in the early stages of extension in this tectonic setting (Lageson,

2009). Hike back to parking lot and return to vehicles.

20.9 2.7 Turn left (east) on Highway 287.

21.7 0.8 Red Canyon Fault scarps are visible as a series of step faults trending east-west on the slope to the north.

23.4 1.7 Cross Grayling Creek.

24.5 1.1 Crossing the 11,000-15,000 year old Grayling Creek alluvial fan (Haller et al., 2002). The Red Canyon Fault scarp is visible to the north. The Hebgen Lake Paleoseismic Working Group excavated a trench at this site and found that the 1959 earthquake reactivated a 66-foot (20-m) wide graben flanked by a 19.7-foot (6-m) high scarp in the footwall. There are antithetic scarps that are 3.3 to 6.6 feet (1-2 m) high on the hanging wall (Haller et al., 2000a, 2000b). Paleoseismic data indicate that one Holocene earthquake preceded the 1959 earthquake; a the total alluvial fan surface displacement resulting from both earthquakes is only about 6.6 feet (2 m), after correcting for back tilting and graben development below the main scarp (Haller et al., 2002).

25.6 1.1 Duck Creek Wye. Turn right (south) on Highway 191. The small rise in Highway 191 just north of this intersection is the Red Canyon Fault. A scarp of approximately five feet (1.5 m) offset the highway here in 1959. Surface rupture along the Red Canyon Fault continues 1.4 miles (2.3 miles) southeastward before dying out close to the boundary of Yellowstone National Park.

25.9 0.3 Cross Duck Creek.

26.6 0.7 Cross Cougar Creek. After crossing Cougar Creek, Highway 191 traverses a

broad surface that is sloping very gently to the northwest. It is composed primarily of obsidian sand covering an area of about 97 square miles (250 square km) to an average depth of 40 feet (25 m). The glassy sand was derived from obsidian rhyolite flows that erupted south and east of West Yellowstone shortly after Bull Lake glaciers retreated from the Hebgen Lake Basin (Richmond, 1964). Obsidian hydration-rind studies indicate that this broad alluvial plain was deposited during early the Pine-dale glaciation, about 30,000 years ago (Pierce et al., 1976), as deposits of glacial outwash and glacial outburst floods (Pierce, 1979) known as *jökulhlaups*.

30.4 3.8 Cross Madison River. Nash (1984) used the fluvial terrace risers along this reach of the Madison River to develop a morphologic dating technique based on riser (or fault scarp) profiles. The remainder of the trip crosses the obsidian sand plain.

34.3 3.9 Arrive at intersection of Yellowstone Avenue and Canyon Street in West Yellowstone. End of trip.

References

Dewey, J.W., Dillinger, W.H., Taggart, J., and Algermissen, S.T., 1973, A technique of seismic zoning; Analysis of earthquake locations and mechanisms in northern Utah, Wyoming, Idaho, and Montana: *in* Proceedings of the International Conference on Microzonation for Safer Construction in Research and Applications: Seattle, University of Washington, v. 2, p. 879-894.

Doser, D.I., 1985, Source parameters and faulting processes of the 1959 Hebgen Lake, Montana, earthquake sequence: *Journal of Geophysical Research*, v. 90, p. 4537-4555.

- Fraser, G.D., Witkind, I.J., and Nelson, W.H., 1964, A geological interpretation of the epicentral area—The dual-basin concept: *in* The Hebgen Lake, Montana, earthquake of August 17, 1959: U.S. Geological Survey Professional Paper 435-J, p. 99-106.
- Hadley, J.B., 1964, Landslides and related phenomena accompanying the Hebgen Lake earthquake of August 17, 1959: *in* The Hebgen Lake, Montana, earthquake of August 17, 1959: U.S. Geological Survey Professional Paper 435-K, p. 107-138.
- Haller, K.M., 2000a, Prehistoric surface faulting on the Red Canyon Fault, Montana: Geological Society of America Abstracts with Programs, v. 32, no. 7, p. 442.
- Haller, K.M., Hiroyuki, T., Machette, M.N., Essex, J., and Hancock, D., 2000b, Paleoseismology of the Grayling Creek site, Red Canyon Fault: EOS, Transactions of the American Geophysical Union, v. 81, no. 48, p. 1169-1170.
- Haller, K.M., Tsutsumi, H., Machette, M.N., Essex, J., and Hancock, D.A., 2002, Paleoseismic Investigation of the 1959 Red Canyon Fault, Southwestern Montana: Geological Society of America Abstracts with Programs, v. 34, no. 4, p. 4.
- Hecker, S., Stenner, H.D., Schwartz, D.P., and Hamilton, J.C., 2000, Paleoseismic results from the central part of the 1959 Hebgen Fault rupture, Montana: Geological Society of America Abstracts with Programs, v. 81, p. 1170.
- Hecker, S., Stenner, H.D., Costa, C.H., Schwartz, D.P., and Hamilton, J.C., 2002, New paleoseismic results from the central part of the 1959 Hebgen Fault rupture, Montana: Geological Society of America Abstracts with Programs, v. 34, No. 4, p. 4.
- Lageson, D.R., 2009, Hebgen Lake-Red Canyon normal fault system, MT; an example of early-stage structural inversion: Geological Society of America Abstracts with Programs, v. 41, p. 54-54.
- Myers, W.B., and Hamilton, W., 1964, Deformation accompanying the Hebgen Lake earthquake of August 17, 1959: *in* The Hebgen Lake, Montana, earthquake of August 17, 1959: U.S. Geological Survey Professional Paper 435-I, p. 55-98.
- Nash, D.B., 1984, Morphologic dating of fluvial terrace scarps and fault scarps near West Yellowstone, Montana: Geological Society of America Bulletin, v. 95, p. 1413-1424.
- Pierce, K.L., 1997, History and dynamics of glaciation in the northern Yellowstone National Park area: U.S. Geological Survey Professional Paper 729-F, 90 p.
- Pierce, K.L., Lageson, D.R., Ruleman, C.A., and Hintz, R.G., 2000, Holocene paleoseismology of Hebgen Lake normal fault, Montana—The Cabin Creek site of the Hebgen Lake paleoseismology working group: EOS, Transactions of the American Geophysical Union, v. 81, no. 48, p. 1170-1170.
- Pierce, K.L., Obradovich, J.D., and Friedman, I., 1976, Obsidian hydration dating and correlation of Bull Lake and Pinedale glaciations near West Yellowstone, Montana: Geological Society of America Bulletin, v. 97, p. 703-710.
- Richmond, G.M., 1964, Glacial geology of the West Yellowstone basin and adjacent parts of Yellowstone National Park: *in* The Hebgen Lake, Montana, earthquake of August 17, 1959: U.S. Geological Survey Professional Paper 435-T, p. 223-236.

Ryall, A., 1962, The Hebgen Lake, Montana earthquake of August 18, 1959; P waves: Bulletin of the Seismological Society of America Bulletin, v. 52, p. 235-271.

Savage, J.C., Lisowski, M., and Prescott, W.H., 1985, Strain accumulation in the Rocky Mountain states: Journal of Geophysical Research, v. 80, p 10,310-10,320.

Savage, J.C., Lisowski, M., Prescott, W.H., and Pitt, A.M., 1993, Deformation from 1973 to 1987 in the epicentral area of the 1959 Hebgen Lake, Montana, earthquake ($M_s = 7.5$): Journal of Geophysical Research, v. 98, p. 2145-2153. doi:10.1029/92JB02410

Schwartz, D.P., Hecker, S., Stenner, H.D., Haller, K.M., Pierce, K.L., Lageson, D.R., and Machette, M.N., 2009. The 1959 Hebgen Lake, Montana, surface rupture and record of late-Pleistocene-Holocene earthquakes: Geological Society of America Abstracts with Programs, v. 41, no. 7, p. 53-54.

U.S. Army Corps of Engineers, 1960, Madison River, Montana, report on flood emergency, Madison River slide, v. 1, main report: Omaha, Nebraska, U.S. Army Engineer District, Sept. 1960, 28 p.

U. S. Society on Dams, 2011, 21st Century Dam Design—Advances and Adaptations: Proceedings of the 31st Annual USSD Conference, San Diego, California, April 11-15, 2011, p. 1399-1420, <http://ussdams.com/proceedings/2011Proc/1399-1420.pdf>

Van der Woerd, J., Benedetti, L., Caffee, M.W., and Finkel, R., 2002, Slip-rate and earthquake recurrence time on the Hebgen Lake Fault (Montana); Constraints from surface exposure dating of alluvial terraces

and bedrock fault scarp: EOS, Transactions of the American Geophysical Union, v. 81, no. 48, p. F1160.

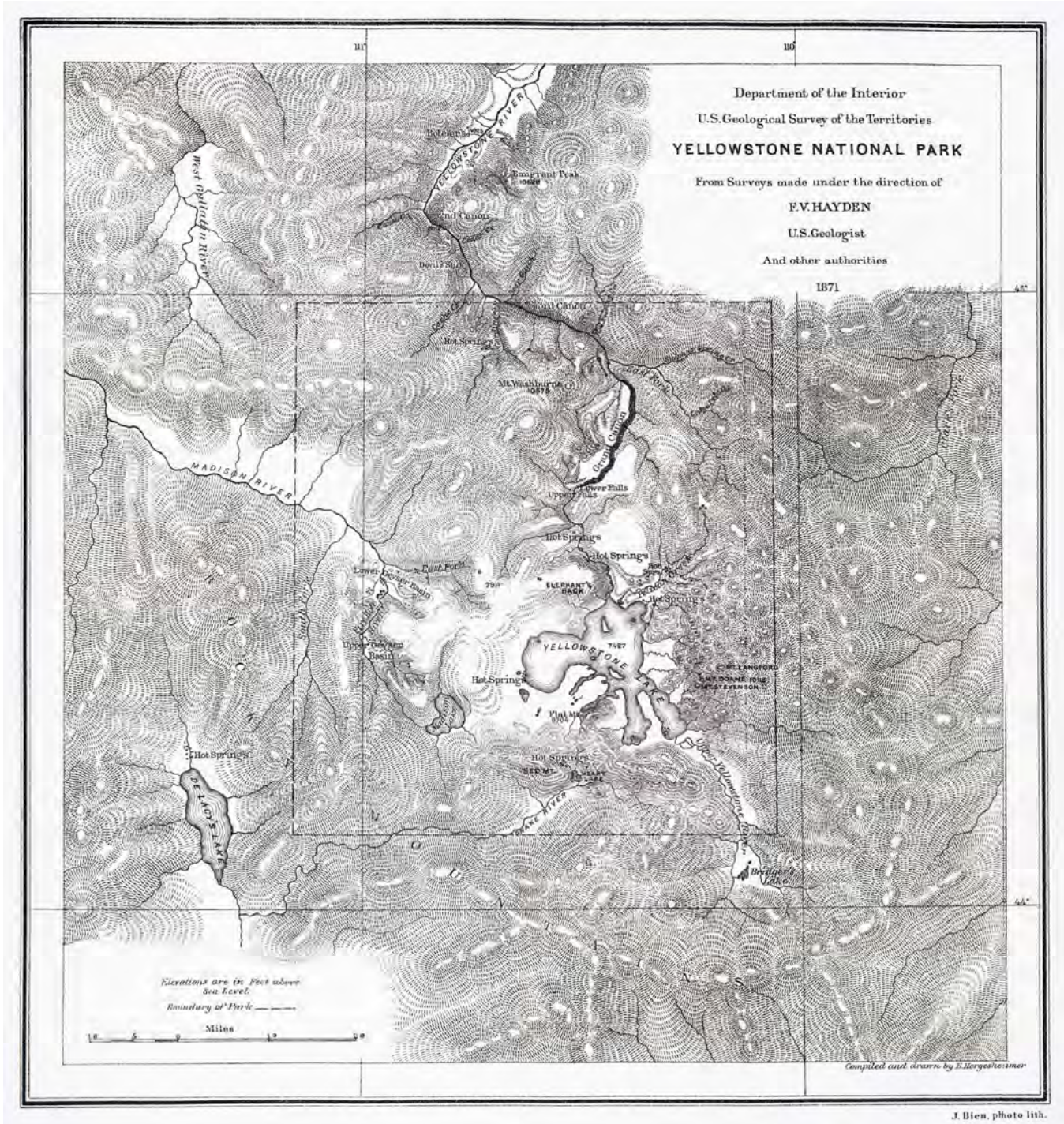
Wallace, R.E., 1980, Degradation of the Hebgen Lake fault scarps of 1959: Geology, v. 8, p. 225-229.

Witkind, I.J., Hadley, J.B., and Nelson, W.H., 1964, Pre-Tertiary stratigraphy and structure of the Hebgen Lake area: *in* The Hebgen Lake, Montana, earthquake of August 17, 1959: U.S. Geological Survey Professional Paper 435-R, p. 199-207.

Zreda, M. and Noller, J.S., 1998, Ages of prehistoric earthquakes revealed by cosmogenic chlorine-36 in a bedrock fault scarp at Hebgen Lake: Science, v. 282, p.1097-1099.



Geologist Ferdinand Vandever Hayden during the Yellowstone expedition, 1871. Photo by William Henry Jackson. Courtesy National Park Service.



Hayden's 1871 map of Yellowstone.

FIELD GUIDE TO THE EOCENE IGNEOUS ROCKS OF THE CENTENNIAL AND HENRY'S MOUNTAINS, IDAHO AND MONTANA

Dan Moore, Chris Sant*, Rebecca Wood*, Barry Miller*, Steve Hansen*, Ryan Shurtliffe*, and Samuel Grover*

Department of Geology, Brigham Young University – Idaho, 525 S Center St, Rexburg, ID, 83460-0510, moored@byui.edu

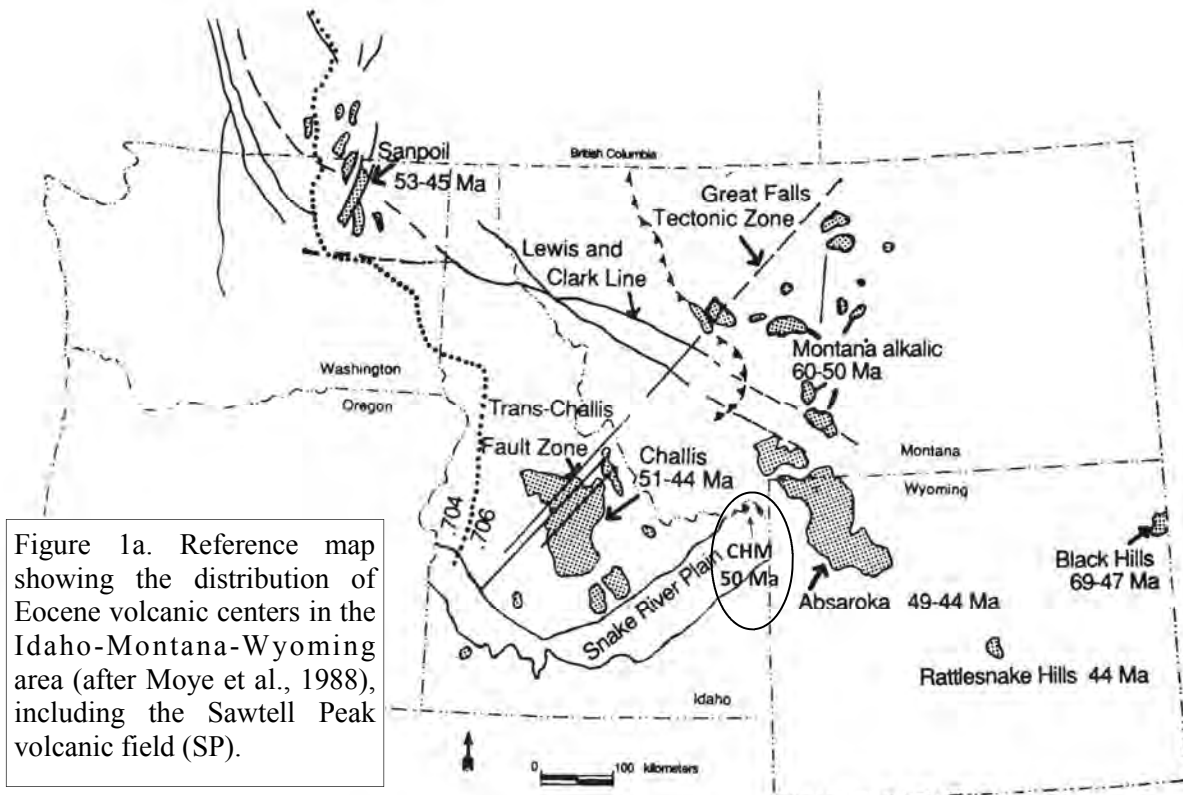
* These individuals are no longer at BYU-Idaho; they participated in the project as undergraduates.

Introduction

The Centennial and Henry's Mountains lie on the Montana-Idaho border and are, respectively, E-W- and N-S-trending ranges located inside the Yellowstone tectonic parabola near the eastern margin of the Basin and Range Province (Figure 1). The Eocene rocks exposed in these ranges represent a deeply eroded Eocene volcanic field, which we informally refer to as the Sawtell Peak volcanic field (SP). This volcanic field is exposed in three areas, from west to east: in the Centennial Mountains, west of Mount

Jefferson, and at Sawtell Peak and in the Henry's Mountains near Mount Two Top (Figure 1). During the Eocene, this area lay just south of the Madison-Gravelly Arch, a N-S trending topographic high (Chetel et al., 2011). The SP lies between two of the largest Eocene volcanic fields in North America—the Absaroka and Challis Volcanic Fields, located ~80 km to the east and ~120 km to the west, respectively.

The Absaroka volcanic field was dominated by composite volcanoes, was primarily active ~55-44 Ma, and records composi-



tions typical of subduction settings (Armstrong, 1991; Luedke, 1994; Bray, 1999; Hiza, 1999; Feeley et al., 2002; Feeley, 2003; Feeley and Cosca, 2003; Lindsay and Feeley, 2003; Chandler, 2006). The Challis volcanic field, which is part of the Challis-Kamloops volcanic belt, contains remnants of composite volcanoes and calderas, was active ~51–45 Ma, and records compositions interpreted to represent the opening of a window in the underlying subducted slab (Ekren and McIntyre, 1985; Lewis and Kiilsgaard, 1991; Norman and Mertzman, 1991; Luedke, 1994; Jellinek, 1994; MacDonald et al., 1998; Breitsprecher et al., 2003; Feeley, 2003; Chandler, 2006). Because of their location, the petrology of SP rocks may yield useful insights into the petrotectonic history of western North America during Eocene time.

Field Relations and Petrography

The SP consists of a ~350-meter-thick sequence of dike-fed, shoshonite aa lava

flows representing eruption of at least 40 cubic kilometers of magma. These lava flows overlie local Paleozoic strata and are best exposed at Sawtell Peak (Figure 1). The Huckleberry Ridge (~2.1 Ma) and Lava Creek (~0.63 Ma) Tuffs, from the nearby Yellowstone Plateau volcanic field, onlap these rocks at lower elevations (Figure 1).

The volcanic features and petrography of SP rocks are remarkably uniform—they consist almost exclusively of sequences of shoshonite aa flows that are one to ten meters thick. These flows typically consist of a thin, lower breccia zone; a dense interior; and a thicker, upper breccia zone. Where slopes are steep the cross sections of individual flow lobes are exposed. SP flows are sometimes vesicular or amygdaloidal; are crystal rich; contain euhedral clinopyroxene (cpx) phenocrysts and subhedral olivine (ol) phenocrysts that are commonly altered to iddingsite; and contain microlites of plagioclase and Fe-Ti oxides (Figure 2). Mo-



Figure 1c. Annotated satellite image (taken from Google Earth) of the field trip route, starting at the junction of U.S. Route 20 and Sawtell Peak Road and ending on top of Sawtell Peak. The path is outlined in blue. The yellow numbers are the locations referred to below.

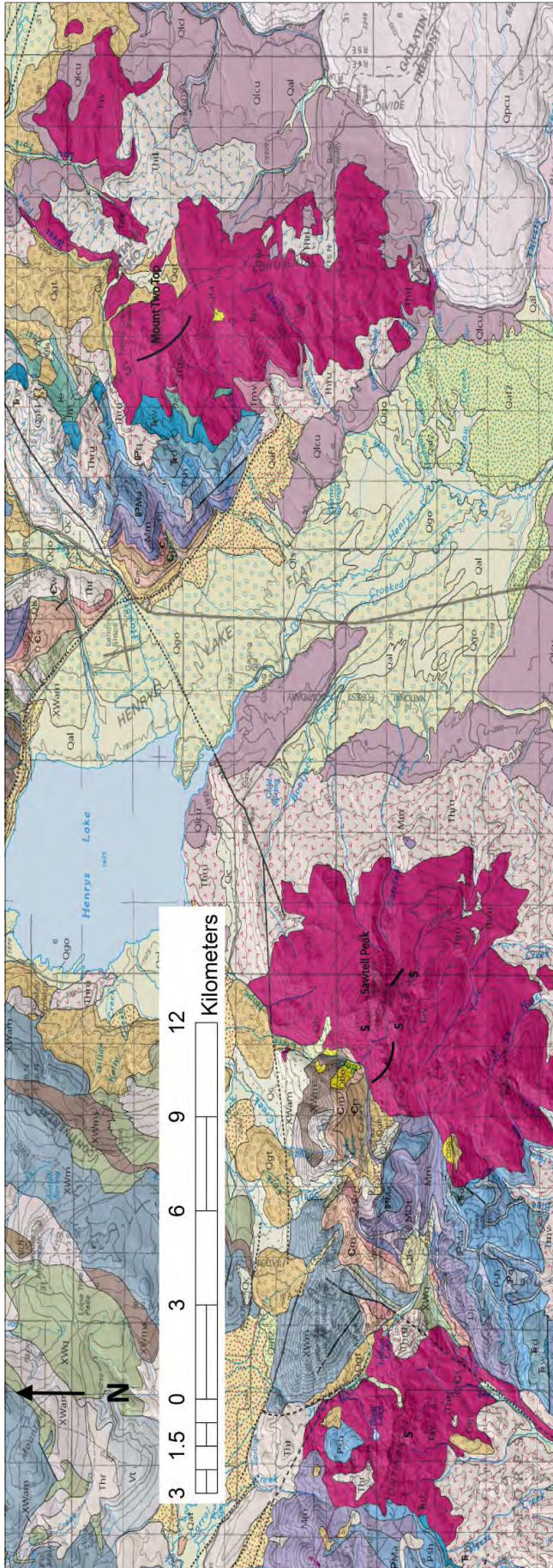


Figure 1b. Geologic map showing the distribution of the Eocene SP and surrounding units (O'Neill and Christiansen, 2004). Hot pink (Tav) – shoshonites of the SP; thick black lines are dikes; 'S' indicates sediments. Light pink, some with "v" (Thru, Thr) – Huckleberry Ridge Tuff. Light purple (Qlcu) upper member of the Lava Creek Tuff. Yellows (Qal, Qls, Qc, Qta, Qat, Qaf, Qgt, Qgo) – Surficial deposits. Other colors and symbols – Precambrian metamorphic and Paleozoic sedimentary rocks.

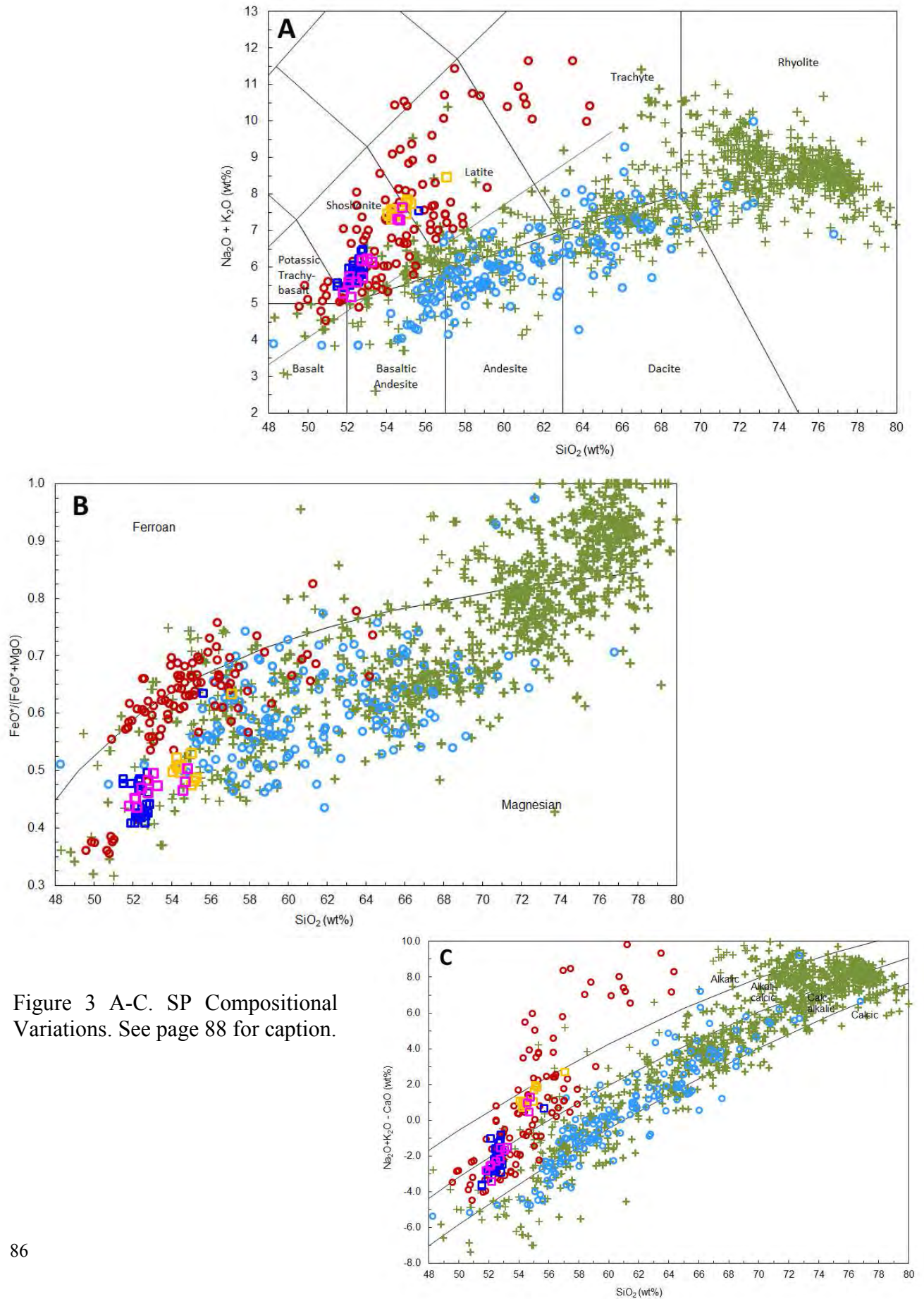
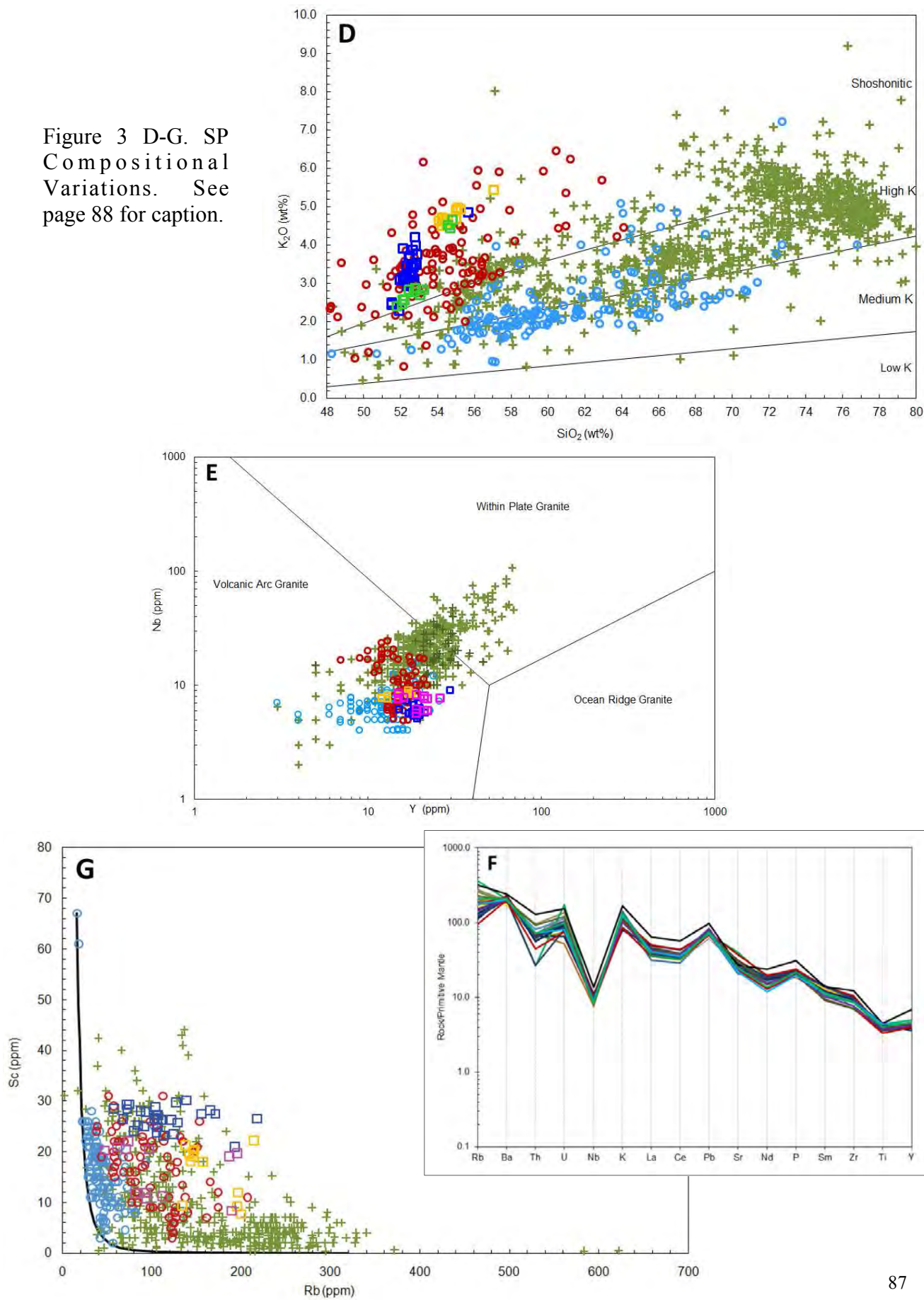


Figure 3 A-C. SP Compositional Variations. See page 88 for caption.

Figure 3 D-G. SP Compositional Variations. See page 88 for caption.



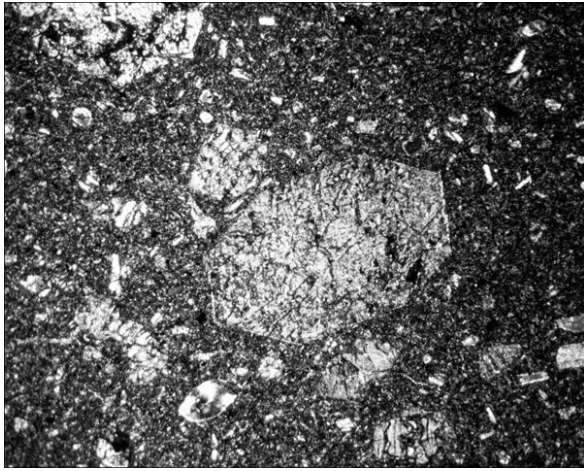


Figure 2. Photomicrograph in crossed polarized light of a Henry's Mountain shoshonite (HM-1) showing euhedral clinopyroxene and subhedral olivine phenocrysts in a felty groundmass of plagioclase, Fe-Ti oxides, clinopyroxene, olivine, and glass.

dal proportions are 61-69% groundmass, 22-34% cpx, and 5-12% ol. Modal proportions of clinopyroxene and olivine are inversely correlated, i.e., rocks with more clinopyroxene contain less olivine. Three units contain phlogopite. The lava flows are cut by northwest-southeast trending vertical feeder dikes that are typically one to five meters thick. Some dikes have chilled margins, while others are surrounded by zones of hydrothermal alteration. Surface exposures of the large dikes are 10-100 m long (Figure 1).

No pyroclastic rocks or lahar deposits were observed. In a very few locations (indicated

with an 'S' in Figure 1) there are small deposits of volcanic sediments between lava flows. Most are located in the voids of the upper breccia zone of flows. One deposit contains highly angular clasts up to one meter in diameter in a matrix of fine-grained volcanic sediments; another deposit consists entirely of laminated, fine-grained volcanic sediments.

Field relations and age dates suggest the lava flows were erupted during a very short period in the early Eocene. Three $^{40/39}\text{Ar}$ age measurements were performed on the following samples: the oldest and youngest flows exposed at Sawtell Peak and the youngest flow from the area west of Mount Jefferson. The reported dates are unable to resolve a difference between the initiation and cessation of volcanism in the SP, suggesting the flows erupted in a short period at ~50 Ma (Turrin, 2011).

Composition and Petrogenesis

Figure 3 shows the basic compositional characteristics of SP rocks. SP rocks are uniformly shoshonitic (K_2O 2-5%), silica-oversaturated, magnesian, and calc-alkalic (Figure 3a-d). SP compositions share many characteristics with compositions from the Absaroka and Challis volcanic fields, but they are most similar to those of the shoshonite series (Sunlight Group) from the Absaroka volcanic field (Moore et al., 2010). Figure 3e shows that SP, Absaroka,

Figure 3 (pages 86-87). SP Compositional Variations. Symbol key: Squares are from the SP – blue squares are samples from Sawtell Peak, yellow squares are samples from the Henry's Mountains, and purple squares are samples from west of Mount Jefferson; circles are from the Absaroka Volcanic Field – red circles are from the shoshonite series, blue circles are from the calc-alkalic series; crosses are from the Challis Volcanic Field. For a full list of the references for the Absaroka and Challis compositional data see Moore et al. (2010). A) Total alkalis versus SiO_2 IUGS classification diagram (Le Bas et al., 1991). B) SiO_2 versus $\text{FeO}_{\text{total}}/(\text{FeO}_{\text{total}}/\text{MgO})$ diagram of Frost (2001), using the dividing line of Miyashiro (1974). C) SiO_2 versus modified alkali-lime diagram of Frost (2001). D) SiO_2 versus K_2O using the dividing lines of Ewart (1982). E) Y versus Nb tectonic discrimination diagram of Pearce (1984) showing that all SP samples plot within the volcanic arc field. F) SP trace element concentrations normalized to the primitive mantle values of McDonough (1995) G) Rb versus Sc plot with a basic Rayleigh fractional crystallization model (solid line). For model parameters see Moore et al. (2010).

and early Challis compositions plot in the volcanic arc field, whereas late Challis compositions plot in the intraplate field. Figure 3f shows that SP compositions share the incompatible element enrichment and niobium depletion characteristic of subduction-related rocks. Both major and trace element variations in SP compositions are relatively small and do not follow straightforward liquid lines of descent. Basic Rayleigh fractionation modeling suggests that mixing of primitive and evolved magmas was important in the genesis of SP compositions (Figure 3g). Based on major and trace element characteristics we infer that SP rocks are subduction related and evolved by mixing of magmas and fractional crystallization of the observed phases. More detailed and comprehensive compositional modeling will yield additional insights into the petrogenesis of SP magmas and their relationship to magma genesis in the Absaroka and Challis Volcanic Fields.

Road Log

Exposure of and access to the Eocene volcanics and near-surface intrusive rocks in the SP is best along the road leading to Sawtell Peak, National Forest Road 024. This road is well-maintained and easily accessible in most vehicles. For a dirt road, it receives a lot of traffic, so when you stop to study the rocks pull to the side in an area where you can be easily seen from both directions. Watch for cars while on the outcrop. This field trip can easily be completed in half a day.

0.0 miles Road log mileages are measured from the junction of Sawtell Peak Road (National Forest Road 024) and U.S. Route 20 (Lat: 44.5217°, Long: -111.3275°). You will stay on Sawtell Peak Road for the entire trip. While you will be passing them, do not turn off onto any side roads, e.g.,

Strawberry Rd., Shadow Ridge Rd., National Forest Roads 052 or 455, or Stamp Meadows Rd.

2.0 miles Location 1 – The Lava Creek Tuff (Figure 1), which produced the Yellowstone III caldera, is poorly exposed in the woods on either side of the road. This tuff overlies the Huckleberry Ridge Tuff, which is exposed at Location 3 and produced the Yellowstone I caldera. These units unconformably overlie and onlap the Eocene volcanics.

3.8 miles Location 2 – As you drive by, you can begin to see Eocene volcanics in the float. Weathered surfaces of unaltered material are typically brown and smooth. Fresh surfaces of unaltered material are generally gray to black. Altered material commonly displays rounded weathering patterns and contains dark, euhedral clinopyroxene crystals and reddish olivine crystals that have been altered to iddingsite in a devitrified, gray-purple matrix.

4.1 miles Location 3 – The rounded boulders and outcrops seen to the right (north) of the road are composed of Huckleberry Ridge Tuff. To view the best exposures in this unit, park on the small service road to the right and hike up the small hill.

8.2 miles Location 4 (Lat: 44.5494°, Long: -111.4233°) – Park on the outside bend of the road. On the inside bend there is a resistant unit of shoshonite with subhorizontal cooling joints whose outcrop pattern is roughly linear and extends northwest-southeast on both sides of the road. This dike is more difficult to identify than the other dikes on the map. This is a good place to take your first look at the petrography of these rocks. In almost every unit, euhedral clinopyroxene is abundant, olivine is less common, and plagioclase and Fe-Ti oxides are phases within the groundmass.

8.9 miles Location 5 (Lat: 44.5514°, Long: -111.4351°) – Park uphill from the bend in the road, so that cars from both directions can see your parked vehicle in time to react. Stay on the inside edge of the road and walk back down to the bend. Study the outcrop on the inside of the bend. Notice two main features: the altered flow breccia near road level that locally contains sediment, and the three overlying lava flows. The sediment is fine grained and consists of small, rounded to subrounded grains similar to what is weathering from the lava flows today. Each of the overlying flows consists of a cliff-forming flow breccia top and a slope-forming interior. Presumably, the flow interior forms a gentler slope because it is jointed, allowing blocks to fall out quite easily. This is the usual weathering profile for the thin, unaltered flows that characterize the volcanic field. In contrast, thicker flows on steep slopes expose the entire cliff-forming unit, composed of flow breccias with massive interiors. A possible history for this area is: deposition and alteration of the road-level flow breccia; formation of a small drainage; deposition of sediments in the voids and on top of the flow breccia; extrusion of the first lava flow, which deposited breccia clasts at the flow-front, then flowed over them, working those clasts down into the underlying sediment; and emplacement of the other two flows, which filled and overflowed the small paleodrainage. The current dip of the paleodrainage is about 15 degrees to the southeast.

9.3 miles Location 6 – As you drive past, notice the outcrops of Huckleberry Ridge Tuff on the side of the road. Here, the tuff thinly covers the Eocene volcanics.

10.1 miles Location 7 (Lat: 44.5567°, Long: -111.4384°) – Park in the pullout on the outside of the sharp bend in the road. This is a great spot for an overlook of Is-

land Park, but you can see more from the top so we'll wait to describe what we see in the distance. As you walk up the right side of the road, notice the succession of flows. Figure 4 shows the contact between two flows.



Figure 4. Photo of the contact between the lower part of a thin flow (that lacks a lower breccia zone) and the upper breccia zone of the underlying flow.

10.6 miles Location 8 (Lat: 44.5593°, Long: -111.4463°) – Park on the outside of the sharp bend in the road. Observe the cross-section of the lava tube(s) in the road-cut directly to the north, as shown in Figure 5. Walk to the left (west) side of this outcrop so that you can observe the stacks of flows exposed in the steep, west-facing slope to your north. Figure 6 shows a close-up of a flow that crops out about a quarter of the way down the west-facing slope northwest of Sawtell Peak.

11.5 miles Location 9 (Lat: 44.5618°, Long: -111.4451°) – Once you reach the peak, park in the cleared area to your right (east). On a clear day, the views from this location provide an excellent overview of the geology of Island Park and the surrounding areas. To the northwest you can see the Henry's Mountains and Mount Two



Figure 5. Photo of a cross-section of several lava flow lobes, each with a dense flow interior and a breccia carapace. Dashed lines indicate approximate flow boundaries.

Top, where the eastern exposures of the SP are located. The ridgeline of Mount Two Top is formed by a dike. To the west you can see the Yellowstone Plateau, which is composed of large rhyolite flows that erupted in the Yellowstone III caldera. To the south you can see Ashton Hill and Big Bend Ridge, which form the southern and western rims of the Yellowstone I and II calderas. You can also see the Island Park dam and reservoir. To the southwest you can see the Spencer - High Point Rift Zone and much of the rest of the Eastern Snake River Plain. To the west you can see Mount Jefferson, beyond which lie the western exposures of the SP. If you walk north past the radar station you can see the succession of lava flows that form Sawtell Peak. Be careful; the slopes are very steep and the trail is rugged. If you walk far enough, you can see Henry's Lake and the northwestern Henry's Mountains, which are composed of Precambrian medium-grade metamorphic rocks and Paleozoic sedimentary rocks.

Exploring other parts of the Sawtell Peak volcanic field

The western portion of this volcanic field is exposed west of Mount Jefferson. To explore, follow these instructions: from the

junction of Sawtell Peak Road (NF Road 024) and U.S. Route 20, go south on U.S. Route 20 for 5.1 miles; turn right on Yale-Kilgore road; after 11.9 miles turn right on NF Road 046; and drive about three miles to the gate. The best exposures of the Eocene volcanics are on the west side of the drainage between you and the Continental Divide (just up from Blair Lake). NF Road 046 is well maintained and can be traversed in most vehicles. Hiking from your vehicle to the top and back will require most of a day. A GPS unit will help you navigate the forested slopes near your vehicle.



Figure 6. Photo of a typical SP aa flow showing the thin lower breccia zone, a dense interior, and thick upper breccia zone.

The eastern portion of this volcanic field is exposed in the Henry's Mountains. To explore, follow these instructions: From the junction of Sawtell Peak Road (NF Road 024) and U.S. Route 20, go north on U.S. Route 20 for 4.7 miles; turn right onto Meadow Creek Road (NF Road 060); after 0.8 miles head straight onto Twin Creek Road; after 420 feet turn left (north) onto NF Development Road 061 (i.e., Mount Two Top Trail); and after 1.5 miles stay right on NF Road 061. Continue for about

another six miles as this road winds its way into the heart of the Henry's Mountains; the best exposures of the Eocene volcanics are on the west side of Mount Two Top (the prominent ridge to your southwest). A dike runs the length of, and forms, Mount Two Top. NF Road 061 requires a four-wheel-drive vehicle, particularly when it is wet. Hiking from your vehicle to Two Top, down the west face, then onto the road and back to your vehicle will require a whole day. A GPS unit will help you find NF Road 061 on the west side of Two Top.

References Cited

- Armstrong, R.L., and Ward, P.L., 1991, Evolving geographic patterns of Cenozoic magmatism in the North American Cordillera; the temporal and spatial association of magmatism and metamorphic core complexes: *Journal of Geophysical Research*, v. 96, p. 13201-13224.
- Bray, E.L., 1999, Geochemical and Isotopic Variations in the Absaroka Volcanic Supergroup, Wyoming - implications on Petrogenesis and Magma Sources: M.Sc. thesis, Provo, Brigham Young University.
- Breitsprecher, K., Thorkelson, D.J., Groome, W.G., and Dostal, J., 2003, Geochemical confirmation of the Kula-Farallon slab window beneath the Pacific Northwest in Eocene time: *Geology*, v. 31, p. 351-354.
- Chandler, M.R., 2006, The provenance of Eocene tuff beds in the Fossil Butte Member of the Green River Formation, Wyoming: Relation to the Absaroka and Challis Volcanic Fields: M.Sc. thesis, Provo, Brigham Young University.
- Chetel, L.M., Janecke, S.U., Carroll, A.R., Beard, B.L., Johnson, C.M., and Singer, B.S., 2011, Paleogeographic reconstruction of the Eocene Idaho River, North American Cordillera: *Geological Society of America Bulletin*, v. 123, p. 71-88.
- Ekren, E.B., and McIntyre, D.H., 1985, Eocene cauldron-related volcanic events in the Challis Quadrangle, Northwest Mining Association Convention: Symposium on the Geology and Mineral Deposits of the Challis 1 x 2 degree Quadrangle, Idaho, U.S. Geological Survey, p. 43-58.
- Ewart, A., 1982, The mineralogy and petrology of Tertiary-Recent orogenic volcanic rocks, with special reference to the andesitic-basaltic compositional range: *in* Thorpe, R.S., ed., *Andesites, Orogenic Andesites and Related Rocks*: John Wiley and Sons, p. 25-95.
- Feeley, T.C., and Cosca, M.A., 2003, Time vs. composition trends of magmatism at Sunlight Volcano, Absaroka volcanic province, Wyoming: *Geological Society of America Bulletin*, v. 115, p. 714-728.
- Feeley, T.C., Cosca, M.A., and Lindsay, C.R., 2002, Petrogenesis and implications of calc-alkaline cryptic hybrid magmas from Washburn Volcano, Absaroka Volcanic Province, USA: *Journal of Petrology*, v. 43, p. 663-703.
- Feeley, T.C., 2003, Origin and tectonic implications of across-strike geochemical variations in the Eocene Absaroka volcanic province, United States: *Journal of Geology*, v. 111, p. 329-346.
- Frost, B.R., 2001, A geochemical classification for granitic rocks: *Journal of Petrology*, v. 42, p. 2033-2048.
- Hiza, M.M., 1999, The geochemistry and geochronology of the Eocene Absaroka volcanic province, northern Wyoming and Southwest Montana, USA: Ph.D. thesis, University of Oregon, Eugene.

- Jellinek, A.M., 1994, The Twin Peaks Caldera, Challis, Idaho: a unique window into the emplacement and evolution of a caldera-filling ignimbrite: M.Sc. thesis, University of Idaho.
- Le Bas, M.J., 1991, The IUGS systematics of igneous rocks: *Journal of the Geological Society of London*, v. 148, Part 5, p. 825-833.
- Lewis, R.S., and Kiilsgaard, T.H., 1991, Eocene plutonic rocks in south central Idaho: *Journal of Geophysical Research*, v. 96, p. 13295-13311.
- Lindsay, C.R., and Feeley, T.C., 2003, Magmagenesis at the Eocene Electric Peak-Sepulcher Mountain Complex, Absaroka volcanic province, USA: *Lithos*, v. 67, p. 53-76.
- Luedke, R.G., 1994, Map showing distribution, composition, and age of early and middle Cenozoic volcanic centers in Idaho, Montana, west-central South Dakota, and Wyoming: U.S. Geological Survey Miscellaneous Investigations Series Map I-2291.
- MacDonald, W.D., Palmer, H.C., and Hayatsu, A., 1998, Structural rotation and volcanic source implications of magnetic data from Eocene volcanic rocks, SW Idaho: *Earth and Planetary Science Letters*, v. 156, p. 225-237.
- McDonough, W.F., 1995, The composition of the Earth: *Chemical Geology*, v. 120, p. 223-253.
- Miyashiro, A., 1974, Volcanic rock series in island arcs and active continental margins: *American Journal of Science*, v. 274, p. 321-355.
- Moore, D.K., Hansen, S., Shurtliff, R., and Grover, S., 2010, Petrology of the igneous rocks of the Centennial and Henry's Mountains, Idaho, U.S.A.: Geological Society of America, Abstracts with Programs v. 42, p. 104.
- Moore, D.K., Wood, R.E., Sant, C.J., Miller, B.C., and Jordan, B.R., 2009, Petrology of the igneous rocks of Sawtell Peak, Idaho, U.S.A.: Geological Society of America, Abstracts with Programs v. 41, p. 114.
- Moye, F.J., Hackett, W.R., Blakley, J.D., and Snider, L.G., 1988, Regional geologic setting and volcanic stratigraphy of the Challis volcanic field, central Idaho: *in* Hughes, S.S., and Thackray, G.D., eds., *Guidebook to the Geology of Central Idaho*, Idaho Geological Survey, p. 87-99.
- Norman, M.D., and Mertzman, S.A., 1991, Petrogenesis of Challis Volcanics from central and southwestern Idaho; trace element and Pb isotopic evidence: *Journal of Geophysical Research*, v. 96, p. 13279-13293.
- O'Neill, J.M., and Christiansen, R.L., 2004, Geologic map of the Hebgen Lake Quadrangle, Beaverhead, Madison, and Gallatin Counties, Montana; Park and Teton Counties, Wyoming; and Clark and Fremont Counties, Idaho: U. S. Geological Survey Scientific Investigations Map 2816.
- Pearce, J.A., Harris, N.B.W., and Tindle, A.G., 1984, Trace element discrimination diagrams for the tectonic interpretation of granitic rocks: *Journal of Petrology*, v. 25, p. 956-983.
- Turrin, B., 2011, Unpublished $^{40/39}\text{Ar}$ ages, Rutgers University.

An early Yellowstone visitor. Courtesy National Park Service.



THE YELLOWSTONE VOLCANO CALDERA MARGIN, QUATERNARY VOLCANICS, AND SELECTED THERMAL FEATURES BETWEEN NORRIS GEYSER BASIN AND THE UPPER GEYSER BASIN, YELLOWSTONE NATIONAL PARK

Marc S. Hendrix

Department of Geosciences, University of Montana, Missoula, MT 59812

Yellowstone National Park contains the densest collection of active geothermal features occurring anywhere on Earth, including roughly one-half of the world's active geysers. The heat driving these geothermal features comes from an active thermal plume under the Yellowstone Volcano that has produced three major caldera-forming eruptions over the past 2.1 million years, in addition to large outpourings of rhyolite and minor eruptions of basalt between major caldera-forming events.

The northwestern margin of the most recent caldera is exposed in western Yellowstone Park. The caldera collapsed 640,000 years ago following the eruption of the Lava Creek Tuff. Since then, the caldera has largely been filled in with younger rhyolitic volcanics. This one-day field trip focuses on these geologic features east and south of Madison Junction and also provides an introduction to some of the active thermal features in the Norris and Upper Geyser Basins. A geologic map showing the field trip stops is provided as Figure 1 (modified from Christiansen, 2001). Radiometric dates are as reported by Christiansen (2001).

0.0 miles (0.0 km): Start at West Entrance to Yellowstone National Park

Beginning at the West Entrance, the West Entrance Road crosses glacial outwash overlying the Madison River Basalt (0.13-0.40 Ma), one of several post-caldera flows. At 6.4 miles, the road enters a can-

yon and passes by good exposures of the Mount Jackson rhyolite (0.609 ± 0.006 Ma), another of the pre-caldera flows. By 9.5 miles, post-caldera rhyolite flows of the West Yellowstone Flow ($.110 \pm 0.001$ Ma) form the canyon wall to the south. The caldera rim is less than a mile to the south along this stretch of the West Entrance Road, although it is largely covered by rhyolite flows of the Central Plateau Member, including the West Yellowstone Flow.

11.5 miles (18.5 km): Madison Junction: proceed left toward Norris Geyser Basin

Between Madison Junction and Gibbon Falls, the Grand Loop Road parallels the former margin of the caldera. The escarpment forming the south face of Purple Mountain is the topographic expression of this segment of the caldera margin, which is covered nearly everywhere else by younger volcanic flows. Across the Gibbon River to the south is the Nez Perce rhyolite flow, one of several voluminous post-caldera flows. We will examine parts of the Nez Perce Flow at Stop 4.

Purple Mountain, located between Madison Junction and Stop 1, consists of Lava Creek Tuff (0.640 ± 0.002 Ma) and is outside of the caldera. Christiansen and Blank (1972) subdivided the Lava Creek Tuff into an upper and lower member. Both members consist mainly of densely welded ash flow tuff, and the two members are separated by a widespread air fall tuff of low density. In this part of Yellowstone, the Lava Creek

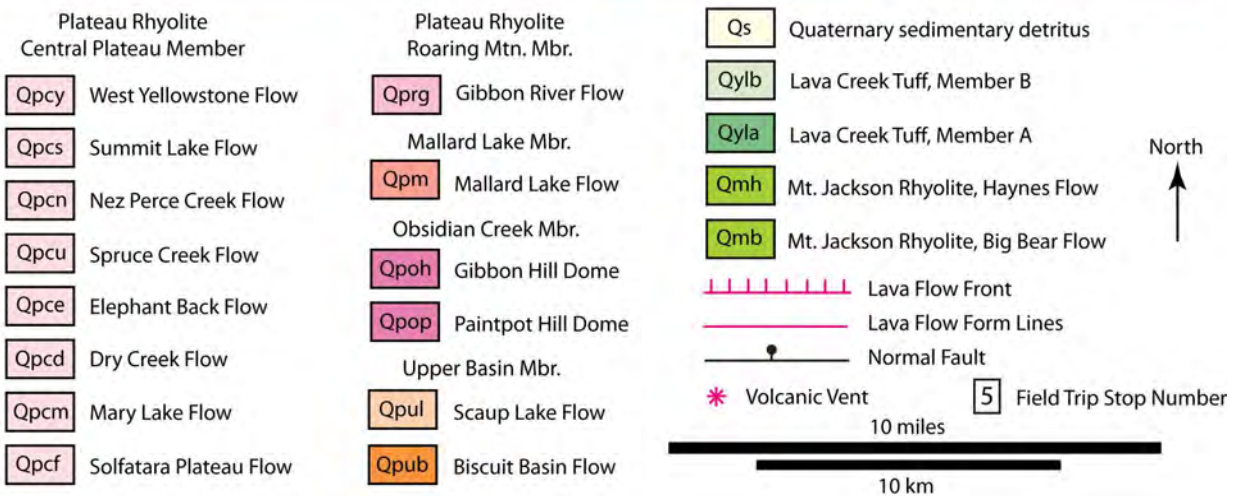
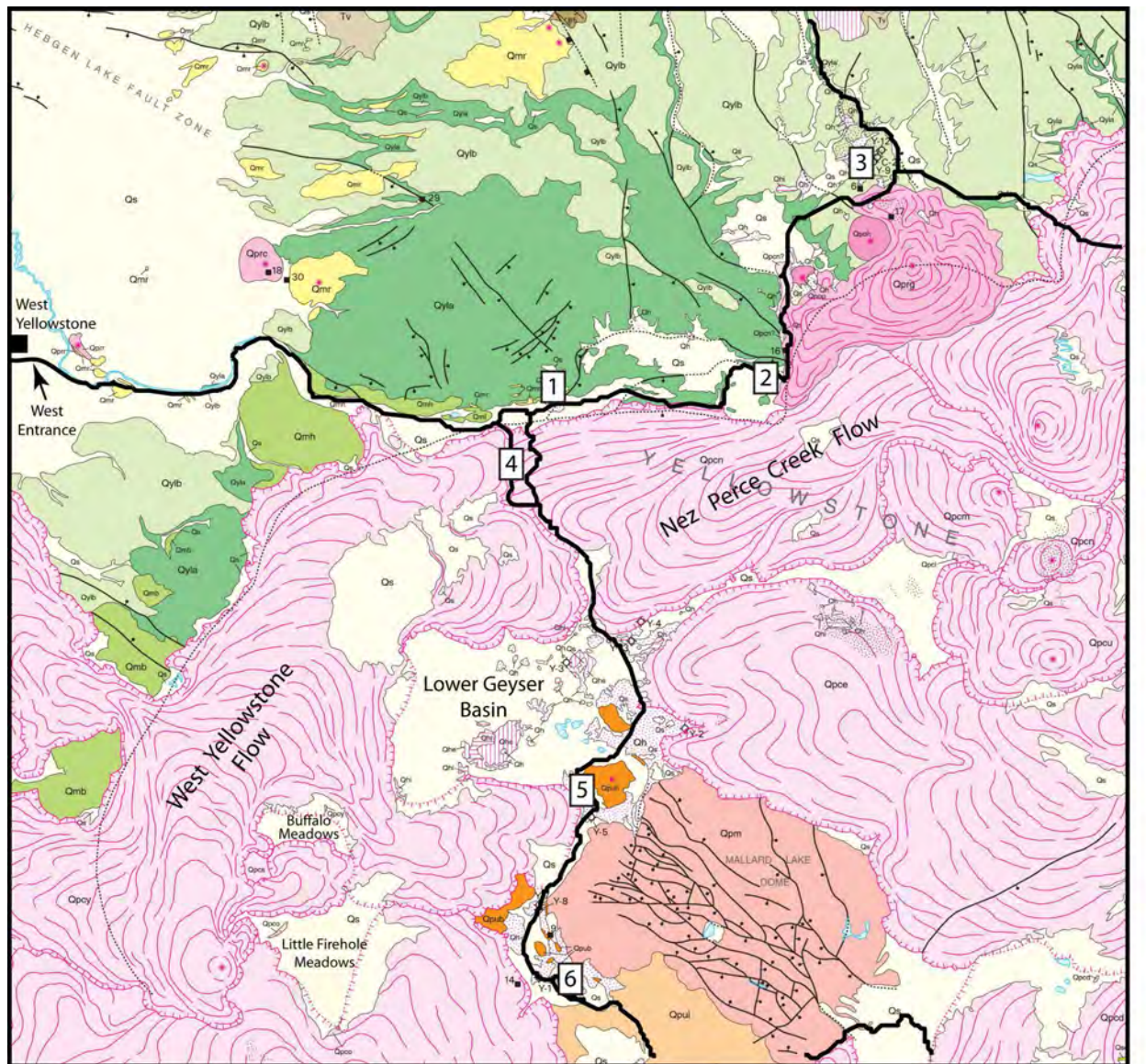


Figure 1: Geologic map of west central Yellowstone National Park, showing location of field trip stops (modified from Christiansen, 2001).

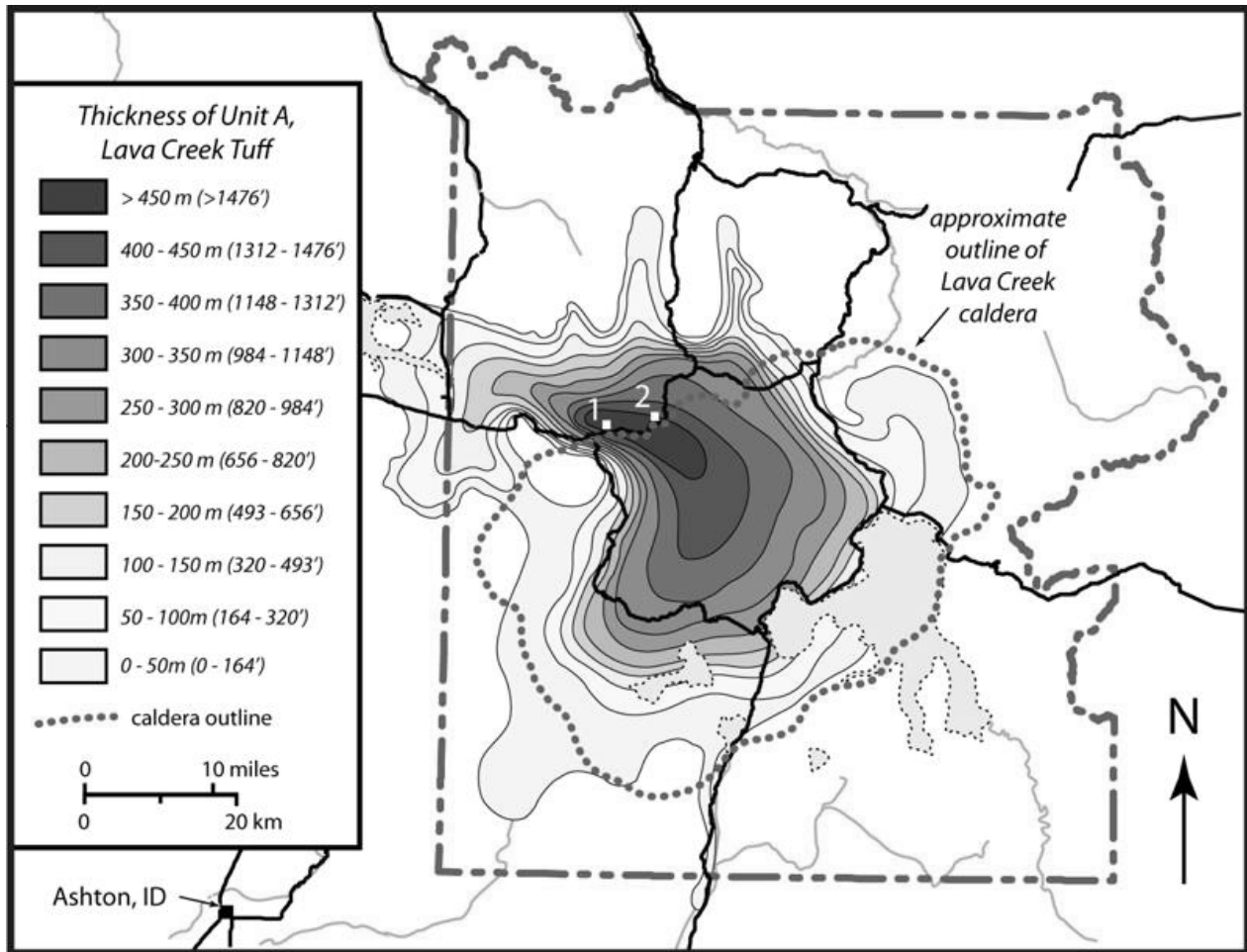


Figure 2: Isopach map of Lava Creek Tuff, Member A (modified from Christiansen, 2001). Location of field trips stops 1 and 2 are highlighted in white.

Tuff consists entirely of Member A, which is over 450 m thick and has an estimated initial volume of 510 km³ (Figure 2; Christiansen, 2001). Based on isopach trends, Member A likely erupted from the ring fracture system along this part of the caldera margin.

STOP 1 13.3 miles (21.4 km):
Stop 1: Tuff Cliff

Tuff Cliff (Figure 3) is an exposure of the lower part of Member A. At this stop, the lower part of Member A consists of a low-density ash flow breccia that has undergone vapor phase recrystallization. Several individual ash flows can be distinguished in the lower cliff, and large pumice clasts are abundant.

Continue east on Grand Loop Road. The Grand Loop Road passes several small road cuts of welded Lava Creek Tuff (Member A) before curving north near Gibbon Falls. About half a mile after turning north, the road climbs out of the Gibbon River Canyon up onto a flat surface formed by the top of the Lava Creek Tuff, here mantled by a thin cover of Quaternary alluvium.

18.0 miles (29.0 km):
Stop 2: Turn out loop on north side of road. **STOP 2**

From this vantage point, a prominent escarpment of Lava Creek Tuff is visible to the north, across the Gibbon River Canyon (Figure 4). This escarpment formed by collapse of a large slump block of Lava Creek



Figure 3: Tuff Cliff at Stop 1. Tuff Cliff is formed by the lower part of Member A and consists of at least two ash flows. Note the presence of large angular pumice clasts.

Tuff into the caldera shortly after it had collapsed. The slump block formed by catastrophic subsidence of the caldera floor along the main ring-fracture zone, followed by inward slumping of the oversteepened caldera walls. The slump block is about five miles in length (east-west) and about a mile across (north-south) and it extends from the vicinity of Stop 2 westward to the region between Madison Junction and Tuff Cliff (Figure 1).

Continue northward towards Norris Geyser Basin. From Stop 2, the Grand Loop Road drops off the slump block and re-enters the Gibbon River Canyon. The prominent canyon wall to the west consists of Member A

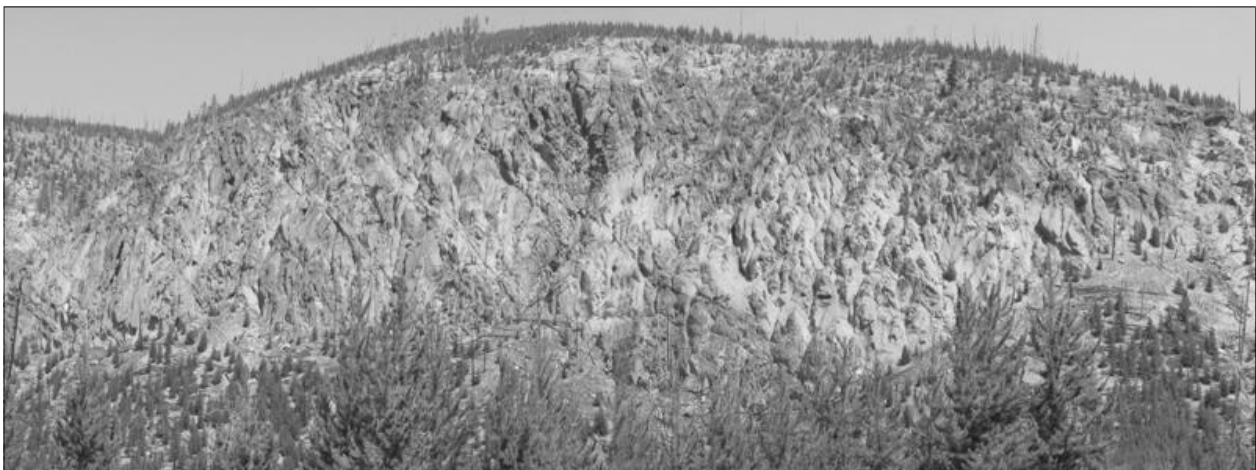


Figure 4: View to the north from Stop 2. The prominent escarpment consists of Member A of the Lava Creek Tuff and is the footwall of a large slump block that collapsed into the caldera shortly after it formed. Stop 2 is located on the slump block.

of the Lava Creek Tuff. The east wall of the Gibbon River Canyon is the Gibbon River Flow (0.090 ± 0.002 Ma). The road climbs slowly out of the Gibbon River Canyon and crosses Gibbon Meadows before traversing over a low ridge formed by both members of the Lava Creek Tuff. The tuff underlies the Norris Geyser Basin which is located several kilometers beyond the ridge.

25.1 miles (40.4 km):

Stop 3: Turn left (west) to
Norris Geyser Basin

STOP 3

The Norris Geyser Basin is located just outside the northwestern edge of the Yellowstone Caldera and is the most geologically unstable of Yellowstone's thermal areas. North-trending faults of the Norris-Mammoth corridor intersect the ring faults that define the caldera's margin, providing a fracture network that extends deep into the subsurface. The fracture network allows deep thermal water to reach the surface at Norris Geyser Basin.

Nearly every year, usually in August or September, thermal features across the basin undergo multiple simultaneous and generally temporary changes during a geothermal disturbance. Based on weekly sampling

and monitoring of eight different thermal features in Norris Geyser Basin in 1995, Fournier et al. (2002) concluded that the geothermal disturbance reflects a seasonal lowering of the water table that decreases the hydrostatic pressure in deep, superheated water sources under the geyser basin and promotes mixing of different water sources within the plumbing system of the basin.

Based on chemical and isotopic analysis, Fournier et al. (2002) suggested that the deepest source of thermal water in Norris Geyser basin is 0.5 mile (0.8 km) or more below the surface, clear blue, and >270 degrees C, although some estimates exceed 300 degrees C. Situated above this hot water is a reservoir of cooler water, estimated to be <250 degrees C. Relative to the water below it, this reservoir is acidic and cloudy because of suspended clay derived from altered volcanic rocks. The top layer is dominated by meteoric water derived from surface runoff.

Fournier et al. (2002) concluded that lowering of the water table during the geothermal disturbance causes superheated water at depth to flash to steam, and promotes mixing between acidic, cloudy water from intermediate depths and clear blue water from



Figure 5: Pearl Geyser in 2008; the milky color of the thermal water indicates that it has suspended silica colloids.

the deeper reservoir. This mixing causes acidic, muddy water to discharge from thermal features that normally are dominated by the clear blue water from the deeper reservoir. Other changes in the basin's thermal features that have been observed during past geothermal disturbances include temperature fluctuations, more frequent geyser eruptions, more vigorous boiling of some hot springs, and temporary conversion of some springs to fumaroles.

Proceed south along the Back Basin boardwalk to Pearl Geyser, a good example of a fountain geyser that has undergone significant changes in water chemistry and hydrology over the past several decades. In 1969, Pearl Geyser contained relatively clear, blue water reflecting the presence of dissolved silica colloids. During a particularly strong geothermal disturbance in August, 2003, Pearl Geyser lost its surface water and became a fumarole. Photographs of the geyser in 2008 show that it was bluish and milky, indicating that it contained dissolved silica as well as larger solid particles of suspended silica.

Continue west along the boardwalk to Porkchop Geyser, the site of a hydrothermal explosion in 1989. Hydrothermal explosions occur as superheated water in the subsurface flashes to steam, causing explosive ejection of overburden and the development of a crater. Such explosions can occur due to seasonal or climate-related decreases in hydrostatic pressure related to water table lowering or seismic energy. Although the Porkchop Geyser hydrothermal explosion was relatively small, much larger explosion craters have been documented along the northern margin of Yellowstone Lake, including Indian Pond (0.4 km diameter), Turbid Lake (1 km diameter), and Mary Bay (2.4 by 2.8 km), which may be the world's largest recognized hydrothermal explosion crater.



Figure 6: Porkchop Geyser with surrounding debris field from 1989 hydrothermal explosion.

The 1989 hydrothermal explosion of Porkchop Geyser was preceded by significant changes in the behavior and hydrology of the feature during the prior two decades (Fournier et al., 1991). Between 1960 and 1971, Porkchop Geyser was an unobtrusive vent a few centimeters across from which thermal water occasionally seeped. Beginning in 1971, infrequent eruptions began to occur, with spouts of water rising up to about 5 m. Presumably the transition from a thermal spring to a geyser resulted from precipitation of silica within the geyser vent and the development of a constriction. Additional silica precipitation and vent constriction caused the frequency of eruptions to increase, and by 1985 the geyser had developed into a perpetual spouter that produced a loud roar and formed a jet of thermal water about 9 m high.

The hydrothermal explosion occurred during the early afternoon of September 5, 1989, when the spout height more than doubled for several seconds before the geyser exploded. The explosion propelled large fragments of sinter outward as far as 60 m, leaving a crater about 11.5 x 13 m across and over one meter deep. The explosion likely resulted from sudden release of pressure as part of the constriction gave way,

reducing the confining pressure on superheated water within the geyser's plumbing system and leading directly to the explosion.

Return to bus by continuing clockwise around the Back Basin to the parking lot.

From Norris Geyser basin, backtrack to Madison Junction. Reset odometer at Madison Junction and proceed south on the Grand Loop Road.

0.5 miles (0.8 km): Stop 4: Turn right (west) into one-way Firehole River Canyon drive; continue to a small pull-out on left at 1.3 miles.

STOP 4

Collectively, the post-caldera rhyolite flows were so voluminous that they have filled in much of the youngest caldera. Forty individual post-caldera rhyolites across Yellowstone have been mapped, ranging in size and shape from relatively small domes less than 2.6 km² in area to gigantic flows exceeding 260 km² (Christiansen, 2001). Most are so large that it is difficult to appreciate their overall shape from the ground. The biggest individual flows are about 32 km across and nearly 300 m thick.

Vent locations have been determined by mapping flow boundaries and flow lines formed perpendicular to the direction of lava movement (Figure 1). Weathering of the rhyolite has produced thin, nutrient-poor soil unable to support diverse tree species. As a result, Yellowstone's forests consist almost exclusively of lodgepole pine (*Pinus contorta*) and are susceptible to large wildfires.

The first post-caldera rhyolites to erupt belong to the Upper Basin Member and range in age from 0.516 to 0.486 Ma. These flows were followed by emplacement of several relatively small rhyolite domes and the eruption of basalt flows, ranging in age from 0.399 to 0.151 Ma.

Massive outpourings of rhyolite forming the Central Plateau Member of the Plateau Rhyolite took place between 0.165 and 0.070 Ma – the age of the most recent eruptions from the Yellowstone Volcano. Differences in composition between Upper Basin Member and Central Plateau Member rhyolites, combined with the lack of widespread volcanism between the two members, suggest that rhyolites of the Central Plateau Member may represent the start of a new eruptive cycle of the Yellowstone Volcano.

Among the two largest flows in the Central Plateau Member are the Nez Perce Creek Flow and the West Yellowstone Flow, both of which are exposed in the Firehole River Canyon. The Nez Perce Creek Flow erupted 0.160 ± 0.002 Ma from a vent in the Mary Mountain region and traveled over 19 km west, reaching just beyond the Firehole River at Stop 4 (Figure 1).

The West Yellowstone Flow erupted 0.108 ± 0.001 Ma from a vent near the southwestern edge of the caldera and flowed about 24 km to the northeast, reaching nearly all the

way to what is now Madison Junction (Figure 1). The western end of the Nez Perce Creek Flow impeded the progress of the West Yellowstone Flow.

The front of the West Yellowstone Flow forms the canyon wall on the far (west) side of the Firehole River at Stop 4. The patterns visible on the canyon wall were formed by mixing of the moving lava along the flow front and formation of hyaloclastite by hydrothermal alteration along permeable zones within the lava.

Rocks exposed along the east (left) side of the road provide superb views of the internal structure of the Nez Perce Creek Flow, including interlayering of flow-banded and autobrecciated rhyolite (Figure 7). About 75 m up the canyon from the pullout are angular clasts of black obsidian encased in a light-colored, ash-rich matrix. The fact that the clasts are made of obsidian sug-

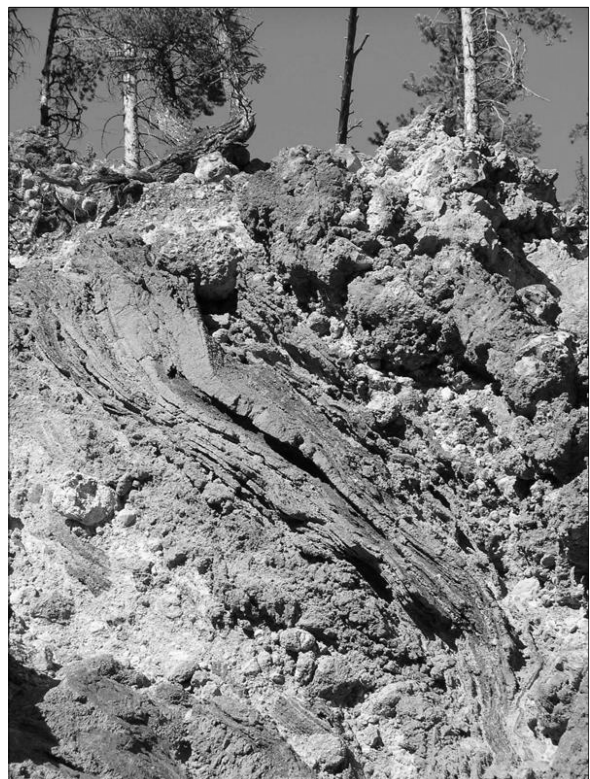


Figure 7: Interstratification of flow-banded and autobrecciated rhyolite in the Nez Perce Creek Flow at Stop 4.

gests that the lava cooled very rapidly, and the angularity of the clasts suggests that this process was violent enough to brecciate the quenched lava. Perlite, hydrated obsidian preserved as masses of BB-sized spherules, also is common at Stop 4 (Figure 8), suggesting that the Nez Perce Creek Flow may have encountered a body of cold water or glacial ice at this point.

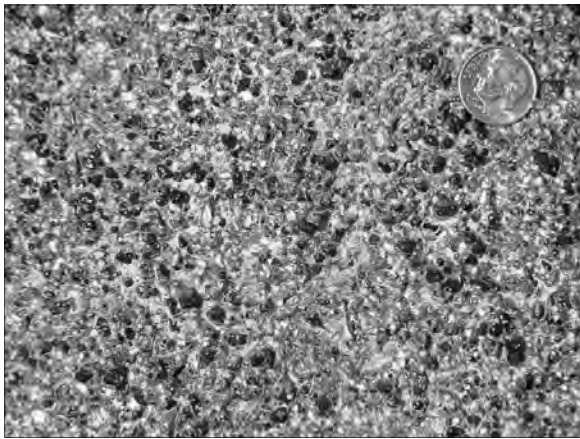


Figure 8: Perlite in rhyolite of the Nez Perce Creek Flow at Stop 4.

Similar perlite forms a sheath along the eastern margin of the West Yellowstone Flow at the Little Firehole Meadows, Buffalo Meadows, and Lower Geyser Basin (Christiansen, 2001). At those locations, the flow also contains several odd reentrants (Figure 1), suggesting that the lava may have encountered lobes of glacial ice. Cosmogenic dating of erratic boulders in the Yellowstone region (Licciardi et al., 2001; Licciardi and Pierce, 2008) suggests that the Bull Lake glaciation had reached its maximum advance as little as 12,000 years before the West Yellowstone Flow erupted, permitting the interpretation that there may have been ice lobes remaining from the Bull Lake glaciation during the eruption.

From Stop 4, return to Grand Loop Road and proceed south.

Mile 10.4 (16.7 km): Stop 5, small pullout on east side of road just beyond the turn-off to Midway Geyser Basin.

STOP 5

Stop 5 provides a good view of the Biscuit Basin Flow (Figure 9), one of two relatively small post-caldera flows belonging to the Upper Basin Member. The Upper Basin Member predates the massive rhyolite outpourings of the Central Plateau Member. The Biscuit Basin Flow is dated at 0.516 ± 0.007 Ma and is the first recognized volcanic rock to have erupted after the Lava Creek Tuff and caldera collapse. The Biscuit Basin Flow vent is approximately 1.6 km northeast of Stop 5.



Figure 9: The Biscuit Basin Flow at Stop 5.

Flow banding is well developed at the base of the Biscuit Basin Flow at Stop 5. The flow banding contrasts with fragmented and brecciated rhyolite at the top of the exposure, indicating that the upper surface of the flow had started to cool and solidify while the hotter interior behaved plastically. In several places there are centimeter-scale recumbent folds in the flow banding (Figure 10); larger meter-scale folds also are present though less obvious.

The Biscuit Basin Flow at Stop 5 also contains abundant spherical lithophysae, likely formed from vapor-phase precipitation of



Figure 10: Recumbent folds in the lower part of the Biscuit Basin Flow at Stop 5.

finely crystalline minerals on the interior of gas bubbles formed in the lava. Note that the lithophysae are absent in the dark gray rhyolite at the base of the outcrop on its southern end but increase in abundance upward, reflecting the decrease in pressure at higher levels within the flow.

Abundant clear or white oligoclase feldspar crystals also characterize the lowest parts of the flow. Gansecki et al. (1996) demonstrated that the ages of individual crystals in Upper Basin Member rhyolites vary widely despite similar appearance and co-occurrence. Termed xenocrysts (from Greek for ‘stranger’), many of the crystals were interpreted by Gansecki et al. (1996) to have been derived from older rhyolites forming the vent walls that the magma passed by during the eruption, rather than forming from the cooling melt directly. Abundant perlite also characterizes the lower part of the Biscuit Basin Flow at Stop 5.

From Stop 5, continue south on Grand Loop Road

15.8 miles (25.4 km): Stop 6: Upper Geyser Basin. Take the Upper Geyser Basin

STOP 6

exit and follow the signs to Old Faithful Lodge and Old Faithful.

Located in the upper reaches of the Firehole River drainage, the Upper Geyser Basin contains a wide variety of geothermal features, including Old Faithful, Yellowstone’s most famous geyser. Start at the Visitor Center and proceed to the boardwalk surrounding Old Faithful Geyser.

Old Faithful Geyser was named on September 18, 1870, by members of the Washburn-Langford-Doane expedition. It is a good example of a cone geyser in which siliceous sinter surrounding the vent forms a cone, and a constriction in the vent causes thermal water to be erupted as a vertical jet. The constriction of the vent is produced by precipitation of amorphous sinter spicules on the vent interior. The spicules are elongate and grow inward, forming a palisade-style fabric that resists destruction by the erupting thermal water. Ongoing precipitation of sinter in the geyser conduit can change the style and frequency of eruptions and ultimately seal the conduit altogether, causing the geyser to become inactive. The presence of inactive sinter mounds in the vicinity of Old Faithful suggests that cone geysers similar to the currently active geyser existed here recently.

Episodic geyser eruptions like those of Old Faithful are produced by heated groundwater and are a function of the shape of the geyser conduit. Too little water in the plumbing system will result in a fumarole, whereas too much water or insufficient heat will produce a thermal spring. A constriction that delays the escape of steam to the surface is needed for pressure to build enough to initiate an eruption.

Following an eruption, a geyser’s plumbing system is refilled by the thermal water draining back into the vent, by lateral flow from shallow groundwater, and from upward circulation of thermal water from greater depths. As the plumbing system re-

fills, hydrostatic pressure causes superheating of thermal water to beyond the boiling point. As the superheated water circulates upward and hydrostatic pressure decreases, some of it turns to steam which rises in the plumbing system, heating cooler water at shallower depths and escaping out the geyser's vent. Some of the steam can become trapped at constrictions within the conduit. As the size of the steam bubble grows, some of the overlying water is forced out of the vent, lowering the confining pressure in the conduit below. The pressure decrease causes superheated water in the shallower parts of the plumbing system to boil, initiating the main eruption as water and steam are forced past the constriction. The escape of this water in turn lowers pressure at greater depths within the main reservoir, causing superheated water there to flash to steam and sustaining the eruption until insufficient water remains or the temperature drops enough to prevent further mass boiling.

Between 1983 and 1994, Hutchinson et al. (1997) lowered a video camera, thermometers, and pressure gauges down the uppermost portions of Old Faithful geyser's conduit. They found that Old Faithful's conduit is dominated by a single, east-west, mostly vertical opening. It contains a constriction roughly 10.5 cm wide and no more than two meters long at a depth of about 6.4 m. Hutchinson et al. interpreted the constriction to be a choke point and estimated that during the peak of an eruption, thermal fluids move past the choke point at about 70 m per second or 253 km per hour (157 miles per hour).

Although widely regarded as perhaps the most predictable geyser on Earth, both long-term and short-term variations in eruptive behavior of Old Faithful Geyser have been observed. Hurwitz et al. (2008) correlated the eruptive interval over multi-

year periods with the discharge of the Madison River, to which the Firehole River is a tributary. During years when flow in the Madison River is high, more water is available to fill the plumbing system, increasing hydrostatic pressure and resulting in more frequent eruptions. During low-flow years, less water is available, decreasing hydrostatic pressure and leading to less frequent eruptions. Seasonal variations in runoff also affect the eruptive interval. The longest intervals typically occur in the spring and summer, during and after peak runoff when cooler water infiltrates the system. The shortest eruptive intervals occur in the fall and winter when warmer water infiltrates the plumbing system and the thermal water there heats more quickly.

Earthquakes also have affected the eruptive behavior of Yellowstone's geysers. Old Faithful's eruptive interval increased immediately after the 1959 Hebgen Lake earthquake (Marler, 1964) and again after the 1983 Borah Peak earthquake in Idaho (Hutchinson, 1985). Variations in eruptive behavior related to earthquakes likely result from physical alteration of the plumbing system or conduit or both as sediment or rock is dislodged and affects the circulation of thermal water.

From Old Faithful, proceed east across the footbridge and onto the boardwalk towards Pump Geyser (Figure 11). Pump Geyser is a good example of a fountain geyser in which hot water erupts from an open pool and splashes back into and around the vent. This process produces the surging eruption characteristic of Pump Geyser and rapidly refills the geyser conduit, typically within a few seconds. Although much of the water flows back into the vent following each surge, some flows into the surrounding moat or runs off in a small stream that passes under the boardwalk.

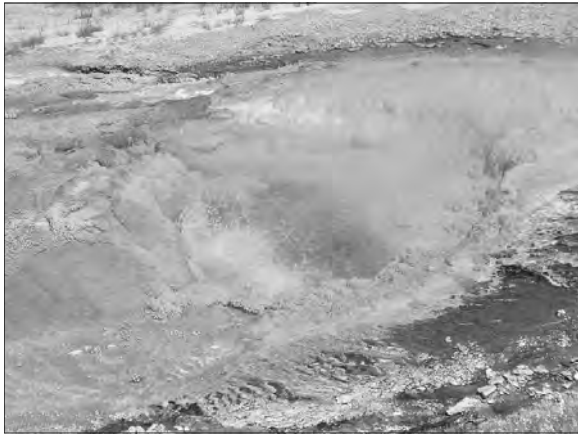


Figure 11: Pump Geysers, a good example of a fountain geysers.

The thermal water erupting from Pump Geysers is about 86 degrees C and supports a community of thermophilic archaea and bacteria. Chlorophyll and carotenoid compounds in the microorganisms produce the bright colors of the sinter in the geyser pool and the stream draining away from it. Distinct color zonations of the sinter result from the specific temperature tolerances of the different thermophiles.

Sinter morphologies around Pump Geysers vary depending on their proximity to the vent and the runoff stream produced by the geyser. Complete submergence or constant wetting of sinter produces a botryoidal (globular) habit. This habit is formed by elongate silica spicules oriented perpendicular to the growth surface. The spicules form a palisades-type structure similar to that observed in the conduits of fountain geysers. More unusual are the small mushroom-like knobs that occur around the rim of the geyser's vent and within and along the small stream of water running from the geyser. The knobs form from episodic wetting and drying of their upper surface. Sinter precipitates more rapidly there than on the narrower columns underneath which are constantly wet.

From Pump Geysers, proceed northward along the boardwalk to Doublet Pool, a

good example of a thermal spring. The deep blue color of the thermal water is particularly striking. Although water has a natural blue color due to preferential absorption of red wavelengths within the visible spectrum, the more intense blue color of Doublet Pool is caused by Rayleigh scattering of the blue portion of the visible spectrum by silica colloids in the water. The longer molecular chains of silica (between 0.1 and 0.5 μm) are particularly effective at scattering blue wavelengths of light.

The water below the surface in the deepest parts of Doublet Pool also appears to shimmer faintly, similar to the way that salt or sugar water poured into a glass of freshwater produces a shimmering as the different density fluids mix and the refractive index varies. In Doublet Pool, local variations in the amount of dissolved silica alter the refractive index in the turbulently-circulating fluid to produce the shimmering.

The white crust protruding into Doublet Pool from its margins is characteristic of many thermal springs. The lower surface of the crust is approximately level with the water surface and is constantly wet. In contrast, the top of the crust is usually dry and slopes slightly away from the edge of the



Figure 12: Doublet Pool. The striking blue color is produced by Rayleigh scattering of silica colloids in the water.

pool. Numerous lobe-shaped protrusions characterize the crust, which extends from the pool edges out and over the water surface about ten cm. The tips of the lobes are bright white, whereas the crust a few centimeters away from the water's edge weathers to gray. Further away from the water's edge, the crust is covered by loose sediment weathered from the surrounding ground surface. Examining similar crusts in hot springs from Yellowstone, Braunstein and Lowe (2001) found that the crust is laminated and very porous, and that seasonal changes in air temperature altered the rate of precipitation. Sinter precipitation rates were highest in the fall, winter, and spring and lowest in the summer, consistent with the observed inverse relationship between the temperature of the thermal water and silica concentration.

Time permitting, other examples of thermal features can be viewed by continuing around the Upper Geyser Basin boardwalk. Return to bus.

End of field trip.

Return to West Yellowstone via Grand Loop Road to Madison, then west on West Entrance Road.

References

Braunstein, D., and Lowe, D. R., 2001, Relationship between spring and geyser activity and the deposition and morphology of high temperature (>73°C) siliceous sinter, Yellowstone National Park, Wyoming, U.S.A.: *Journal of Sedimentary Research* 71, p. 747–63.

Christiansen, R. L., 2003, The Quaternary and Pliocene Yellowstone Plateau Volcanic Field of Wyoming, Idaho, and Montana: U.S. Geological Survey Professional Paper 729-G, 145 p.

Christiansen, R.L., and Blank, H.R., Jr., 1972, Volcanic stratigraphy of the Quaternary rhyolite plateau in Yellowstone National Park: U.S. Geological Survey Professional Paper 729-B, 18 p.

Fournier, R. O., Thompson, J.M., Cunningham, C.G., and Hutchinson, R.A., 1991, Conditions leading to a recent small hydrothermal explosion at Yellowstone National Park: *Geological Society of America Bulletin* 103, p. 1114–20.

Fournier, R.O., Weltman, U., Counce, D., White, L.D., and Janik, C.J., 2002, Results of weekly chemical and isotopic monitoring of selected springs in the Norris Geyser Basin, Yellowstone National Park during June-September, 1995: U.S. Geological Survey Open-File Report 02–344, 49 p.

Gansecki, C.A., Mahood, G.A., and McWilliams, M.O., 1996, $^{40}\text{Ar}/^{39}\text{Ar}$ geochronology of rhyolites erupted following collapse of the Yellowstone Caldera, Yellowstone Plateau Volcanic Field: implications for crustal contamination: *Earth and Planetary Science Letters* 142, p. 91–107.

Hurwitz, S., Kumar, A., Taylor, R., and Heasler, H., 2008, Climate-induced variations of geyser periodicity in Yellowstone National Park, USA: *Geology*, v. 36, p. 451–54.

Husen, S., Smith, R.B., and Waite, G.P., 2004, Evidence for gas and magmatic sources beneath the Yellowstone Volcanic Field from seismic tomographic imaging: *Journal of Volcanology and Geothermal Research* 131, p. 397–410.

Hutchinson, R.A., 1985, Hydrothermal changes in the Upper Geyser Basin, Yellowstone National Park, after the 1983 Borah Peak, Idaho, earthquake: *Proceedings of Workshop XXVIII on the Borah*

Peak, Idaho, Earthquake: National Earthquake Prediction and Hazard Programs Open-File Report 85-290, Vol. A.

Hutchinson, R.A., Westphal, J.A., and Kieffer, S.W., 1997, In situ observations of Old Faithful Geyser: *Geology*, v. 25, p. 875–878.

Licciardi, J.M., Clark, P.U., Brook, E.J., Pierce, K.L., Kurz, M.D., Elmore, D., and Sharma, P., 2001, Cosmogenic ^3He and ^{10}Be chronologies of the late Pinedale northern Yellowstone Ice Cap, Montana, USA: *Geology*, v. 29, p. 1095–1098.

Licciardi, J.M., and Pierce, K.L., 2008, Cosmogenic exposure-age chronologies of Pinedale and Bull Lake glaciations in greater Yellowstone and the Teton Range USA: *Quaternary Science Reviews* 27, p. 814–831.

Marler, G.D., 1964, Effects of the Hebgen Lake earthquake of August 17, 1959, on the hot springs of the Firehole geyser basins, Yellowstone National Park: *in* The Hebgen Lake, Montana, earthquake of August 17, 1959, U.S. Geological Survey Professional Paper 435-Q, p. 185–97.

Ohsawa, S., Kawamura, T., Takamatsu, N., and Yusa, Y., 2002, Rayleigh scattering by aqueous colloidal silica as a cause for the blue color of hydrothermal water: *Journal of Volcanology and Geothermal Research* 113 (1–2):49–60.



Norris Geyser Basin, 1902. Courtesy National Park Service.

CENTENNIAL VALLEY—EAST TO WEST: A FIELD TRIP CROSSING THE GREAT DIVIDE (TWICE)

B.E. Cox and Jo-Ann Sherwin

Compilers of road log and references

Introduction

An intricate geologic story for Montana's Centennial Valley has been quietly assembled by many of our geologic colleagues over the past few decades. As with any truly good story, it gets better with time. Recent work has emphasized the topographic expression of Holocene faults and the evolution of major, Late Pleistocene faults which bound and transect the valley and Centennial Range to the south. Observations of F.E. Petrik (2010) introduce several features to be seen and discussed on this trip: "The present Centennial Mountains are subdivided into two stratigraphically different blocks by the Odell Creek normal fault. The eastern Centennial Mountains are interpreted as the upthrown block of the Odell Creek normal fault exposing Precambrian and Paleozoic rock along the northern face of the range. The western Centennial Mountains are interpreted as the downthrown block of the Odell Creek normal fault exposing Cretaceous and younger rocks. Both eastern and western segments of the Centennial Mountains are then offset along the range-bounding Centennial normal fault. Offset along the Centennial normal fault started approximately 2.1 Ma as evidenced by the displacement of the 2.1 Ma Huckleberry Ridge tuff. It is believed that prior to the emplacement of the 2.1 Ma Huckleberry Ridge tuff, the Centennial Mountains had minimum to no surface relief. The majority of offset along the Centennial normal fault has occurred within the Late Pleistocene with estimated slip rates of 0.65-0.82 mm/yr. Late Pleistocene surface offsets along the Centennial Mountains

have an average of 9.1-9.6 meters with similar offsets seen along the eastern and western segments."

The road log presented here, between miles 18.5 and 62.9, is condensed from a detailed log prepared by W.J. McMannis and Fred Honkala for the Billings Geological Society's ("BGS") 11th annual field conference in 1960. Their log has been updated and annotated to include new stops for inspection and discussion. The reader/traveler is encouraged to track the BGS log as well. Note: there are no services for the next 100 miles (82 miles are unpaved); be sure your tank is topped-off and spare tires ready.

Road Log - The field trip route and planned stops are shown on Figure 1.

Leave West Yellowstone and drive west on State Highway 20.

Set Odometer to 0.0 at the junction of State Highways 287 and 20. Turn west and stay on Hwy 20 for 13 miles.

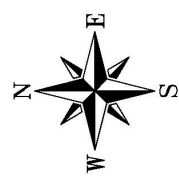
9.0 Targhee Pass. Cross the Continental Divide and enter Idaho.

13.0 Junction of Hwy 20 and Hwy 87. Turn RIGHT (NW) on Hwy 87. The highway eventually wraps around the north shore of Henry's Lake. Black Mountain, rising north and east above the lake, is underlain by Lower Proterozoic metamorphic rocks.

18.5 Junction of Hwy 87 and Henry's Lake Drive (US Forest Service Road 055).



FIGURE 1
CENTENNIAL VALLEY FIELD TRIP



EXPLANATION

● FIELD TRIP STOP
STOP 3

Figure 1. Route Location Map for the Centennial Valley Road Log. Approximately 100 miles east to west; eight Field Trip Stops noted.

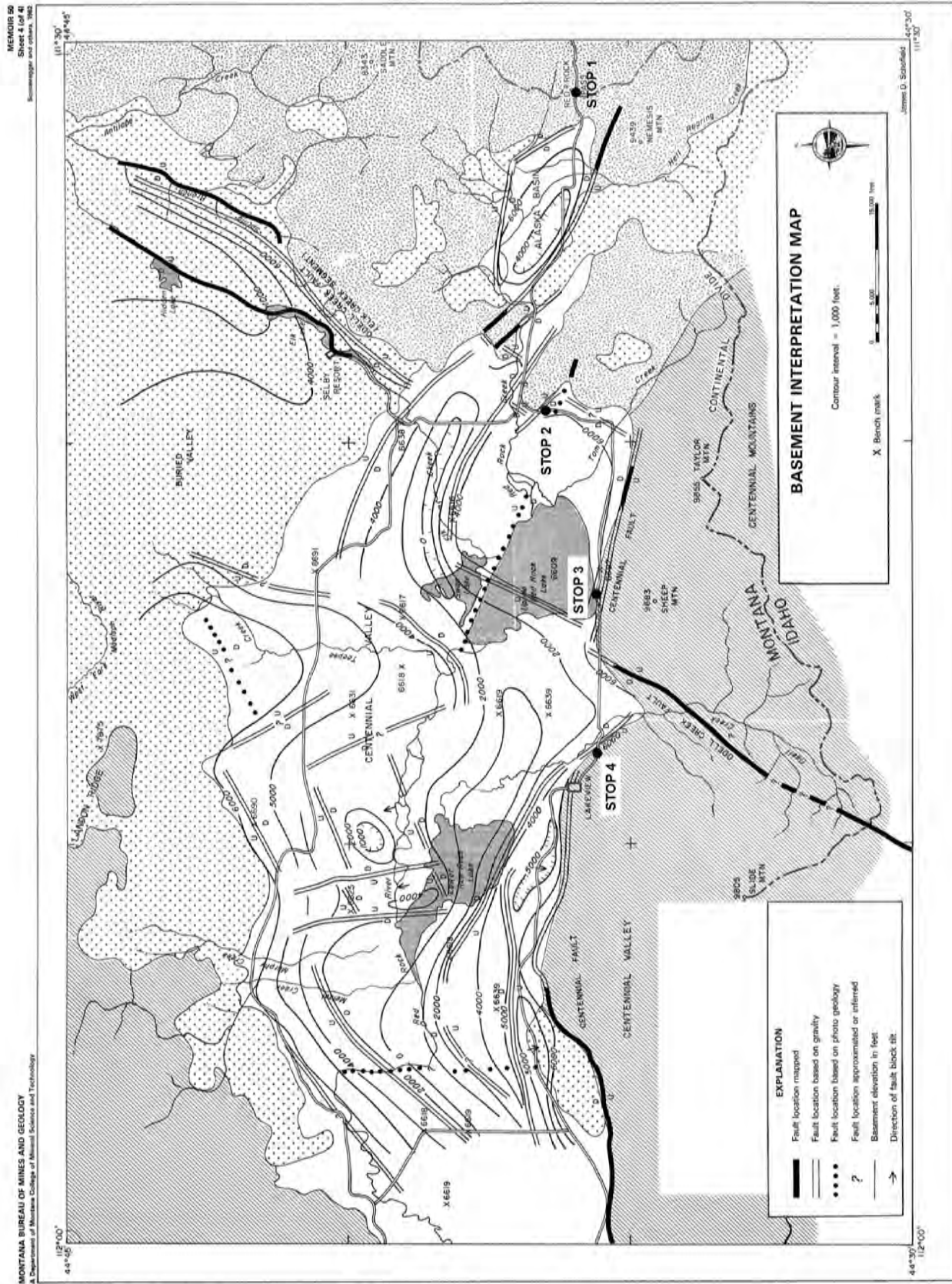


Figure 2. Eastern Centennial Valley Basement Interpretation Map. Modified from Sheet 4 by J.D. Schofield in Sonderegger et al. (1982). Field Stops 1-4 are shown.

The BGS road log mileage here is 14.05 [sic]. Turn LEFT (SW). There are rhyolite outcrops and boulders for the next six miles. They are locally lithophysal, which is likely to have formed during the flow from vapor-phase precipitation of finely crystalline material on the interior of gas bubbles in the lava (Hendrix, M., this volume).

24.4 Junction of Henry's Lake Drive and USFS Road 053 (Red Rock Road), STAY RIGHT (SW) toward Red Rock Pass. Road name changes from Red Rock Road to Red Rock Pass Road.

STOP 1 **29.0** STOP 1: Red Rock Pass, Elev. 7,150 feet. This is a mature erosional surface with a terminal moraine in the timber at left. This is the eastern margin of the complex faulted terrain of Centennial Valley including the Alaska Basin, a basement depression that was geophysically interpreted (Figure 2). Cross the Continental Divide and re-enter Montana.

32.8 Roadcuts to the left are composed of rhyolite.

33.4 We are travelling parallel to a young fault scarp on the left.

34.0 At 3:00 there is a NW-trending fault offsetting the rhyolite.

34.4 Up-faulted remnant of an erosional surface in front of Paleozoic cliffs of the Centennial Range. Peaks of the Snowcrest Range are at 1:00.

35.8 Boundary of Red Rock Lakes Migratory Waterfowl Refuge.

36.5 Junction of USFS Road 053 and Elk Lake Road, STAY LEFT (south). To the left are Precambrian carbonate strata which

have been contorted and silicified. Road name changes to County Route 509 (South Valley Road).

37.0 STOP 2: This stop is on the trace of a suspect normal fault which forms the linear north shore of Upper Red Rock Lake. The high escarpment ahead (south) is a west-northwest trending strand (?) of the Centennial fault. Note the terminal moraines of small valley glaciers at the base of the Range. On aerial photos, some of these moraines appear to override beach lines of an old Pleistocene Red Rock Lake.

38.8 Cross Tom Creek.

42.4 STOP 3: Upper Lake Campground. Lunch.

45.4 Cross Odell Creek.

45.8 STOP 4: Junction of County Road 509 and Odell Creek Road. This is on the down-thrown block of the Odell Creek-Elk Creek fault and is underlain by Cretaceous Frontier Formation. Triassic and Permian rocks (including phosphorites of the Phosphoria Formation) form the crest of Sheep Mountain on the up-thrown block on the skyline to the southeast. This field trip will not follow the phosphate mine side trip noted in the BGS road log. Continue STRAIGHT, westward toward Monida.

46.0 Lake View. Headquarters for Red Rock Lakes Migratory Waterfowl Refuge.

47.0 Baldy Mountain, elev. 9,889 feet, to the left. It is composed of Cretaceous sediments overlain by Tertiary volcanics. Lower Red Rock Lake is at 2:00.

47.6 Landslide from 10-12:00 developed

along the Centennial fault. This fault scarp is characteristically unstable and there are many landslides evident along the fault between here and Monida.

48.9 Views of Baldy Mountain, left, for about the next mile. Note volcanic neck on spur to left of peak.

54.1 Young scarp along Centennial fault expressed by local steepening at base of slope, 9:00.

56.0 Slump along scarp at left.

STOP 5 **57.1** STOP 5: Small knob at 2:00 has outcrops of suspect pillow basalts underlain by two or more rhyolite flows. These strata are dipping steeply northward toward the center of the Centennial Valley. Outcrops north and east of Stop 5 may be offset segments of this volcanic sequence.

58.6 Aspen-covered hills to left are in Cretaceous (Colorado Group) rocks, which are folded into the Peet Creek Anticlinorium.

59.3 Note southwest-dipping slopes off flanks of folds in Cretaceous rocks at 9:00.

60.4 Scarp cuts stream deposits at mouth of small creek at 9:00.

STOP 6 **62.9** STOP 6: Junction of Blacktail-Deer Creek Road 202. The road log turns northward here on Price Lane, crosses Red Rock River, and makes two stops on the northern side of the Centennial Valley before arriving at I-15 at Lima. Persons wishing a more direct route to the paved road can continue westward. That route follows the trace of the Centennial fault for 2.6 miles, then traverses alluvial fan deposits and the Beaverhead Formation for another 6.4 miles to I-15 at Monida.

From Stop 6, TURN RIGHT (north) across the Centennial Valley. The Snowcrest Range is straight ahead. This valley is typical of many intramontane structural basins in Southwestern Montana. It is far too large to have been formed by the westward-flowing Red Rock River, and contains remnants of larger Pleistocene lakes that once occupied it. Pleistocene and Recent sediments cover the valley floor and may overlie older Tertiary volcanics.

66.0 Price Lane turns left. STAY RIGHT on Road 202.

66.2 Bridge over Red Rock River. Snowcrest Range ahead. Antone Peak is the highest point on skyline. From 9 to 12:00, the range crest is underlain by rocks of the Cretaceous Beaverhead Formation in a broad syncline resting unconformably on older rocks.

66.5 Junction of Blacktail-Deer Creek Road 202 and North Valley Road 204. Turn LEFT (NW) and stay on Road 202 – the TRGS trip leaves the BGS trip at this junction.

67.1 Road 202 makes a 90-degree turn northward.

70.6 Road 202 makes a 90-degree turn westward. For the next ~2.6 miles, the road follows the contact between Quaternary alluvial fan deposits (left) and Beaverhead Formation rocks (right).

70.9 Cross First Wolverine Creek.

71.8 Cross Second Wolverine Creek.

72.7 Cross Sandy Creek.

73.2 Pass Sandy Creek Road on right. STAY ON ROAD 202 which bends southwest.

74.5 Junction. Blacktail-Deer Creek Road 202 turns westward. TURN HARD LEFT (south) on Road 205 toward Lima.

75.0 Cross main channel of Clover Creek.

76.0 Road 205 makes a 90-degree turn westward.

STOP 7

76.2 STOP 7: Head-scarp and discussion of Lateral Spread flanking the Lima Reservoir. Along the north side of Lima Reservoir, there are a number of landslides on the hills flanking the Centennial Valley, and on the gently sloping valley floor. Bartholomew et al. (2002) interpret a large area (at least 5.5 km in the east-west direction and about 5 km from north to south) as a low-angle landslide or lateral spread that was most likely associated with liquefaction of valley sediments during strong seismic shaking accompanying a large earthquake. A headscarp, with right-angle bends and up to 20-foot high offsets, defines the top of the lateral spread where it cuts the alluvial fan gravels of Clover Creek. The lateral spread obliterates the geomorphic expression of the Lima Reservoir fault where the fault trends into the landslide mass. An unusual linear drainage with perpendicular branches is roughly collinear with the Lima Reservoir fault and may reflect its presence below the slide mass. The lower part of the landslide closest to Lima Reservoir is underlain by Pleistocene lacustrine deposits that have a “churned” appearance in aerial photographs; these lacustrine sediments may have played a crucial role in the movement of the lateral spread. A trench excavated across the Lima Reservoir fault in 1986 provides evidence for six earthquakes that ruptured at the surface during the late Quaternary (Bartholomew et al., 2002).

Continue on Road 205 for approximately 8.4 miles, crossing Shineberger Creek and Trail Creek en route. Beaverhead Formation rocks are north of the road; Quaternary lake deposits and Lima Reservoir are to the south. Most of this distance is on or near the trace of the landslide headwall.

84.5 STOP 8: Continued discussion of the Lima Reservoir lateral

STOP 8

spread. From here, a USDI Bureau of Land Management guide will lead a 3/4 mile round-trip walking traverse to the Merrell Paleontology / Archaeology site. Note: visitors are welcome to examine and photograph (but not touch) any fossils and artifacts that may be exposed. These items are protected under the Antiquities Act and it is important that they be preserved.

Donald Merrell, a lifelong resident of Lima, Montana, discovered fossil bones at Lima Reservoir and brought them to the attention of the Bureau of Land Management in 1988. Since then, the Merrell Site has been the focus of several paleontologic and archaeological investigations (Hill and Davis, 2005). Site stratigraphy is comprised of Late Pleistocene alluvium, lacustrine, and debris flow sediments overlain by colluvial soils. Researchers have identified over 19 species of Pleistocene fauna including a mammoth, scimitar cat, horse, Yesterday’s camel, and a Trumpeter swan. This was the first trumpeter swan fossil found in Montana. Finite radiocarbon (C14) dates for these fauna range from ca. 49,000 to 19,000 years BP. The Merrell Site has yielded fewer than 100 plains paleoindian artifacts including four stone tools. Sadly, a reliable chronology of the artifacts has been compromised by bioturbation and erosion.

Return to vehicles, continue westward on Road 205.

92.9 Four-way intersection. BEAR RIGHT (westward) and stay on Road 205.

98.4 Lima, Montana. US I-15 junction is 0.5 miles south (left).

End of Road Log.

Acknowledgements

When the designated trip leaders were unable to attend, this road log was cobbled together with excellent support and contributions from Liz Younggren, Michael Stickney, Larry Johnson, and Falene Petrik. Many thanks to you all.

References

Bartholomew, M.J., Stickney, M.C., Wilde, E.M., and Dundas, R.G., 2002, Late Quaternary paleoseismites: Syndepositional features and section restoration used to indicate paleoseismicity and stress-field orientations during faulting along the main Lima reservoir fault, southwestern Montana: *in* Ettensohn, F.R., Rast, N. and Brett, C.E., eds., *Ancient Seismites: Boulder, Colorado*, Geological Society of America, Special Paper 359, p. 298-47.

Hill, C.L., and Davis, L.B., 2005, *The Merrell Locality (24BE1659) and Centennial Valley Southwest Montana: Pleistocene Geology, Paleontology, and Prehistoric Archaeology*: U.S. Bureau of Land Management Cultural Resources Series No. 4, Billings, Montana, 166 p.

McMannis, W.J., and Fred Honkala, 1960, *Geologic Road Log, Madison Canyon Slide to Southern Gravelly Range via Centennial Valley*: Billings Geological Society 11th Annual Field Conference, pages 284-288.

Mumma, S. A., Whitlock, Cathy, and Pierce, Kenneth, 2012, A 28,000 year history of vegetation and climate from Lower Red Rock Lake, Centennial Valley, Southwestern Montana, USA: *Palaeography, Palaeoclimatology, Palaeoecology*, v. 326-328, p. 30-41.

Petrik, F.E., 2008, *Scarp analysis of the Centennial Normal Fault, Beaverhead County Montana and Fremont County, Idaho*: Master of Science thesis, Montana State University, Bozeman, Montana.

Sonderegger, J.L., Schofield, J.D., Berg, R.B., and Mannick, M.L., 1982, *The Upper Centennial Valley, Beaverhead and Madison Counties, Montana*: Montana Bureau of Mines and Geology, Memoir 50, 53 p.

Witkind, L.J., 1975, *Geology of a strip along the Centennial fault, southwestern Montana and adjacent Idaho*: U.S. Geological Survey Map I-890, scale 1:62,500, 1 sheet.



Tourists at Old Faithful Inn, 1922. Courtesy National Park Service.

FIELD GUIDE TO THE SEDIMENTARY DEPOSITS, TECTONIC SETTING, PALEOENVIRONMENT, AND BASIN EVOLUTION OF THE PALEOGENE RENOVA FORMATION IN THE UPPER RUBY RIVER BASIN OF SOUTHWESTERN MONTANA

Kevin Lielke

Geosciences Department, University of Montana, Missoula, MT 59712

Robert C. Thomas

Environmental Sciences Department, University of Montana Western, Dillon, MT 59725

Introduction

The initiation and early evolution of the intermontane basins of southwestern Montana is a subject of considerable controversy. Particularly disputed issues include: 1) the timing of the initial formation of the basins; 2) the mechanisms responsible for the formation of accommodation space for sediment accumulation, in particular the importance of active normal faulting relative to erosional incision; 3) the existence of Paleogene paleotopography and its influence on the nature of basin sedimentation; 4) temporal changes in basin tectonics, climate, and volcanism and their influence on sedimentary depositional environments and accommodation space; and 5) the relationship of intermontane basins to the underlying geology and the influence of earlier events, such as late Cretaceous orogeny and igneous intrusion, on Cenozoic basin evolution.

Previously proposed models for Cenozoic basin formation fall into three distinct categories:

1) Models which assume that modern basins had a direct Paleogene ancestor and that active normal faulting was an important, probably dominant, factor in the evolution of intermontane basins and the formation of accommodation space (Fields et

al., 1985; Hanneman, 1989, 1991; Ruppel, 1993).

2) Models which propose a two-phase development of intermontane basins. In the first phase, a largely featureless, tectonically inactive volcanic plateau was situated between surrounding volcanic highlands during the Paleogene (Challis-Absaroka-Lowland Creek volcanic centers). During the second phase, this low-relief plateau was dissected, first by a major middle Miocene tectonic event, which formed a regional angular unconformity and northeast-trending half-grabens, and later by northwest-trending normal faults related to uplift along the flanks of the Yellowstone hotspot (Sears, 1995; Sears et al., 1995; Sears and Fritz, 1998; Sears and Thomas, 2007).

3) Models similar to the second class, but which recognize distinct sub-basins, generally correlated to late Cretaceous orogenic and igneous remnants within a larger Paleogene basin system. In this model, differential erosion, climate change, volcanic flows, and drainage disruption were major influences on the basin evolution of a complex but tectonically inactive Paleogene basin (Rothfuss et al., 2012; Lielke, 2010; Rothfuss, 2010).

This trip will examine the early Cenozoic geologic record of the Timber Hill area.

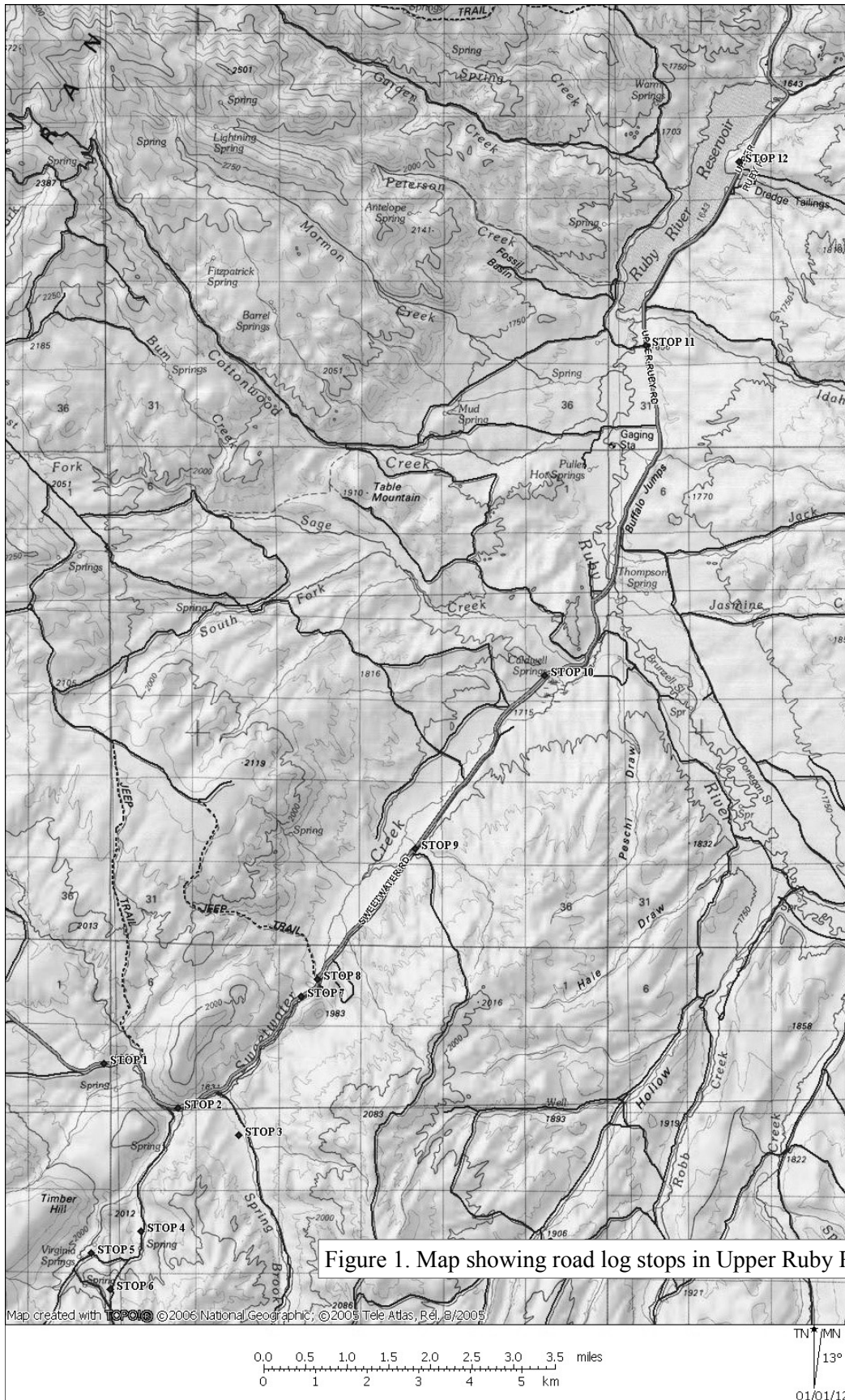


Figure 1. Map showing road log stops in Upper Ruby River Valley.

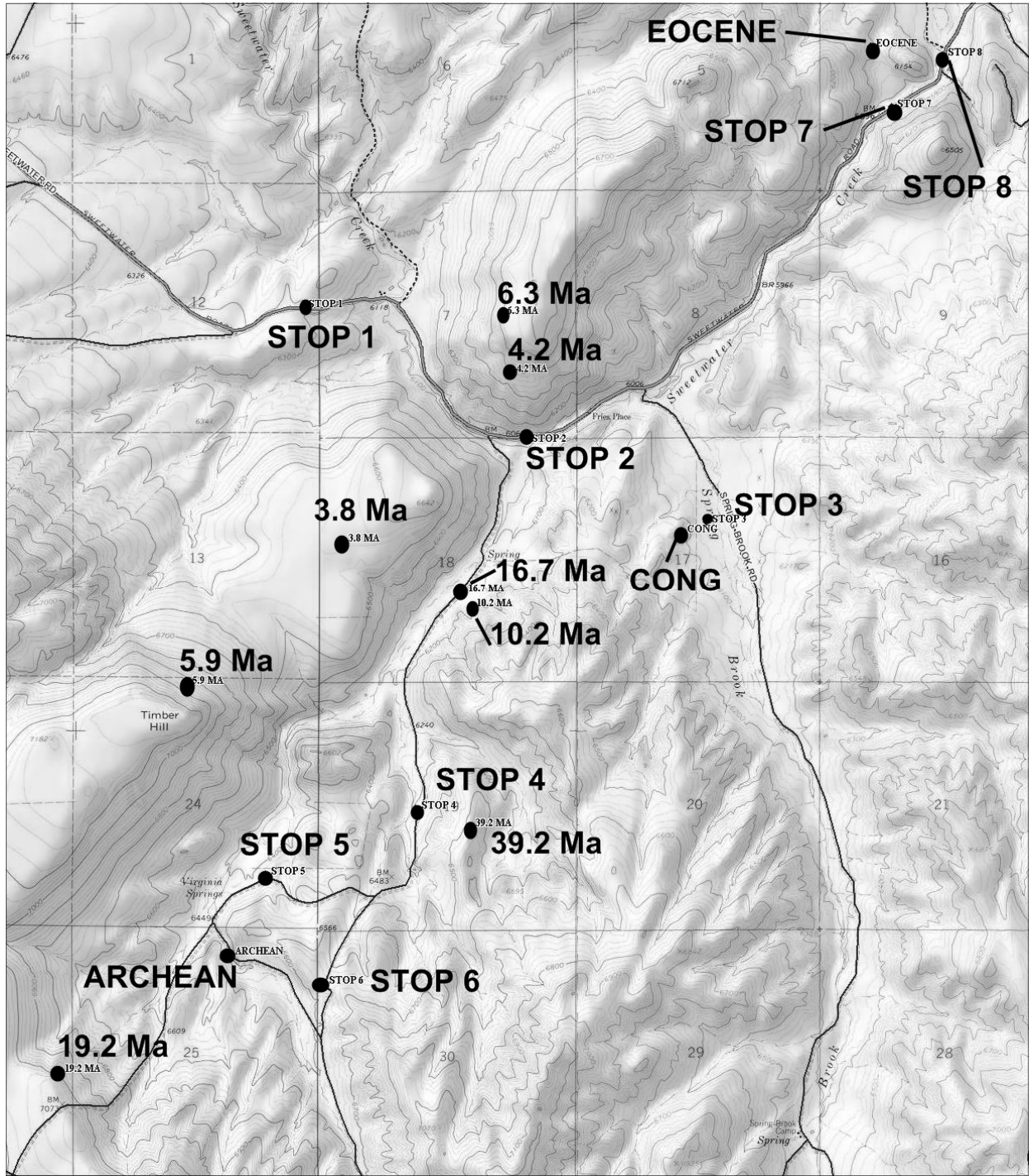


Figure 2. Map showing road log stops and radiometric age dates in Timber Hill area.

Local stratigraphy consists of Archean basement; middle Eocene Lower Dillon volcanic rocks; a basal conglomerate unit informally referred to here as the Spring Brook conglomerate; the Climbing Arrow, Dunbar Creek and Passamari Members of the late Eocene to early Miocene Renova Formation; and the Neogene Sixmile Creek Formation. The Timber Hill area presents several features of interest relevant to the Paleogene history of southwestern Montana. In particular, the existence of Paleogene paleotopography and the nature of the basal Renova sediments and their relation to Archean basement and Eocene volcanics will be examined.

The purpose of this field guide is to examine the localities listed above that are relevant to the interpretation of early Cenozoic basin evolution. Preferred interpretations, which reflect the opinions of the authors, will be offered in the hope that they will clarify the issues involved and the evidence required to test them, provoke discussion of possible alternatives, and encourage further research.

Itinerary and Methodology

This field trip will start at Dillon, Montana, and travel over the Sweetwater and Ruby roads to the Ruby Reservoir in the Upper Ruby River Valley. The roads are mostly unpaved. Most stops will be along the main road; however, the field trip will venture off the main road in the Timber Hill area to visit several key outcrops (Figure 1). The stops on this road log can all be viewed from a vehicle, but several stops also include optional walking trips to observe important outcrops firsthand. All road and walking stops have been located in the field with a handheld GPS and these coordinates (in UTM units) are provided in Appendix 1 as an aid to navigation.

Road Log – Dillon to Ruby Reservoir

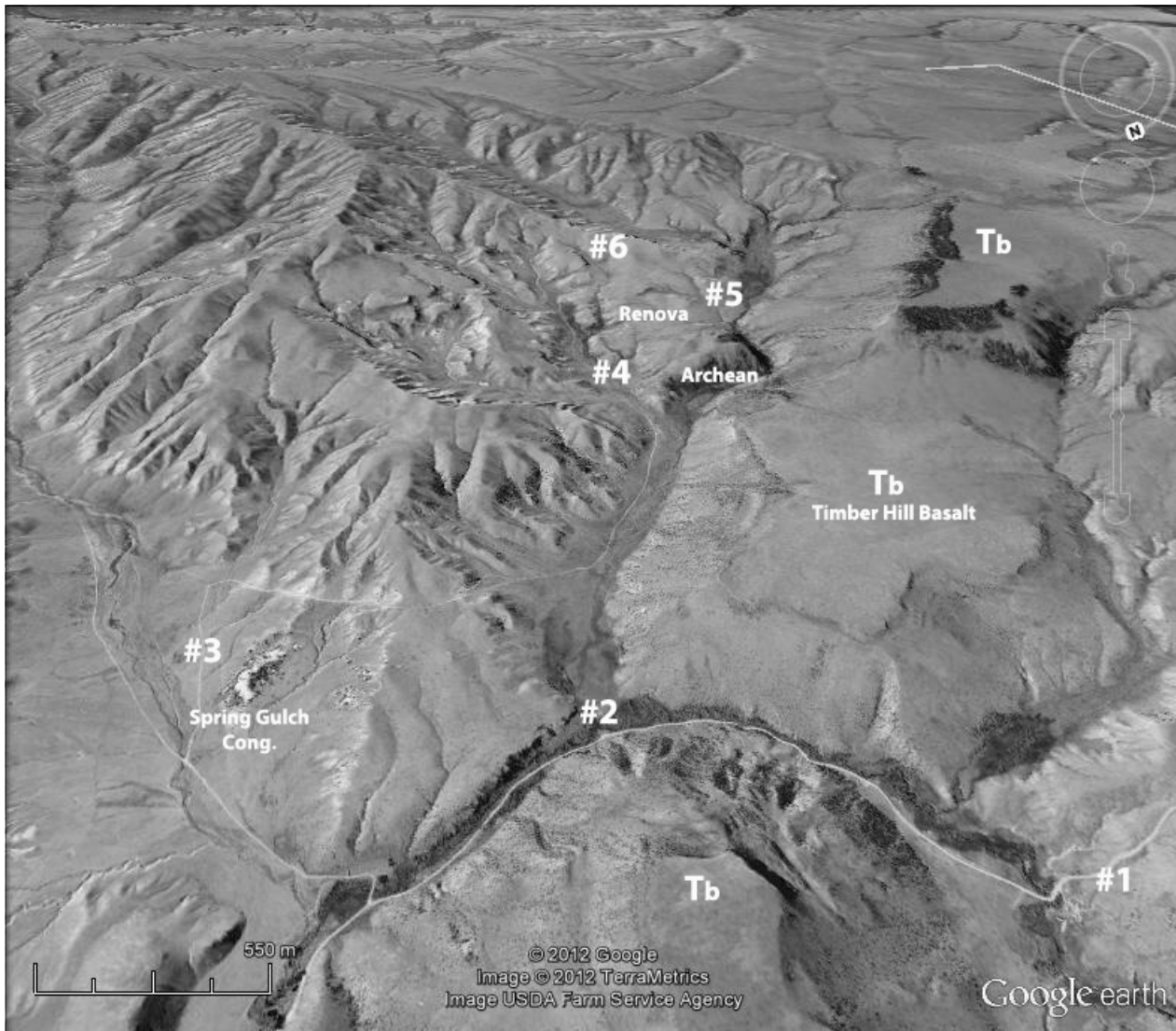
Meet at a convenient location in Dillon. Proceed to Beaverhead County High School just past the intersection of Helena and Atlantic Streets and drive east on Thompson Avenue. Proceed four blocks and then turn left onto Oliver Lane. Take the first right onto Sweetwater Road and drive east toward the Ruby Range. The road log proper will start at an overview of the Timber Hill locality. Cenozoic geology along the Sweetwater Road to the southern Ruby Range mostly involves Neogene to recent normal faulting and related sedimentation (Sears et al., 1995); however, at some points remnant surfaces of an Archean basement unconformity can be seen. This surface appears to continue to the east, where it underlies sediments of the Paleogene Renova Formation. North of the Sweetwater Road near Sweetwater Pass, an Eocene basalt flow (41.5 ± 0.9 Ma age from K/Ar) directly overlies this erosional surface (Sears et al., 1995; Fritz et al., 2007).

Approximately 10 miles southeast of Sweetwater Pass, the road abruptly bends toward the north and descends a steep hill. The road log proper begins just before this steep descent.

Mileage

Stop 1 – Overview of Timber Hill locality (Figure 2). Turn out to the left where jeep track intersects main road. This locality provides a good overview of the Timber Hill area. Sweetwater Creek has cut a narrow canyon through which the main road passes. The post-Middle Miocene history of this area is dominated by the interplay between a northeast-trending Neogene paleovalley, which parallels the Cretaceous Snowcrest/Greenhorn thrust

STOP 1



system, and a younger system of northwest-trending normal faults related to deformation along the flanks of the Yellowstone hotspot. For a more comprehensive discussion of the late Cenozoic history and stratigraphy of this area refer to the road log of Sears et al. (1995) - Stop #5 of this earlier road log corresponds to the current locality.

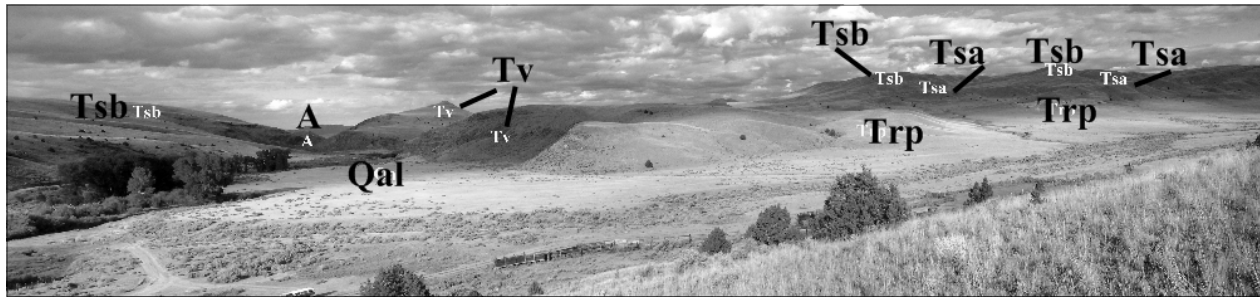
Proceed downhill toward ranch buildings.

0.1 Gray outcrop forming low scarp to the left is a terrestrial hot spring or lacustrine limestone deposit (Ripley, 1995).

0.3 Ranch buildings to left at base of hill. Cross Sweetwater Creek at bridge.

Figure 3. Overview of Timber Hill area looking south. Numbers correspond to road log stops in figure 2. T_b = Timber Hill Basalt (~6 Ma).

0.7 Archean outcrops are present along the road. Archean basement here is overlain by the Big Hole Member of the Neogene Sixmile Creek Formation. Whole rock K/Ar age dates, ranging from 4.2 ± 0.2 to 6.3 ± 0.2 Ma, have been reported from basalt flows within the Sixmile Creek Formation (Marvin et al., 1974; Fritz et al., 2007). These lava flows are likely related to explosive caldera volcanism in the Heise volcanic field of eastern Idaho, which pro-



duced voluminous felsic tuffs in addition to lesser amounts of basalt. Specifically, these basalt flows closely correspond in age to the ~4.3-Ma Kilgore tuff and the 6.3- to 6.5-Ma Walcott tuff (Pierce and Morgan, 1992; Anders et al., 2009). Basalt flows further south near Timber Hill may correspond to the eruption of the ~6.0-Ma Conant Creek tuff (Morgan, 1992; Anders et al., 2009). These age dates, and their close correlation to known caldera eruptions in the Heise volcanic field, suggest that multiple individual basalt flows are present in this area and that these flows are genetically related to Yellowstone hot spot volcanism.

STOP 2 1.2 Stop 2 – Virginia Springs Gulch. Stop at turnout along right shoulder of road (Figure 3). To the south of the road, Virginia Springs Gulch cuts through sediments of the Sixmile Creek Formation. A gentle dip slope of about 6-Ma Timber Hill basalt caps the flat-topped hills to the southwest. The Sweetwater normal fault offsets the Timber Hill basalt flow, which is also bisected by Sweetwater Creek Canyon. Field trip will eventually proceed up this gulch. To the north of the road is a cliff composed of Archean basement buried by Sixmile Creek sediments and later exposed by the down-cutting of Sweetwater Creek. This Archean knob represents Paleogene paleotopography related to the erosional surface exposed along Sweetwater Pass to the west. This Archean outcrop can be visited provided that caution is exercised

Figure 4. Spring Gulch looking northeast. A = Archean, Tv = Eocene volcanics, Trp = Renova (Passamari Member), Tsa = Sixmile Creek (Anderson Ranch Member), Tsb = Sixmile Creek (Bighole Member), Qal = Quaternary alluvium.

while crossing the road. When finished, return to vehicles and continue east along main road.

1.5 Fries Place: old ranch buildings.

1.7 Intersection with Spring Brook Road. Turn right and take Spring Brook Road past gates and corrals. You may need to open and close these gates when area is being used for grazing.

2.2 Road forks – take right (west) fork. Note small forested hill to right front. This hill is composed of Spring Gulch conglomerate, an informal unit at the base of the Paleogene sedimentary section. To the northeast, Archean basement is present at the base of the deep canyon cut by Sweetwater Creek (Figure 4). Middle Eocene Lower Dillon volcanic rocks form the conical hill on the skyline and the prominent cliffs above the Archean basement rocks.

At the base of the hill directly to the east are lacustrine shales and limy mudstones belonging to the Passamari Member of the Renova Formation. Passamari playa lakebeds onlap the Eocene volcanics to the northeast. The Neogene Sixmile Creek For-

mation overlies the Renova sediments. Cross-bedded tephtras of the Anderson Ranch Member form the prominent white bluffs about halfway up the hill. Well-rounded fluvial conglomerate of the Big Hole Member overlies these tephtras and forms the treeless and barren hill tops.

STOP 3 2.4 Stop 3 – Spring Gulch Conglomerate. Stop along fence line and proceed on foot toward bluffs near top of small hill. This unit is composed predominantly of crudely cross-bedded to horizontally bedded coarse sandstone and conglomerate. Individual clasts are almost exclusively composed of angular to sub-rounded cobbles of Archean felsic gneiss in a matrix of weathered Archean material. Crossbeds and imbricated cobbles indicate flow from the north-northwest (N09W). This unit is interpreted to be the proximal portion of an alluvial fan sourced in the Archean rocks of the southern Ruby Range.

The age of the deposit is uncertain, but based on its stratigraphic position and clast provenance it appears to be at least middle Eocene in age. A lack of exotic cobbles and reworked Renova mudstone differentiates this unit from typical Sixmile Creek conglomerates. No obvious Eocene volcanic lithologies are present, suggesting that this unit predates the emplacement of Lower Dillon volcanic rocks. If this age assessment is correct, then this high energy alluvial fan suggests the presence of significant relief in the southern Ruby Range during early Paleogene time. The early Miocene playa lakebeds of the Passamari Member directly onlap Eocene volcanics at the head of Spring Gulch, implying the dominance of subaerial erosion, not deposition, prior to this time.

Similar basal conglomerates, dominated by local bedrock lithologies and lacking younger sedimentary clasts, have also been described from the southern Tobacco Root Mountains to the east (Lielke, 2008a) and the northern Boulder basin to the north (Rothfuss et al., 2008; Rothfuss et al., 2012). Recent provenance studies, employing both detrital zircon analysis and traditional methods, also suggest the presence of relict paleotopography during deposition of the Renova Formation (Lielke, 2008b; Lielke, 2010; Rothfuss, 2010; Rothfuss et al., 2012).

2.7 Return to vehicles and continue along road over the hill towards Virginia Springs Gulch. Proceed through gate. This road cuts up section through Sixmile Creek Formation sediments.

3.0 Driving through white, cross-bedded tephtra deposits of the Anderson Ranch Member of the Sixmile Creek Formation. Generally treeless hills above Anderson Ranch are composed of well-rounded fluvial conglomerates of the Big Hole Member of the Sixmile Creek Formation.

3.2 Proceed through gate and downhill into Virginia Springs Gulch. Small rounded hill to right across fence line is composed of Big Hole conglomerate. Flat topped hills on skyline are held up by ~6.0-Ma Timber Hill basalt flow. This flow, sourced in Idaho, traveled down a long-lived north-east-trending paleovalley and was later cut and tilted by a series of northwest-trending, down-to-the-east normal faults (Sears et al., 1995). Sweetwater Creek follows one of these later grabens which crosscut the Miocene Ruby paleovalley (Sears et al., 1995).

4.0 There are impressive cliff exposures of the Anderson Ranch Member of the Six-

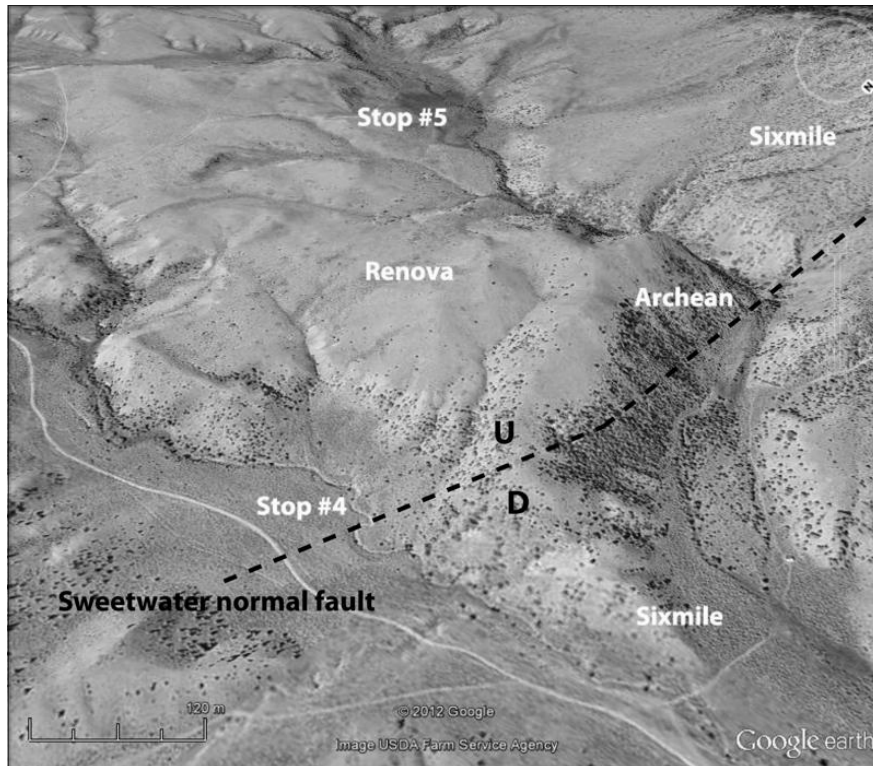


Figure 5. Buttress unconformity at Virginia Springs looking southwest. The Renova sediments onlap Archean basement in the footwall of the Sweetwater normal fault. Archean spur represents Eocene topography exposed by the modern erosion of Renova sediments.

mile Creek Formation along the left side of the road. Whole rock K/Ar age dates on rhyolite tuff from this locality range from 16.7 ± 0.3 Ma at the base of the section to 10.2 ± 0.4 Ma in the upper cliff exposures (Fritz et al., 2007). These age dates would bracket eruptive activity from the 15-16 Ma McDermitt volcanic field in southeastern Oregon to the ~10-Ma Picabo volcanic field in east-central Idaho. In particular, the ~10.2-Ma age date corresponds closely to the eruption of the Blackfoot Caldera that deposited the widespread Arbon Valley tuff (10.34 ± 0.01 Ma at Arbon Valley, ID; 10.41 ± 0.02 at Grand Valley, ID; 10.3 ± 0.6 Ma at Jackson Hole, WY – dates from Anders et al., 2009). The ~16.7-Ma age date suggests that deposition in the Ruby paleovalley probably began during, or im-

mediately after, the beginning of extension associated with the outbreak of the Yellowstone hot spot around 17 Ma in the Middle Miocene. The Anderson Ranch Member varies greatly in thickness depending on its original position in the Miocene Ruby paleovalley.

4.2 Continue along main road. Side road to the right leads to old ranch building along Virginia Springs Creek. Rounded cobble hills along right side of road are Big Hole Member sediments located in the hanging wall of the

Sweetwater normal fault. Sixmile Creek Formation sediments are in fault contact with Archean basement and Renova sediments in the footwall of the Sweetwater fault. Prominent cliff along west side of hill (benchmark 6,607 feet), which can be seen in the distance, is composed of Archean basement. The Sweetwater fault offsets Timber Hill basalt on skyline to the west.

4.5 Stop 4 – Buttress unconformity. Stop along main road where white **STOP 4** Renova Formation sediments can be seen past outcrops of the Big Hole conglomerate along the west side of main road (Figure 5). Proceed on foot to Renova Formation outcrops. The Sweetwater fault separates Big Hole Member conglomerates in the down-dropped hanging wall from Archean basement and Renova Formation sediments in the uplifted footwall. The Renova Formation passively onlaps the Archean basement, which can be seen in the cliff immediately to the west of this location. These



Figure 6. Buttress unconformity looking north. Sixmile Creek sediments (Ts) and Timber Hill basalt formerly covered Renova (Tr) and Archean rocks in axis of Miocene Ruby paleovalley.

relations provide further evidence that the Timber Hill area was an area of positive relief gradually buried by the encroaching Renova Formation during the early Paleogene.

In the Timber Hill area, there is no evidence of fault movement between the Renova Formation and any of the older rocks it overlies; therefore this contact probably represents a buttress unconformity. Renova sediments slowly buried an Eocene or older erosional surface whose original topography is gradually being revealed by modern erosion and normal faulting. On the hill to the east of the road, a rhyolite shard in the Renova Formation yielded a K/Ar age date of 39.2 ± 3.0 Ma providing a maximum age date for the Renova at this location (Fritz et al., 2007). The Renova sediments onlapping basement here appear to be older than those at the entrance to Spring Brook, where the early Miocene Passamari Member onlaps Eocene volcanics. This suggests that the unconformity at the base of the Renova is diachronous even over short distances.

Return to vehicles and continue along main road.

5.0 Road forks – take right (west) fork and proceed toward Virginia Springs.

6.3 Stop 5. Virginia Springs overlook. Stop along turnout just before road heads down hill toward Virginia Springs, the green marshy **STOP 5** area along the base of Timber Hill. Walk to top of small hill for overview of area (Figure 6). The flat-topped, forested hill to the west is named Timber Hill and is topped by the Timber Hill basalt flow. A whole rock K/Ar age date of 5.9 ± 0.2 Ma was obtained from the basalt flow near the steep north edge of Timber Hill (Fritz et al., 2007). This age closely corresponds to the reported K/Ar age of 5.99 ± 0.06 Ma for the Conant Creek tuff of the Heise volcanic field (Morgan, 1992; Anders et al., 2009) suggesting a possible genetic relationship.

Immediately to the north, Archean basement is exposed in the cliff directly to the east of Virginia Springs Creek. Rolling topography between here and this hill is Renova Formation onlapping exhumed Paleogene topography developed on the Archean basement. About a mile to the south, a K/Ar date of 19.2 ± 0.4 Ma was obtained


from a rhyolite tuff near the top of the exposed Renova section at an elevation about 500 feet higher than the current locality (Fritz et al., 2007). This gives a rough estimate of the amount of Renova sediment removed by recent erosion. The Sweetwater fault cuts across the hill to the northeast near location of Stop #4. The smaller hill to the south is also formerly buried Archean basement which will be visited at next stop. On the skyline to the north and east are Sixmile Creek outcrops, including prominent white tephras of the Anderson Ranch Member, in the hanging wall of the Sweetwater normal fault.

Proceed downhill toward Virginia Springs. Caution – the road beyond this point is narrow and of poor quality especially when wet. You may wish to skip, or visit on foot, the weathered Archean gneiss at mileage marker 6.8. An alternative route to Stop #6 is to return to the fork in the road at mileage marker 5.0 and then take the east fork of the main road.

6.6 Road forks past creek crossing. Take left fork and proceed through tall sagebrush towards exposed outcrops of Archean basement rocks on small hill directly to the east.

6.8 Weathered felsic gneiss is exposed along the road at this location. This small basement spur is another example of relict paleotopography slowly being exposed as erosion strips away overlying Renova sediments. Since this outcrop has been uncovered relatively recently, the high degree of weathering likely reflects Paleogene subaerial exposure and provides further evidence of an extensive area of pre-Renova relief in the southern Ruby Range. Proceed uphill to the intersection with the main road.

7.0 Across fence line, bluffs on skyline are composed of a relatively complete section of Sixmile Creek Formation in the hanging wall of the Sweetwater normal fault.

7.3 Stop 6 – Over-view of Timber Hill area. From the top of this hill, the gross structure of the Timber Hill area can be easily seen. The main structural element is the northwest-trending Sweetwater normal fault which tilts Timber Hill southwest and uplifts it relative to the lower, flat-topped hill directly to the northeast. Both of these hills are capped by the ~6.0-Ma Timber Hill basalt flow which serves as a useful regional datum (Sears et al., 1995; Sears and Thomas, 2007). Other remnants of this flow can be seen offset and tilted by related northwest-trending normal faults towards the south in the direction of the Blacktail Deer Creek drainage (Sears et al., 1995). The Sweetwater fault cuts the eastern edge of “Hill 6607” and obliquely crosses the main road roughly following the line of low hills to the east of the road.

The higher hills in the background, within the down-dropped hanging wall of the fault, are composed of sediments of the Sixmile Creek Formation. The white, cliff-forming Anderson Ranch Member is a useful visual cue which broadly outlines the hanging wall area of the fault. In the footwall of the Sweetwater fault, Renova Formation sediments form the low rolling topography in the immediate foreground. Recently exhumed remnants of Archean basement poke through this thin veneer of Paleogene sediments. The Sixmile Creek Formation overlies the Renova and forms the top of Timber Hill, capped by the Timber Hill basalt flow.

Return to vehicles and follow the main road north back to the intersection of Spring

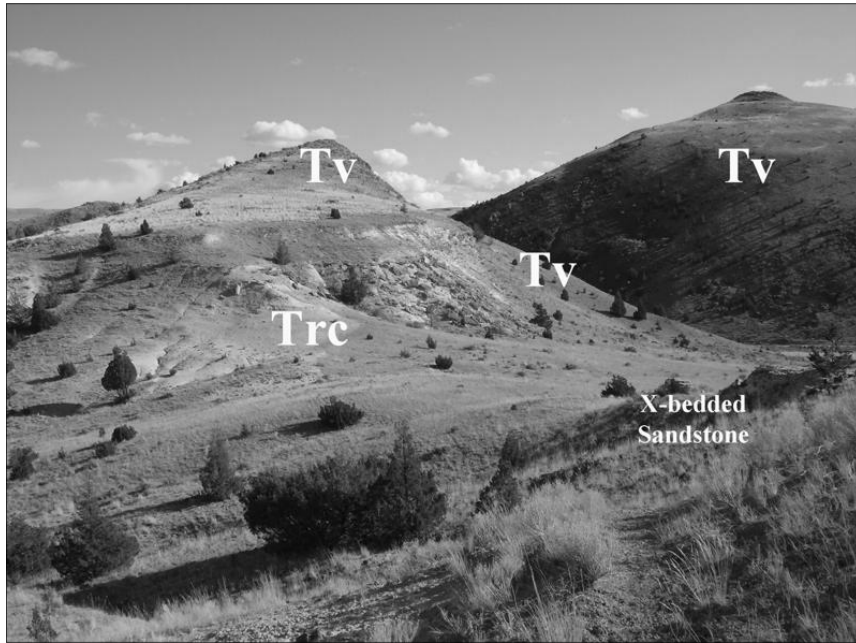


Figure 7. Renova Climbing Arrow sediments (Trc) onlapping Eocene volcanics (Tv) at Cone Hill (the Anthill) looking south. Highly cross-bedded fluvial sandstone located to right.

Brook Road with the Sweetwater Road (mileage marker 1.7).

11.2 Turn right onto Sweetwater Road at junction with Spring Gulch Road. Drive through narrow canyon cut by Sweetwater Creek. Sweetwater Creek is likely a superposed stream which cut downward from a Sixmile topographic surface until it incised buried Archean basement.

11.5 Cliffs on both sides of road are composed of highly silicified Eocene volcanic rocks. Alteration of original volcanic material was likely hydrothermal in origin. Note fracture sets which may have localized hydrothermal fluids.

12.0 Archean felsic gneiss is exposed in road cuts. These gneisses are overlain by Eocene volcanic rocks and the Big Hole Member of the Sixmile Creek Formation. Sweetwater Creek is likely controlled by

the same northwest-trending normal fault system which offsets the Timber Hill basalt flow over most of its area of exposure (Sears et al., 1995). From an original Miocene or Pliocene fluvial-alluvial surface, Sweetwater Creek has incised a narrow into these crystalline Eocene volcanic and Archean metamorphic rocks.

12.7 Stop 7 – Eocene Dillon volcanics overview. Turn out at the wide shoulder on the left side of the

road adjacent to Sweetwater Creek. On the south side of the road, a barren cone-shaped hill of Eocene volcanic rock forms a prominent landmark; the hill is variously known as Cone Hill or the Anthill. To the north of the road, a continuation of these Eocene volcanic rocks forms the prominent cliff above the bend of the road. In the swale directly to the north, Renova sediments can be seen onlapping the volcanic rocks. These sediments belong to the late Eocene Climbing Arrow Member of the Renova Formation (Monroe, 1976). This area will be visited at the next stop. Proceed east along the Sweetwater Road.

STOP 7

12.9 Round corner. Silicified cliffs of Eocene volcanics to the left are separated from the bulk of Cone Hill by incision of Sweetwater Creek.

13.1 Stop 8 – Park at BLM sign just before road crosses cattle guard and fence line. Proceed west on foot following fence line along northern side of hill composed of Eocene volcanics. Caution

STOP 8

should be taken crossing creek bed especially during periods of wet weather. Walk to swale on northwest side of hill. At this location, approximately horizontal sediments of the Climbing Arrow Member of the Renova Formation onlap middle Eocene volcanic and volcanoclastic sedimentary rocks (Figure 7). Looking to the north, Climbing Arrow sediments also underlie the bluffs which stretch into the distance roughly paralleling the Sweetwater Road. These sediments contain a late Eocene (early Chadronian NALMA) fossil mammal fauna (Monroe, 1976). These relations suggest that the initial Renova deposition in this area filled topographic depressions in an erosional terrain developed on the middle Eocene volcanic rocks. These late Eocene Climbing Arrow sediments are significantly older than the early Miocene Passamari sediments which onlap the Eocene volcanics at the head of Spring Gulch, further illustrating the diachronous nature of this erosional surface. No evidence of normal faulting is apparent.

Volcanics and related sediments have been silicified to a high degree, probably by hydrothermal fluids during or soon after emplacement of the volcanic rocks. On the west side of the swale is a low ridge formed by a white, trough cross-bedded, fluvial sandstone. A similar sandstone bed, across the Sweetwater Road from this location, was previously interpreted as having been deposited on a relatively featureless volcanic plateau (Thomas, 1995; Sears et al., 1995). More recent studies, which include sandstone detrital zircon analysis, suggest Renova deposition occurred in distinct sub-basins separated by relict paleotopography which included an ancestral Ruby Range (Lielke, 2010; Rothfuss, 2010; Rothfuss et al., 2012). Neither of these models invokes active normal faulting during deposition of the Renova Formation, in contrast to earlier

models proposed for Renova deposition (Pardee, 1950; Kuenzi and Fields, 1966; Fields et al., 1985; Hanneman, 1989, 1991).

Return to vehicles and proceed north along Sweetwater Road. Warning: beyond this point, localities off the main road are on private ranch land. Respect private property and do not visit any sites off of the main road without obtaining landowner permission first. All field trip stops beyond this point are road stops.

16.0 Note flat-topped mesa of Renova sediments to the west.

16.9 Stop 9 - Gravel pit. Stop at gravel pit in modern alluvium on right side of road. From this vantage point, the relationships between the Renova Formation and both overlying and underlying units can be observed. Sediments of the late Eocene (Chadronian) Climbing Arrow Member of the Renova form the low line of bluffs to the west. These Renova sediments occur in the footwall of the northwest-trending Stone Creek fault whose surface trace is usually expressed by a change in topography between easily eroded Renova mudstones to the south and resistant, coarse clastic Sixmile Creek sediments to the north. In the hanging wall of the Stone Creek fault, Sixmile Creek sediments form resistant upper bluffs underlain by light-colored, calcareous playa lakebeds of the early Miocene (Arikarean) Passamari Member.

STOP 9

On the skyline overlooking the Sage Creek drainage to the north is a prominent cliff of Sixmile Creek sediments overlying the type section of the Passamari Member. The angular unconformity between the Renova and Sixmile Creek Formations is well exposed here. This angular relationship devel-



Figure 8. Soft sediment deformation in Miocene lacustrine limestone of the Passamari Member of the Renova Formation. Prograding delta sandstone deformed unconsolidated offshore lake carbonates during a lake level lowstand.

oped during the well-recognized middle Miocene extension, which formed the northeast-trending Ruby paleovalley (Sears et al., 1995; Sears, 1995; Sears and Fritz, 1998). This paleovalley likely formed by extensional collapse of the Snowcrest/Greenhorn thrust system, tilting the Renova sediments toward the southeast. Sixmile Creek Formation sediments and volcanic material later filled the half-graben formed by this tilted fault block. The northwest-trending Stone Creek fault is a younger feature probably related to crustal realignments caused by passage of the Yellowstone hotspot (Anders and Sleep, 1992; Sears et al., 1995; Sears and Fritz, 1998; Sears and Thomas, 2007).

Late Eocene Climbing Arrow sediments represent a low energy fluvial environment, with a few mature cross-bedded sandstones encased in an apron of fine-grained over-

bank sediments which show variable degrees of paleosol development. Closer to the Ruby Range, alluvial fans and high energy, coarse-grained fluvial sandstones and conglomerates indicate significant relief in the area of the modern Ruby Range. Our preferred interpretation is that Renova sediments passively overlapped this ancestral Ruby Range, although this relationship is generally obscured by younger sediments and faulting. Detrital zircon age dates from Renova sandstone on the western side of the Ruby Range also suggest the presence of relict Paleogene paleotopography in the area of the modern Ruby Range (Rothfuss et al., 2010; Rothfuss et al., 2012).

tal zircon age dates from Renova sandstone on the western side of the Ruby Range also suggest the presence of relict Paleogene paleotopography in the area of the modern Ruby Range (Rothfuss et al., 2010; Rothfuss et al., 2012).

17.8 Crossing cattle guard. Ranch buildings to left. Low hills beyond irrigated fields are Passamari Member lakebed sediments.

19.5 Stop 10 – Caldwell Springs. Stop along edge of road opposite steep bluffs just past irrigated fields.

STOP 10

The bluffs to the west expose a coarse clastic, lake-margin facies that is rare in the Passamari Member (Monroe, 1976, 1981). The early Miocene (Arikarreen) Passamari Member represents a radically different depositional environment compared to earlier Renova sediments. Following a trend towards a cooler, drier, and more seasonal climate regime (Lielke et al., in press), a closed basin containing a playa lake developed by late Oligocene or early Miocene time flanking the ancestral Ruby Range (Monroe, 1976, 1981; Ripley, 1995).

Coarse clastic fluvial and deltaic facies drained radially into the lake, interfingering with mixed lake-margin and open-lake carbonate facies (Monroe, 1976, 1981).

At this locality, a siliciclastic delta sequence prograded into an open water carbonate environment. Coarse sandstone and conglomerate (which can be identified by their darker color and resistant topography) compose most of the northern part of the bluffs. Fine-grained lacustrine limestone forms the white, less resistant southern part. Spectacular soft-sediment deformation can be seen where the weight of the prograding delta contorted the underlying lakebeds (Figure 8). This suggests that the lake deposits were saturated, soft, and unconsolidated when deformed. Overlying the delta deposits, across the top of the bluffs, is an undeformed open-lake carbonate bed of considerable lateral extent. This bed can be traced to the north and west and represents a major expansion of the lake. These stratigraphic relations, similar to those observed at other Passamari outcrops, suggest that lake level fluctuations were common during the lifecycle of Lake Passamari. Monroe (1981) concluded that tectonic adjustments likely influenced changes in lake level; however, a lack of direct evidence for contemporary seismicity or normal faulting suggests the possibility of climate-induced lake fluctuations. Playa lakes are known to be highly susceptible to even minor variations in climate, especially precipitation (Cohen, 2003).

19.8 To the left, on the north side of Sage Creek drainage, is Neogene normal-fault contact between white Passamari lakebed sediments to the left, and Sixmile Creek conglomerates to the right.

20.1 Buildings to left (Ball Place) are surrounded by cliffs of Sixmile Creek con-

glomerate, most likely the basal Sweetwater Member.

20.3 Note change in attitude of Sixmile Creek beds in cliffs to left. Crossing the Ball Place normal fault, which separates the older Sweetwater Member from younger Big Hole Member conglomerates (Monroe, 1976).

21.4 Crossing bridge over Ruby River.

21.9 Junction with Ruby Road. Take left fork and proceed north toward Ruby Reservoir. Cliffs along both sides of the road to the reservoir are composed of sediments of the Sixmile Creek Formation. Light-colored Renova outcrops can be seen further to the west. Cenozoic sediments are oldest along the Ruby Range front and generally decrease in age toward the east. The entire Cenozoic section appears to be tilted southeast into the normal fault along the Greenhorn Range front. This fault likely became active during the middle Miocene tectonic event and formed the Neogene Ruby paleovalley (Sears et al., 1995).

A major normal fault has historically been mapped along the Ruby Range front as well, but convincing evidence for Paleogene tectonism is not apparent in the Renova Formation; this relationship appears to be one of passive onlap. Active faulting may have started later, during the Neogene, but the simple presence of Cenozoic sediments located against Archean basement is not sufficient evidence to deduce a fault relationship. This could be a buttress unconformity similar to those seen in the Timber Hill area only on a much larger scale. Minor Neogene normal faulting may have accommodated extension in a half-graben controlled by the dominant Snowcrest/Greenhorn normal fault system to the east. Northwest-trending Neogene

extensional faults, such as the Stone Creek fault, later cut through the entire Ruby Valley including the Archean core of the Ruby Range.

22.6 There are prominent cliffs of the Sweetwater Member of the Sixmile Creek Formation along this section of road. Note calcic paleosol layers which separate distinct conglomerate units.

24.2 Gravel road ends and pavement begins.

STOP 11 **24.3** Stop 11 – Overview of Fossil Basin area. Cottonwood Creek Road intersects the Ruby Road to left. Turn off at a convenient point at this juncture. Northwest, to the right of the Cottonwood Creek Road, is the Fossil Basin locality, where a drainage basin developed in the eastern foothills of the Ruby Range without a modern perennial stream. The stratigraphy of the Fossil Basin area consists of Climbing Arrow and Dunbar Creek sediments overlain unconformably by the Big Hole Member of the Sixmile Creek Formation (Figures 9 and 10). This area is important to the study of the evolution of Paleogene climate and vegetation since it contains multiple fossil plants at different stratigraphic positions across the Eocene-Oligocene boundary (Becker, 1960, 1961, 1972 and 1973; Lielke et al., in press).

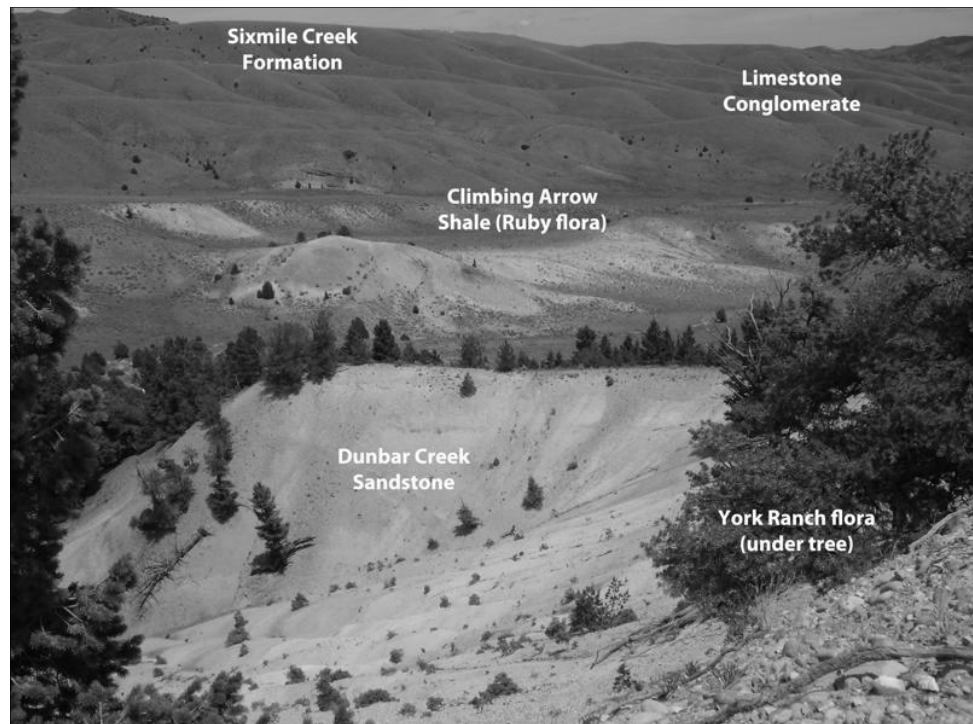


Figure 9. Fossil Basin area looking north. Oligocene Dunbar Creek fluvial sandstone conformably overlies late Eocene-early Oligocene Climbing Arrow lake shales which host the Ruby paleoflora. Big Hole Member of Sixmile Creek Formation overlies the Renova Formation with angular unconformity. Note red limestone conglomerate on skyline to right.

Revisions in the age of closely related fossil floras and changes to the NALMA time scale have refined the dating of the Fossil Basin paleofloras to the late Eocene-early Oligocene, and refute their prior assignment to the early Miocene Passamari Member (Figure 10). Paleoclimate estimates, based on leaf morphology and nearest living modern analogs, indicate a cooling and drying trend across the Eocene-Oligocene transition with the most important trends being increased seasonality and summer dry conditions (Lielke et al., in press). Subtropical and warm, temperate species were replaced by cool temperate forms of more modern aspect. A dry-adapted (xeric) element also became pronounced during the early Oligocene (Becker, 1961). The pres-

Fossil Basin Stratigraphic Section

Upper Ruby River Valley
Southwestern Montana
2011

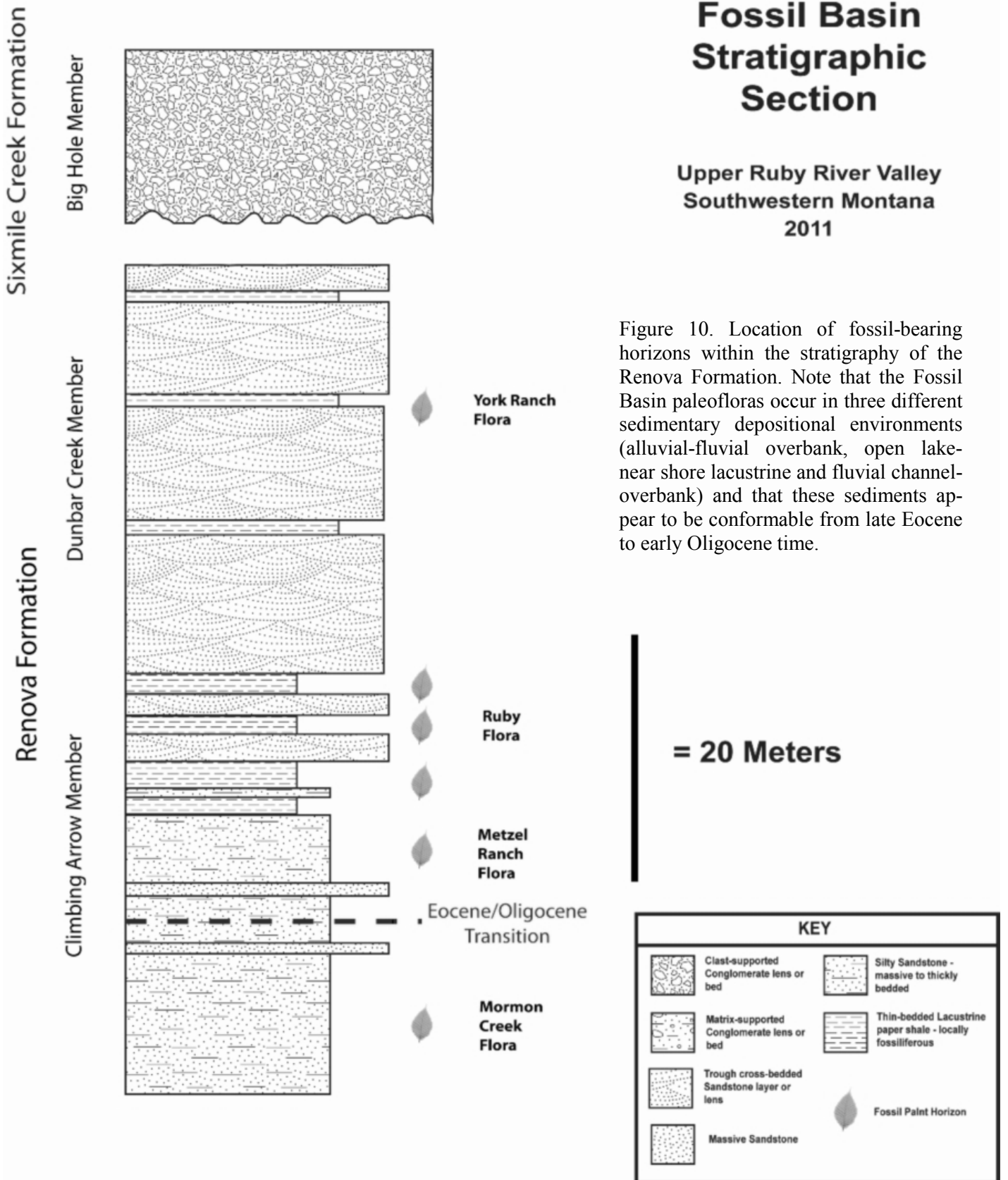


Figure 10. Location of fossil-bearing horizons within the stratigraphy of the Renova Formation. Note that the Fossil Basin paleofloras occur in three different sedimentary depositional environments (alluvial-fluvial overbank, open lake-near shore lacustrine and fluvial channel-overbank) and that these sediments appear to be conformable from late Eocene to early Oligocene time.

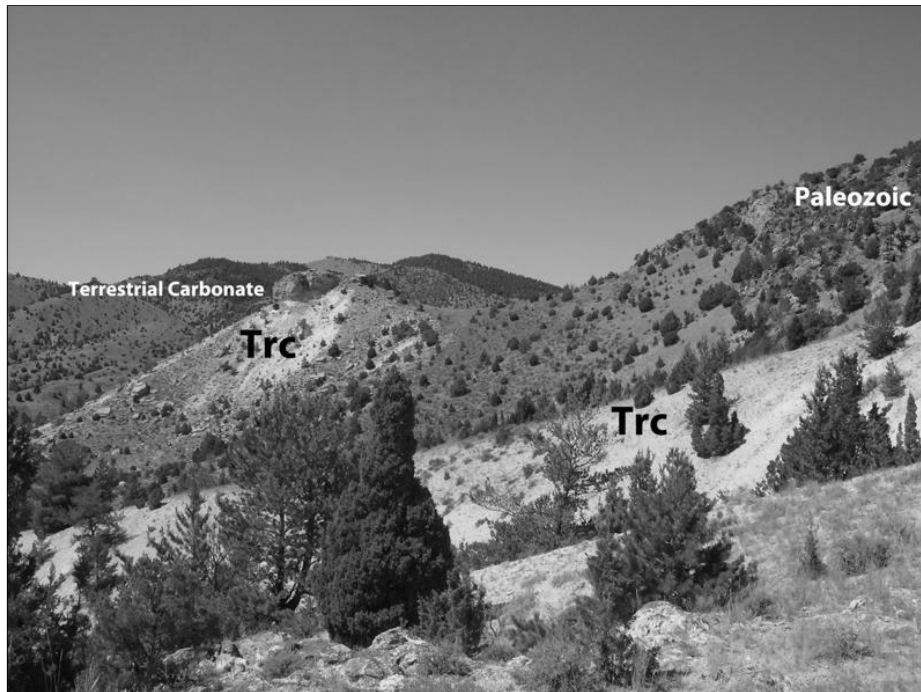


Figure 11. Late Eocene (early Chadronian NALMA) sediments overlain by a cliff of terrestrial hot springs-lake carbonate. Renova sediments onlap Paleozoic marine limestone to right. This hot springs algal carbonate unit may correlate with similar rocks to the south at Table Mountain and along the western margin of the Madison Valley to the east.

ence of high altitude coniferous genera (*Abies* [Fir], *Picea* [Spruce], *Pinus* and *Pseudotsuga* [Douglas Fir]) preserved in lake deposits is independent evidence of high-elevation Paleogene paleotopography (Becker, 1961).

STOP 12

27.0 Stop 12 – Ruby Reservoir Overview.

Turn left into Ruby Reservoir campground and park at the top of the hill. From this vantage point, several features of interest are visible. The Cenozoic sedimentary section is tilted east-southeast toward the Greenhorn Range. Because of this tilting, the Cenozoic sediments are oldest in the west, along the Ruby Range front, becoming progressively younger toward the east. These basin-fill

sediments overlie an older Paleogene erosional surface developed on Archean, Paleozoic, and Paleogene age rocks. Looking east, Sixmile Creek coarse, clastic sediments occupy most of the area between Ruby Road and the Greenhorn Range. To the north, just to the right of the Ruby Dam, is a prominent mountain composed of Archean basement intruded by an Eocene volcanic plug. The Archean

rocks tend to be more heavily vegetated than the volcanic rocks at higher elevations.

Archean and Paleozoic basement rocks comprise the high ground to the west of the dam. These basement rocks are onlapped by Renova sedimentary rocks. In the Spring Creek drainage, directly south of the basement exposures, early Chadronian NALMA fossils have been found in sediments deposited in alluvial and fluvial environments sourced from the ancestral Ruby Range. Overlying the Renova sediments are rounded-clast conglomerates of the Big Hole Member of the Sixmile Creek Formation, and an enigmatic terrestrial limestone of apparent hot spring or lake provenance. Tumbled blocks of these terrestrial carbonates can be seen along the western shore of the reservoir and are found in place further to the west where they cap the Renova sediments and in turn are overlain by Sixmile Creek gravels (Figure 11).

Similar terrestrial carbonates occur at Table Mountain (Monroe, 1976), which can be seen on the far southern horizon, and along the western margin of the Gravelly and Greenhorn Ranges to the east (Hadley,



Figure 12. Unusual limestone conglomerate found on ridge north of Fossil Basin. Gray angular limestone clasts cemented by a reddish matrix. This unit appears to occur near the top of the Sixmile Creek Formation in this area.

1980). One hypothesis for the formation of these basin-margin hot spring carbonates, which stratigraphically appear to cap the Renova Formation, is that they formed as a response to the greatly increased tectonic activity which accompanied the middle Miocene tectonic event. More research on the nature and stratigraphic position of these hot spring deposits is necessary to evaluate their significance to the Cenozoic history of the area. Prominent red horizons may represent paleosols associated with the middle Miocene climatic optimum (Thompson et al., 1981).

Directly across the reservoir from this point, the hills between Spring Creek and Fossil Basin are composed of the Sweetwater Member of the Sixmile Creek Formation, which directly overlies Renova sediments at this locality. The red-orange unit at the top of the hill nearest to Fossil Basin is an enigmatic conglomerate composed of grey fragments of carbonate rock supported by a red-orange matrix (Figures 9 and 12). Interpretations of this unit range from Cretaceous Beaverhead conglomerate (Dorr and Wheeler, 1964) to Pleistocene landslide

deposits (Monroe, 1976). Our favored interpretation is that this unit is located within the Sixmile Creek Formation although its significance is uncertain.

End Road Log – Return to Dillon via Alder and Twin Bridges or back the way you came.

References

Anders, M., and Sleep, N., 1992, Magmatism and extension: the thermal and mechanical effects of the Yellowstone hotspot: *Jour. Geophysical Research*, v. 97, no. B11, p. 15,379-15,393.

Anders, M., Saltzman, J., and Hemming, S., 2009, Neogene tephra correlations in eastern Idaho and Wyoming: Implications for Yellowstone hotspot-related volcanism and tectonic activity: *Geological Society of America Bulletin*, v. 121, no. 5/6, p. 837-856.

Becker, H., 1960, The Tertiary Mormon Creek flora from the upper Ruby River basin in southwestern Montana: *Palaeontographica Abt. B.*, v. 107, Lfg 4-6, p. 83-126.

Becker, H., 1961, Oligocene plants from the upper Ruby River basin, southwestern Montana: *Geological Society of America Memoir* 82, 127 p.

Becker, H., 1972, The Metzel Ranch flora of the upper Ruby River basin, southwestern Montana: *Palaeontographica Abt. B.*, v. 141, Lfg 1-2, p. 1-61.

Becker, H., 1973, The York Ranch flora of the upper Ruby River basin, southwestern Montana: *Palaeontographica Abt. B.*, v. 143, Lfg 1-4, p. 18-93.

- Chadwick, R., 1981, Chronology and structural setting of volcanism in southwestern and central Montana: Montana Geological Society 1981 field conference, p. 301-309.
- Cohen, A., 2003, Paleolimnology – the history and evolution of lake systems: Oxford University Press, 500 p.
- Constenius, K., 1996, Late Paleogene extensional collapse of the Cordilleran foreland fold and thrust belt: Geological Society of America Bulletin, v. 108, no. 1, p. 20-39.
- Dorr, J., and Wheeler, W., 1964, Cenozoic paleontology, stratigraphy and reconnaissance geology of the upper Ruby River basin, southwestern Montana: Contributions of the Museum of Paleontology, University of Michigan, v. 13, p. 297-339.
- Dunlop, D., 1982, Tertiary Geology of the Muddy Creek Basin, Beaverhead County Montana: University of Montana, Ph.D. Dissertation, 133 p.
- Fields, R., Rasmussen, D., Tabrum, A., and Nichols, R., 1985, Cenozoic rocks of the intermontane basins of western Montana and eastern Idaho: A summary: in Flores, R., and Kaplan, S., eds., Cenozoic paleogeography of west-central United States, SEPM-RMS, p. 9-36.
- Fritz, W., Sears, J., McDowell, R., and Wampler, J., 2007, Cenozoic volcanic rocks of southwestern Montana: Northwest Geology, v. 36, p. 91-110.
- Hadley, J., 1980, Geology of the Varney and Cameron Quadrangles, Madison County, Montana: U.S. Geological Survey Bull. 1459, 108 p.
- Hanneman, D., 1989, Cenozoic basin evolution in a part of southwestern Montana: Ph.D. dissertation, University of Montana, 347 p.
- Hanneman, D., and Wideman, C., 1991, Sequence stratigraphy of Cenozoic continental rocks, southwestern Montana: Geological Society of America Bulletin., v. 103, no. 10, p. 1335-1345.
- Janecke, S., 1994, Sedimentation and paleogeography of an Eocene to Oligocene rift zone, Idaho and Montana: Geological Society of America Bulletin, v. 106, p. 1083-1095.
- Janecke, S., McIntosh, W., and Good, S., 1999, Testing models of rift basins: structure and stratigraphy of an Eocene-Oligocene supradetachment basin, Muddy Creek half graben, southwest Montana: Basin Research, v. 11, p. 143-185.
- Janecke, S., 2007, Cenozoic extensional processes and tectonics in the northern Rocky Mountains: southwest Montana and eastern Idaho: Northwest Geology, v. 36, p. 111-132.
- Kuenzi, W., 1966, Tertiary stratigraphy in the Jefferson basin, Montana: Ph.D. dissertation, University of Montana, 293 p.
- Lielke, K., 2008a, The Butcher Creek conglomerate: an enigmatic Paleogene deposit from the northern Gravelly Range of southwestern Montana: Northwest Geology, v. 37, p. 85-96.
- Lielke, K., 2008b, Paleogeographic Reconstruction of the Renova Formation in southwestern Montana: AAPG Bulletin, v. 92, no. 11, p. 1605.
- Lielke, K., 2010, Paleogene topography, drainage patterns, and climate change in southwestern Montana: AAPG abstracts 2010 annual convention and exhibition, v. 19, p. 149.

- Lielke, K., Manchester, S., and Meyer, H., *in press*, Reconstructing the environment of the northern Rocky Mountains during the Eocene/Oligocene transition: Constraints from the paleobotany and geology of southwestern Montana, USA: *Acta Palaeobotanica*.
- Marvin, R., Weir, K., Mehnert, H., and Merritt, V., 1974, K-Ar ages of selected Tertiary igneous rocks in southwestern Montana: *Isochron West*, no. 10, p. 17-20.
- Monroe, S., 1976, Vertebrate paleontology, stratigraphy and sedimentation of the upper Ruby River basin, Madison county, Montana: Ph.D. dissertation, University of Montana, 301 p.
- Monroe, S., 1981, Late Oligocene-early Miocene facies and lacustrine sedimentation, upper Ruby river basin, southwestern Montana: *Journal of Sedimentary Petrology*, v. 51, no. 3, p. 939-951.
- Morgan, L., 1992, Stratigraphic relations and paleomagnetic and geochemical correlation of ignimbrites of the Heise volcanic field, eastern Snake River plain, eastern Idaho and western Wyoming: *Geological Society of America Memoir 179, Regional geology of eastern Idaho and western Wyoming*, p. 215-226.
- Pardee, J., 1950, Late Cenozoic block faulting in western Montana: *Geological Society of America Bull.* v. 61, no. 4, p. 359-406.
- Pierce, K., and Morgan, L., 1992, The track of the Yellowstone hot spot: volcanism, faulting and uplift: in Link, P., Kuntz, M., and Platt, L., eds., *Regional geology of eastern Idaho and western Wyoming*, Geological Society of America Memoir 179, p. 1-54.
- Ripley, A., 1995, Tertiary carbonates in the Upper Ruby and Jefferson River valleys, Montana: *Geologic history of the Dillon area, southwestern Montana: Northwest Geology*, v. 25, p. 47-78.
- Rothfuss, J., Weislogel, A., and Michalak, S., 2010, Influence of ancestral and syndepositional tectonic regimes on sediment dispersal pathways in intermontane basins: Facies and paleoflow evidence from the Renova Formation, southwest Montana: *AAPG abstracts 2010 annual convention and exhibition*, v. 19, p. 219.
- Rothfuss, J.L., Schwartz, T., and Schwartz, R.K., 2008, Alluvial facies of the Eocene Red Hill map unit of the Renova Formation, southwest Montana—Paleotopographic and extensional tectonic significance: *Geological Society of America Abstracts with Programs*, v. 40, no. 2, p. 83.
- Rothfuss, J. L., Lielke, K., and Weislogel, A. L., 2012, Application of detrital zircon provenance in paleogeographic reconstruction of an intermontane basin system, Paleogene Renova Formation, southwest Montana: in Rasbury, E.T., Hemming, S.R., and Riggs, N.R., eds., *Mineralogical and Geochemical Approaches to Provenance: Geological Society of America Special Paper 487*, p. 63-96.
- Ruppel, E., 1993, Cenozoic tectonic evolution of southwest Montana and east-central Idaho: *Montana Bureau of Mines and Geology Memoir 65*, 62p.
- Sears, J., 1995, Middle Miocene rift system in SW Montana: Implications for the initial outbreak of the Yellowstone hotspot: *Geologic history of the Dillon area, southwestern Montana, Northwest Geology*, v. 25, p. 43-46.

Sears, J., Hurlow, H., Fritz, W., and Thomas, R., 1995, Late Cenozoic disruption of Miocene grabens on the shoulder of the Yellowstone hotspot track in southwest Montana: Field guide from Lima to Alder, Montana: Northwest Geology, v. 24, p. 201-219.

Sears, J., and Fritz, W., 1998, Cenozoic tilt domains in southwestern Montana: Interference among three generations of extensional fault systems: Geological Society of America Special Paper 323, p. 241-247.

Sears, J., and Thomas, R., 2007, Extraordinary middle Miocene crustal disturbance in southwest Montana: Birth record of the Yellowstone hot spot?: Northwest Geology, v. 36, p. 133-142.

Smith, R., and Braile, L., 1993, Topographic signature, space-time evolution, and physical properties of the Yellowstone-Snake River Plain volcanic system: the Yellowstone hotspot: in Snoke, A., Steidtmann, J. and Roberts, S., eds., The Geology of Wyoming, Geological Survey of Wyoming Memoir 5, p. 694-754.

Sonder, L., and Jones, C., 1999, Western United States extension: How the west was widened: Annual Review of Earth and Planetary Sciences, v. 27, p. 417-462.

St. Jean, Z., and Teeter, D., 2004, Geologic map of the Ruby Dam area southwestern Montana: Montana Bureau of Mines and Geology Open File Report 488, 12p.

Thomas, R., 1995, Tectonic significance of Paleocene sandstone deposits in southwestern Montana: Field Guide to geologic excursions in southwest Montana, Northwest Geology, v.24, p. 237-244.

Thompson, G., Fields, R., and Alt, D., 1981, Tertiary paleoclimates, sedimentation patterns and uranium distribution in southwestern Montana: Montana Geological Society 1981 field conference, p. 105-109.

Appendix 1 - GPS coordinates (UTM)

Road Log #1 – Timber Hill and Upper Ruby Valley

Zone, Easting, Northing	Locality
12T, 399797, 4990917	STOP #1 Timber Hill north overlook
12T, 401241, 4990013	STOP #2 Head of Virginia Springs Gulch
12T, 402411, 4989468	STOP #3 Spring Brook
12T, 402248, 4989409	CONG Spring Brook Conglomerate outcrop
12T, 400480, 4987624	STOP #4 Buttress Unconformity – Hill 6607
12T, 399493, 4987211	STOP #5 Virginia Springs overview
12T, 399251, 4986693	ARCHEAN Archean basement outcrop
12T, 399864, 4986498	STOP #6 Timber Hill south overlook
12T, 403661, 4992165	STOP #7 Anthill (Cone Hill) overview
12T, 403995, 4992496	STOP #8 Volcanic intrusion – Ant (Cone) Hill
12T, 403534, 4992564	EOCENE Eocene sediments onlapping volcanics
12T, 405927, 4995006	STOP #9 Gravel Pit – Renova Fm. overview
12T, 408510, 4998363	STOP #10 Caldwell Springs – Passamari delta
12T, 410563, 5004782	STOP #11 Cottonwood Creek – Fossil Basin overview
12T, 412437, 5008349	STOP #12 Ruby Reservoir overview



Yellowstone visitors in 1896 repairing their buggy. Courtesy National Park Service.

FIELD GUIDE TO PALEOGENE VOLCANICS, SEDIMENTARY DEPOSITS, TECTONIC SETTING, PALEOENVIRONMENT, AND BASIN EVOLUTION OF THE BEAVERHEAD CANYON, MUDDY CREEK AND SAGE CREEK AREAS OF SOUTHWESTERN MONTANA, USA

Kevin Lielke

Geosciences Department, University of Montana, Missoula, MT 59712

Robert C. Thomas

Environmental Sciences Department, University of Montana Western, Dillon, MT 59725

Introduction

This field guide examines the depositional systems, paleoenvironments, and tectonic settings of the Paleogene sedimentary and volcanic rocks of southwestern Montana. During the first leg of the journey, from the area south of Dillon through Beaverhead Canyon, the field trip will examine Paleogene volcanic rocks and explore the role of pre-existing paleovalleys and topography on the development of early intermontane basins. During the second and third legs of the trip, to the Sage Creek and Muddy Creek basins respectively, Paleogene sediments deposited under different tectonic boundary conditions will be examined. The field trip will also examine the influence of the topographic inversion of the volcanic rocks in the Beaverhead Canyon area on later Paleogene sedimentary depositional environments.

Itinerary and Methodology

This field trip will start at Dillon, Montana and travel south along Interstate 15 to Barretts Park at the head of Beaverhead Canyon. From there, the trip will travel mostly along side roads to Clark Canyon Reservoir, regaining Interstate 15 at that point and ultimately arriving at Dell, Montana. Two separate trips will then visit Sage

Creek basin to the east and Muddy Creek basin to the west of Dell. Most stops will be along main roads, but several stops involve optional walking trips to observe key outcrops firsthand. These walking tours are included because several important areas, such as the Sage Creek Formation type section, cannot be accessed by vehicle but are still vital to understanding the Paleogene history of the region. All road and walking stops have been located in the field with a handheld GPS and these coordinates (in UTM units) are provided in Appendix 1 as an aid to navigation.

Road Log

Leg 1– Dillon to Dell, Montana

Meet at a convenient location in Dillon. Proceed to Interstate 15 and drive south. The road log proper will begin at Barretts Park. Leg 1 of the road log through Beaverhead Canyon will examine the thick section of Paleogene volcanic rocks which are exposed along the narrow canyon cut by the Beaverhead River. As you drive south, the Blacktail Mountains stretch across your center of vision, cut by the notch of the Beaverhead River Canyon directly ahead. Modern topography along the Blacktail Mountains is controlled by the still-active Blacktail normal fault. This fault has been

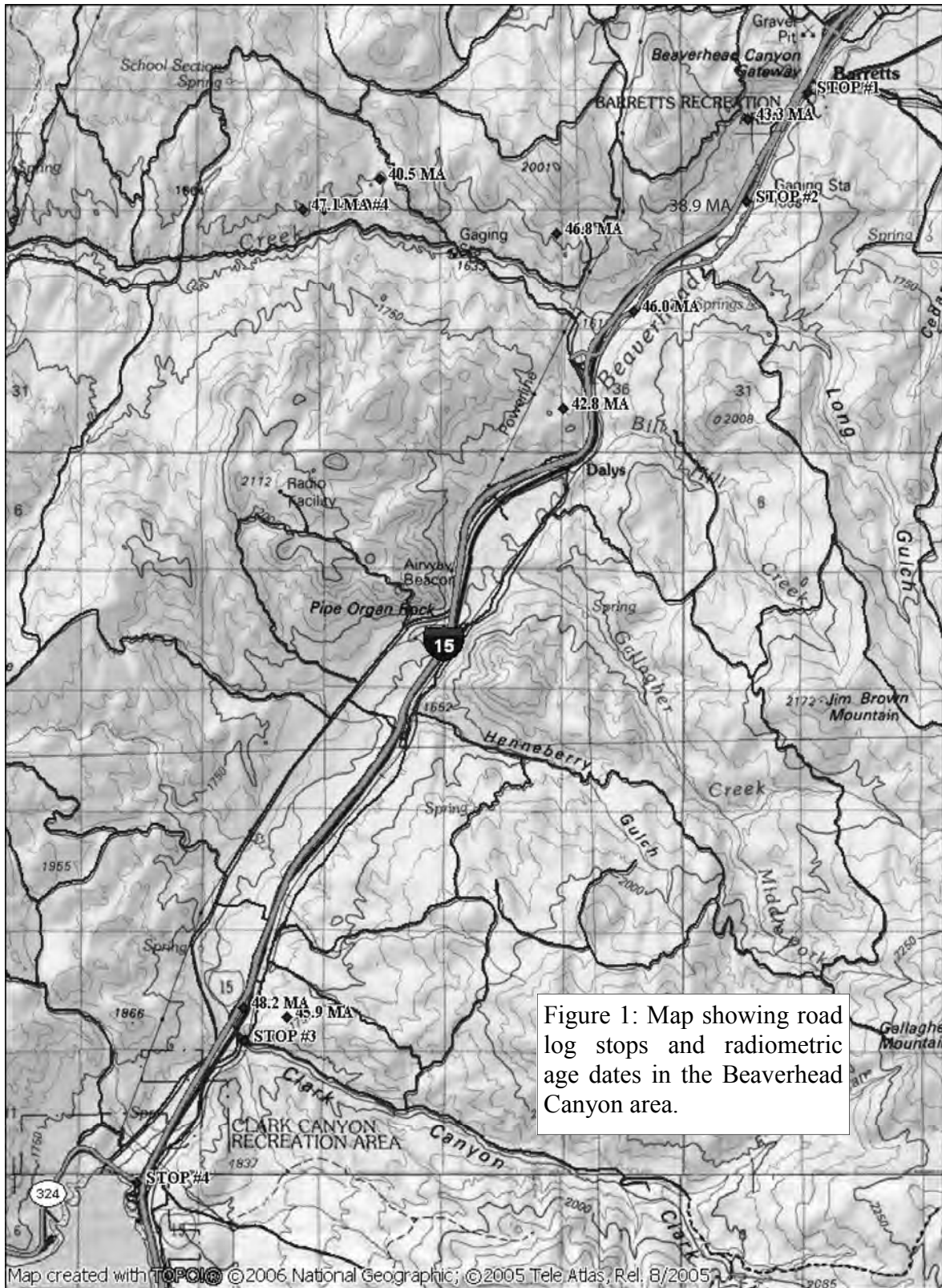
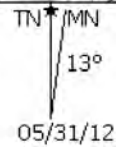
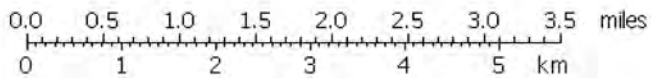


Figure 1: Map showing road log stops and radiometric age dates in the Beaverhead Canyon area.



active for approximately 6 Ma and likely represents an example of extension occasioned by motion of the North American plate over the Yellowstone hot spot (Sears and Thomas, 2007). Uplift of the Blacktail Mountains disrupted a northeast-trending Miocene paleovalley, with the modern Beaverhead River likely an antecedent stream still following its original Miocene course (Sears et al., 1995). Stream gravels of the Big Hole Member of the Sixmile Creek Formation were deposited in this Beaverhead paleovalley, remnants of which still exist as cut surfaces above the level of the modern river valley (Sears et al., 1995; Sears, 2007).

Turn off of the Interstate at Exit 56 and turn left at intersection. After crossing beneath underpass, turn right onto State Highway 91 and proceed to Barretts Park at entrance to Beaverhead Canyon.

Mileage

STOP 1

0.0 Stop 1 – Barretts Park (Figures 1 and 2).

Stop at parking lot near grassy area. There is an impressive cliff of black basaltic lava across the stream whose continuation can be seen across the interstate to the west. The Lower Dillon Volcanics have at least 600 feet of relief at this point. A whole-rock K/Ar age date of 43.3 ± 2.3 Ma was obtained from a rhyolite tuff interbedded with basalt flows across the highway approximately 0.5 mile to the south (Fritz et al., 2007). Volcanic lithologies in Beaverhead Canyon include sub-alkalinic andesite and dacite tuffs interbedded with low-silica alkaline basalts (Leeth, 1998).

Since lava and pyroclastic flows follow the path of least resistance under gravity's influence, this area must have been a topographic low during deposition of the Eocene

Lower Dillon Volcanics. The exposed thickness of Eocene volcanic rocks is over 200 meters which suggests that this area was a significant early to middle Eocene paleovalley. The volcanic source was nearby (Leeth, 1998), probably one of the easternmost Challis volcanic centers. The presence of Cretaceous volcanic flows on the western flank of Beaverhead Canyon (Leeth, 1998) suggests that this was a paleovalley with Cretaceous ancestry. It drained the Sevier orogenic highlands, given its orientation perpendicular to the Cretaceous overthrust belt. For a discussion of the Neogene tectonics of this area, see Stop #4 of Sears et al. (1995).

1.1 Road cut of basalt to right across from railroad bridges. End of pavement just past basalt outcrop.

1.5 Waterfall to east of basalt cliffs.

2.0 Silhouette of buffalo on top of basalt cliff across stream. This surface has been interpreted as a Miocene valley remnant (Sears, 2007), and will be part of the next stop.

2.1 Stop 2 – Basalt along railroad cut. Cross **STOP 2** bridge and railroad tracks, park along side of road. Carefully proceed north along railroad tracks to outcrop of black basalt. Fine-grained black basalt is well exposed in the cliff along the right side of the railroad tracks. Multiple intersecting fracture sets are visible in this otherwise massive basalt flow. A sample from a rhyolite porphyry, a little to the south along the west bank of the river, yielded a K/Ar age date of 38.9 ± 1.7 Ma (Chadwick, 1978). This rhyolite tuff likely underlies the basalt at this location.

Return to vehicles and proceed south on frontage road.

2.4 More basalt to left of road. Note near vertical fracture sets.

2.6 Purplish-red basaltic tuff along side of road. A K/Ar age date of 46 ± 2.0 Ma was obtained from basalt near this location (Chadwick, 1980).

2.7 Grasshopper Creek drainage located to right (west) across highway. Paleogene volcanic rocks make up the hills (white tuffs overlain by reddish-brown basalt flows) on the north side of the drainage. Cretaceous volcanic rocks underlie these Cenozoic volcanics further to the west (Leeth, 1998). Modern landslide deposits flank the east side of the basalt flows above the interstate. There are Paleozoic rocks on the south side of Grasshopper Creek which form the local basement which was buried by younger volcanic rocks. The well-layered rocks to the left (south) directly across the interstate are Triassic marine carbonates of the Dinwoody Formation.

2.9 Road turns to the right and crosses railroad tracks. The dirt road intersects with a paved road. Turn left onto pavement, cross bridge and then drive through interstate underpass.

3.2 Intersection – turn left and regain Interstate 15 South (Idaho Falls).

3.5 White Rattlesnake Cliff to right composed of Pennsylvanian Quadrant quartzite. Around corner, swale composed of Permian Phosphoria Formation separates the Quadrant from overlying Dinwoody Formation. These Paleozoic marine rocks likely represent early Cenozoic topography buried by Eocene volcanic flows that have been exposed by erosion. Eocene volcanics across the river include white rhyolitic ash and basalt flows.

4.4 Take Exit 51 (Daly's Spur). Turn

left at the intersection and drive through Interstate 15 underpass, then turn right onto High Bridge Road.

6.0 Cross bridge – to right note spectacular columnar jointing in massive basalt cliff (Pipe Organ Rocks). Hummocky terrain to south represents modern landslide deposits. Basalt continues across river.

6.8 Valley widens ahead. Reddish-orange rocks occur in railroad cuts to left. These are Cretaceous Beaverhead siliciclastics in the footwall of the Sevier overthrust belt. Paleozoic sedimentary rocks in the hanging wall of the overthrust belt can be seen on the western skyline in several localities along the road.

7.0 Road turns to the right and continues through I-15 underpass. At turn in paved road, a dirt road continues straight ahead and can be used to access Beaverhead sedimentary rocks.

7.8 Reddish Beaverhead sedimentary rocks in railroad cut to left (east) are visibly tilted to the north.

9.5 Railroad cut to left (southeast) is same outcrop which will be observed from Stop #3. From this vantage point, horizontal white tephra (Anderson Ranch Member of Neogene Sixmile Creek Formation) can be seen overlying older Eocene volcanics (mostly reddish basalt but also a white tuff bed) on north side of the railroad cut.

9.7 Cross under bridges – Beaverhead River to right. Impressive basalt cliff located directly ahead along left side of road.

9.9 Dirt road to left travels up steep slope and can be used to access railroad cut.

STOP 3 10.0 Stop 3 – Turn onto wide shoulder to right alongside river. On the skyline to the north-east is an outcrop of rounded-cobble conglomerate of the Big Hole Member of the Neogene Sixmile Creek Formation which overlies Eocene volcanic rocks with angular unconformity (Figure 3). To the north, white Anderson Ranch tephra underlies the Big Hole Member and overlies red-brown Eocene basalt, and a silicified white tuff on the far northern end of the railroad cut.

During the middle Miocene, this area was tilted and onlapped by Sixmile Creek Formation sediments within the Beaverhead paleovalley (Sears et al., 1995; Sears 2007). This area was later uplifted as a fault block in the footwall of northwest-trending normal faults related to the Yellowstone hot spot (Sears and Thomas, 2007). The Beaverhead River is likely an antecedent stream, a modern day remnant of the middle Miocene paleovalley (Sears et al., 1995; Sears, 2007). A thin veneer of Sixmile Creek sediments is still present in Beaverhead Canyon overlying older volcanic and basement rocks, often preserved within isolated Miocene valley surfaces (Sears, 2007). The railroad cut which exposes these relationships can be accessed from the steep dirt road at the curve of the main road at mileage marker 9.9.

Return to vehicles and continue south along frontage road.

11.4 Cross interstate overpass, drive through four-way intersection and into

gravel parking area to left of interstate on-ramp.

11.5 Stop 4 – Clark Canyon Reservoir. Stop at gravel parking area between interstate onramp and dam. From this locality, the gross structure of the area can be observed. Across the dam, Cretaceous synorogenic Beaverhead conglomerate is present in the footwall of the Sevier fold and thrust belt. The leading edge of the overthrust hanging wall is represented by Paleozoic carbonates, which make up the ridge on the skyline above the dam. It is hypothesized that Paleogene volcanic rocks occupy a paleovalley oriented perpendicular to the overthrust belt (Figure 2). This thick pile of durable volcanic rocks was later topographically inverted by differential erosion and supplied sediment to the middle Eocene (Bridgerian NALMA) vol-



Figure 2: Google Earth image showing road log stops in relation to Cenozoic volcanic rocks and Cretaceous fold and thrust belt.



Figure 3: Sixmile Creek Formation Big Hole Member fluvial conglomerates (Tsb) and white Anderson Ranch Member tephra (Tsa) overlying red-brown Eocene volcanics (Tv) in railroad cut east of Beaverhead River.

caniclastic sandstones of the Sage Creek Formation. These sediments will be examined on the second leg of this road log. For a discussion of the middle Miocene and younger history of this area, see Stop #1 of Sears (2007).

Return to vehicles and drive across dam. Proceed along lake front road several miles to Stop 5.

11.8 Road cut in Cretaceous Beaverhead conglomerate on west side of dam. The Beaverhead Formation is a synorogenic conglomerate located in the footwall of the Sevier overthrust belt. The Beaverhead conglomerate at this point is composed mostly of limestone clasts in a yellowish carbonate matrix. These carbonate clasts were derived from Paleozoic limestone in the hanging wall of the overthrust belt.

12.0 White Carboniferous limestone makes up the cliffs on the skyline to the west. These marine carbonates represent the eastern margin of the Sevier fold and thrust belt in this area.

12.9 Island to left. Limestone outcrops in

road cut to right contain several unusual breccia deposits. For a discussion of the significance of these breccias see Stop #5 of Sears (2007).

13.9 Horse Prairie campground entrance to left. The open valley to the right represents the Archean core of the Armstead anticline, a Cretaceous orogenic feature. Multiple stacked thrust sheets occur in this area. Paleozoic marine rocks make up the hanging walls of these thrust sheets and roughly outline the structure of the overthrust belt in this region.

14.9 Road cut exposes the Great Unconformity – the contact between the Archean basement and the basal Phanerozoic sedimentary section, here represented by the Cambrian Flathead sandstone and overlying green Wolsey shale. A weathered layer occurs at the top of the Archean basement.

16.0 Road cut in prominent cliff of Pennsylvanian Quadrant quartzite.



Figure 4: Tilted Oligocene lake beds along road cut west of Clark Canyon Reservoir. These lake beds were deposited in a Paleogene basin controlled by active low-angle normal faulting. The lake beds are tilted east into the Grasshopper/Muddy Creek fault zone. Variations in climate may have also played a role in controlling lake level fluctuations and sediment deposition.

18.0 Horse Prairie basin opens ahead. Crossing into area of Paleogene normal faulting which is interpreted by Janecke (2007) as a low-angle normal fault, the Muddy Creek/Grasshopper fault zone.

20.0 Medicine Lodge basin opens to left.

22.6 Bannack Bench road to right. For next couple of miles, road cuts to left expose thin-bedded, fossiliferous lake-deposited shales.

25.6 Mansfield Lane intersects the main highway to right. This road goes to the ghost town of Bannack, now a Montana state park. Spectacular cliff of layered Oligocene lake beds to left.

25.8 Stop 5 – Stop **STOP 5** along right side of road at western edge of prominent road cut developed in layered lake deposits (Figure 4). These tilted lakebed sediments represent deposition in an area of active Paleogene extension, the Grant Protobasin of Janecke (2007). This area of extension coincides with the trace of the Cretaceous fold and thrust belt, and is likely the result of extensional collapse of unstable, over-thickened crust. Alternating layers of sedimentary rock, mostly siliciclastic shales and fine-grained carbonates, are likely due to lake level fluctuations caused by a variable climate or tectonic movements. Coarse-grained sediments are not common here, which, along with the thin-bedded nature of the sediments, suggests a

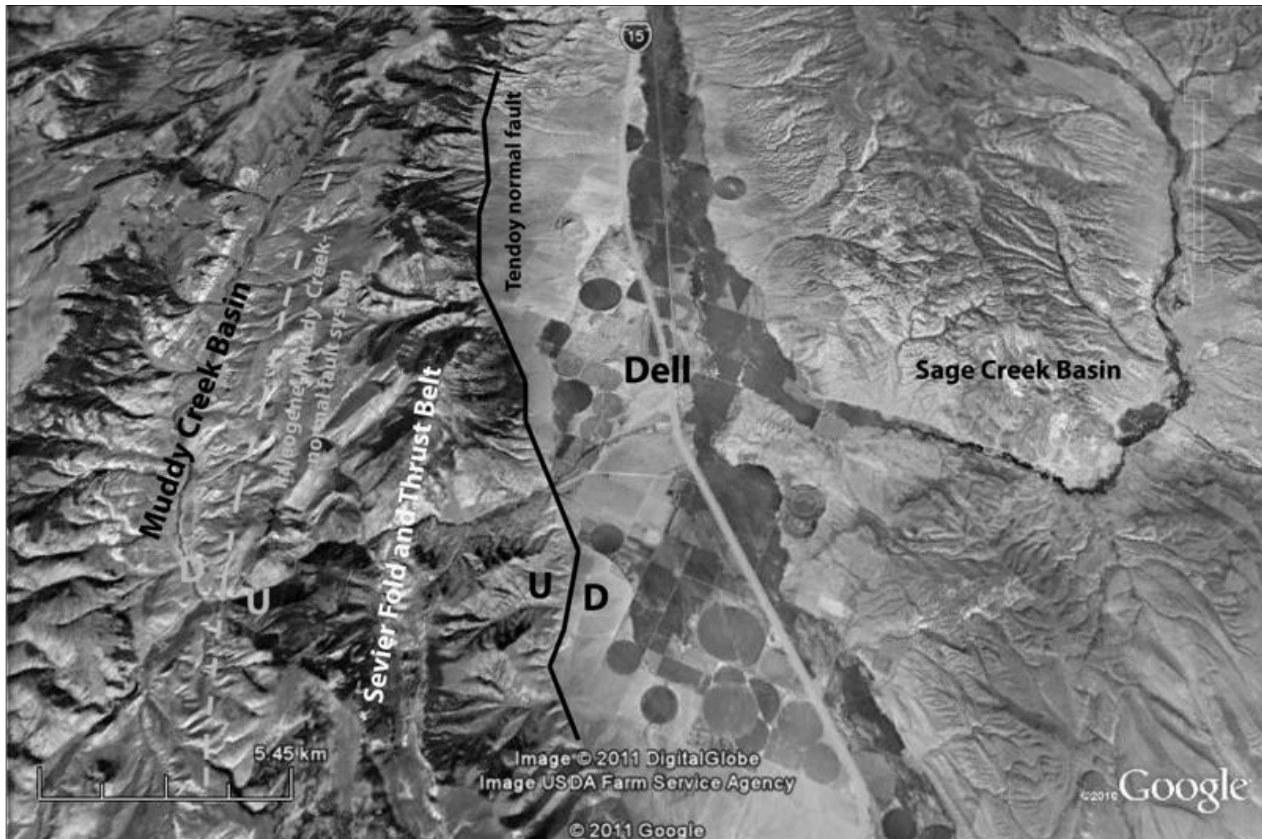


Figure 5: Google Earth image showing Paleogene Muddy Creek and Sage Creek Basins in relation to Cretaceous fold and thrust belt and Paleogene low-angle, Muddy Creek fault zone. The Muddy Creek/Grasshopper fault zone likely represents extensional collapse of the Cretaceous fold and thrust belt. Sediments in Muddy Creek and Sage Creek basins, despite their proximity, were deposited under very different tectonic boundary conditions.

calm, relatively deep-water environment. Other interpretations are possible however.

These road cuts, modified from their original form by later road work, host the Horse Prairie (Grant) section of the Beaverhead Basins paleoflora of Becker (1969). This fossil plant flora is early Oligocene in age and contains vegetation from multiple habitats which surrounded the lake basin. A high elevation coniferous forest association indicates the presence of high relief in close proximity to the lake basin. Fossil plant specimens can still be found in this area, especially in the finely-laminated lake-deposited shales. These deposits can easily be visited by climbing up the small gully on the western side of the road cut to the wide ledge which runs parallel to the highway. Exercise caution crossing the road.

Return to vehicles, backtrack to Interstate 15 and proceed south to Dell, Montana.

End of first leg of road log.

Leg 2 – Dell to Sage Creek Basin

Mileage

0.0 The remaining two legs of the field trip will examine the sedimentary deposits of the Muddy Creek and Sage Creek basins. These two basins differ from each other in their relation to the Cretaceous overthrust belt and its subsequent extensional collapse (Figure 5). The second leg of the field trip begins at the town of Dell, just off of Interstate 15 and travels to the Sage Creek basin east of the thrust front, outside the zone of Paleogene extension. Proceed to the Dell Merc parking lot. Reset mileage here. Turn left leaving the Dell Merc parking lot, and then turn right at stop sign.

0.5 Proceed north parallel to interstate and then turn right onto the Sage Creek Road and cross railroad tracks.

1.6 Reddish Beaverhead conglomerate in quarry to right. Ranch buildings to left.

2.9 Turn left and cross Sage Creek. To the right, flat-topped basalt ridges can be seen tilting to the south-southwest.

3.6 Turn right at ranch buildings and proceed along Sage Creek Road parallel to north bank of Sage Creek. Red rocks in road cut near ranch buildings are Cretaceous Beaverhead conglomerate.

4.6 Beaverhead conglomerate is exposed in road cuts and hillsides along the left side of the road. To the right, the prominent dark-colored, linear ridge capping the hill south of Sage Creek is the ~6-Ma basalt flow correlated with the Timber Hill basalt. This Pliocene basalt flow outlines a dissected inverted paleovalley of probable middle Miocene ancestry (Sears and Thomas, 2007).

6.4 Gate onto BLM land to left. On eastern side of this narrow draw, an exposure of reddish Beaverhead conglomerate can be seen in a small quarry. These hills may represent relict topography buried by younger Renova and Sixmile Creek sediments that are now being exposed by erosion.

6.7 Well-exposed sandstone layers to left are an isolated outcrop of the Oligocene Cook Ranch Member of the Renova Formation. This outlier demonstrates that the Cook Ranch Member was once more widely distributed and has subsequently been removed by erosion to expose older Renova sediments and Cretaceous rocks. These sediments appear to onlap a hill whose core is composed of Beaverhead conglomerate. This suggests that Renova sediments filled an Eocene terrain developed on the Beaverhead Formation.

**LEG 2
STOP 1**

7.2 **Stop 1** – Turn off to left and proceed on jeep trail onto BLM land. The hills on either side of the primitive road are composed of the dominantly fine-grained Dell Beds Member of the Renova Formation (Figures 6 and 7). This unit contains Uintan NALMA (Eocene) fossils and is interpreted as the fine-grained, distal portion of an alluvial fan flanking higher ground to the west/northwest. Overlying the Dell Beds Member in most places is float derived from the Neogene Sixmile Creek Formation or younger units. From here, the field trip will proceed up the draw to visit several locations of interest in the Dell Beds Member and the older Sage Creek Formation. The primitive jeep track

is impassable beyond a certain point so these locations will have to be visited on foot. This part of the field trip can be physically challenging, so you may prefer to return to the main road and continue on to Stop #2.

If you wish to continue, proceed up the draw as far as you reasonably can and then continue on foot to Waypoint 1a.

Waypoint 1a. At this locality, several coarse-grained sandstone and conglomerate beds can be observed surrounded by typical Dell Beds mudstone and siltstone. Most of these coarse-grained units are in the form of cut channels, some of which show a fining-upward trend from large angular clasts to pebble conglomerate and coarse sandstone.

Clast-supported conglomerates are frequently imbricated and show a consistent flow direction from the west-northwest. Clast compositions indicate derivation from the Cretaceous Beaverhead Conglomerate and the Eocene Hall Springs basalt, both of which outcrop to the west-northwest. These cut channels are interpreted as resulting from high energy discharge events, likely seasonal floods in a dominantly arid environment. Toward the top of this draw, well-developed calcic paleosols, typical of arid climates with alternating wet and dry seasons, are found. Round concretions resembling golf balls in size and shape are also present in the Dell Beds Member.

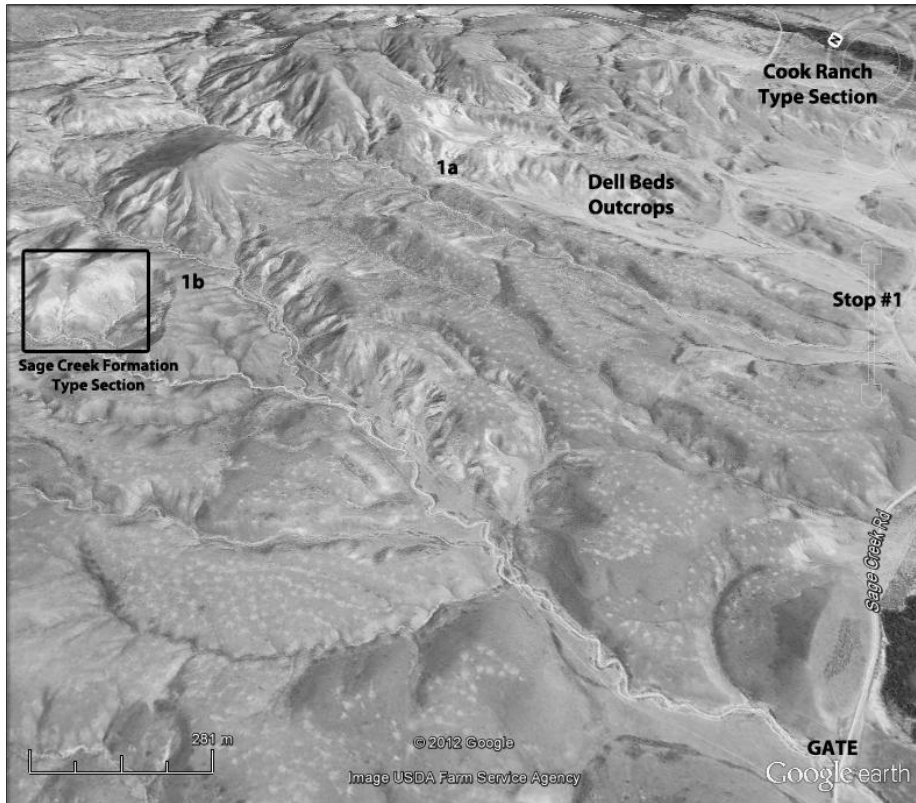
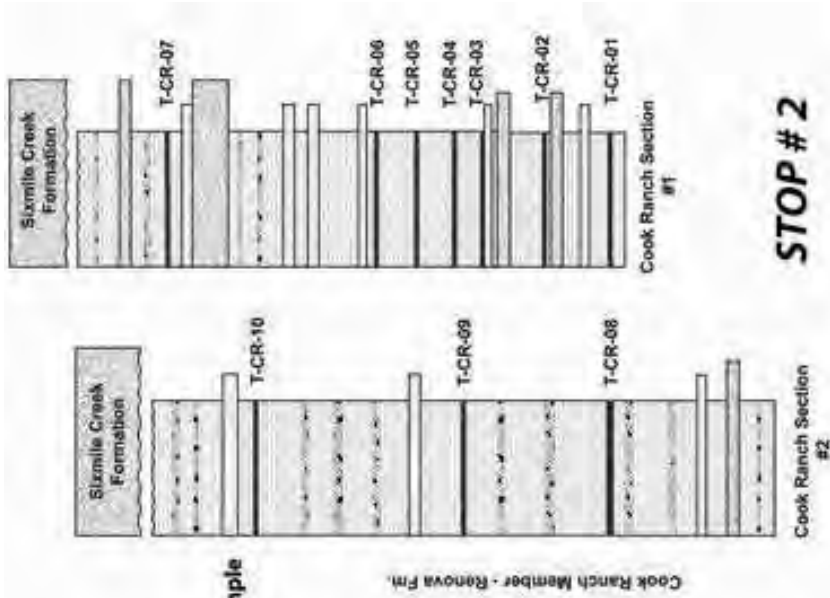
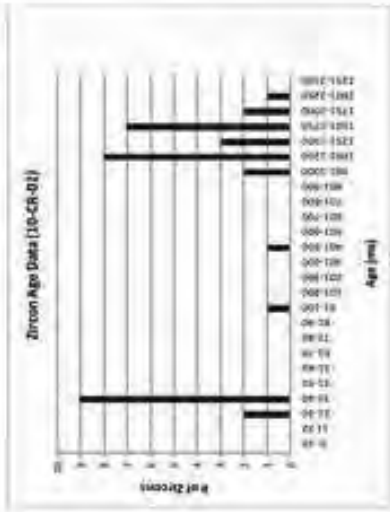
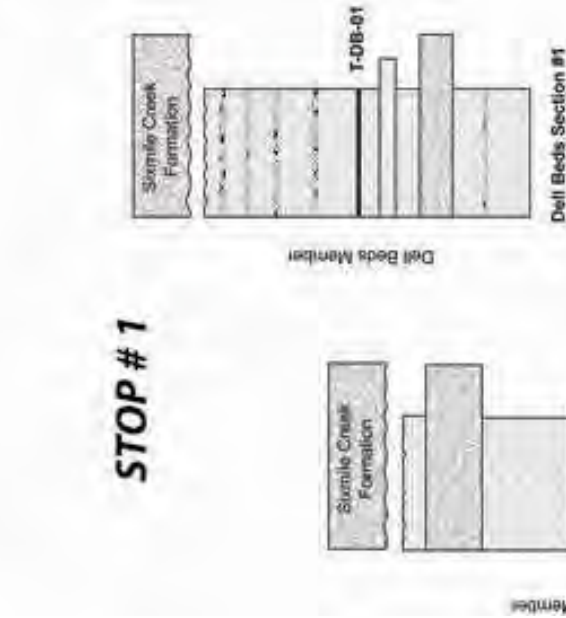


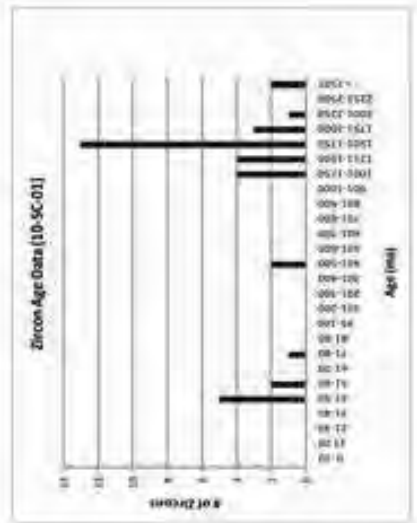
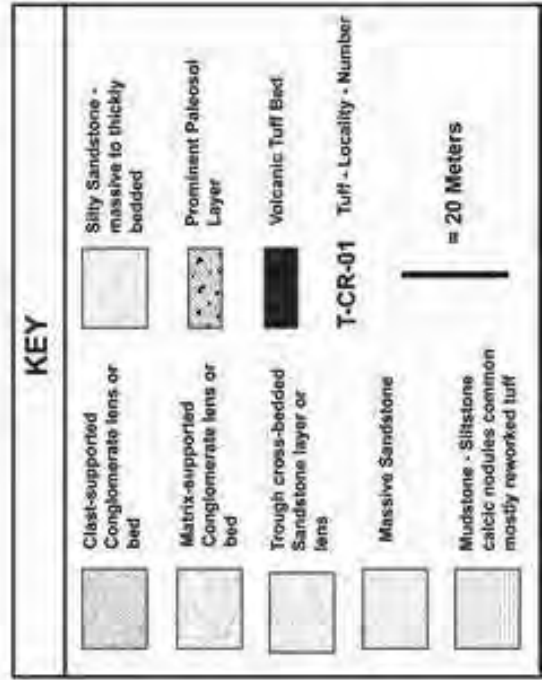
Figure 6: Google Earth image of Big Bend of Sage Creek area looking east. Paleogene sediments young toward the east. Numbers refer to stops on walking tour of area. See Figure 8 for close-up of Sage Creek type section (black box).

Measured Sections - Big Bend of Sage Creek east of Dell, MT

STOP # 1



STOP # 2



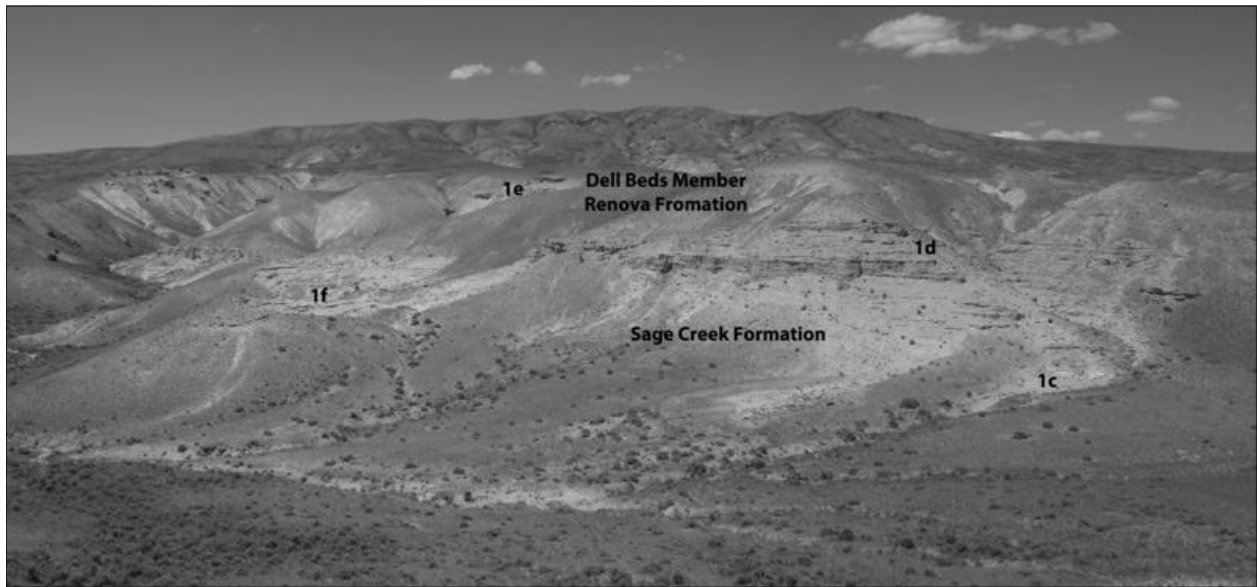


Figure 8: Sage Creek Formation type section looking north. Walking tour stops 1c – 1f are shown. Photo was taken from vicinity of walking tour stop 1b. Major unconformity exists between the Bridgerian Sage Creek Fm. and the Uintan Dell Beds Member of the Renova Fm. Late Cretaceous Beaverhead Formation conglomerate outcrops to the far left.

Proceed northwest in the direction of the Sage Creek type section (toward Waypoint 1b). An alternate route to this area is to return to the gate at mileage marker 6.4 and proceed up that draw. However, this road also washes out short of its destination; the Sage Creek type section area can only be accessed on foot.

Waypoint 1b – The top of this hill provides an excellent overview of the middle Eocene Sage Creek Formation (Figure 8). The Sage Creek Formation is a multistory fluvial sandstone unit which is separated from the overlying Dell Beds Member of the Renova Formation by a major unconformity. To the west, low hills of reddish-weathering conglomerate of the Cretaceous Beaverhead Formation can be seen. Proceed downhill towards Waypoint 1c.

Waypoint 1c – Base of the Eocene Sage Creek Formation. The Sage Creek Formation is composed of trough cross-bedded volcanoclastic sandstone beds stacked on top of each other. Channels have been eroded into older sandstone beds and filled with younger channel deposits. Cross-bed orientations and aligned wood fragments indicate flow from the north-northwest likely off of topographically inverted middle Eocene volcanics in the Beaverhead Canyon area. Near the base of this outcrop, a biotite-rich air-fall tuff (T-SC-01) is present, likely derived from the contemporary Challis volcanic field to the west (Figures 7 and 10). The first prominent sandstone ledge above this tuff was sampled for detrital zircon analysis (Rothfuss et al., 2012). The age of the youngest zircon in this sample suggests that the basal Sage Creek Formation is no older than ~46 Ma which is

Figure 7 (opposite): Measured sections and detrital zircon data from Stops #1 and #2 of Leg 2 of road log. Dell Beds section #1 corresponds to Waypoint 1a, Sage Creek section #1 corresponds to Waypoints 1c-f. Cook Ranch section #1 corresponds to Waypoint 2a, Cook Ranch section #2 corresponds to Waypoints 2b-c. Detrital zircon data were acquired from fluvial cross-bedded sandstones at locations indicated on measured sections.



Figure 9: Cook Ranch Member of the Renova Formation type section. The Oligocene Cook Ranch Member is overlain by the Miocene Big Hole Member of the Sixmile Creek Formation with angular unconformity. Walking tour stops 2a – 2c are shown.

consistent with Bridgerian NALMA fossils (Tabrum et al., 1997). The majority of the zircons are in the 46-47 Ma age range, consistent with derivation from middle Eocene volcanic rocks in the Beaverhead Canyon area (Figure 7, zircon sample 10-SC-01).

Proceed uphill toward Waypoint 1d – this is the area where Sage Creek section #1 (Figure 7) was measured. About a third of the way up, observe the unconformity between the Sage Creek Formation and the Dell Beds. This surface represents a major hiatus in sediment deposition. To the northwest, the Eocene Hall Springs basalt flow was emplaced on this surface.

Waypoint 1d – At this location, a thick conglomerate layer occurs within the Dell Beds Member. This conglomerate fills an eroded surface and contains cobbles which appear to be derived from local sources immediately to the west: the Cretaceous Beaverhead Conglomerate and the Hall Springs Basalt. Conglomerate beds become thicker, laterally continuous, and more abundant toward the west suggesting proximity to source. It is theorized that the smaller, conglomerate-filled channels at Waypoint 1a are the distal equivalents of these near-source conglomerate beds.

Proceed back downhill toward Waypoint 1e. Observe the large scale trough in the Sage Creek sandstone at Waypoint 1e as you approach from above. Also note sandstone onlapping reddish hill across gully. This may be an example of a partly exhumed hill of Beaverhead Conglomerate that was buried and now unearthed by modern erosion.

Waypoint 1e – At this location, sedimentary structures within the Sage Creek sandstones can be easily observed. Trough cross-bedding on multiple scales is present throughout this outcrop. Along the western side of this outcrop, a silicified log is present parallel to the long axis of the trough, oriented in the direction of flow toward the south-southeast. A horizontal layer of gypsum is also present, easily observed along the northern rim of the outcrop. Gypsum is present at intervals within the Sage Creek Formation and is indicative of a seasonally dry climate.

Return to vehicles and backtrack to the Sage Creek Road. You may need to compensate for the mileage driven up the draw. Turn left onto Sage Creek Road.

8.0 Big Hole conglomerate to left of road.

**LEG 2
STOP 2**

8.4 Stop 2 – Cook Ranch Member type section (Figures 7 and 9). Park along the side of the road. The outcrop to the left of the road is the Cook Ranch type section. Renova sediments of the Cook Ranch Member contain Chadronian and Orellan mammal fossils, which along with magnetostratigraphic studies indicate that these sediments straddle the late Eocene-early Oligocene boundary (Tabrum et al., 1997). On this side of the hill, the Orellan Cook Ranch Fauna and a correlated zone of mostly normal polarity suggest that these sediments represent early Oligocene deposition (Tabrum et al., 1997). At the summit of the hill, conglomerate of the Big Hole Member of the Sixmile Creek Formation overlies the Renova sediments with pronounced angular unconformity. Within the Cook Ranch Member, several features of interest relevant to the interpretation of climate and environmental conditions during the early Oligocene are present. The remainder of this stop will consist of a walking tour of this locality.

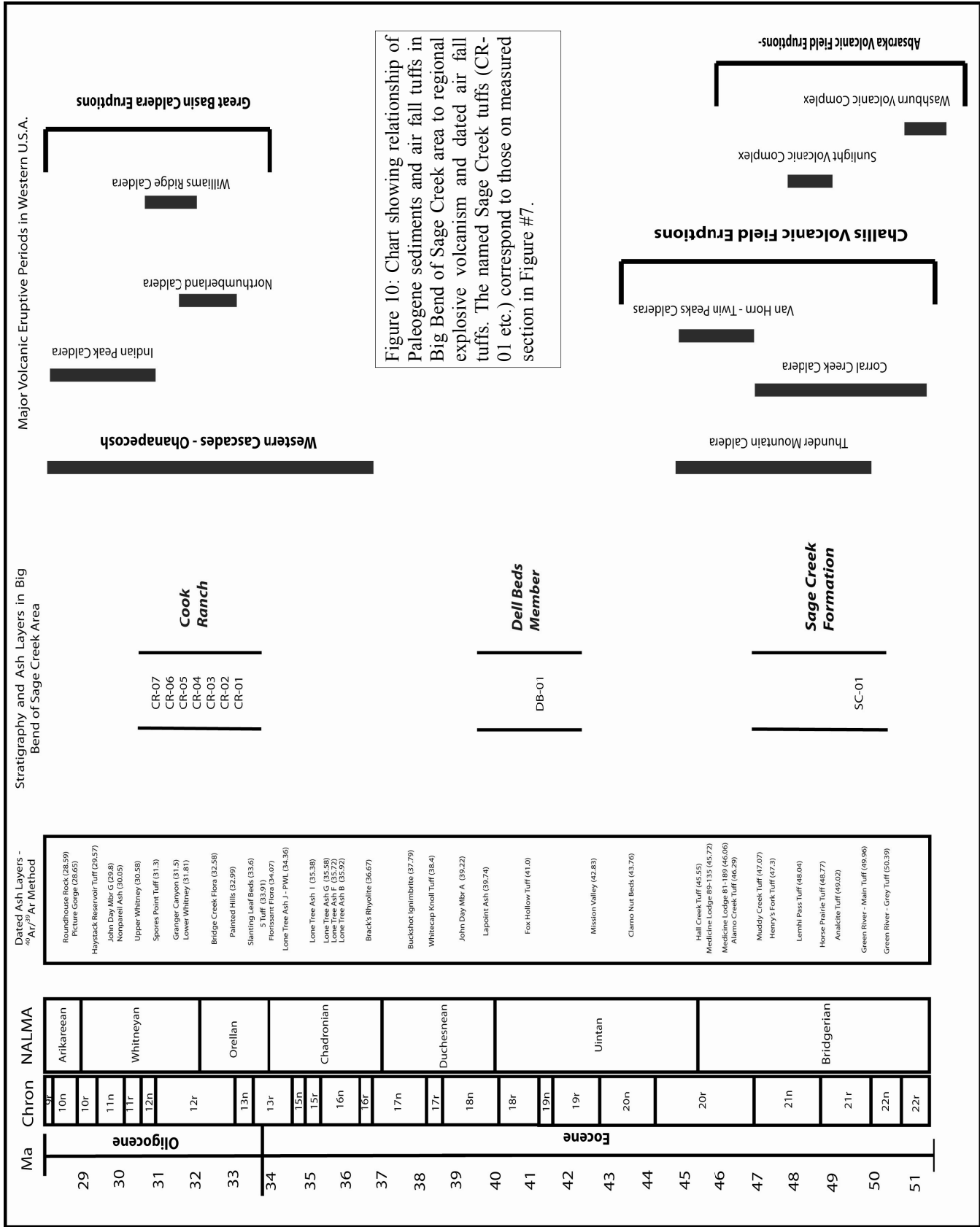
Leave vehicles and proceed north toward GPS waypoint 2a. Note red-black basalt float underlying Cook Ranch Member at this location. The significance of this volcanic material is unknown, but it is possible that it is a basalt flow on the unconformity between the Dell Beds and Cook Ranch Members of the Renova Formation.

Waypoint 2a – Caution: avoid walking on Renova outcrops as footing is unstable especially on unvegetated surfaces. At this location, along the northeastern rim of the outcrop area, about seven discrete air-fall tuffs form prominent white layers which can be traced laterally across the entire out-

crop face (Figure 7, Cook Ranch section #1). These air-fall tuffs are likely fallout from explosive rhyolitic caldera eruptions in the Great Basin (Figure 10). Interlayered mudstones and siltstones contain a high proportion of volcanic material likely reworked from ash deposited at higher elevations by these same eruptions. Prominent ledges and lenses are composed of sandstone and conglomerate layers and channels. Near the top of the hill, toward the center of the outcrop, are several prominent conglomerate lenses. These represent cut channels which contain multiple fining-upward sequences. Each individual sequence is composed of basal breccias which grade upwards to coarse sandstone. The depositional environment is interpreted to be a dominantly fine-grained, distal alluvial fan which contains tabular sheet-flood sandstones; thin, ephemeral cross-bedded fluvial sandstones; and cut channels filled with high discharge flood deposits all encased in volcanoclastic siltstones and mudstones.

Proceed carefully towards the southwest along the base of the outcrop area to Waypoint 2b.

Waypoint 2b – Warning: watch your footing on this outcrop especially on steep and unvegetated slopes. This location presents several features of interest relevant to the interpretation of early Oligocene climate and sedimentary depositional environments. A sheet of thin, cross-bedded sandstone extends across this outcrop several meters above the base. This sandstone has a well-developed pebble lag at the base and is interpreted as a small ephemeral stream which meandered across the low gradient distal portion of an alluvial fan. Very small freshwater gastropods are present in this fluvial sandstone. These are likely dwarfed versions of common freshwater gastropods living in an arid environment (Roth, 1987).



Additional evidence of an arid climate is present in the form of highly developed calcic soil horizons (calcisols). This type of paleosol is characteristic of arid environments with seasonal wet periods, where calcium carbonate is alternately dissolved and re-precipitated (Retallack, 2001). In some places these paleosol layers have become interconnected, forming a three-dimensional web. A couple of tuff layers, which can be visually traced across the outcrop, are also visible. These layers are a useful datum to gauge the southeastern tilt of the Renova section in the direction of the Snowcrest Range which can be seen on the horizon to the south.

Carefully walk to the edge of the outcrop and proceed uphill along the grass fringe which borders the south rim of the outcrop area. Avoid walking off the grassy area as footing on the bare rock surfaces is quite hazardous.

Waypoint 2c – From the top of the hill, the unconformity between the Renova and the Sixmile Creek Formations can be directly observed. Using the white tuff layers as a visual cue, the angular nature of the unconformity can be seen. The rounded cobble, fluvial conglomerate topping the hill is the Big Hole Member of the Sixmile Creek Formation. This unit represents deposition in a major through-going stream and contains exotic clasts with an Idaho provenance. This stream flowed northeast along the middle Miocene Beaverhead paleovalley. Stretching from east to west across the horizon are other remnants of this Miocene paleovalley including more Big Hole Conglomerate as well as a dissected linear ridge of black basalt to the southwest, the ~6.0-Ma Timber Hill basalt flow. For a more detailed discussion of the significance of this Miocene paleovalley see Sears et al. (1995).

Looking northwest, Dell Beds Member sediments are visible. Magnetostratigraphic work and fossil mammal biostratigraphy suggest that the Eocene-Oligocene boundary may be present near the base of this hill. The Chadronian (late Eocene) Little Spring Gulch local fauna is found in a stratigraphically low position in the Cook Ranch Member (Tabrum et al., 1997). To the east across Sage Creek, white fine-grained sediments of the Whitneyan and Arikareean (Oligocene to early Miocene) age Blacktail Deer Creek Member form low undulating hills. The resistant layers capping these hills are conglomerate beds of the Big Hole Member.

End Road Log Leg 2 – Return to Dell.

Leg 3 – Dell to Muddy Creek Basin

Mileage

Field trip begins at the Dell Merc parking lot in the town of Dell, Montana.

Red Butte, the prominent red bluff to the east, is composed of Cretaceous Beaverhead conglomerate. This syntectonic conglomerate was shed from Cretaceous thrust sheets (Medicine Lodge, Tendoy, etc.) to the west. Turn left out of Dell Merc parking lot, drive through stop sign, after stopping, and through interstate underpass.

0.2 Turn left onto Westside Frontage Road at sign for Big Sheep Creek. Tendoy Range directly ahead on horizon. Prominent peaks are Dixon Mountain to the south and Timber Butte to the north separated by Little Water Canyon.

1.5 Good view of the internal stratigraphy of the Beaverhead Conglomerate on south side of Red Butte to left.

1.8 Turn right onto Big Sheep Creek Road.

4.0 Road crosses small linear hill. This hill represents the fault scarp of the active normal fault along the front of the Tendoy Range. Poorly sorted conglomerate of the Sixmile Creek Formation is exposed in this road cut. Road ahead crosses through narrow valley cut by Big Sheep Creek through the Tendoy Range. Canyon walls expose the internal structure of Cretaceous thrust sheets and Paleogene normal fault zone.

4.4 More Sixmile conglomerate in road cut to right.

6.0 South side of Dixon, Mountain. Paleozoic Quadrant quartzite in roadcuts and cliffs to right. Road is crossing through the footwall of the Paleogene Muddy Creek fault zone (Figure 5). This area is also the footwall of the modern Tendoy normal fault. During Cretaceous time, this area was subjected to a considerable amount of crustal shortening as evidenced by the Tendoy, Four Eyes Canyon, and Medicine Lodge thrust sheets.

9.6 Cross cattle guard. Muddy and Big Sheep Creek basins open straight ahead. Note westward-dipping Paleozoic strata in cliffs to north and northeast on flank of Dixon Mountain. Crossing approximate location of Paleogene Muddy Creek normal fault zone.

9.8 Turn right onto Muddy Creek Road (BLM road #1829). Road through Muddy Creek Basin crosses both BLM and private access land; stay on road while crossing private access land. The road cuts generally down section from Oligocene sedimentary basin fill to middle Eocene volcanic and volcanoclastic sediments.

10.2 Crossing fence line and gate. Paleo-

gene sedimentary rocks exposed ahead; resistant ledges are conglomeritic channels cut into fine-grained siltstones and sandstones. Note gentle eastward tilt of Paleogene beds compared to steeply dipping Paleozoic Quadrant quartzite exposed on the southwest slope of Dixon Mountain. Paleogene sediments are tilted eastward into the Muddy Creek fault zone.

10.5 Stop 1. Climb slope to right to view conglomerate lenses cut into fine-grained Paleogene sediments. These deposits correspond to Facies 5 of Janecke et al. (1999) and represent the youngest (Oligocene) basin fill of Muddy Creek basin. Toward the east, the unit becomes coarser grained, grading to alluvial conglomerate deposits along the edge of the Muddy Creek footwall. Clasts are predominately angular boulders and cobbles of Quadrant quartzite derived from the Muddy Creek fault footwall directly to the east (Janecke et al., 1999) documented conglomerate clast compositions which can be traced to individual portions of the footwall, demonstrating the existence of locally derived alluvial fans. Clast imbrication indicates derivation from Dixon Mountain to the east. During the later stages of the evolution of Muddy Creek basin these coarse-grained alluvial deposits prograded throughout most of the basin, covering the older lacustrine and fluvial deposits. This change corresponds roughly to the final descent into ice-house climatic conditions across the Eocene-Oligocene boundary.

**LEG 3
STOP 1**

10.9 Lacustrine and fluvial beds to right are covered with a thin drift of Quadrant quartzite cobbles. These beds correspond to Facies D of Janecke et al. (1999) and are late Eocene to earliest Oligocene (Chadronian NALMA) in age based on the mammal biostratigraphy work of Dunlop

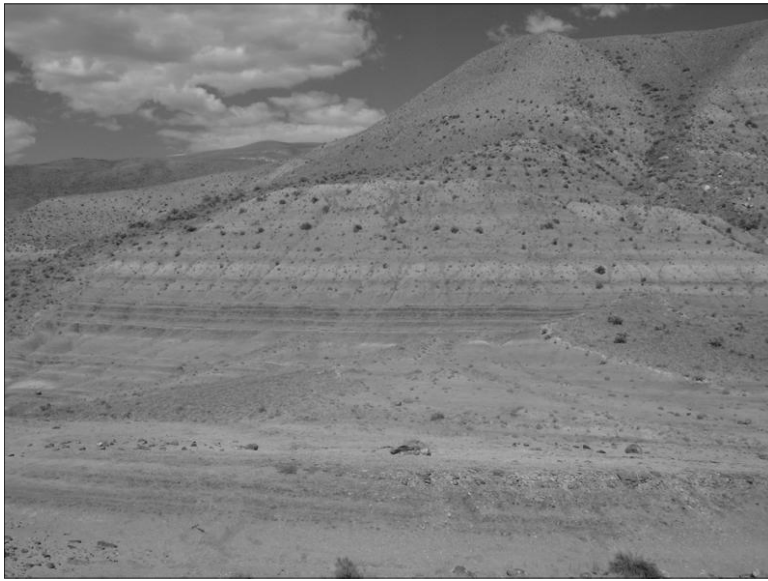


Figure 11: Lake beds in the Muddy Creek Basin. Lake beds tilt eastward into basin bounding Muddy Creek fault system of Paleogene age. These lake deposits are similar to those visited at Stop #5 of Leg 1 of road log, which are controlled by the same fault system, but radically different from the alluvial fan deposits in the Sage Creek area despite their overlapping ages and close proximity to each other. This suggests that the Muddy Creek/Grasshopper normal fault system represents a major Paleogene structural boundary.

(1982). This would make them roughly time equivalent to the alluvial fan deposits of the Cook Ranch type section (Stop #2 of Leg 2 of this road log). Lakebed sediments are commonly organic rich and thin bedded. Note that the organic-rich beds in this unit tend to weather to lighter colors. Lakebeds of this unit continue to the north for several miles. To the east, toward the footwall, these lake sediments eventually grade to conglomerate similar to that at stop #1.

**LEG 3
STOP 2**

12.6 Stop 2 – Trail Creek road. Turn off and park at Trail Creek Road (BLM Road #1830) turnout. Best exposure of organic-rich lacustrine shale facies (Facies D of Janecke et al., 1999) is in semi-circular box canyon to east of road. Dark organic-rich shale (lighter colored when weathered)

predominates but is interlayered with siliceous shale, lignitic coal, limey mudstone, and minor sandstone layers (Figure 11). Ash is uncommon suggesting the cessation of most local igneous activity by this time (Janecke et al., 1999). Sandstone units are well-laminated, tabular and contain abundant crossbeds. Plant debris, especially wood fragments, are common in the dark-brown organic-rich shale layers.

These deposits have been interpreted as shallow freshwater pond- and lake-margin environments (Janecke et al., 1999) considering the interlayered cross-bedded sandstone and interbedded coal seams. However, the presence of well-preserved organic debris and paper shale suggest that poorly oxygenated conditions with little bioturbation were present over a wide area. A deeper lake environment is an alternate explanation if tabular sandstone deposits are either turbidities or representative of temporary lake-level drops. These lake deposits represent a significantly different depositional environment from the roughly contemporary sediments in Sage Creek despite their close proximity to each other.

If you wish to examine these lakebeds up close, proceed across road, cross fence (carefully) and walk to Waypoint 2a. This is one of the most easily accessible areas where the lakebeds are well exposed.

When finished, return to vehicles and continue north.

13.7 Stop 3 – To the right are more lake and fluvial deposits of Facies D of Janecke et al. (1999). Fossil mammal remains from this locality and Stop #2 are early Chadronian (early

**LEG 3
STOP 3**

late Eocene) in age and come primarily from high in the section (Dunlap, 1982). Waypoint 3a marks the location of a thin, laterally persistent cross-bedded sandstone bed containing abundant freshwater invertebrates which can be visited on foot. This sandstone is encased in dark shale and could be a fluvial deposit, or alternatively, a turbidity flow. Correct interpretation of these coarse grained deposits has important implications for the interpretation of the lakebeds especially in regards to their depth and paleoenvironment.

14.2 The Johnson Creek area. To the east along this stretch of road, beyond the Cenozoic lakebeds, are Mesozoic rocks within the hanging wall of the Cretaceous Four Eyes Canyon thrust fault. The modern canyon between Dixon Mountain and Timber Butte is occupied by the Little Water Syncline, a fold in the footwall of the Cretaceous thrust. The south side of Timber Butte is folded by the paired Timber Butte Anticline (Dunlap, 1982). The Paleogene Muddy Creek normal fault appears to be localized above a Cretaceous thrust ramp, an example of fault reactivation likely related to extensional collapse of overthickened and thermally weakened crust.

**LEG 3
STOP 4**

15.4 Stop 4 – Ranch buildings at McNinch Creek. To the east of the corrals, more lake deposits of Facies D can be seen tilted approximately 30 degrees to the east into the Muddy Creek basin normal fault. To the west across Muddy Creek are distinctive white layers of tuffaceous siltstones and shales belonging to Facies C of Janecke et al. (1999). These are well-laminated tuffaceous shales and mudstones with minor sandstone, limestone, and well-rounded and well-sorted pebble conglomerates. These deposits represent a shallow freshwater lake margin, stream, and marsh

setting. Facies C may represent a shallower water setting compared to the organic rich shales of Facies D. Alternatively, it may reflect a reduction in the influx of volcanic material in the later Eocene. The contact between Facies C and D appears to be gradational, suggesting a long-lived lake basin which persisted for approximately 10 Ma. (Janecke et al., 1999). Further to the north-northwest in the higher elevations, Eocene volcanic and related volcanoclastic rocks can be seen. These deposits are synrift volcanics related to the middle Eocene Challis volcanic field in Idaho.

END ROAD LOG HERE – Turn around and return to junction with Big Sheep Creek Road and retrace your path back to Dell.

References

Becker, H., 1969, Fossil plants of the Tertiary Beaverhead basins in southwestern Montana: *Palaeontographica Abt. B.*, v. 127, Lfg. 1-6, p. 1-142.

Chadwick, R., 1978, Geochronology of post-Eocene rhyolitic and basaltic volcanism in southwestern Montana: *Isochron/West*, no. 22, p. 25-28.

Chadwick, R., 1980, Radiometric ages of some Eocene volcanic rocks, southwestern Montana: *Isochron/West*, no. 27, p. 11.

Constenius, K., 1996, Late Paleogene extensional collapse of the Cordilleran foreland fold and thrust belt: *Geological Society of America Bulletin*, v. 108, no. 1, p. 20-39.

Dunlap, D., 1982, Tertiary geology of the Muddy Creek Basin, Beaverhead County Montana: University of Montana, Ph.D. Dissertation, 133 p.

- Fields, R., Rasmussen, D., Tabrum, A., and Nichols, R., 1985, Cenozoic rocks of the intermontane basins of western Montana and eastern Idaho: A summary: in Flores, R., and Kaplan, S., 1985, Cenozoic paleogeography of west-central United States, SEPM-RMS, p. 9-36.
- Fritz, W., Sears, J., McDowell, R., and Wampler, J., 2007, Cenozoic volcanic rocks of southwestern Montana: Northwest Geology, v. 36, p. 91-110.
- Janecke, S., McIntosh, W., and Good, S., 1999, Testing models of rift basins: structure and stratigraphy of an Eocene-Oligocene supradetachment basin, Muddy Creek half graben, southwest Montana: Basin Research, v. 11, p. 143-185.
- Janecke, S., 2007, Cenozoic extensional processes and tectonics in the northern Rocky Mountains: southwest Montana and eastern Idaho: Northwest Geology, v. 36, p. 111-132.
- Leeth, D., 1998, Geology, age and chemistry of Cretaceous and Tertiary volcanics near the mouth of Grasshopper Canyon, Beaverhead county Montana: M.S. thesis, Georgia State University, 74 p.
- M'Gonigle, J., and Dalrymple, G., 1996, Ar⁴⁰/Ar³⁹ ages of some Challis volcanic group rocks and initiation of Tertiary sedimentary basins in southwestern Montana: United States Geological Survey Bulletin 2132, 17 p.
- Retallack, G., 2001, Soils of the past – an introduction to paleopedology: Blackwell Science, 2nd edition, 404 p.
- Roth, B., 1986, Land mollusks (Gastropoda: Pulmonata) from early Tertiary Bozeman group, Montana: Proceeding of the California Academy of Sciences, v. 44, no. 11, p. 237-267.
- Rothfuss, J. L., Lielke, K., and Weislogel, A. L., 2012, Application of detrital zircon provenance in paleogeographic reconstruction of an intermontane basin system, Paleogene Renova Formation, southwest Montana: in Rasbury, E.T., Hemming, S.R., and Riggs, N.R., eds., Mineralogical and Geochemical Approaches to Provenance: Geological Society of America Special Paper 487, p. 63-96.
- Sears, J., Hurlow, H., Fritz, W., and Thomas, R., 1995, Late Cenozoic disruption of Miocene grabens on the shoulder of the Yellowstone hotspot track in southwest Montana: Field guide from Lima to Alder, Montana: Northwest Geology, v. 24, p. 201-219.
- Sears, J., and Thomas, R., 2007, Extraordinary middle Miocene crustal disturbance in southwest Montana: Birth record of the Yellowstone hot spot?: Northwest Geology, v. 36, p. 133-142.
- Sears, J., 2007, A field guide to Middle Miocene karstified erosional surface and debris flows and neotectonic faults near Clark Canyon Reservoir, southwest Montana: Northwest Geology, v. 36, p. 251-260.
- Tabrum, A., Prothero, D., and Garcia, D., 1997, Magnetostratigraphy and biostratigraphy of the Eocene-Oligocene transition, southwestern Montana: in Prothero, D.R., and Emry, R.J., eds., The Terrestrial Eocene-Oligocene transition in North America, Cambridge University Press, p. 278-311.
- Tabrum, A., Nichols, R., Barnosky, A., 2002, Tertiary paleontology of southwest Montana and adjacent Idaho: Museum of the Rockies Occasional Paper no. 3.

Appendix 1 - GPS coordinates (UTM)

Road Log Leg #1 – Dillon to Dell via Beaverhead Canyon

Zone, Easting, Northing	Locality
12T, 363131, 4998594	STOP #1 – Barretts Park
12T, 362289, 4997158	STOP #2 – Railroad Cut – volcanics
12T, 355239, 4986075	STOP #3 – Sixmile overlying volcanic
12T, 355426, 4986474	VOLCANICS – along railroad cut
12T, 353871, 4984287	STOP #4 – Clark Canyon Overview – overthrust belt
12T, 333466, 4985952	STOP #5 – Grant roadcut – tilted lake beds
12T, 333648, 4985951	LAKE BEDS – bench above road
12T, 365346, 4953632	DELL MERC - end road log here

Road Log Leg #2 – Dell to Sage Creek Basin

Zone, Easting, Northing	Locality
12T, 365346, 4953632	Dell Merc - begin road log here
12T, 374963, 4955284	STOP #1 – BLM access road
12T, 374906, 4956621	Waypoint 1a – Dell Beds conglomerate
12T, 373967, 4956866	Waypoint 1b – Overview of Sage Creek type section
12T, 373946, 4956979	Waypoint 1c – Cross-bedded sandstone and tuff
12T, 373921, 4957015	Waypoint 1d – Unconformity - Sage Creek and Dell Beds
12T, 373563, 4957379	Waypoint 1e – Conglomerate in Dell Beds
12T, 373941, 4957011	Waypoint 1f – Sage Creek trough crossbeds and fossil log
12T, 376238, 4956184	STOP #2 – Cook Ranch Member type section
12T, 375955, 4956359	Waypoint 2a – Air-fall tuffs in Cook Ranch Member
12T, 376047, 4956209	Waypoint 2b – Paleosols and fluvial sandstone bed
12T, 375955, 4956125	Waypoint 2c – Unconformity between Sixmile and Renova

Road Log Leg #3 – Dell to Muddy Creek Basin

Zone, Easting, Northing	Locality
12T, 365346, 4953632	Dell Merc - begin road log here
12T, 356531, 4944598	STOP #1 – Conglomerate
12T, 354514, 4947342	STOP #2 – Trail Creek turnout
12T, 354547, 4947643	WAYPOINT 2a – Lake Beds
12T, 353832, 4948543	STOP #3 – Lake Beds overview
12T, 354154, 4948543	WAYPOINT 3a – Fluvial bed
12T, 353599, 4949233	JOHNSON CREEK - Overthrust overview
12T, 352767, 4951413	STOP #4 – McNinch Creek



*Oregon Short Line depot at West Yellowstone, about 1908.
Courtesy National Park Service.*